Addressing regression architecture for the robust mitigation of environmental and operational variations in wind turbine blade monitoring

THE UNIVERSITY
of EDINBURGH

Callum Roberts

School of Engineering

The University of Edinburgh

A thesis submitted for the degree of

Doctor of Philosophy (Ph.D)

2023

If you torture the data long enough, it will confess to anything.

Ronald H. Coase

Acknowledgements

Principally, I would like to express my deepest gratitude to Dr. David Garcia Cava for his continued, unwavering and unequivocal support. Your advice on my work has been invaluable in finishing. Additionally, I would like to extend my appreciation to Dr. Luis David Avendãno-Valencia for his contributions towards my work, primarily through his extensive knowledge of the applied theory. No habria terminado este trabajo sin su conocimiento y experiencia, al menos no con los estandares de ahora. No podria haber pedido por unos mejores colegas para trabajar tan cercanamente durante los ultimos años. Gracias sinceramente e infinitamente.

I am deeply indebted my funder The Carnegie Trust for the Universities of Scotland. The support from the board has been exceptional, especially Dr. Patricia Krus and Sarah Huxtable. I am grateful for their support during my mental health problems, for the extension and for the sense of community that I have felt during my studies. I hope that in the future I can give back to the trust so that other students can have the wonderful experience that I had.

I would be remiss if I did not extend special thanks to my fellow PhD students Dr. Artur Movsessian and Mateusz Stajuda for the discussions about work and for their support during my studies. Additionally, I would like to recognise the contributions of Prof. Yong Lu for his helpful comments and Dr. Tcherniak for providing the data for the V27 wind turbine.

I could not have undertaken this journey without the love and support of my wonderful partner, Tegan Fraser. I cannot thank you enough for all you have done for me. From helping me through self-doubt and overcoming the worst of my mental health problems, you have always been there and this work would not have been completed without your resolute support. Finally, I would also like to thank my family for their support. I know it has not been easy at times but I am grateful for all that you have done for me.

Abstract

Whilst wind power is a promising alternative to wasteful and polluting fossil fuels, there are a number of issues that must be addressed. Many difficulties lie in the maintenance of the ever increasing size of the blades, especially in offshore environments. The current industry standard of visual inspection is outdated and needs to be replaced with real-time and online monitoring. Vibration-based Structural Health Monitoring (VSHM) has been proposed as a potential solution to this problem. However, the presence of Environmental and Operational Variations (EOVs) causes VSHM methods to struggle to differentiate between damaged and undamaged observations. The Damage Sensitive Features (DSFs) measured from the wind turbine blades are heavily influenced by the EOVs and effort has to be made to mitigate their effects to ensure the damage detection is reliable. Through regression analysis, relationships can be established between the DSFs and measured Environmental and Operational Parameters (EOPs). Subsequently, EOP-normalised DSFs are created by the difference between the original DSFs and those predicted by the regression models.

The reliability in the predictions, beyond what they were trained with, is an extremely important but often overlooked aspect of regression design. Uncertainty can easily be introduced by overfitting model orders, including non-influential EOPs and by benign trends present in the training data. Through considered design, this work aims to address such issues through the application of a comprehensive nonlinear forward stepwise regression method for the purpose of monitoring an operational wind turbine blade. The proposed methodology employs methods to remove collinear variables, identify the most influential EOPs, reduce model orders and determine which DSFs should be regressed. The combination of these methods facilitates a compact regression basis, purged of as much uncertainty as possible. Lasso regression is used for comparison, as it is a similar and established type of stepwise regression. Ultimately, reducing biases and overfitting through considered design will increase the robustness of the system, as well as increasing confidence in the decision making process.

Keywords: Structural Health Monitoring, environmental and operational variations, multivariate nonlinear regression, forward stepwise regression, Lasso regression, mutual information, F-statistic, Mahalanobis distance

Lay Summary

As climate change continues to get worse, it is important for more research to be done into renewable sources of energy, such as wind. One of the main problems with wind turbines is that they are difficult to maintain. At the moment, maintenance of wind turbine blades is most commonly done by an engineer inspecting by eye while suspended high in the air. What is needed is a remote system that can assess the condition of the wind turbine blade. Vibration-based structural health monitoring has been proposed to accomplish this. However, the measurements from the sensors required for the remote system can become distorted by changes in the weather and how the turbine is operating.

So that the remote system can separate damage from the changing conditions, regression models are used to understand the cause-effect relationship between the changing conditions and the sensor measurements. By understanding the relationships, it is possible to mitigate against the changing conditions by comparing the predicted value to the measured value. Modelling the measurements from the sensors is very difficult because the signals are noisy.

To ensure that the models are accurately predicting the sensor measurements, a new method is proposed. The proposed method aims to overcome a number of common problems. These include: only selecting influential predictors, avoiding overcomplicated models and deciding whether having a model provides any benefit. It is essential for the system to be sensitive to damage but more importantly, for the method to be robust. By considering and addressing the problems, the proposed method is able to design a dependable system.

Overcoming the problem with the changing conditions will allow a remote system to make more reliable decisions. Having more confidence in the decision making on maintenance results in fewer wind turbine blade breakages and enables the wind turbines to operate for longer. These factors will make operating wind turbines more cost efficient, making them more attractive compared to fossil fuels.

Declaration of Originality

I declare that I composed the the work presented in this thesis, "Addressing regression architecture for the robust mitigation of environmental and operational variations in wind turbine blade monitoring". Except in cases where indicated in the text, the presented work was completed in its entirety by me. Furthermore, I declare that none of the included work has been submitted for any other degree or professional qualification. Sections of the thesis that have already been published have been clearly noted in the text.

_____

Callum Roberts

Publications

Journal contributions:

Roberts, C., García Cava, D., Avendaño-Valencia L.D. (2023). Addressing practicalities in multivariate nonlinear regression for mitigating environmental and operational variations. In: Structural Health Monitoring, vol 22. Sage. Available at: https://doi.org/10.1177/14759217221091907

Roberts, C., Avendaño-Valencia, L.D., García Cava, D. (Under review). Robust Mitigation of EOVs Using Multivariate Nonlinear Regression within a Vibration-Based SHM Methodology. In: Mechanical Systems and Signal Processing. Elsevier. Available at SSRN: https://ssrn.com/abstract=4387099

Book chapters:

García Cava, D., Avendaño-Valencia, L.D., Movsessian, A., **Roberts, C.**, Tcherniak, D. (2022). On Explicit and Implicit Procedures to Mitigate Environmental and Operational Variabilities in Data-Driven Structural Health Monitoring. In: Cury, A., Ribeiro, D., Ubertini, F., Todd, M.D. (eds) Structural Health Monitoring Based on Data Science Techniques. Structural Integrity, vol 21. Springer, Cham. https://doi.org/10.1007/978-3-030-81716-9_15

Conference papers:

Roberts, C., Cava, D.G., Avendaño-Valencia, L.D. (2021). Understanding the Influence of Environmental and Operational Variability on Wind Turbine Blade Monitoring. In: Rizzo, P., Milazzo, A. (eds) European Workshop on Structural Health Monitoring. EWSHM 2020. Lecture Notes in Civil Engineering, vol 127. Springer, Cham. Available at: `https://doi.org/10.1007/978-3-030-64594-6_12`

Roberts, C., Garcia, D., Tcherniak, D. (2020). A Comparative Study on Data Manipulation in PCA-Based Structural Health Monitoring Systems for Removing Environmental and Operational Variations. In: Wahab, M. (eds) Proceedings of the 13th International Conference on Damage Assessment of Structures. Lecture Notes in Mechanical Engineering. Springer, Singapore. Available at: `https://doi.org/10.1007/978-981-13-8331-1_13`

Roberts, C., Isbister, S., Murphy, C., Nisbet, C., Sweeney, P., Tcherniak, D., García Cava, D. (2018). Strain estimation using modal expansion approach via virtual sensing for structural asset management. In: 1st International Conference on Structural Integrity for offshore energy industry. Available at: `https://strathprints.strath.ac.uk/65677/`

Contents

List of Figures

List of Tables

Nomenclature

α	A damage sensitive feature
$\bar{\boldsymbol{\beta}}$	Mean of the baseline observations
$\boldsymbol{\alpha}$	Measured damage sensitive feature
$\boldsymbol{\xi}$	Vector of environmental and operational parameters
$\breve{\boldsymbol{\alpha}}$	Combined measured and regression corrected damage sensitive feature
γ	Critical F-statistic
$\hat{\boldsymbol{\alpha}}$	Estimated damage sensitive feature
$\hat{\boldsymbol{\xi}}$	Vector of environmental and operational parameters, excluding one entry
$\hat{\mathbf{W}}$	Estimated coefficient matrix
Λ	Regularisation parameter
$\ln \mathcal{L}$	Log likelihood
$\hat{\boldsymbol{\Sigma}}_{\mathbf{u}}$	Innovations covariance
$\boldsymbol{\Sigma}_{\boldsymbol{\beta}}$	Covariance of the baseline model
$\mathbf{A}$	Collection of damage sensitive features
$\mathbf{C}$	Covariance
$\mathbf{D}$	Diagonal matrix of eigenvalues

$\mathbf{f}(\xi)$	Univariate functional representation
$\mathbf{f}(\boldsymbol{\xi})$	Multivariate functional representation
$\mathbf{F}(\mathbf{X})$	Collection of multivariate functional representations
$\mathbf{g}(\boldsymbol{\xi})$	Nonlinear representation of $\boldsymbol{\xi}$
$\mathbf{S}$	Diagonal matrix containing singular values
$\mathbf{T}$	Principal component analysis transformed data
$\mathbf{U}$	Principal component analysis transformation matrix
$\mathbf{u}$	Innovations matrix
$\mathbf{V}$	Unitary matrix
$\mathbf{W}$	Regression coefficient matrix
$\mathbf{X}$	Standardised extracted information
μ	Threshold for damage
$\otimes$	Kronecker product
$\overline{I}$	Average mutual information
ρ^2	Squared Pearson correlation coefficient
σ	Innovations
σ^2	Variance
Σ_ϵ	Diagonal matrix containing variances
Σ_λ	Diagonal matrix containing eigenvalues
Σ_{tot}	Diagonal matrix containing eigenvalues and variances

$\text{Var}(\hat{\mathbf{W}})$	Variance-covariance
$\tilde{\boldsymbol{\alpha}}$	Regression corrected damage sensitive feature
$\tilde{\mathbf{T}}$	Reduced form of principal component analysis transformed matrix
$\tilde{\mathbf{U}}$	Reduced form of principal component analysis transformation matrix
ξ	An environmental and operational parameter
$d...\Delta$	Damage group
E	Cross correlation
F	F-statistic
$j...J$	Sensor number
$k...K$	Number of k-fold
$l...L$	Environmental and operational parameter number
MSE_{LOO}	Leave-one-out cross validation error
N	Number of observations
$n...N$	Observation number
N_T	Number of training observations
P	Probability density
p_2	Number of parameters in the second model
$q...Q$	Length of damage sensitive feature prior to the application of principal component analysis
$r...R$	Damage sensitive feature number
S	Sensitivity

T	Temperature
Y	Modulus of elasticity
y_0	Modulus of elasticity at 0^oC
y_1	Rate of change of modulus of elasticity
$z...Z$	Order of regression model

List of Abbreviations

ANN Artificial neural network

AUC Area underneath ROC curve

CNN Convolutional neural network

DSF Damage sensitive feature

EOP Environmental and operational parameter

EOV Environmental and operational variation

FEM Finite element model

FT Fourier transform

FTBF Frequency transformation based feature

GPR Gaussian process regression

IQR Interquartile range

LOOCV Leave-one-out cross validation

ML Machine learning

MSD Mahalanobis squared distance

NIQR Normalised interquartile range

OMA Operational modal analysis

PC Principal component

PCA Principal component analysis

PCC Pearson Correlation Coefficient

ROC Receiver operating characteristic

RSS Residual sum of squares

SCADA Supervisory control and data acquisition

SHM Structural health monitoring

SSI Stochastic subspace identification

STD Standard deviation

SVM Support vector machine

UFR Univariate functional representation

VSHM Vibration-based structural health monitoring

1 | Introduction

In this chapter, the background to the work in thesis will be laid out. The research motivation will introduce the importance of wind power and the increased targets outlined for the future of the technology. The problem that will be addressed in this work is clearly presented in the problem statement, with the specific aims of the work stated in the objectives. Finally, the contribution to knowledge of the work is detailed.

1.1 Research motivation

As the severity of the impact of global warming and climate change continue to worsen, action is required to prevent the Earth reaching a temperature at which irreversible damage will be done. The likelihood of extreme climate events is increasing along with significant sea level rises, events that will see devastating effects on both human communities and the ecosystems that we rely upon [1]. The urgency of the action needed cannot be understated, a fact that has been highlighted for some time [2]. Ultimately, emphasis must be put on technologies that move away from traditional fossil fuel sources and on to greener, renewable sources of energy.

A large step forward in recognising the importance of reducing global emissions came in 2015 with the Paris Agreement [3]. The Paris Agreement is a legally binding treaty that was adopted by 196 countries. Although one country has since left the agreement [4], it still remains the cornerstone of limiting climate change. In the treaty, a limit of a 1.5^{o}C rise in atmospheric temperature by 2025, compared to pre-industrial levels, was set to attempt to limit the impact of global warming [5]. A comprehensive report on the steps that must be taken to mitigate the effects has been published by The Intergovernmental Panel on Climate Change [6].

One alternative energy source that has been widely exploited is wind power. Whilst wind power has been harnessed for a variety of purposes over 5000 years [7], it is now predominantly used for converting kinetic energy into electrical energy. Some European countries (such as Scotland, Denmark and Germany) have installed a large number of wind turbines in order to offset their carbon emissions. For instance, Scotland has almost tripled its output from renewable sources in the last 10 years, of which the majority is wind power [8]. This meant that Scotland only narrowly missed out on its target of generating 100% of their electricity from renewable sources in 2020 [9].

In 2022, four European countries came together to sign the Esbjerg Declaration, in which they pledged to increase their combined offshore wind output in the North Sea to 150GW [10]. To achieve this, two options are available. The first would be to build a large number of turbines. The second, and more attractive option, would be to build fewer turbines, but ones with a much larger output. The downside of this second approach, however, is that the construction and operation of the wind turbines increases in cost and complexity.

Another significant and frequent issue that arises in the operation of wind turbines is the length of time in which they can be operated [11]. In a large number of cases, wind turbines are given a set operational period and decommissioned once this has been reached. For example, wind turbine blades are typically given a lifespan of 20 years [12]. However, it is quite probable that the turbine itself would be perfectly safe and capable of operating for many more years [13]. The largest barrier to overcoming this issue is gaining a reliable understanding of the condition of the structure throughout its lifetime.

Therefore, what is desperately needed is the development of robust monitoring systems that are able to provide support in the decision making process. A monitoring system capable of doing so would provide vital information on the immediate condition of the structure, as well as its historical loads. Real-time condition monitoring and extending the useful life of the wind turbine would increase its efficiency in terms of both cost and production, further enhancing its desirability as an alternative to fossil fuels.

1.2 Problem statement

As wind turbines continue to grow in size [14], the monitoring of their structural condition becomes more and more complex, especially in the case of offshore and remote structures. The current industry standard for inspection of wind turbine blades is done through visual inspection methods, such as the physical inspection by an engineer or through images captured using a drone or similar

devices [15]. These methods are dangerous, expensive and sparse [16]. This problem, therefore, requires a solution capable of working online, in real-time and in remote locations [17].

An alternative method that has been proposed for the monitoring of wind turbine blades is *Vibration-Based Structural Health Monitoring* (VSHM). VSHM systems are implemented in order to evaluate the present condition of the structure [18]. They remove the need to physically visit the structure to carry out the inspection. However, the design of the VSHM system is critical to its successful function [19]. The extracted vibration features must be repeatable, in the sense that they are similar for the undamaged condition, but still contain information that is sensitive to damage. A VSHM system that cannot differentiate between undamaged and damaged observations or cannot confirm a future observation is undamaged are equally inadequate. Therefore, a crucial aspect of robust VSHM is creating vibration features that contain pertinent information for aiding in the decision making process.

An additional benefit of VSHM is that the system is implemented over the lifetime of the structure. By tracking the vibrations over the operational period, a more accurate estimation of the loads that the structure has experienced can be calculated. By comparing the experienced loads to the design assumptions, the operational lifetime of the structure can be extended [20]. If the loads are below the design assumptions, the structure can be safely operated beyond its assumed 20 year lifespan [13]. Likewise, preventative maintenance can be performed if the experienced loads exceed the design assumptions.

However, one major problem that has plagued VSHM is the presence of environmental and operational variations. For example, on its own, temperature has been shown to have more of an effect on the dynamics of a structure than instances of damage [21]. Therefore, methods that are to be implemented must

be capable of removing any influence arising from the presence of varying conditions without discarding the potential impact of the damage on the vibration responses [22].

The effect of the varying environmental and operational conditions leads to convolution within the VSHM system, making damage detection more difficult by masking the effects of the damage itself [23, 24]. Furthermore, decoupling the effects of varying conditions from the effects of damage is extremely difficult since they manifest in the same way within the VSHM system. The problem is further worsened in the case of offshore structures, where the conditions it experiences are much harsher [25]. By accounting for, or purging, the aforementioned effects, a more robust and reliable damage detection system can be implemented.

A variety of methods have been implemented to mitigate the effects of varying conditions. These include: principal component analysis [26, 27, 28], cointegration [29, 30, 31] and various types of neural networks [32, 33, 34], amongst others. However, these methods often lack the interpretability required to make informed decisions. Furthermore, some of the methods are based on linear models that do not represent real conditions very accurately. Ultimately, an interpretable and nonlinear method could advance the maintenance of wind turbines, making them a more desirable choice for green energy.

In this thesis, a methodology based around multivariate nonlinear regression is applied to correct for the effects of the varying conditions within the vibration response. Furthermore, a number of other statistical methods are applied to better understand the data and to increase the robustness and reliability of the overall methodology. The methodology is tested on data obtained from an operational wind turbine in order to demonstrate its benefits. Additionally, it is important to understand the limitations of such a method to gain the most accurate evaluation.

1.3 Aims and objectives

Based on the information contained within the problem statement, and for the reasons explored in the research motivation, the main aim of this thesis can be summarised as:

To design a robust, interpretable and automatic data-driven vibration-based structural health monitoring system capable of mitigating the effects of varying environmental and operational conditions without discarding the influence of damage.

In order to achieve this aim, the following objectives (Obj) have been defined:

Obj.1a. Demonstrate the ability of a multivariate nonlinear regression method to model the relationships between vibration data and environmental and operational parameters within a VSHM framework for wind turbine blades. (Chapter 3)

Obj.1b. Compare the performance of the multivariate nonlinear regression method to a well-established implicit framework, such as principal component analysis, in order to understand the benefits and downsides of each. (Chapter 3 and Chapter 5)

Obj.2a. Design a robust optimisation procedure for the design of regression models by addressing practical considerations in the application of an interpretable vibration-based structural health monitoring system on a real structure. (Chapter 4)

Obj.2b. Establish a framework for creating a more robust baseline from training data by considering the value of regression and by determining the true nature of the training covariance. (Chapter 4)

Obj.3. Establish damage sensitive features that capture a broad range of frequency content of the vibrational response of a wind turbine blade and purge the unwanted effects of environmental and operational conditions. (Chapter 5)

Obj.4. Explore the application of vibration-based structural health monitoring on operational structures to identify the need for crucial design elements. (Chapter 6)

1.4 Contribution to knowledge

Working towards addressing the objectives and main aim, the contribution to knowledge presented within this thesis is based on addressing the more intricate details of the design of the methodology for removing the influence of environmental and operational variations in a vibration-based structural health monitoring system. Consequently, a more robust and reliable system can be designed, one which is more likely to see implementation on real structures. Furthermore, a nonlinear forward stepwise regression procedure is implemented which has not been seen before in the context of vibration-based structural health monitoring.

In order to support new developments in the field of vibration-based structural health monitoring, this thesis makes the following contributions to knowledge (CtK):

CtK.1. Developed the understanding of the cause-effect relationship between environmental and operational parameters and damage sensitive features.

CtK.1a. Implemented a sensitivity study to determine which parameters are most influential in VSHM for wind turbine blades. (Chapter 4)

CtK.1b. Demonstrated the effect of using non-influential parameters within regression modelling. (Chapter 3 and Chapter 5)

CtK.1c. Included a method for the automatic discarding of correlated and collinear variables that negatively affect regression models. (Chapter 4)

CtK.2. Created a holistic method for automatic optimisation of regression models.

Ctk.2a. A forward stepwise regression was developed in a nonlinear setting to select the most influential parameters at their preferred order. (Chapter 4)

Ctk.2b. An implementation of an order reduction method to reduce overfitting in order to achieve an appropriate and compact regression basis. (Chapter 4)

CtK.3. Furthered the knowledge in the fundamental principles of designing robust regression within a VSHM framework for wind turbine blades.

Ctk.3a. Implemented a method for automatically determining which damage sensitive features should be regressed and which should not. (Chapter 4)

CtK.3b. Optimised the outlier analysis to reflect the true variability in the training data. (Chapter 4)

2 | Literature Review

This chapter presents an overview of the current literature that is relevant to this thesis. The chapter will begin with a brief history on the application of structural health monitoring, noting the most important progressions. Furthermore, the advantages and disadvantages of the two main types, model-based and data-driven, will be discussed in more detail. Following this, an introduction to the main problem, variations in environmental and operational conditions, faced by structural health monitoring will be presented. A detailed review of state-of-the-art methods aimed at mitigating these conditions will then be given. These methods are split into three main groups: implicit, explicit and black-box methods. Finally, the application of structural health monitoring will be covered in the context of wind turbine blades. This section includes the different failure modes and types of breakage a wind turbine blade experiences, as well as the current and future methods for assessing the structural health of the blade.

2.1 History of structural health monitoring

The term *Structural Health Monitoring* (SHM) is one that began to see use in the 1990s as a way to characterise a variety of different methods for assessing the current damage state of civil structures in order to improve the information available to operators [35]. Monitoring of civil structures existed prior to this, but the advent of computing technologies has increased the quantity and quality of information that can be gathered from structures. As these technologies continue to advance, so too do the potential applications of SHM. With more advanced SHM systems, it will be possible to extend the useful remaining lifetimes of structures as well as detecting and preventing damage in a more reliable and timely fashion.

The primary driver in the advances of SHM was safety. This began in such industries as oil and gas, nuclear and aircraft design [36]. Given the potential catastrophic events caused by a disaster in these areas, it is natural for the importance of SHM to have originated from here. In comparison, residential and commercial properties have received far less consideration due to the fact that the proprietors have to address any problems that arise. One method that has been implemented in order to rectify this is to increase building insurance premiums as well as enforcing building standards [37].

Ultimately, SHM systems are advanced algorithms capable of damage identification. Rytter [38] and Farrar [39] defined a hierarchical structure for defining five different stages of the SHM process:

Stage 1. Detection - The first, and arguably the most critical, stage is the initial detection of the presence of damage in the structure.

Stage 2. Localisation - In the second stage, the location of the damage is estimated.

Stage 3. Classification - The classification stage aims to identify the type of damage that is present.

Stage 4. Assessment - In the assessment stage, the severity of the damage is quantified.

Stage 5. Consequences - The final stage aims to determine the safety of the structure following the damage incurred.

In order to achieve all stages of the SHM process, the structures need to be fitted with a number of sensors. The type of sensors required depends on the structure in question, and can range from accelerometers and strain gauges to temperature sensors and anemometers. A cost efficient and reliable SHM system comprising of these sensors can drastically reduce the operational and maintenance costs of a structure [17]. Furthermore, SHM systems can also extend the lifetime of structures through thorough monitoring and maintenance.

The application of SHM systems is not exclusive to new structures. They can also be applied to existing structures to estimate their current operational condition. A number of cases where SHM could be applied were identified in [40] and [41] and summarised by Brownjohn [35]:

Case 1. Structural changes to in-situ structure.

Case 2. Structures subjected to changes due to external works.

Case 3. Structures being demolished.

Case 4. Where degradation and/or long-term movement have affected the structure.

Case 5. As a means to improve the design of similar structures in the future.

Case 6. Structural fatigue assessment.

Case 7. Structures constructed of novel arrangement.

Case 8. Assessment of structures following an earthquake or other natural disaster.

Case 9. Where the maintenance requirements continue to increase.

Case 10. Where performance-based design is being implemented.

Fundamentally, a SHM system continuously monitors data observed from a structure which is subjected to time-dependent variations. The data taken is used to create models, whether physical or parametric, of the so-called normal condition of the structure. Further observations are then compared to the model to assess for the presence of anomalies [42]. In theory, damage in the structure will lead to changes in its properties which can then be detected.

There are two main types of SHM monitoring: model-based methods and data-driven methods. Model-based methods are typically focused around physical or computer generated models, often represented by finite element models. These methods were commonly used in the early stages of SHM and benefited from interpretability, as they are built around known physical relationships. However, when complex structures and dynamics are modelled computationally, they can be extremely time-consuming and expensive to create and operate [43]. On the other hand, data-driven methods are constructed purely on data obtained from the structure. These methods can lack interpretability but can also incorporate physical properties or physical laws in order to alleviate this. Whilst they are often computationally less expensive, they also need to be designed meticulously so that they operate in an appropriate manner [19]. The following sections aim to go into more detail about the two different methods.

2.1.1 Model-based methods

As the name suggests, model-based SHM is based around the creation of models to represent a structure. The majority of these models, certainly in the modern era, are created using a *Finite Element Model* (FEM). Often referred to as a digital twin, an updated FEM behaves as closely as possible to the real structure. The method that is used for updating the FEM is know as *Operational Modal Analysis* (OMA). OMA continuously monitors the fundamental modal parameters of the structure to ensure that the digital replica matches what is happening in reality [44]. The difficulty that comes with the continuous monitoring of modal parameters is that they are constantly changing due to changes in operational and environmental conditions. Nevertheless, once the relationships are understood, the FEM can be used to test "what-if" scenarios, such as extreme weather conditions [45].

The concept of being able to test unknown scenarios is one of the main benefits of model-based SHM. This can be especially useful in cases where there is not a large amount of training observations available. As long as there is sufficient information to perform OMA, the FEM can be used to generate new observations. A further advantage of this is that damage can be simulated in the model and, thus, prior information on what damage responses might look like can be obtained [46]. The same goes for simulating different environmental conditions. The combination of these aspects allows for a robust baseline to be created. However, if there is insufficient data on the material properties of the structure, such as damping and elastic modulus, the correlation between the FEM and the real structure can decrease, leading to inaccurate evaluations of the structure's health [47].

Given the number of processes that need to occur simultaneously for model-based SHM, computational costs can be huge. Consequently, the computational speed must be balanced with the accuracy of the FEM model [48]. This often

leads to meshes that are more coarse and, thus, less accurate. Alternatively, the complexity of the model of the system can be reduced, or replaced with a surrogate, to ease the computational cost [49]. Whilst the computational power will remain an issue, the advancement of technology is constantly bringing in more and more powerful computers that will be able to perform the same tasks faster.

However, not all model-based SHM methods require expensive and time-consuming FEMs. One such method uses virtual distortion to update a numerical model [50]. The virtual distortion method is capable of tracking stiffness, mass and damping. When the values no longer match those of the numerical model, damage is detected. Notably, this was only proven on a numerical simulation.

Data aggregation between sensors using smart sensor networks can substantially reduce the amount of data communication [51]. The smart sensors themselves contain microprocessors which can carry out some of the preemptive data processing, reducing the amount communicated to the central system. This reduction in information can be used in collaboration with numerical models or even reduce the computational costs of FEMs.

Like all methods, model-based SHM has many advantages but also disadvantages. The main benefit of model-based SHM is that once the model has been updated to behave as closely as possible to the real structure, more data can be created to evaluate situations that the training data has not experienced, this includes both instances of damage and unexpected environmental conditions. The second benefit is that the models are mostly interpretable and give outputs in terms of physical units, in comparison to feature units [48]. The major disadvantage of most model-based SHM methods is that they are computationally expensive, as well as being time-consuming to establish and operate. However, as computing technologies continue to advance, this issue might naturally be negated.

2.1.2 Data-driven methods

The main difference between the data-driven and model-based methods is that the data-driven methods do not require complex physics-based models. Instead, data-driven SHM methods rely only on data obtained from the structure. Whilst model-based SHM is almost always confined to updating numerical models or FEMs, data-driven approaches vary in the types of sensors and methods that are employed. Therefore, the versatility that they offer has made them the more attractive option [52]. Another aspect that has aided in propelling data-driven methods forward has been the advancement of technology. New technology has allowed for increased data collection, as well as the ability to apply more complex analysis techniques [53].

Whilst data-driven approaches rely on data measured from a structure, they still require some form of baseline model to compare against. However, the baseline model in this case is based on numerical or analytical representations of the structural data [54]. The baseline model is used as a reference from which to compare any future observations. Therefore, the baseline is only made up of observations that were recorded in the early stages of the monitoring campaign [55] . If the future observations deviate from the baseline, this is often an indication of the presence of damage in the system. In an ideal situation, information would be available in advance about the damage, though, this is seldom the case. For this particular case, supervised learning can be employed to distinguish more easily between undamaged and damaged observations. In the majority of cases, unsupervised learning is used since information on damage is rarely available [56].

One of the main disadvantages of data-driven approaches is often a lack of interpretability. For example, once the *Damage Sensitive Features* (DSFs) have been extracted, they often lose their spatial correlation and, thus, it becomes difficult to locate damage [57]. Furthermore, the DSFs themselves can also

be void of any physical meaning, making explaining trends very problematic. However, with the advent of physics-informed machine learning, some of the interpretability can be reclaimed. Through introducing constraints to the data-driven approaches, physical assumptions and known physical relationships can be incorporated within the methods [58].

Data-driven approaches have many advantages. They are easier to implement and operate, they do not require computationally expensive and complex physics-based models and they are able to work with noisy data, which model-based methods are unable to do [53]. However, the data-driven approaches often lack in interpretability which makes them less likely to be implemented. Some of the interpretability issue can be overcome through the implementation of regression modelling or physics-informed SHM. In reality, the most appropriate method for representing a structure might come through a combination of both model-based and data-driven approaches.

2.2 Challenges associated with environmental and operational variations

Civil structures, such as bridges, dams, buildings and energy infrastructure, are most often exposed to *Environmental and Operational Variations* (EOVs). The EOVs will affect the way the structure behaves and, therefore, the data taken from the measurement sensors. Consequently, different responses will be observed for the same structural condition. This can lead to problems when determining the current structural state.

It has been established for many years that the behaviour of a structure is highly influenced by changing temperatures [59]. The changing temperature affects the stiffness of the structure and, thus, its natural frequencies and vibrational characteristics. Temperature alone can have a greater effect on the dynamic responses than damage itself [21]. This is because the global system is affected by the changing temperature. However, where perhaps only minor

damage has occurred, this only changes the vibrational properties at a local level. As such, differentiating effects from temperature and from damage can be extremely difficult. It could be detrimental to the integrity of a structure if a temperature effect has been assumed when in reality the structure is damaged.

In addition to the changes to the stiffness of a structure, the temperature can also affect the boundary conditions. Whilst the changing boundary conditions affect the global vibrational behaviours, the effect can be different due to varying materials or, in the case of large structures, a temperature gradient [23]. In one work [60], the authors found that the changes in eigenfrequencies was an order of magnitude higher for the changing temperatures in comparison to the presence of damage. In two other works, one found a 5% variation in the eigenfrequencies within a day [61] and the other 10% across a full years monitoring [62]. Therefore, the effect of temperature variation cannot be ignored when creating SHM systems, given the magnitude of the effect.

A further environmental element that can affect a structure is the wind. The wind loading that a structure experiences is caused by two main factors; mean wind speed and turbulence intensity [63]. The work by Hu et al., highlights the importance of properly modelling the wind load across multiple wind turbines given that the wind loading at different locations result in different effects. Another work [64] showed the effect on fatigue life of individual wind turbine blades. Here, it was found that the wind load has a large influence. Furthermore, the authors demonstrated that neglecting shear and transverse stresses would lead to overestimates of remaining life. Altogether, environmental variations can lead to substantial changes in the structural behaviour, variations that can be sufficient to mask the effect of damage.

In addition to the above environmental effects, operating conditions can also have a significant impact on a SHM system. The loading of a structure can cause big changes in the vibrational responses, especially in bridges where traffic loads constantly vary. If a limited amount of data is available from a short-term

monitoring campaign, this can cause major issues in the future predictability of the structural condition [65]. A separate study [66] investigated the effects of extreme loading on a bridge. It found that the design of the bridge was conservative and that the analysis could be used for the better design of similar bridges in the future.

Another operating variant that can affect the SHM system is rotational speed, a prominent aspect in wind turbines. The rotational speed of the turbines is constantly changing with wind fluctuations. This leads to non-stationary behaviour which, again, affects the dynamic behaviours [67]. One of the behaviours that has been studied in more detail is the aerodynamic damping which varies with rotational speed, with additional effects around resonance [68]. A separate work [69] found that the rotational speed had the second largest influence, alongside temperature. Ultimately, the varying rotational speeds can lead to a significant change in the structural responses [70].

To summarise, EOVs can have a significant impact on the damage detection capabilities of a SHM system. Whether it is changing the stiffness or boundary conditions of the structure, the EOVs lead to changes in structural behaviours which, in turn, lead to many different structural responses for the same condition. In a similar manner, damage also affects structural behaviours. Thus, the EOVs can effectively hide the indicators of damage, which is extremely detrimental to SHM. Consequently, there will potentially be an increase in the number of false alarms, as well as undetected damage. The result of this is that the systems cannot be considered robust or reliable unless action is taken to mitigate the effects of EOVs.

2.3 Addressing environmental and operational variations

As highlighted in the previous section, the issues caused by EOVs can have a significant impact on the separation of damaged and undamaged observations.

Efforts should be made to try and mitigate these effects, where possible by the means of data normalisation. The remainder of this section explores a number of different methods for addressing the issue. The data normalisation methods are separated into three main groups; implicit, explicit and black-box methods. Black box methods can be either implicit or explicit, but fundamentally lack interpretability. A graphical representation of the implicit and explicit methods of normalisation can be found in Fig. 2.1.

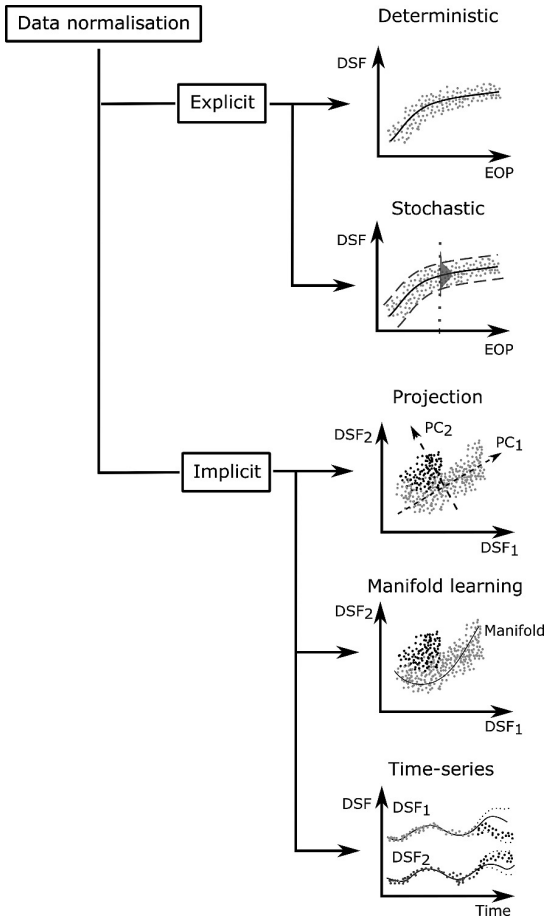

Figure 2.1: Graphical representation of different data normalisation methods in VSHM [71].

2.3.1 Implicit methods

In an implicit method, no information about the varying conditions is given to the SHM system. Instead, the mitigation of any variations in the data are

assumed to be a result of the EOVs. Since the varying conditions are the most likely cause of the most significant variations within the system, the assumption is very plausible. Many different methods have been applied to construct an SHM system in an implicit manner, ranging from simple linear transformations [72] all the way up to complex machine learning approaches, such as artificial neural networks [73].

One of the benefits of an implicit method is that less information is required from the in-situ monitoring and data acquisition system [74]. This benefit can become three-fold. Firstly, the SHM system can be less complex with fewer inputs. Secondly, the measurements taken from the environmental sensors will contain some inaccuracies and, therefore, the total uncertainty in the system can be reduced by not including the data from the environmental sensors [75]. Finally, fewer pieces of expensive sensing equipment is needed for the measurements and it can bypass the requirement for complex programs to estimate conditions between adjacent turbines within a wind farm, a problem associated with wind effects [76].

There are also a number of disadvantages to an implicit method, the first of which is that often a number of assumptions have to be made. For example, DSFs are often discarded because they are assumed to be affected by EOVs and, therefore, detrimental to the SHM system. Assumptions that turn out to be incorrect can have negative consequences for a system [77], especially in cases where information about damage can be unknowingly discarded. A further disadvantage is that the interpretability of a model might decrease. For example, when a number of outliers begin to appear, it can be difficult to justify the reason for their presence when only information about the vibrations is available [71]. It can be possible to increase the interpretability through the application of additional explicit methods [78]. However, this leaves the possibility of just using an explicit method in the first instance. In the following sections, two

of the most commonly applied implicit methods, in the context of SHM, are discussed in detail.

2.3.1.1 Principal component analysis

Principal Component Analysis (PCA) has been a popular choice of linear transformation, projection, method used for SHM. It is a diverse method which has been applied across a number of scientific fields including facial recognition [79] and monitoring land coverage [80]. The aim of PCA is to transform an often complex data set into a lower dimension set that describes the most important trends in the data [27].

The purpose for the implementation of PCA in SHM has varied depending on the specific application. A common use for PCA is for noise reduction of the raw vibration responses. In the work by Tang [81], PCA is used to de-noise the signal as well as for extracting DSFs. In the work, it was found that the ability of the system to detect damage can be improved with the reduction of noise, as well as increasing the number of baseline data sets. Similarly, a study on facial recognition found that by selecting specific principal components, an increase in the classification accuracy could be achieved [82].

The use of PCA for DSF extraction is common in SHM since data sets often have very high dimension. The aptly named *curse of dimensionality* can often cause problems with sampling and optimisation when analysing large data sets [83]. PCA has been applied along with the wavelet transform to highlight the most important ridges [26]. In this case, the method provided results that were more clear, as well as being more accurate. Furthermore, the work by Tibaduiza et al. [84] uses PCA to create baseline DSFs as well as for projecting data from new experiments for damage detection.

PCA is often used in combination with other methods as an initial step for noise or dimensionality reduction. In the work by Lederman et al. [85], PCA was first used to reduce the dimension of the signals. Kernel regression was then

used to try and relate the condition of the bridge to the obtained signals. In two recent studies [86, 87], the PCA-reduced dimension DSFs were then used as inputs for a Gaussian process regression and multivariate nonlinear regression respectively. In both cases, the length of the original DSFs would have made the regression models difficult to implement since a different model had to be created for each DSF.

The implementation of PCA can also be used to mitigate the effects of varying environmental and operational conditions [88]. In the work by Qadri et al. [89], an explanation is given which suggests that the lower principal components correspond to the information most sensitive to varying conditions, the moderate principal components link with information about the structure that is insensitive to the varying conditions and the higher components which consist mainly of noise. To mitigate the effects of the varying conditions, the principal components corresponding to the insensitive information is used for the damage detection method. In the work by Kumar et al. [90], a similar approach is taken where only mid-range principal components are considered. Likewise, Worden et al. [91] projected the data on to the ten smallest minor components. However, there is a limitation to this approach: by discarding information from higher variance components, potential information on damage is lost.

2.3.1.2 Application of principal component analysis for vibration-based structural health monitoring

Although the primary purpose of PCA is dimensionality reduction, it has had varied applications in SHM. A number of previous works have used it for its original purpose. Zang and Imregun [92] used PCA to reduce the dimension of frequency response data to avoid a drawback associated with artificial neural networks. Mujica et al. [93] also used PCA for dimension reduction whilst developing a multivariate statistics approach for detecting and localising damage in an aircraft wing.

Another use for PCA in VSHM was to capture and remove the influence of environmental and operational variations by removing the eigenvectors thought to be associated with these changes [88, 94]. A summary of this method is shown in Fig. 2.2. PCA can also be used as a means to extract structural DSFs [81, 87] as well as being used to differentiate between undamaged and damaged structures [95, 96]. In this thesis, PCA is used for two purposes. It is used as a combination of dimensionality reduction with DSF extraction to create the DSFs that are used on the case study of the operational wind turbine blade.

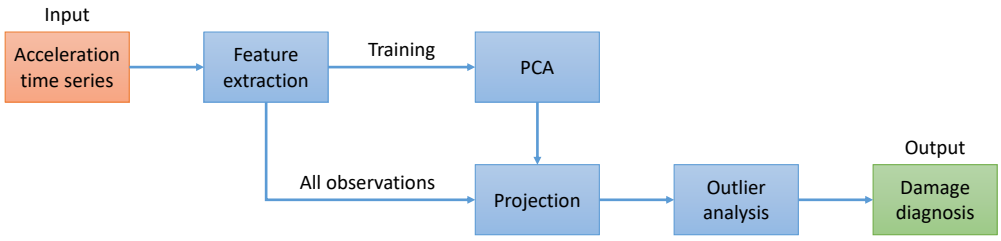

Figure 2.2: Schematic representation of the overall implicit method for VSHM.

2.3.1.3 Cointegration

The cointegration approach to SHM has its origins in economics and belongs to the time-series arm of Fig. 2.1. It was first introduced in the context of SHM in 2011 by Cross et al. [97], where it was demonstrated to work on both an example model, as well as a real example. In cointegration, if the linear combination of two non-stationary signals are stationary, then the signals can be said to be cointegrated. The residual of this process can then be used as a DSF for damage detection. In another article, Cross and Worden [29] go into more detail about why cointegration can be implemented in SHM, justifying why it can be applied despite the philosophical differences in the understanding of non-stationarity in economics.

The environmental and operational variations often cause nonlinear effects in measured variables. Since the cointegration procedure is based on a linear

approach, adaptions to the method must be made. Shi et al. [31] combined cointegration with Gaussian process regression for the application on the Z24 bridge in Switzerland. While the method was able to detect damage to a reasonable extent, the authors also recognised the limitations of the method where the Gaussian process may fail to model accurately under regime changes. In order to counter this, Shi et al. [98] then implemented a regime switching cointegration procedure. This method created multiple cointegration models to overcome the previous problem. The outcome of this was that the damage detection capabilities were enhanced over the previous work.

Another alternative approach was offered, again, by Shi et al. [99]. In this work, a Trigonometric, Box-Cox ARMA Trend, Seasonal model is applied to the data prior to the application of cointegration. The method was applied to an experimental foot bridge where the model was able to extract the daily cycles, accounting for the majority heteroscedasticity within the data. The method provided promising results with the cointegration residual showing high sensitivity to the damage observations.

In recent years, cointegration has also been applied in the context of SHM for wind turbine blades. Qadri et al. [30] applied a robust cointegration approach, based on the same Johansen cointegration procedure [100] used by Cross et al. and Shi et al., on data taken from an operational Vestas V27 wind turbine. In this example, a crack was introduced to the trailing edge of the blade. By using an outlier analysis based on the Q-statistic, Qadri et al. were able to compare the performance of cointegration compared to a PCA-based approach. It was found that while the PCA-based approach was able to detect damage to an extent, the cointegration procedure provided far superior detection results. However, a limitation of this work is that method was only tested on a very small number of observations and a narrow range of EOVs.

2.3.2 Explicit methods

In an explicit method, information on the varying conditions is made available to the SHM system. *Environmental and operational parameters* (EOPs) can be used to model the variations in the measurements. In this sense, the variations in the data can be directly attributed to the EOPs. Therefore, the majority of explicit methods are based on some type of regression model. The regression models themselves vary in complexity depending on their application. These range from very basic, deterministic linear regression models [101] all the way up to complex, stochastic Gaussian process regression models [86], see Fig. 2.1.

As mentioned, one of the main benefits of explicit methods is that there is a functional relationship between the EOPs and the measured response of the structure [71]. This type of relationship is often referred to as cause-effect [102]. Since the relationship is directly modelled, it can often be easier to explain the origin of outliers in the data [103]. Additionally, it is also possible to fit empirical models into the SHM system. With all these aspects combined, explicit models are often more interpretable than their implicit counterparts.

However, there are many issues that must addressed in the application of explicit procedures. Firstly, the measured EOPs cannot always explain the variabilities in the data [71]. The measured responses themselves will contain uncertainties and if no effort is made to correct for these, it can be detrimental to the predictability of the designed regression models [104]. Furthermore, the selection of the variables used within the model is not trivial. A poor selection of variables may lead to overfitting, characterised by unreliable predictions and decision making [105]. Addressing these problems to create a robust SHM method forms the inspiration behind the work in this thesis.

2.3.2.1 Linear regression

Linear regression is the most basic form of regression that can be implemented. In this method, it is assumed that the variations in the EOPs have a linear

effect on the response variable. This type of model was implemented in the early stages of SHM. Sohn et al. [24], used linear regression models to predict the fundamental frequencies of the Alamosa Canyon Bridge in New Mexico. It was found in this work that by creating models using two different temperature sensors, it was possible to accurately predict the fundamental frequency of the bridge from previous measurements. The author also noted that the method was very application specific and could not be straightforwardly applied to a different data set.

However, in a one year long monitoring campaign of the Z24 bridge in Switzerland, Peeters and De Roeck [23] found that the relationship between the temperature and the natural frequencies was either nonlinear or piecewise linear. In this instance, the authors implemented a bilinear regression model. They found that this model outperformed a "static" linear regression model. By studying the natural frequencies, it was possible to detect damage by checking if the prediction for the frequencies was within the confidence intervals established during the modelling [59]. Whilst the bilinear model performed well at predicting the natural frequencies, it makes more sense to model the effects using a nonlinear model if the data exhibits nonlinear behaviour.

Since the behaviour exhibited in the system is often nonlinear, a sort of middle-of-the-road approach can also be taken. In a work by Dervilis et al. [106], generalised linear regression models were employed to consider nonlinear behaviour in a linear perspective. The primary aim of this work was to address the effect of "inclusive outliers" due to unusual environmental and operational conditions, a problem that had previously arisen in a work by the same authors [77]. Whilst this approach employs linear models, it is still able to accurately model nonlinear behaviour.

A linear model can, however, be the most appropriate regression model. In the work by Schlechtingen and Santos [107], it was found that the relationship between the temperatures in the stator and bearings of a generator in a wind

turbine was highly linear. The linear model was compared to two different neural network implementations. While the linear model was simpler and easier to interpret, it did not perform to the same degree as the neural networks, not being able to detect the onset of damage as early. The linear regression model is still an appropriate choice because of its simplicity and interpretability. The authors also state here that the models are application specific and no general statement about which is most appropriate can be made.

2.3.2.2 Nonlinear regression

As mentioned in the previous section, the effects of varying conditions often manifests as nonlinear effects in the measured responses. In a separate work on the Z24 bridge by Wah et al. [108], nonlinear regression models were fitted to natural frequencies obtained from a bridge. Interestingly, this work would actually be considered pseudo-implicit but has been included in this section since the method is most commonly applied in an explicit manner. By considering the effects as nonlinear, the authors were able to more accurately predict the presence of damage in the bridge. In a similar pseudo-implicit manner, structural properties have been used to estimate cumulative plastic deformation and residual deformation for the purpose of damage detection in tall buildings [109].

Multivariate nonlinear regression has been implemented a number of times to model the vibration response of a wind turbine blade. In the work by Roberts et al. [87], multivariate nonlinear regression was applied to try and determine which EOPs are most influential on the vibration DSFs. As expected, the most influential parameter was the temperature. However, this study was not extensive and only considered three EOPs. In a more recent work by the same authors [103], a larger number of EOPs were considered for modelling. The most important aspect of this work was that the authors began to address the issues associated with the design of regression models. However, the work in this thesis aims to fully focus on these issues.

In a separate work by Qadri et al. [89], the authors went a step further and directly compared three different methods, two implicit and one explicit. The methods used were: PCA, cointegration and a combination of PCA and multivariate nonlinear regression. The work produced some interesting results. Firstly, they demonstrated that PCA DSFs that were regarded as EOV-insensitive contained more information than their EOV-sensitive compatriots. The second method implemented was cointegration, which performed the best being able to discriminate almost perfectly between damaged and undamaged observations, as well as being devoid of any trends. In the final method, the regressed DSFs were able to discriminate well between damaged and undamaged observations, but clear trends remained present in the data. The observed variability could be due to the nature of the models being used. The main novelty of this thesis comes as a result of this problem, investigating the design and robustness of regression models.

2.3.2.3 Application of nonlinear regression for VSHM

The main application of multivariate nonlinear regression within VSHM is for the mitigation of EOVs. In most cases, the dependent variables are the DSFs obtained from the structure. The independent variables are the measured environmental and operational parameters such as: temperature, wind speed, wind direction and information about the excitation of the structure [77, 87, 110]. The overall explicit process is summarised in Fig. 2.3.

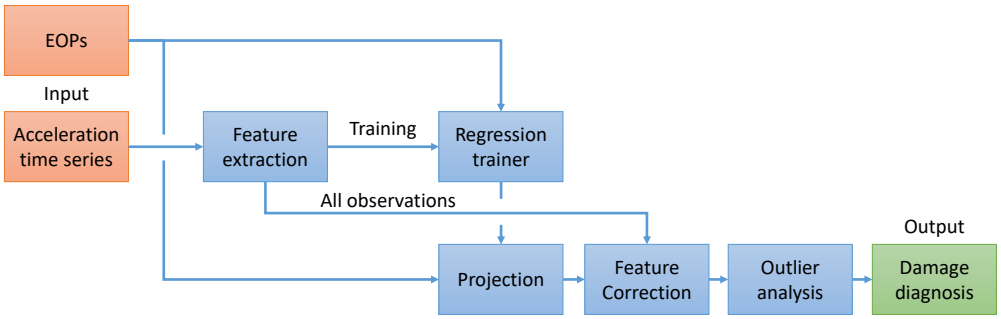

Figure 2.3: Schematic representation of the overall explicit method for VSHM.

In addition to traditional regression schemes, there have been more novel approaches, applied where the natural frequencies were used as both dependent and independent variables [108]. In this study, each natural frequency was modelled considering one other natural frequency. The authors showed that this method provided superior results to one that considered temperature as an independent variable. Although this work has its merits, it is inconclusive in demonstrating an improvement over a traditional multivariate nonlinear regression.

2.3.2.4 Gaussian process regression

Both linear and nonlinear regression are examples of deterministic methods. In contrast, *Gaussian Process Regression* (GPR) is a probabilistic method, where each prediction comes with a corresponding boundary of error [71]. GPR is a very powerful tool in modelling unknown or deeply embedded functions in data by creating distributions across different functions [111]. Furthermore, machine learning methods can be easily incorporated as part as of a GPR method, creating an even more powerful modelling tool [112]. There are many different variations of GPR where different kernels can be used to model the data. A consequence of this is that some Bayesian regression methods can be altered to behave like a GPR, if some assumptions about the kernel are adhered to [113].

GPR is becoming increasingly popular in the application of SHM. It has been implemented in many different structures, such as high-speed rail track slab [114], bridges [115, 116] and wind turbines [117, 118]. In the work by Dervilis et al. [119], GPR is applied to data from the Z24 bridge in Switzerland in combination with manifold learning to explore the SHM data. The purpose of the GPR is to give a more robust training model, given the assumption that benign outliers are present. Whilst this objective is achieved, the optimisation procedure in the design of the hyperparameters in the model is a complex procedure. Rogers et al. recognised this problem and began to address it their work

[120]. The work aimed to determine if more complex optimisation procedures were required in hyperparameter optimisation or whether more basic methods were adequate.

Zhang et al. [121] used GPR as part of a grey-box model for predicting bridge deflections obtained from the Tamar bridge in Plymouth. The grey-box model allowed for additional learning, meaning that it could use information analysed from the prior knowledge to improve the model prediction. It was found that the model extrapolates easier when using a shorter length-scale. This indicates that the model is more heavily influenced by the physical mean function, a preferable quality for grey-box models. Zhang et al. also recognise the difficulties with the optimisation procedure for the hyperparameters. Overall, the work demonstrated the benefits of a grey-box GPR approach in the context of SHM.

In a recent work by Qu et al. [122], GPR was applied to remove the influence of environmental and operational parameters for the purpose of enhancing the detection of scour at the base of an offshore wind turbine tower. By modelling the natural frequencies of the structure based on the wave height using GPR, it was possible to mitigate the variations that were present in the data. A point that can be highlighted from this work is that while GPR is a powerful tool, nothing is done with the uncertainty that accompanies the mean function. This is also true of other works. In this case, it might have been possible to apply a simpler regression model and obtain the same results.

One work that addresses the application of GPR on wind turbine blades, and also the Humber bridge, was produced by Avendaño et al. [102]. This work analysed the identification of modal parameters based on both the short-term and long-term responses. In addition, principal component regression was also used to optimise the selection of model orders. It was found that, whist the RSS/SSS (residual sum of squares/signal sum of squares) error increased, it was possible to match the posterior to the prior more accurately. The benefit

of this is that fewer hyperparameters have to be estimated. The GPR method offered a promising alternative to deterministic methods for modelling complex dynamics under varying environmental and operational conditions. However, a limitation was identified in the definition of the innovations variance which may affect the accuracy of the method, as the vibration response varies under changing power. A further limitation was addressed in the overall context of the application of GPR models, where the range of training conditions capable of producing robust training models was noted. This limitation was put under scrutiny in a further work by the same author [123].

An extremely thorough study based on GPR was also carried out on an operational wind turbine blade by Avendaño et al. [86]. In it, the vibration responses were separated into low and high-frequency groups. The low-frequency group was used to identify the structural dynamics of the blade in which a 30 second period was used. The high-frequency group was used to determine the transmission properties of the blade. The work showed that the high-frequency group yielded superior damage detection as well as discriminating between healthy and damaged at any operational regime. Whilst the work identified temperature, wind speed and turbulence intensity as the most influential parameters affecting the vibration responses, the author also acknowledged that other parameters might emerge as influential over a longer period of study. The author also recognises that whilst the low-frequency group has poorer damage detection qualities, it performs better on the task of identifying the structural dynamics and fatigue loads.

2.3.3 Black-box methods

Machine Learning (ML) methods form a significant portion of black-box methods and have been included in a separate section since they are complex and can be either implicit or explicit in nature, existing in a grey area between the

two. ML is a constantly evolving field, spread across numerous different topics. Due to their inherent lack of interpretability, methods have been applied to overcome this [78]. Interpretability is, and will remain, a talking point in the world of ML.

The application of ML approaches is widespread in the SHM literature. The methods have been applied in a range of different structures, including bridges [124, 125, 126], buildings [127, 128, 129] and dams [130, 131]. The purpose of the ML methods in each case can vary. In a number of studies, ML is applied to aid structural identification, such as estimating natural frequencies, mode shapes and damping ratios. In other works, ML methods are used to mitigate the effects of varying environmental and operational conditions, or to expand training data sets for example.

ML methods have regularly been applied to wind turbines [132, 133, 134]. ML itself is a blanket term and covers a variety of different methods [135]. In the context of wind turbine blades, a number of these of these different methods have been applied. The following is not an exhaustive list of examples, but gives an overview of the most commonly applied ML methods.

2.3.3.1 Artificial neural networks

In one study [32], *Artificial Neural Networks* (ANNs) were applied to model a novelty index based on the DSFs obtained from an operational wind turbine blade. It was found that whilst the damage scenarios were not easily distinguishable from each other, the overall damage detection rate was better compared to a standard novelty index approach. The improvement in detection, especially in the early stage of damage, was attributed to the ability of the ANN to mitigate the effect of varying environmental and operational conditions. A further study replicated this finding, suggesting ANNs are an accurate method for the detection of damage within wind turbine blades [136]. The work found that an ANN

was best at classifying six different delamination scenarios during a laboratory experiment compared to a k-nearest neighbours method.

2.3.3.2 Convolutional neural networks

A ML method which is often implemented within image-based SHM is *Convolutional Neural Networks* (CNNs). Using labelled data, the CNN is able to learn how to classify different types of damage which can occur on wind turbine blades. Yu et al. [34], were able to achieve a damage classification of almost 100% on images captured during a standard visual inspection of a wind turbine blade. These results are especially promising given the method was tested on a real structure and with a very small training sample size. A similar study explores the use of images captured using drones alongside a CNN to classify damage on a real wind turbine blade [137]. This work found a high detection rate of over 90% for multi class classification. Whilst both these examples are applied to images, there is no reason they could not also be applied to VSHM.

2.3.3.3 Support vector machines

Support Vector Machines (SVMs) are another ML method that has been implemented to wind turbine blades, most commonly as a classifier. SVM has been applied both as a linear and nonlinear classifier for detecting the presence of ice on a blade [138]. The nonlinear classifier achieved a minimum accuracy of 95% for the different damage scenarios. However, the method was tested in a laboratory setting, so it is not known if these results could be replicated for a real turbine. A similar approach was later used for damage detection alongside a number of different ML methods [139]. Whilst they also produced accurate results, they were not tested on a real structure.

2.3.3.4 Alternative black-box methods

There are many other ML methods that have been implemented as part of wind turbine blade SHM. K-nearest neighbour classification has assisted in the detection of anomalies such as ice [138] and mud [140], as well as for general damage detection [139]. XGBoost has been used for both damage detection in wind turbine foundations [141] and wind turbine blades [78]. Autoencoders and back-propagation methods have also been used to detect breakages in wind turbine blades [33, 142].

2.3.4 Overfitting models

The more detailed design of regression-based models can often be overlooked when using them within a SHM framework. It is relatively simple to introduce some data to a system and achieve promising results. However, there are a lot of practical issues that must be addressed in the design of the regression-based models. Failure to do so reduces the reliability of decisions, a key component in the robustness of a VSHM system. For example, DSFs contain uncertainties which can be detrimental if no action is taken to reduce the effect of bias [104]. When many inputs are available, it is not straightforward to know which ones to use and even which are actually influential [71]. Furthermore, the selection of the variables used within the model is not trivial. A poor selection of variables may lead to overfitting. Additionally, dependency between inputs can lead to severe problems with instability in parameter estimates, large sampling variances and an inability to decouple the effects of different predictors, which can affect the interpretability of the regression model [143].

The problem of overfitting, characterised by poor generalisation from observed to unseen data [144], has long been an issue in the ML community. In real data sets, there is a finite number of training observations and, as a result, neural networks excessively weight around the training observations, consequently reducing the generalisation ability [145]. One method that is often

applied to address the generalisation problem is pruning. Pruning reduces the complexity of a network by methodically discarding parameters from it [146], creating a lower dimension and less intricate network, but at the cost of a small reduction in accuracy. Alternatively, the dimension of networks can be reduced through the application of weight sharing [147]. The weight sharing approach relies on the bits-back argument that can be achieved through defining a more appropriate prior and an uncertainty limited posterior distribution.

Complexity regularisation can also be embedded within a neural network to prevent overfitting [148]. Additional terms in the form of penalty functions can be added to the optimisation function to reduce the occurrence of large weights or large numbers of weights [145]. While all these methods proactively seek to reduce overfitting to the training data, data sets that contain noisy predictors and responses can still pose serious problems. Additionally, the design of neural networks, as well as other ML approaches, often fundamentally lack interpretability. The consequence of this is that while parameters are being reduced, there is an absence of understanding as to the effect of the particular relationship.

On the other hand, when less-complex traditional regression models are applied, they are less susceptible to the level of overfitting of neural networks. However, this comes at the cost of the accuracy of the prediction of the training observations. Nevertheless, this does not mean that traditional regression models cannot be overfitted. Similar methods to those used in ML must also be applied to traditional regression schemes. For example, methods akin to pruning and complexity regularisation can be used to help identify the most influential parameters and determine which DSFs should be and should not be regressed.

Stepwise regression is often used in the optimisation of traditional regression models. Forward stepwise regression is usually applied for linear models and is a tool that has been in use for many years, recently being applied in the context

of SHM [149]. In each stage of a forward stepwise regression, the variable that best describes the trend in the data is selected until the error no longer decreases. Lasso regression is a backward stepwise regression first introduced by Tibshirani [150], also for the purpose of linear regression. The Lasso is capable of performing subset selection by introducing a penalty function in the least squares estimate [151], identical to the approach used in complexity regularisation.

In both stepwise regression methods, the move to nonlinear is challenging but important given the complex relationships that exist in real applications. Previous works have sought to linearise the formation of the model through a suitable transformation [152]. One such method requires the expansion of each EOP with its corresponding order to form a new input vector. For example, if temperature is considered to have a cubic effect, the input to the model would require temperature, temperature squared and temperature cubed. However, this can become impractical if there are a large number of EOPs, especially so if the inter-parameter relationships are being considered.

In summary, the overfitting of models can have major adverse effects on their predictability if not addressed. There are many methods available in the literature to reduce overfitting through subset selection and the addition of penalty functions to reduce function orders. However, knowing when and where to apply each method is not a straight forward decision. The development of a single all-inclusive method that addresses all the issues associated with overfitting would be of benefit to the wider VSHM community. In this thesis, a framework is developed to achieve this target.

2.4 Application of structural health monitoring to wind energy

The last section of this literature review puts into context the current and future application of SHM in wind energy; specifically, information pertinent to the

monitoring of wind turbine blades. The maintenance and monitoring of wind turbine towers is well-established and implemented in the industry. However, the current industry standard for maintenance of the blades appears archaic in comparison. This is particularly unusual given that the blades are the most expensive component of the overall wind turbine [153]. The damage caused to the blades can have a significant impact on the performance of the wind turbine and, whilst, there is a plethora of research being undertaken to develop more modern methods for monitoring, little has seen implementation on real structures. To better understand the types of damage experienced by wind turbine blades, Fig. 2.4 shows a typical internal construction. The remainder of this section will demonstrate the necessity for monitoring as well as the current, and future, methods for monitoring wind turbine blades.

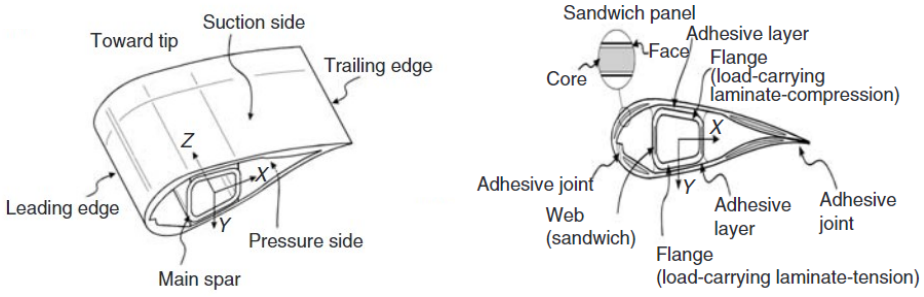

(a) (b)

Figure 2.4: (a) Wind turbine blade aerofoil section with main spar and outer shells (aerodynamic profile). (b) Design details of typical wind turbine blade [154].

2.4.1 Damage mechanisms

Owing to their location in exposed and often harsh environments, wind turbines are impacted by many conditions that can lead to damage in the structure. Such damage is frequently unavoidable and can cause a reduction in the efficiency of energy generation. There follows a brief review of different failure modes that cause damage, followed by the specific types of damage that can occur.

2.4.1.1 Failure modes

A significant failure mode in the operation of wind turbines is leading edge erosion. Due to precipitation and the presence of particulates in the air, serious damage can occur on the leading edge of the blades. Furthermore, accumulation of debris such as insects can also affect the energy output performance of the turbine, especially in cases where the accumulation and erosion has built up in the high speed tip region [155]. Pugh et al. [156] found that raindrop erosion alone can lead to a 4% reduction in the energy production of a blade. Even small losses like this can lead to substantial losses if the damage goes undetected and unrepaired.

Another failure mode that can arise from precipitation is blade icing. The areas in which onshore wind turbines are typically placed are often high-altitude where the climate is colder and more humid. Because of this, the blades are more susceptible to icing [157]. Ice build-up on the blades can change the aerodynamics as well as modal parameters, leading to reduced performance as well as potential accidents. Hochart et al. [158] found that icing could cause a significant reduction in the lift produced by the blade, and as much as 40% at the tip. As a result, the power output is greatly reduced. Due to the weight of the ice, increased load is added to the structure which causes more fatigue [159], shortening the lifespan of the turbine.

Another issue with the open location of turbine installations is that it makes them prone to lightning strikes. The turbine blades themselves are the most likely part to be damaged, making up 75% of all cases in which damage occurs on large turbines [160]. Lightning strikes to unprotected blades can cause a number of issues and are very expensive to repair. The strikes can cause superficial damage to the skin as well as much more serious damage such as shell detachment or complete tip detachment [161]. Furthermore, the lightning can cause significant internal damage too through a process called sideflash [162].

Lightning strike protection is already common but challenges remain on scaling up as the blades continue to increase in size.

Another unavoidable failure mode is fatigue loading due to constantly changing wind speeds. These lead to fluctuating mechanical stresses, which cause the gradual deterioration of mechanical components. If the components are not properly monitored, they will eventually fail [163] and the lifetime of the turbine can be significantly reduced. In addition, it has also been found that turbines that are downstream from other turbines within wind farms experience greater fatigue loads due to the turbulent air produced by their upstream neighbours [164].

Altogether, there are many failure modes that must be considered in the design of wind turbines. In addition to the failure modes that arise as a result of the location of wind turbines, other faults such as sensor failure can occur [165]. Replacing or fixing turbines can be very expensive because of such factors as transport, asset downtime and materials. Therefore, it is important to try and monitor the conditions to avoid unnecessary losses in operation. However, this can be extremely difficult since there are a number of different types of damage that can result from the failure modes.

2.4.1.2 Damage types

The overall failure of a wind turbine can occur as a consequence of many types of damage that arise in the blade skins and the main spar [166]. The seven types of damage that occur have been defined by Debel [166] and have been adopted in other works [167, 168]. The damages are summarised as follows:

Type 1. Adhesive debonding - Growth in damage of adhesive layer between main spar flanges and blade skin.

Type 2. Skin adhesive failure - Growth in damage of adhesive layer between adjoining skin.

Type 3. Sandwich debonding - Growth in damage of interface between sandwich core and face in either skin or main spar web.

Type 4. Delamination due to tension or buckling - Growth in internal damage of skin or spar flanges due to tensional or buckling load.

Type 5. Fibre failure - Failure of fibres in tension or laminate in compression in the skin or main spar.

Type 6. Buckling induced debonding - Debonding between skin and adhesive because of buckling. Type 6. damage is a particular variation of Type 1. damage.

Type 7. Gel-coat failure - Either formation of cracks in the gel-coat layer or debonding between gel-coat layer and skin.

Several of the damage types are associated with the debonding of sections of the wind turbine blade, so it is often considered the most common and important form of damage [167]. Along with the failure modes that lead to instances of damage, incidents during transport and irregularities stemming from the manufacturing process can exacerbate the problems. Cavities in the adhesive layer can propagate into cracks, and once a critical level is reached, debonding will occur. Since the glass fibre composites, that are most commonly used in wind turbine blade construction, are strong in tension, debonding most often happens due to buckling. Consequently, it is especially important to monitor this type of damage in wind turbine blades in order to prevent failures and ensure their safe and effective operation.

2.4.2 Current inspection methods

The current industry standard for assessing wind turbine blades involves visual inspection. These can be relatively quick and inexpensive for onshore wind turbines but the process becomes more complex and dangerous for inspecting offshore wind turbines. In order to inspect the wind turbine blades, the turbine must be stopped [169], further adding to the overall cost of inspection. The three main methods used for inspecting wind turbine blades are: via rope access, images captured with drones and ground-based cameras.

A common practice for inspections is via rope access. Fig. 2.5 shows the scale of the inspection task. A highly skilled workforce is required for such operations, with engineers being suspended high in the air to repair and clean the wind turbine blades. Often, the workers recruited are already proficient abseilers and climbers [170]. Nevertheless, this method is still dangerous, and safety is a massive concern. Wind speeds have to be at a safe level and the rotor has to be braked and locked in place. Despite all precautions being taken, inspectors are still susceptible to issues with eye strain or fatigue [171]. One of the benefits of rope access inspection is that repairs can often be made as and when they are found. However, the inspections can take a significant amount of time to perform.

Inspections carried out by drones and ground-based cameras work on the same principle. Captured images are analysed using algorithms to detect defects [15]. To alleviate some of the problems associated with offshore inspections, such as rough weather and large waves, Kim et al. [172] proposed a camera-based system that is built upon a robot climber for inspecting the blades. Whilst this solution is elegant and fit-for-purpose, it further adds to monitoring expense, especially with the increasing number of turbines being installed. Drone-based inspection can be beneficial as it is relatively inexpensive and can access harder

(a) (b)

Figure 2.5: Wind turbine blade inspection by engineers via rope access (a) from afar and (b) close up [170].

to reach locations. However, operators must still visit each turbine for inspection, and engineers access via rope for any required repairs.

In any case, engineers will still be required to access the structure to perform repairs. Given that the longer the crack, the more expensive it is to repair. Operators must then decide if it is worth the cost of repair meaning it is important for the damage to be identified as soon as possible so that the repairs remains feasible. While the current inspection methods already require the presence of an engineer, it might be too late by the time the inspection comes around. Therefore, an online monitoring method can alert operators in more time to allow for a more timely repair.

The task of maintaining the structures will continue to become more challenging as the wind turbine blades continue to increase in size [14]. Furthermore, visual inspections are limited to detection of external defects [171]. In order to assess for internal damage, more complex and expensive non-destructive testing

methods, such as ultrasonic testing or thermography, must be used. The problems discussed in this section highlight the need for more efficient and detailed inspections that can be carried in real-time [17].

2.4.3 Future monitoring

With the advancements in sensing equipment and technology, it is possible to embed sensing equipment within the wind turbine blades in order to monitor its condition. The sensing equipment is able to provide real-time monitoring of wind turbine blades, including those located in remote areas, such as offshore turbines [173]. There are numerous types of sensor that have already been installed for this purpose, such as: conventional strain gauges [174], fibre optic sensors [175] and accelerometers [176]. While each sensor operates in a different manner, they all aim to capture the dynamics of the wind turbine blade.

The main problem of embedded sensors is that they are difficult to replace if they themselves break. However, there are a number of ways in which the sensor network can be designed in order to avoid such a problem. The first is to select sensors that have design lives in excess of the 20 year lifespan of the wind turbine blade [12]. However, if the purpose of the monitoring is to try and extend the lifetime of the blade, then selecting sensors is difficult. The second option is to design the sensor network with redundancy [177]. In this case, if a sensor were to fail then there are additional sensors that can be used in its place.

The problem does not lie in the implementation of the sensors, but instead with the methods that are used to process the obtained information. The main reason being the problems associated with EOVs, as discussed in Section 2.2. Several of the methods, discussed in Section 2.3, have been shown to overcome these problems, but there has been little uptake within the industry. Once VSHM methods have been shown to be robust and reliable, they will be able

to be implemented. The future of wind turbine blade monitoring is heading towards VSHM, but more research is required to get it over the final hurdle.

2.5 Chapter summary

VSHM encompasses a broad range of methods, varying in complexity and in implementation. The incorporation of VSHM into the monitoring of wind turbine blades is an exciting opportunity, but not one that comes without its difficulties. The presence of EOVs makes detecting damage more difficult. Without mitigation, there will be an increase in the number of false alarms, as well as in instances of undetected damage. Separating the effects of damage from the effects of the EOVs is a challenge at the forefront of VSHM for wind turbine blades. Detection of the damage is crucial since the output of the turbine is heavily influenced by the condition of the blades. Furthermore, if left undetected, the damage will grow and can cause the entire turbine to fail, an expensive and undesirable consequence.

The methods that have been used for the purpose of mitigation in data-driven VSHM can be separated into two main categories. Implicit methods, such as PCA and cointegration, consider the effects of EOVs to be embedded in the DSFs, and attempt to mitigate them without information on the EOPs. Many studies have demonstrated success with these methods, but are often limited by assumptions made in their application. On the other hand, explicit methods use information on the EOPs to create cause-effect relationships between the EOPs and the DSFs. Similar to the implicit methods, explicit methods have been demonstrated to work but there are some key aspects in their design which are often overlooked. These aspects can have a significant impact on the robustness of the system if left untreated. ML methods are powerful and growing in interest, and can be either implicit or explicit depending on their design. However, they often lack interpretability, making them less desirable for implementation

on operational structures. Fundamentally, every method aims to remove the influence of the EOVs without affecting the system's ability to detect damage.

When using explicit methods, their design is very important in ensuring that the VSHM system is robust and reliable. The overfitting of model orders and EOPs can severely affect the prediction of future observations. Many methods are required to address potential flaws in the design of regression models. To demonstrate the problem, Chapter 3 explores the implementation of PCA and multivariate nonlinear regression. Chapter 4 introduces the concepts used to overcome the design problems. An operational wind turbine blade is used to analyse the corresponding effects of the introduced concepts in Chapter 5.

3 | Vibration-Based Structural Health Monitoring: An introduction and identifying the challenges

The purpose of this chapter is to introduce the foundations of Vibration-Based Structural Health Monitoring. Firstly, a macroscopic overview of a system will be presented. Two types of procedures, namely implicit and explicit, will then be detailed with a specific method presented for each in more detail. In this work, principal component analysis is used as a benchmark study with which to compare the proposed method. The methods presented in this chapter form the basis on which the proposed method of this thesis is built. The main novelty of this thesis does not lie in this chapter but instead, it is primarily used to demonstrate the necessity of the framework developed in Chapter 4. Finally, an illustrative example is used to demonstrate the performance of the two method types, as well as demonstrating common issues that occur in the design of VSHM systems for implementation on wind turbine blades. The work developed in this chapter is based upon two previously published works in which I was lead author [87, 103].

3.1 Vibration-based structural health monitoring

This section will provide the main structure of the VSHM methodology. The aim of this section is to form an understanding of the overall function of a VSHM method. The most important stages of VSHM systems are presented in more detail, starting from the outline of a typical system.

3.1.1 Foundations of a vibration-based structural health monitoring system

All VSHM systems can be broken down into three main components, as shown in Fig. 3.1. The overall complexity of the system then falls to the user who designs it and the purpose for which it is required. The input into the system is most commonly time series data. Typically in VSHM, this is acceleration measurements but can also be strain [178], acoustic [179] or others [180]. In addition to the time series data, a number of methods require information regarding different environmental or operational conditions.

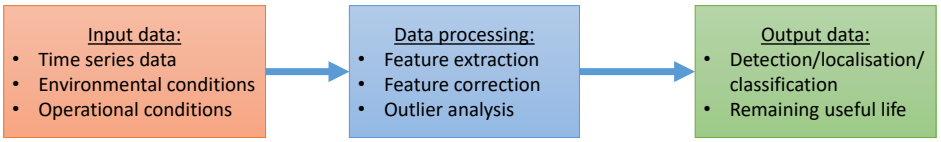

Figure 3.1: Outline of the main stages of a VSHM method.

The middle section of the system tends to be the most complex. The data processing stage typically has a number of functions to compute. This is also the section where the methodologies are developed. The first data processing task is to is extract the DSFs from the time series data. Following this, the system then applies a selected method capable of performing feature correction.

Subsequently, an outlier analysis is used to make decisions on what the current health of the structure is.

In the final stage of the VSHM system, a damage diagnosis is given. This is typically made up of the main steps defined by Rytter [181], see Section 2.1. Each of the individual steps is a difficult task in itself and requires a large amount of research. Accordingly, this thesis focuses on only the first step, damage detection.

3.1.2 Damage sensitive feature extraction

The extraction of DSFs is a critical aspect in the VSHM framework. The reason being that sensors themselves cannot measure damage [182]. There are many different types of DSF that can be used, but the important aspect is to capture the essence of the vibrations. The information contained within DSFs will describe the vibrations of the structure across many conditions. However, the information must also be sensitive to changes due to damage. The DSF must be selected carefully as the more sensitive it is to damage, the more sensitive it is likely to be EOVs [183]. Therefore, the chosen DSF must be compatible with both the structure in question, as well as the information obtainable from it.

Another aspect of DSF design is related to the physics behind the vibrations themselves. Whilst the fundamental physics is always present, it might not be possible to extract. For instance, a DSF based on the structural modal parameters of a structure has high interpretability [184], more so than an abstract DSF which correlates the information obtained from each sensor. Whilst the physics-based DSFs are more interpretable, the alternative can still be very powerful. More research is being conducted to include more interpretability into previously low interpretability models [78, 185]. In an ideal scenario, the DSFs should be as interpretable as possible. However, this is not always practical, particularly in cases where it is not possible to take the measurements necessary to create the physical models.

It is desirable to have a single value or vector as the DSF for each observation of the structure. This allows for easier comparison between observations. It follows that there must be a DSF for each observation, otherwise it is not possible to assess the condition of the structure at that point.

When constructing VSHM systems, the observations can come either labelled or unlabelled. A labelled observation is in a known condition, whereas an unlabelled observation's condition is unknown. Creating a system using labelled observations is a type of learning known as supervised learning [186]. This type of learning is not well suited to VSHM as data about damage must be available to create reliable models. In real structures, it is not practical to damage the structures to obtain the required information, hence the absence of supervised learning in the context of VSHM. Conversely, unsupervised learning, a system created using unlabelled observations, is more appropriate for VSHM as it negates the need for a significant amount of prior monitoring of the structure [187].

In this thesis, a semi-supervised approach is used for damage detection. In semi-supervised learning, the models are trained with a limited amount of labelled data [188]. This means that a baseline model is created using only labelled, undamaged observations from the structure, with the remaining conditions unknown. All future observations are compared with this baseline, so it is important that it is representative of an undamaged state. Whilst damage can still be present in the baseline, a fundamental axiom of SHM defined by Worden et al. [183], damage growth or new damage should still be able to be detected, allows for pre-existing damage. It is also important to note that a number of undamaged, labelled, observations are also kept and used to validate the baseline model. Fig. 3.2 illustrates the split of observations, as detailed above.

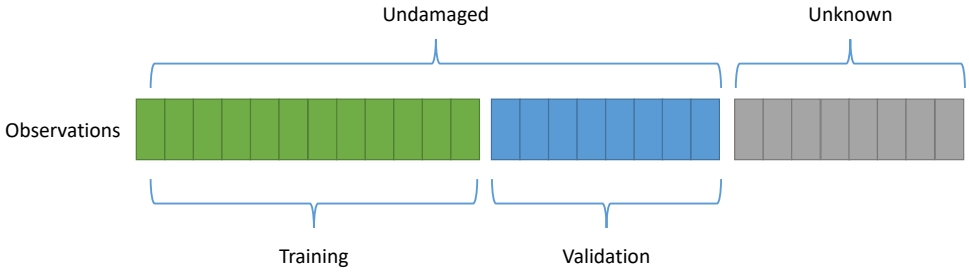

Figure 3.2: Representation of separation of observations in a semi-supervised VSHM system.

3.1.3 Outlier analysis

In order for a VSHM system to be able to differentiate between undamaged and damaged observations, a measure must be used to compare new observations to a defined baseline. This type of method is known as an outlier analysis and uses a so-called novelty index which is most often a function of the distance between the new observation and the baseline. The expectation of the novelty index is that it will change significantly when damage is present. However, outliers can also appear due to extreme weather conditions or other unknown peculiarities. In a robust system, it is important to be able to discriminate between which outliers arise from benign events and those that arise from the presence of damage.

A common novelty index that is used in VSHM methods is the *Mahalanobis Squared Distance* (MSD) [32, 87, 176, 189]. The MSD is similar to the Euclidean distance in that it computes the square of the difference between the new observation and the mean of the baseline. However, the MSD also takes into account the covariance of the baseline which gives an indication of the shape of the data in an R-dimensional space. The form of the MSD used in this work is given in Eq. 3.1.

$$MSD_n(\boldsymbol{\alpha}_n, \boldsymbol{\Sigma}_{\boldsymbol{\beta}}) = (\boldsymbol{\alpha}_n - \bar{\boldsymbol{\beta}})^{\mathrm{T}} \boldsymbol{\Sigma}_{\boldsymbol{\beta}}^{-1} (\boldsymbol{\alpha}_n - \bar{\boldsymbol{\beta}}) \tag{3.1}$$

where $\boldsymbol{\alpha}_n \in \mathbb{R}^R$ is the DSF of the n-observation, R is the length of each DSF, $\bar{\boldsymbol{\beta}} \in \mathbb{R}^R$ is the mean of the observations of the baseline model and $\boldsymbol{\Sigma}_{\boldsymbol{\beta}} \in \mathbb{R}^{R \times R}$ is the covariance of the observations of the baseline model.

A simple binary damage diagnosis can be created based on the value of the MSD for each observation, along with a threshold value, μ, which is defined from the baseline model. The definition of the threshold can be done in several ways based on the type of novelty index being used. The output of the MSD is a Chi-Squared, χ^2, distribution. The threshold that distinguishes between undamaged and damaged is a decision that is made by the user. The number of degrees of freedom of the distribution is dependent on the definition of the DSFs $\boldsymbol{\alpha}$ and is equal to the dimension of the DSFs.

Since the damage diagnosis is binary, and that the expectation is that the damaged observations will change with respect to the baseline, damage classification can be concluded according to the hypotheses in Eq. 3.2a and Eq. 3.2b, assuming the baseline is created using undamaged observations.

$$\mathrm{H}_u : MSD_n \leq \mu \rightarrow \text{Undamaged} \tag{3.2a}$$

$$\mathrm{H}_d : MSD_n > \mu \rightarrow \text{Damaged} \tag{3.2b}$$

3.1.4 Decision making

In order for an operator to make decisions based on the hypotheses in Eq. 3.2a and Eq. 3.2b, a visual representation of the results is required. A number of methods for choosing models and making real-time decisions are outlined in this section, namely: control charts, receiver operating characteristic curves and the area under receiver operating characteristic curves. Examples are provided for each to gain a better understanding of how to interpret the results.

3.1.4.1 Control charts

A control chart is a type of figure that can be used to interpret the results from the outlier analysis [87]. Fig. 3.3, below, shows an example control chart. The four types of observations that can be obtained from the outlier analysis are: true negative, true positive, false positive and false negative. In this case, the negatives and the positives are the observations below and above the threshold.

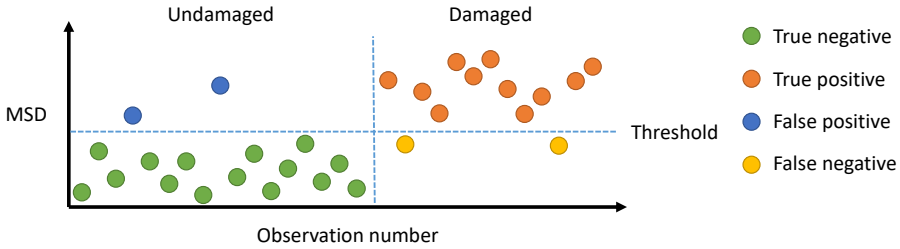

Figure 3.3: Example control chart showing regions of outlier analysis.

The threshold for damage is defined from the training data in the VSHM system. Its definition is dependent on the particular novelty index and the distribution of the observations in the training data. In the case of the MSD, the observations obey a Chi-squared distribution. The operator can decide at which rate of outliers they are comfortable with, this could be 10%, 5% or 2% for example. The threshold can then be found by finding the corresponding value of the distribution that matches the percentage of outliers.

The first group, true negatives, are undamaged observations that exist below the threshold. These are true negatives since they abide by the hypothesis in Eq. 3.2a and they are known to be undamaged. The second most populated group are the true positives. These are damaged observations that exist above the threshold, following Eq. 3.2b. These two types are what would be considered ideal cases. The converse to these then are the false positives and the false negatives. The false positives occur where undamaged observations would be

classified as damage [55], above the defined threshold. As such, these observations violate the hypothesis in Eq. 3.2a. The false negatives are the opposite of this. In VSHM, it is important to reduce the number of false positives and false negatives as much as possible [190].

3.1.4.2 Receiver operating characteristic curves

Receiver Operating Characteristic (ROC) curves are used to quantify the results seen in the control charts. They are primarily used to visualise the rate at which false positives appear in comparison to the number of true positives [191]. Other works [103] have also used ROC curves to analyse the overlap between observations that belong to the same damage category. The ROC curves compare any given damage scenario against the validation observation set. Fig. 3.4 below shows three examples of ROC curves.

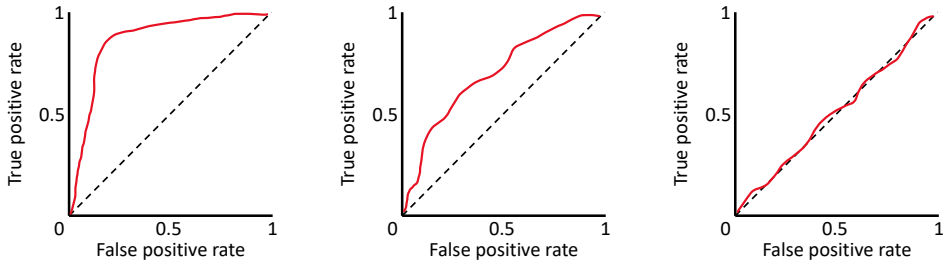

(a) (b) (c)

Figure 3.4: Examples of three different ROC curves: (a) Good separation between scenario and validation, (b) poor separation between scenario and validation and (c) no separation between scenario and validation.

Fig. 3.4a is an example of a case where there is good separation between the scenario being analysed and the validation observation set. The true positive rate is able to stay high even for small false positive rates. In essence, the *Area Under the Curve* (AUC) needs to be maximised for separation between classes, maximum 1. Maximising the AUC does not always give the best result, however, it is a good general criteria [192]. Fig. 3.4b has poor separation between classes.

For there to be a high true positive rate, there will also be a high false positive rate. Fig. 3.4c is a result that will be obtained when comparing two observation sets that display no separation.

3.1.4.3 Assessing the similarity between training and testing observations

An important aspect in a robust VSHM system is for the testing observations to behave as similarly as possible. Differences in the testing observations could indicate that damage is present when there is none. The consequence of this being that the observations beyond training are no longer reliable.

To assess the similarity between the training and testing observations, a figure similar to the ROC curves is used, hereon referred to as similarity curves. Instead of comparing the true positive rate to the false positive rate, the rate of testing observations is compared to the rate of training observations. Fig. 3.5 below, gives examples of the distributions of training and testing observations, along with their corresponding similarity curves.

In its essence, the similarity curves tell us what percentage of testing observations that have occurred for a given percentage of training observations. An ideal case, as shown in Fig. 3.5a and Fig. 3.5d, follows perfectly the line between [0,0] and [1,1]. Any deviation from this line indicates a dissimilarity between the training and testing observations. An example of poor overlap between training and testing observations is shown in Fig. 3.5b and Fig. 3.5b. The ideal case has an area of 0.5 under the similarity curve. A limitation of this method of comparison is demonstrated in Fig. 3.5c and Fig. 3.5f, where the area under the curve would also be 0.5 despite not following the ideal path. However, the area under the similarity curve can still be used as an appropriate estimation of the similarity between the training and testing observations.

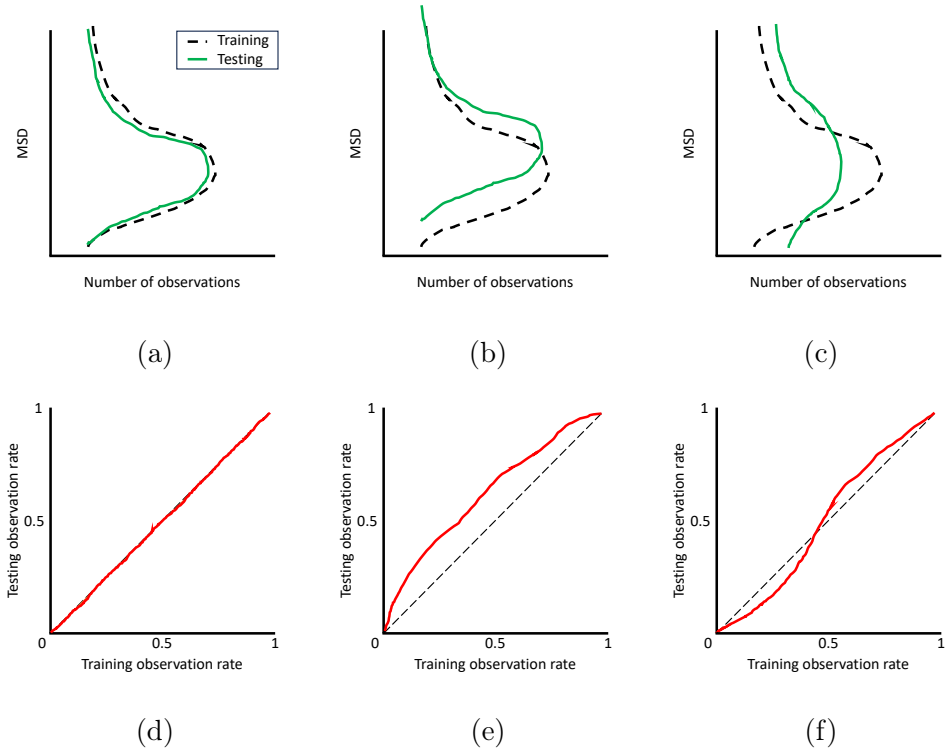

Figure 3.5: Distributions of training and testing observations (a) - (c) and similarity curves (d) - (f) for three different scenarios: (a) + (d) good overlap between training and testing, (b) + (e) poor overlap between training and testing and (c) + (f) ideal area under ROC curve but poor overlap.

3.1.4.4 Area under the receiver operating characteristic curve

As mentioned in the previous section, the AUC can be used to determine the separation between classes. It can also be used to compare various models to identify the highest performing. Furthermore, variations in AUC have also been used to compare models whilst also varying the amount of input information [103]. Fig. 3.6 shows two examples of how the AUC might change for two methods with varying amounts of input information.

In the example in Fig. 3.6a, the clear choice of model is the second since it is consistently higher than the first. However, in Fig. 3.6b, the choice is less straightforward. While model 1 finished higher, it has a much lower AUC for less information. A potential solution here is to combine the two models to maximise the AUC. The decision on model is made more difficult when

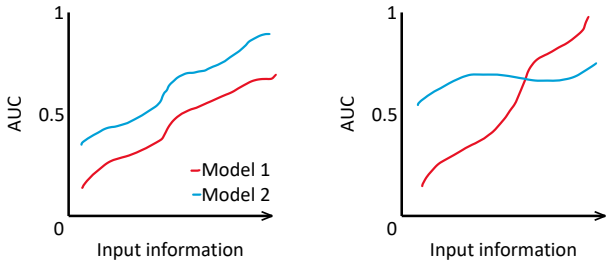

(a) (b)

Figure 3.6: Examples of variations in AUC for two competing models, (a) clear winner and (b) ambiguous decision.

considering that larger amounts of input information may lead to overfitting in the training model, leading to an artificially increased AUC. This effect has been witnessed in previous work [103]. Therefore, while the AUC is good way to choose between models, further aspects in the model must also be considered.

3.2 Implicit Procedure

This section will cover the methodology and application of an implicit procedure, a system in which the environmental and operational parameters are not directly considered. The chosen implicit method is principal component analysis. This method was chosen since it has been a commonly applied method in the field of VSHM for a number of years [26, 81, 82, 84, 94, 193]. PCA is an important method within this work as it is used for both dimensionality reduction and as a benchmark study. The purpose for its inclusion is for it to be used to demonstrate differences compared to a proposed explicit method based on multivariate nonlinear regression, introduced in Section 3.3.1. The benefits and drawbacks of each method can then be more easily analysed and discussed.

3.2.1 Principal component analysis method

Since the aim of PCA is to perform a linear transformation, this must first be defined. The transformation is described in Eq. 3.3. The transformation is per-

formed on information extracted from the structural system. The information is represented by $\mathbf{X}$, which consists of N observations with Q readings.

$$\mathbf{T} = \mathbf{U}^{\mathrm{T}}\mathbf{X} \tag{3.3}$$

where $\mathbf{T} \in \mathbb{R}^{Q\times N}$ is the transformed data, $\mathbf{X} \in \mathbb{R}^{Q\times N}$ is the standardised extracted information matrix, $\mathbf{U} \in \mathbb{R}^{Q\times Q}$ is the transformation matrix and $(\cdot)^{\mathrm{T}}$ is the transpose. Q indicates the length of the DSF prior to the application of PCA. Prior to the transformation, the extracted information matrix is standardised according to Eq. 3.4.

$$\mathbf{X}_{n,r} = \frac{\mathbf{x}_{n,r} - \bar{\mathbf{x}}_r}{\sigma_{\mathbf{x}_r}} \tag{3.4}$$

where $\mathbf{x}_{n,r}$ is the extracted information from the r-DSF of the n-observation, $\bar{\mathbf{x}}_r \in \mathbb{R}^Q$ is the mean of the r-DSF and $\sigma_{\mathbf{x}_r} \in \mathbb{R}^Q$ is the standard deviation of the r-DSF.

The transformation matrix must allow for the transformed DSF matrix's covariance to be diagonal so that the minimal redundancy goal is achieved. The covariance for the DSF matrix is given in Eq. 3.5a. Since the covariance $\mathbf{C}_{\mathbf{X}} \in \mathbb{R}^{Q\times Q}$ is symmetrical, it can be diagonalised according to Eq. 3.5b.

$$\mathbf{C}_{\mathbf{X}} = \frac{1}{N-1}\mathbf{X}\mathbf{X}^{\mathrm{T}} \tag{3.5a}$$

$$\mathbf{C}_{\mathbf{X}} = \mathbf{U}\mathbf{D}\mathbf{U}^{\mathrm{T}} \tag{3.5b}$$

where N is the number of observations, $\mathbf{U}$ is a matrix containing eigenvectors and $\mathbf{D} \in \mathbb{R}^{Q\times Q}$ is a diagonal matrix containing eigenvalues λ_r.

The Singular Value Decomposition, Eq. 3.6, can be used to calculate the eigenvectors and eigenvalues of the standardised extracted information matrix.

$$\mathbf{X} = \mathbf{U}\mathbf{S}\mathbf{V}^{\mathrm{T}} \tag{3.6}$$

where $\mathbf{V} \in \mathbb{R}^{N \times N}$ is a unitary matrix and $\mathbf{S} \in \mathbb{R}^{Q \times N}$ is a diagonal matrix containing singular values s_r.

The form of the covariance in Eq. 3.5b is equal to the covariance obtained by substituting Eq. 3.6 into Eq. 3.5a, as demonstrated in Eq. 3.7.

$$\mathbf{C_X} = \frac{1}{N-1}\mathbf{U}\mathbf{S}\mathbf{V}^{\mathrm{T}}\mathbf{V}\mathbf{S}^{\mathrm{T}}\mathbf{U}^{\mathrm{T}} = \frac{1}{N-1}\mathbf{U}\mathbf{S}^2\mathbf{U}^{\mathrm{T}} \tag{3.7}$$

where the eigenvalues can be written as a function of the singular values, $\mathbf{D} = \frac{\mathbf{S}^2}{N-1}$.

Once the eigenvectors and eigenvalues have been determined, the eigenvectors are then sorted from high to low based on their corresponding eigenvalue. In order to reduce the dimension of the transformed data, the dimension of $\mathbf{U}$ must also be reduced. This is achieved by reducing the number of eigenvectors that are used in the transformation. The transformed data can then be calculated using the transformation in Eq. 3.8.

$$\tilde{\mathbf{T}} = \tilde{\mathbf{U}}^{\mathrm{T}}\mathbf{X} \tag{3.8}$$

where $\tilde{\mathbf{U}} \in \mathbb{R}^{Q \times P}$ (where $P < Q$) is the reduced form of transformation matrix $\mathbf{U}$ and $\tilde{\mathbf{T}} \in \mathbb{R}^{P \times N}$ is a reduced dimension form of transformed matrix $\mathbf{T}$. The dimension of $\tilde{\mathbf{U}}$ is dependent on the number of eigenvectors, *Principal Components* (PCs), that are chosen to be kept. The total number of PCs is equal to the original length of the DSF. The PCs that correspond to higher eigenvalues contain the directions of the largest variances in the DSFs. Lower order PCs are normally attributed to noise in the system.

3.2.2 Application of principal component analysis for vibration-based structural health monitoring

The application of PCA within a VSHM framework is implemented as described in Section 2.3.1.2. In this work, the transformation matrix is defined exclusively using undamaged data in the training section of the method. The number of

observations that are used is N_T, as shown in Eq. 3.9. It is important to note that $N_T << N$, since N represents the total number of available observations. Additionally, a transformation matrix was created for the information coming from each sensor separately within the training regime. This allowed for a more accurate representation of the local phenomena as opposed to the global phenomena which would be obtained by combining the information from the sensors together.

$$\mathbf{C}_{\mathbf{X}_\mathrm{T}} = \frac{1}{N_T - 1}\mathbf{X}_\mathrm{T}^\mathrm{T}\mathbf{X}_\mathrm{T} \tag{3.9}$$

where $\mathbf{X}_\mathrm{T} \in \mathbb{R}^{Q \times N_T}$ is the standardised DSF matrix from the training observation set, according to Eq. 3.4.

In a similar manner, the form of Eq. 3.8 should be rewritten to reflect the change in the number of observations. Eq. 3.10 shows the way in which each DSF vector is created using the transformation equation. Every observation is passed through this transformation to ensure every observation is treated in exactly the same way.

$$\tilde{\mathbf{T}}_\mathrm{T} = \tilde{\mathbf{U}}_\mathrm{T}^\mathrm{T}\mathbf{X}_\mathrm{T} \tag{3.10}$$

where $\tilde{\mathbf{U}}_\mathrm{T} \in \mathbb{R}^{Q \times P}$ is the reduced form of transformation matrix from the training observation set $\mathbf{U}_\mathrm{T}$ and $\tilde{\mathbf{T}}_\mathrm{T}$ is the reduced form of transformed DSF matrix from the training observation set $\mathbf{T}_\mathrm{T} \in \mathbb{R}^{P \times N}$. The subscript T denotes that the transformation matrix is defined using only training observations.

3.3 Explicit Procedure

The information in this section relates to the application of an explicit procedure in the context of VSHM, namely a system that directly uses information regarding the environmental and operational variations. The method developed throughout this manuscript is based on a multivariate nonlinear regression. A

multivariate nonlinear regression builds relationships between input variables to establish the nonlinear behaviour of the system. This method is relatively understudied in comparison to PCA but has been shown to offer many benefits [71, 86, 87].

3.3.1 Multivariate nonlinear regression method

In a multivariate nonlinear regression, the dependent variables are regressed based on a number of independent variables. That is to say that, a combination of independent variables can be used to predict the dependent variable. Multivariate nonlinear regression is a very powerful tool for making predictions. In this work, a nonlinear approach was used over a linear approach as it has been shown that the relationship between DSFs and environmental and operational variations is often nonlinear [87]. Trying to model nonlinear behaviour with linear models will lead to large model errors and unreliable predictions. Therefore, using nonlinear models will allow the creation of more representative and reliable models and predictions.

The dependent variables can be modelled according to Eq. 3.11.

$$\boldsymbol{\alpha}_n = \mathbf{W}^{\mathrm{T}} \cdot \mathbf{f}(\boldsymbol{\xi}_n) + \mathbf{u}, \quad \mathbf{u} \sim \mathcal{N}(\mathbf{0}, \boldsymbol{\Sigma}_u) \tag{3.11}$$

where $\boldsymbol{\alpha}_n \in \mathbb{R}^R$ represents the dependent variables for the n-observation, $\mathbf{W} \in \mathbb{R}^{V \times R}$ is the coefficient matrix, $\mathbf{f}(\boldsymbol{\xi}_n) \in \mathbb{R}^V$ is the multivariate functional representation of the independent variables and $\boldsymbol{\xi}_n \in \mathbb{R}^L$ is a vector containing the independent variables. In this case, $\mathbf{u} \in \mathbb{R}^R$ is the innovations matrix which represents any uncertainties in the system that cannot be accounted for using the independent variables. $\mathbf{u}$ is modelled as having zero mean and a normal distribution.

The multivariate functional representation is a method for expressing how the independent variables behave with respect to each other. Each independent variable has an associated order, which can be different to other variables. All

the independent variables are combined using a Kronecker product [102], as shown in Eq. 3.12.

$$\mathbf{f}(\boldsymbol{\xi}_n) = \mathbf{f}_1(\xi_{n,1}) \otimes \mathbf{f}_2(\xi_{n,2}) \otimes \cdots \otimes \mathbf{f}_l(\xi_{n,l}) \otimes \cdots \otimes \mathbf{f}_L(\xi_{n,L}) \tag{3.12}$$

where $\otimes$ is the Kronecker product, $\mathbf{f}(\boldsymbol{\xi}_n) \in \mathbb{R}^V$ is the multivariate functional representation of the n-observation, $\mathbf{f}_l$ is the univariate function (a matrix that contains all order terms for a particular parameter, eg.$\begin{bmatrix} x & x^2 & \dots & x^e \end{bmatrix}$) of the l-independent variable, $\xi_{n,l}$ is the l-independent variable of the n-observation, $\mathbf{f}_l(\xi_{n,l})$ is the univariate representation of the l-independent variable of the n-observation and the subscript L is the total length of the EOP input vector.

In order to proceed to the next step, the multivariate functional representations and the dependent variables must be collected into their own matrices, as shown in Eq. 3.13a and Eq. 3.13b respectively.

$$\mathbf{F}(\mathbf{X}) = \begin{bmatrix} \mathbf{f}(\boldsymbol{\xi}_1) & \mathbf{f}(\boldsymbol{\xi}_2) & \dots & \mathbf{f}(\boldsymbol{\xi}_n) & \dots & \mathbf{f}(\boldsymbol{\xi}_N) \end{bmatrix} \tag{3.13a}$$

$$\mathbf{A} = \begin{bmatrix} \boldsymbol{\alpha}_1 & \boldsymbol{\alpha}_2 & \dots & \boldsymbol{\alpha}_n & \dots & \boldsymbol{\alpha}_N \end{bmatrix} \tag{3.13b}$$

where $\mathbf{F}(\mathbf{X}) \in \mathbb{R}^{V \times N}$ is the collection of multivariate functional representations and $\mathbf{A} \in \mathbb{R}^{R \times N}$ the collection of DSFs across N observations.

Once $\mathbf{F}(\mathbf{X})$ and $\mathbf{A}$ have been calculated, the coefficient matrix, $\hat{\mathbf{W}} \in \mathbb{R}^{V \times R}$, and the innovations covariance, $\hat{\boldsymbol{\Sigma}}_{\mathbf{u}} \in \mathbb{R}^{R \times R}$, can be estimated. The least squares estimate is used to calculate the coefficient matrix, as shown in Eq. 3.14a, with the innovations covariance estimated using Eq. 3.14b.

$$\hat{\mathbf{W}} = (\mathbf{F}(\mathbf{X}) \cdot \mathbf{F}^{\mathrm{T}}(\mathbf{X}))^{-1} \cdot \mathbf{F}(\mathbf{X}) \cdot \mathbf{A}^{\mathrm{T}} \tag{3.14a}$$

$$\hat{\boldsymbol{\Sigma}}_{\mathbf{u}} = \frac{1}{N}(\mathbf{A} - \hat{\mathbf{W}}^{\mathrm{T}} \cdot \mathbf{F}(\mathbf{X})) \cdot (\mathbf{A} - \hat{\mathbf{W}}^{\mathrm{T}} \cdot \mathbf{F}(\mathbf{X}))^{\mathrm{T}} \tag{3.14b}$$

To create new DSFs that are insensitive to the independent variables, the DSFs must first be estimated using Eq. 3.11. The corrected DSFs are simply found by finding the difference between the estimated value and the measured

value. This process is equivalent to finding the regression residual for each DSF. The DSF normalisation process is shown in Eq. 3.15.

$$\tilde{\boldsymbol{\alpha}}_n = \boldsymbol{\alpha}_n - \hat{\boldsymbol{\alpha}}_n \tag{3.15}$$

where $\tilde{\boldsymbol{\alpha}}_n \in \mathbb{R}^R$ is the corrected DSF, $\boldsymbol{\alpha}_n \in \mathbb{R}^R$ is the measured DSF and $\hat{\boldsymbol{\alpha}}_n \in \mathbb{R}^R$ is the nonlinear estimate of the DSF.

3.3.2 Application of multivariate nonlinear regression method for vibration-based structural health monitoring

The application of multivariate nonlinear regression within a VSHM framework is implemented as described in Section 2.3.2.3. As with the implicit method, only a section of the data is used to train the models. The training data is used to learn the relationships between the DSFs and the EOPs. As such, Eq. 3.13a and Eq. 3.13b should now be written in the following manner.

$$\mathbf{F}_T(\mathbf{X}) = \begin{bmatrix} \mathbf{f}(\boldsymbol{\xi}_1) & \mathbf{f}(\boldsymbol{\xi}_2) & \dots & \mathbf{f}(\boldsymbol{\xi}_n) & \dots & \mathbf{f}(\boldsymbol{\xi}_{N_T}) \end{bmatrix} \tag{3.16a}$$

$$\mathbf{A}_T = \begin{bmatrix} \boldsymbol{\alpha}_1 & \boldsymbol{\alpha}_2 & \dots & \boldsymbol{\alpha}_n & \dots & \boldsymbol{\alpha}_{N_T} \end{bmatrix} \tag{3.16b}$$

Since the coefficient matrix is trained using these matrices, it is representative of the training data. To ensure the training data is representative of any condition the structure may experience, as many observations as possible should be used to train the regression models. Using the coefficient matrix and the multivariate functional representation of each observation, an estimate for each DSF can be calculated using Eq. 3.17.

$$\hat{\boldsymbol{\alpha}}_n = \mathbf{W}^{\mathrm{T}} \cdot \mathbf{f}(\boldsymbol{\xi}_n) \tag{3.17}$$

3.4 Illustrative example

This section demonstrates the application of a VSHM system for damage detection. The methods that have been described in Section 3.2.2 and Section 3.3.2 will be applied to data obtained from a simulated model of a wind turbine blade under varying environmental and operational conditions. A number of aspects will be highlighted to emphasise the need for the practical considerations discussed in the following chapter. Additionally, the main benefits and disadvantages of the implicit and explicit methods will be discussed.

3.4.1 Simulated wind turbine case study

The data used in this illustrative example of a simulated wind turbine blade is taken from a previous study [123]. For the sake of completeness, a full description of the simulation is included in this document.

The vibration responses were taken from a simulation of a 60m long, aluminium wind turbine blade. A summary of the most important model parameters are included in Table 3.1. The wind turbine blade model is a tailored aeroelastic model of a 4 element beam in a cantilever arrangement, see Fig. 3.7. Each of the beam elements is modelled as an Euler-Bernoulli element, such that the rotational dynamics can be ignored [194]. The lift and drag forces acting on the blade are determined as a function of the shape of the blade, which in this case is a NACA 64-618 [195].

Table 3.1: Model parameters of simulated wind turbine blade case study [123].

Property	Value
Blade length,L	60m
Blade width	1.00m
Blade thickness	0.25m
Density	2700 kg/m^3
Angle of attack	25^o
Air density	1.2754 kg/m^3

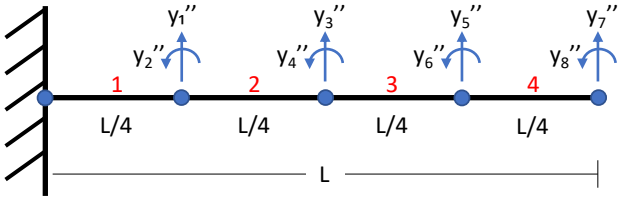

Figure 3.7: 60m long simulated wind turbine blade model made of 4 Euler-Bernoulli elements.

To test the ability of the methodologies to remove the influence of varying conditions, the simulated blade is subjected to varying temperature and wind speed. The temperatures and wind speeds in the simulation are based on the average weather conditions in north-central Switzerland [196, 197]. The modulus of elasticity of the beam elements is modelled as a linear relationship of the temperature [198], according to Eq. 3.18, and the wind excitation through the Turbsim wind simulator [199]. The combination of these models creates a realistic model of conditions, and dynamics, that a wind turbine would experience. Fig. 3.8a and Fig. 3.8b show how the temperature and wind speed, respectively, varied over the simulated monitoring campaign.

$$Y(T) = y_1 \cdot T + y_0 \tag{3.18}$$

where Y is the modulus of elasticity of the aluminium, y_1 is the rate at which Y changes with respect to temperature ($y_1 = -0.06GPa/^oC$) and y_0 is the modulus of elasticity at 0^oC.

For each temperature and wind speed, data is generated at 40Hz for 10 minutes. This process is repeated once an hour. The blade is tested under a number of scenarios in order to test the methodologies. Firstly, the blade is simulated without damage for a total of one year, for the purpose of covering one full seasonal cycle. Subsequently, the blade is tested under extreme weather for one week, again without damage. In this case, the temperature that the blade experiences is higher than any experienced during the first year of measurements,

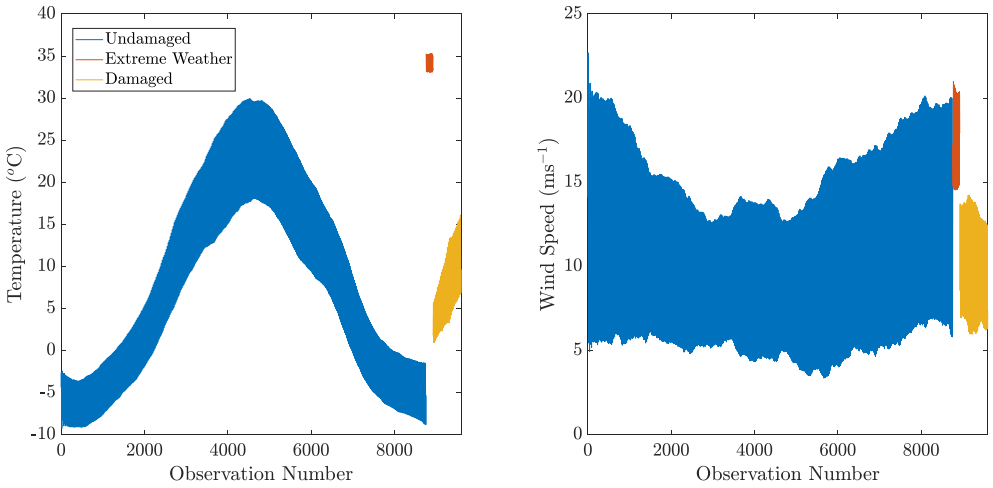

(a) (b)

Figure 3.8: (a) Temperature and (b) wind speed variations over simulated wind turbine blade monitoring campaign.

see Fig. 3.8a. Finally, the blade is simulated with damage over the course of one month. In the first half of the month, the stiffness of beam element 1 was decremented from 100% of its original value to 75%. The stiffness is then held at 75% for the remainder of the month. The total number of observations available for each condition is shown in Table 3.2.

Table 3.2: Total number of available observations for each damage scenario for the simulated wind turbine blade monitoring campaign.

Undamaged	Extreme Weather	Damage
8760	168	672

3.4.2 Case study performance

To study the capabilities of the multivariate nonlinear regression method, the DSFs themselves must be studied to show whether they are suitable for regression models. Firstly, the DSFs for this case study must be defined.

3.4.2.1 Natural frequencies as damage sensitive features

The natural frequencies of a structure are the frequencies at which a structure will oscillate following an excitation to the structure, but without the presence of a continuous or repetitive driving force. They have been extensively used in VSHM for the purpose of damage detection [62, 200, 201, 202]. Unfortunately, the natural frequencies themselves are sensitive to external conditions, such as temperature and a change to the boundary conditions of the structure. However, a large amount of information about the vibration response of a structure is contained in its natural frequencies. When damage occurs in a structure, it can either lead to a reduction of stiffness or mass. Therefore, a change in either of these parameters will lead to a change in the vibration responses. These small changes in the natural frequencies can be exploited by a VSHM method to detect damage if action is taken to mitigate the effect of varying conditions.

In this thesis, the natural frequencies are extracted with the use of *Stochastic Subspace Identification* (SSI). There are three main stages to the covariance output SSI method implemented to obtain the natural frequencies. Firstly, the data is preprocessed using a PCA approach to remove any noise that might be present. Following on, system identification is undertaken through singular value decomposition. Finally, in the modal analysis stage (orders 2-30), the output stabilisation diagram is used to identify the natural frequencies of the structure [203]. The implementation in this work was done through a previously developed code [204]. For each observation, the natural frequencies are automatically selected using target values obtained by studying a number of stabilisation diagrams. The final DSF vector, $\boldsymbol{\alpha}_n$, for each observation n, is shown in Eq. 3.19. The length of this DSF, R, is dependent on the chosen number of natural frequencies. In this work, $R = 6$.

$$\boldsymbol{\alpha}_n = \begin{bmatrix} \alpha_{n,1} & \alpha_{n,2} & \dots & \alpha_{n,r} & \dots & \alpha_{n,R} \end{bmatrix} \in \mathbb{R}^R \tag{3.19}$$

The natural frequency DSFs are used since they are easily detected at lower frequencies as well as being more intuitive for illustrative purposes. The first six natural frequencies from the system were used since they were stable and non-overlapping, this can be seen in the stabilisation diagram in Fig. 3.9. It can be seen from Fig. 3.10 that when each of the natural frequencies are compared to the temperature there is a clear dependency. Fig. 3.11 shows the natural frequencies against the wind speed. While there is a trend present, it is more difficult to discern. Specifically, it is important to consider the relationship between the undamaged observations and the temperature since these are the observations that the regression models are constructed with. As with previous work, the higher natural frequencies experience a larger range of values from the changing temperature than the lower ones [200].

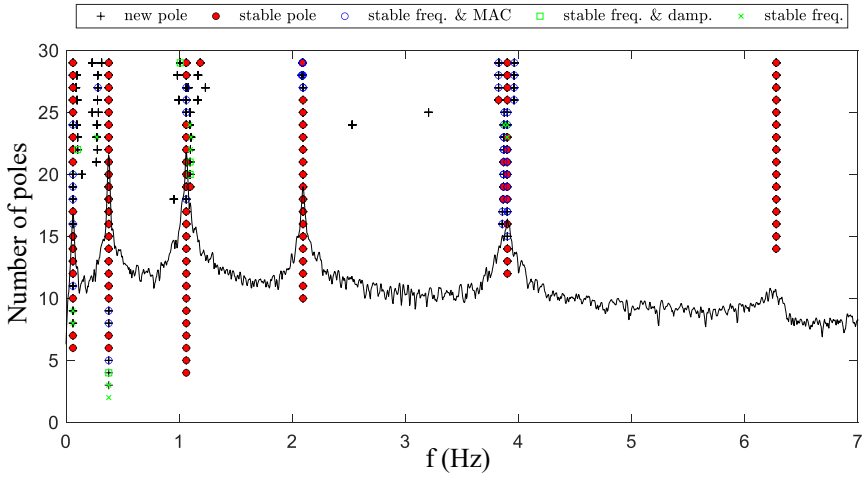

Figure 3.9: Stabilisation diagram showing the first six stable and non-overlapping natural frequencies from the simulated wind turbine blade.

As such, a regression model can be created to model the DSFs based on the temperature and the wind speed, the only two EOPs affecting the system. A separate model was created, using the training data, for each natural frequency. From a visual inspection of each of the DSFs in Fig. 3.10, the natural frequencies

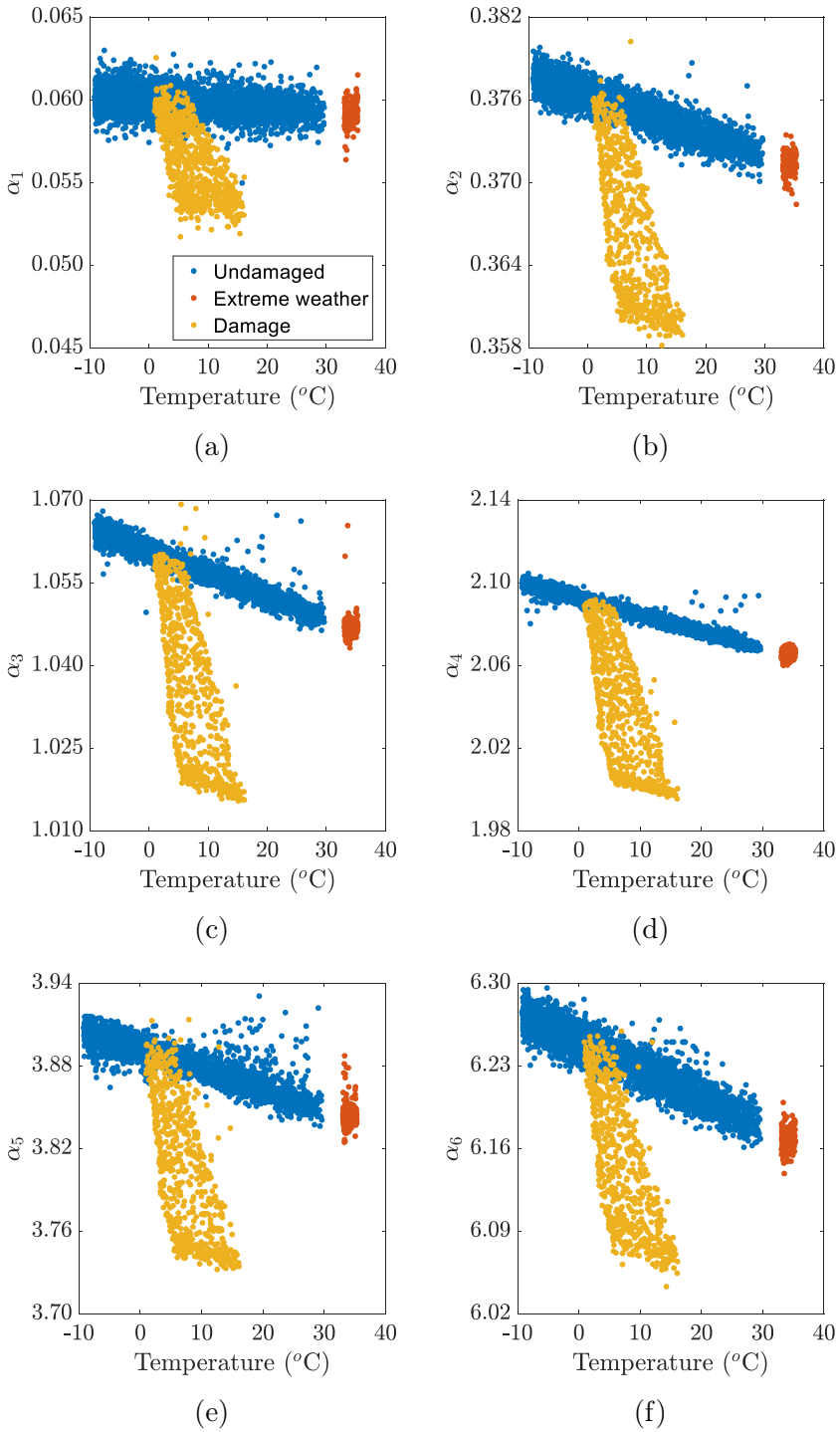

Figure 3.10: Trend of natural frequencies from simulated WTB against temperature for natural frequencies (a)-(f) α_1 to α_6. Each figure shows the natural frequencies for the undamaged, extreme weather and damaged conditions.

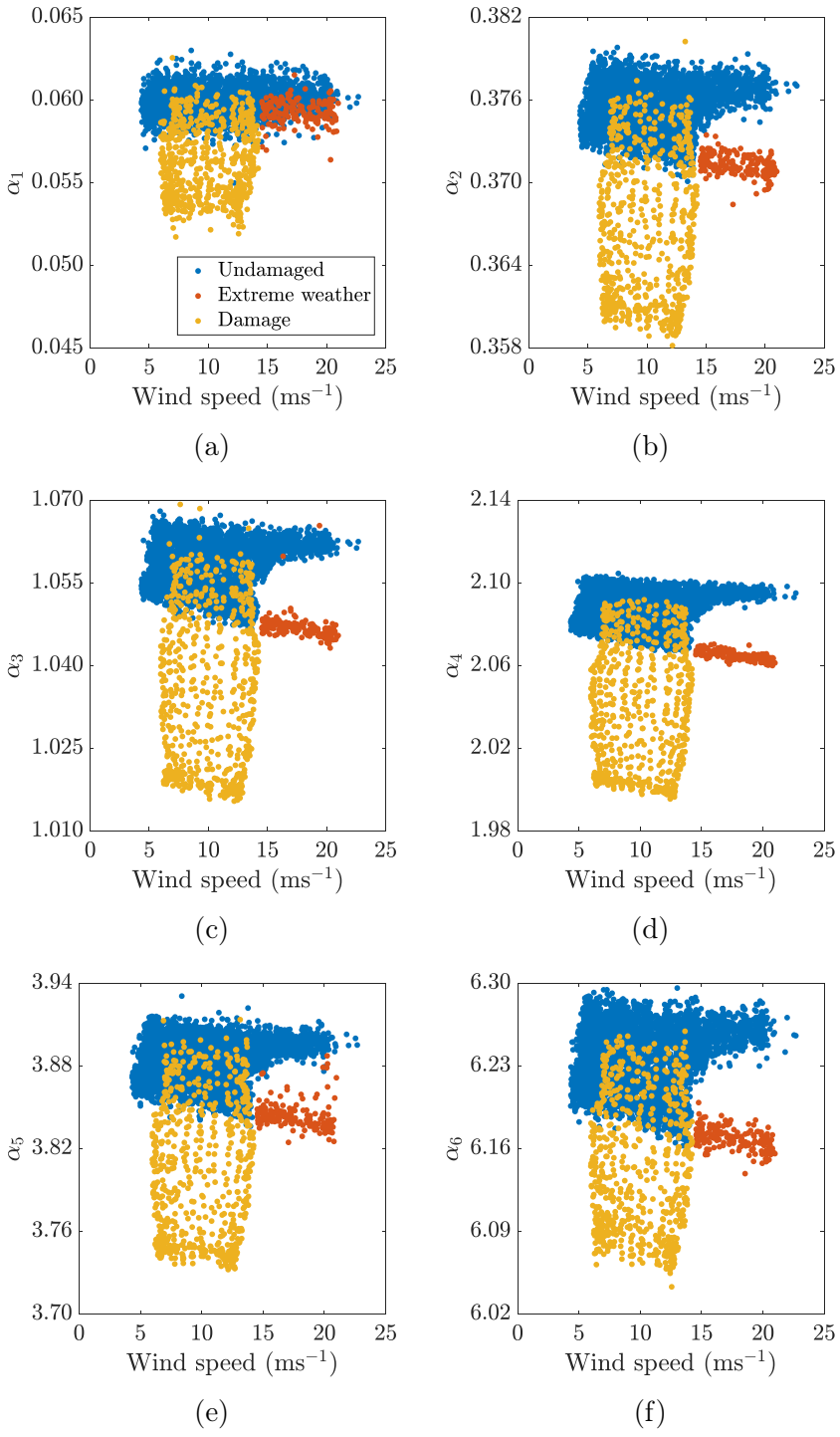

Figure 3.11: Trend of natural frequencies from simulated WTB against wind speed for natural frequencies (a)-(f) α_1 to α_6. Each figure shows the natural frequencies for the undamaged, extreme weather and damaged conditions.

appear to have a linear relationship with temperature. Each DSF was also inspected to determine its relationship with the wind speed. The regression model for each DSF was then created using the linear relationship with temperature and the corresponding order of the relationship with wind speed. Following the implementation of the regression models, values for the DSFs were estimated for all of the damage scenarios, including the, undamaged, training data. As stated in Eq. 3.15, the corrected DSFs were found by taking the difference between the measured and estimated values.

3.4.2.2 Measured, principal component analysis and regression corrected damage sensitive features

Using the defined outlier analysis from Section 3.1.3, a comparison can be made on the damage detection performance of the measured DSFs, PCA DSFs and the regression corrected DSFs. The measured DSFs ($\alpha_n \in \mathbb{R}^6$) are those taken directly from the SSI method. The PCA DSFs ($\breve{\alpha}_n \in \mathbb{R}^4$) will represent the implicit method, where it is assumed the PCA alone has removed the influence of the varying conditions. Similarly, the regression corrected DSFs ($\tilde{\alpha}_n \in \mathbb{R}^6$, ξ_1 = temperature, ξ_2 = wind speed, order $\xi_1 = 2$ and order $\xi_2 = 3$) are the output of the explicit method. The corresponding corrected DSFs can be found in Fig. 3.12.

Fig 3.13 shows the control charts for the three different DSF sets. On initial inspection, the regression corrected DSFs perform on a similar level of damage detection to the measured and PCA DSFs. Notably, the overall performances of the system before and after the correction is very good.

The objective of the regression models is to remove the influence that the EOPs have on the system. By studying the MSD for training and validation in Fig. 3.13a and Fig. 3.13b, an obvious trend is present which correlates well to the temperature curve shown in Fig 3.8a. This is evidence that both the implicit method of PCA and measured DSFs was not sufficient enough to mitigate the

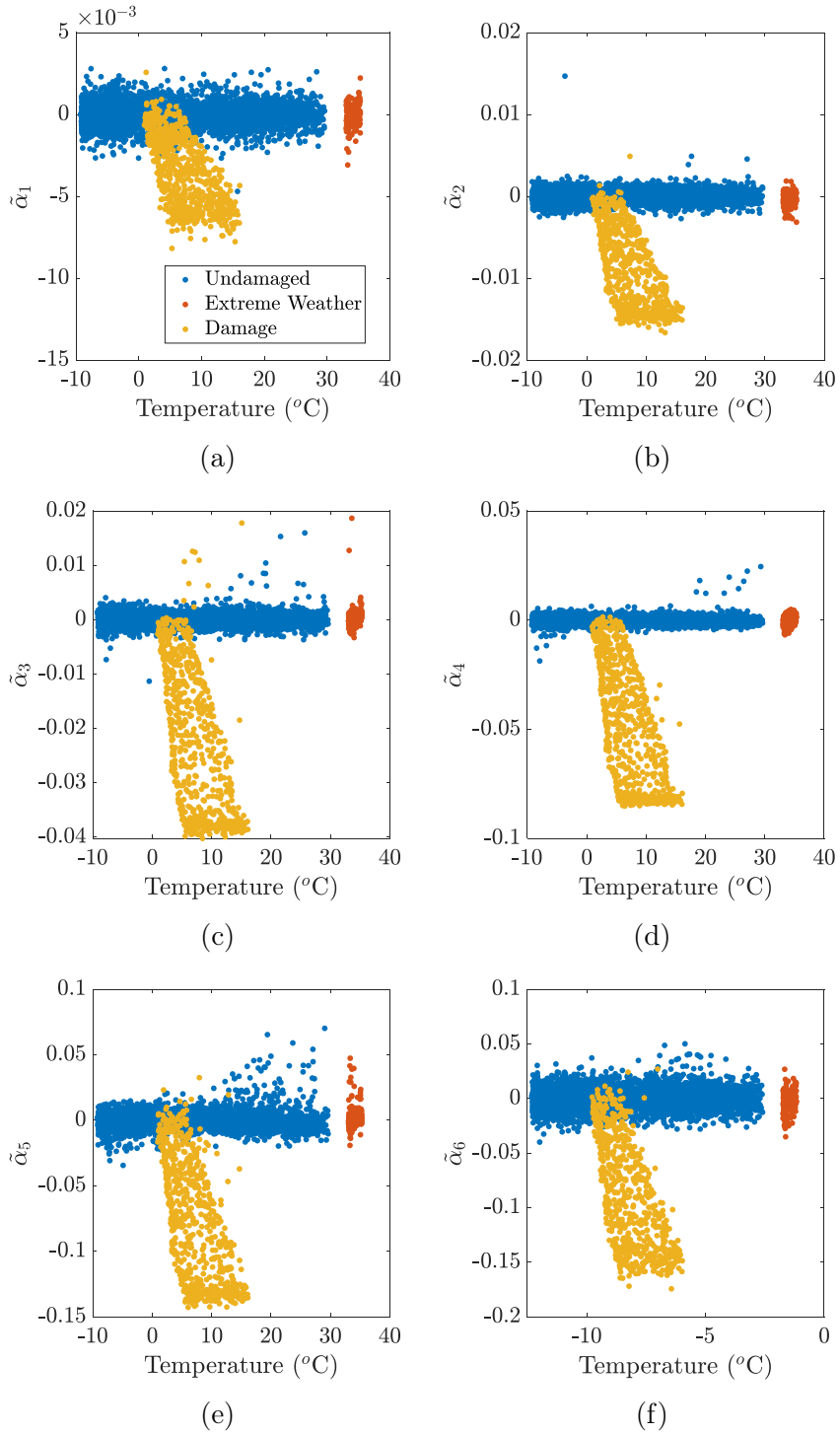

Figure 3.12: Corrected natural frequencies from simulated WTB against temperature for natural frequencies (a)-(f) α_1 to α_6. Each figure shows the natural frequencies for the undamaged, extreme weather and damaged conditions.

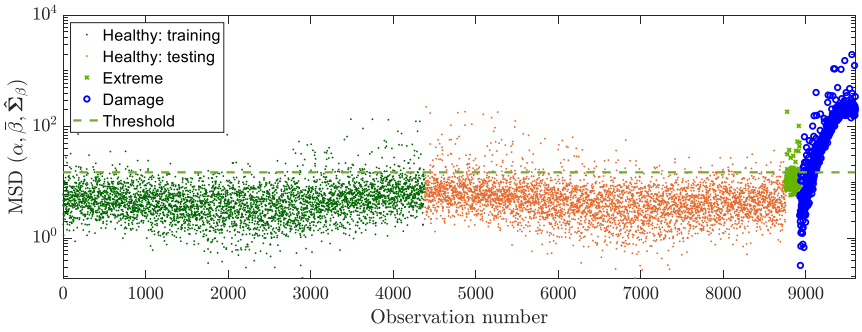

(a)

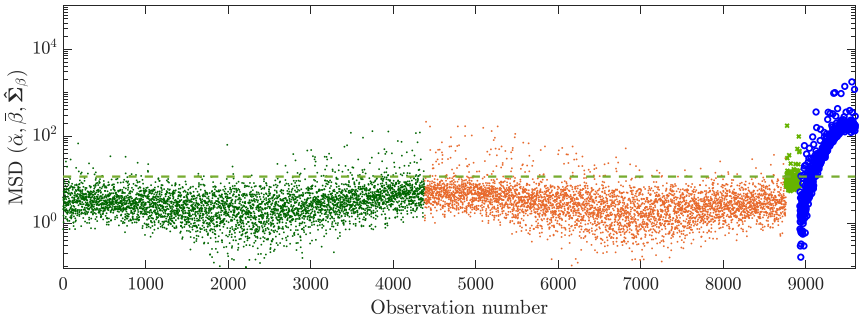

(b)

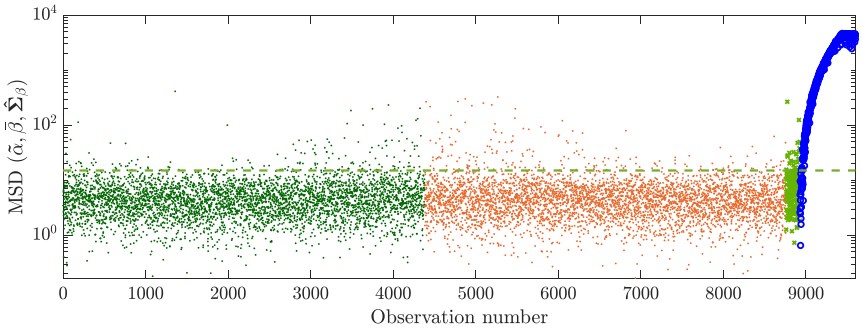

(c)

Figure 3.13: Control chart showing MSD against observation number for simulated data for (a) measured DSFs ($\alpha_n \in \mathbb{R}^6$), (b) PCA DSFs ($\breve{\alpha}_n \in \mathbb{R}^4$) and (c) regression corrected natural frequency DSFs ($\tilde{\alpha}_n \in \mathbb{R}^6$, ξ_1 = temperature, ξ_2 = wind speed, order $\xi_1 = 2$ and order $\xi_2 = 3$).Threshold calculated to represent 98% of values in the training data according to a Chi-squared distribution

temperature trend. Looking at the same region in the corrected DSFs reveals that the trend is no longer present. Unlike the measured DSFs, the behaviour of the extreme weather for the corrected DSFs is now far more similar to that of the other undamaged observations. Rather than being to the top end of the spectrum along with other observations of high temperatures, the observations now fall in line with both the testing and training observations. This is due to the regression model predicting the future behaviour beyond the training range of temperatures. Perhaps the most significant change comes in the damaged observations. There is a clear difference between the measured and PCA DSFs and the regression corrected DSFs, most notably the reduction in variability as the damage progresses. Given the reduction in variation across all the conditions, it can be said that the regression models perform their task of removing the influence of the EOPs. Although it is difficult to determine if the damage detection has improved from the control charts, the regression corrected DSFs provide a more robust system with less sensitivity to the varying environmental and operational conditions.

In order to get a more quantitative understanding of the improvement, a similarity curve and ROC curves are plotted in Fig.3.14 for three scenarios. Firstly for the testing compared to training, then for extreme weather compared to testing and, finally, for the damage compared to the testing.

Considering first Fig. 3.14a, it can be seen that the measured, PCA and regression corrected follow the diagonal between 0 and 1. This suggests that the overlap between the training and testing is good and the two groups behave in the exact same way. Since the extreme weather observations are also undamaged, it would be desirable to witness the same effect in Fig. 3.14b as Fig. 3.14a. However, due to the higher temperatures, the system does not see the observations as the same. In this case, the regression corrected DSFs far outperform the measured DSFs, and even more so the PCA DSFs, since the line

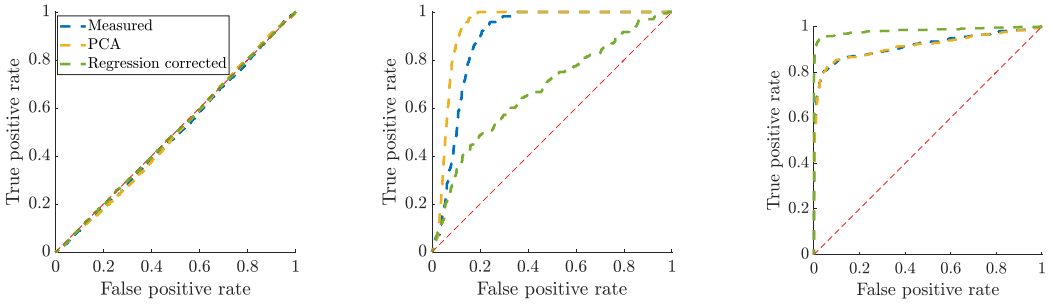

(a) (b) (c)

Figure 3.14: Figures showing measured DSFs, PCA DSFs and regression corrected DSFs for different damage scenarios. (a) similarity curve for training compared to testing, (b) ROC curve for extreme weather compared to testing and (c) ROC curve for damage compared to testing.

is much closer to the 0 to 1 diagonal. This result shows that regression models have compensated for, for the most part, the influence of the EOVs since the regression corrected extreme weather DSFs perform more similarly to the training than the measured or PCA. Fig. 3.14c shows a large improvement in the detection of damage. The corrected DSFs are almost able to perfectly distinguish between undamaged and damaged observations. The reason it is not perfect is due to the very small damage at the start being very similar to the undamaged observations. It is unlikely that any VSHM system would be able to differentiate damaged from undamaged in this scenario since the change due to the damage is so small.

3.4.2.3 Increasing the model order of the regression approach

In the previous example, the orders of the variables were selected by looking at the individual relationships between the EOPs and the DSFs ($\tilde{\alpha}_n \in \mathbb{R}^6$, $\xi_1 =$ temperature, $\xi_2 =$ wind speed, order $\xi_1 = 2$ and order $\xi_2 = 3$). Fig. 3.15 demonstrates the consequence of increasing the order of the input variables of the regression corrected DSFs to a higher value, in this case 5 ($\tilde{\alpha}_n \in \mathbb{R}^6$, $\xi_1 =$ temperature, $\xi_2 =$ wind speed, both EOP's regression orders $= 5$). An assumption that is often made in the instance of a model of this type is that

the coefficients corresponding to higher orders tend to zero. The theory being that as the coefficient tends to zero, so too does its influence on the model.

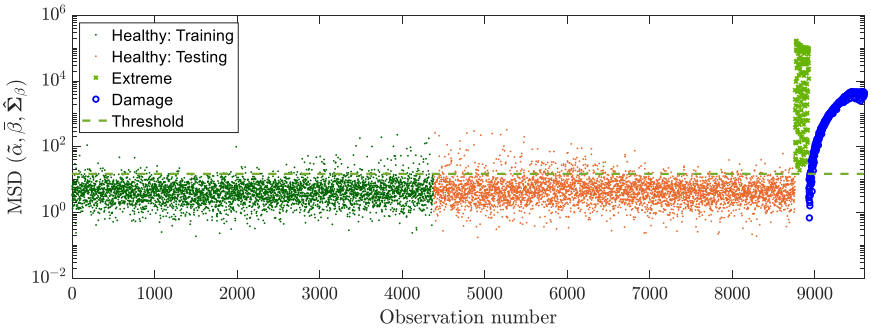

Figure 3.15: Control chart showing MSD against observation number for simulated data for regression corrected natural frequency DSFs with high order models ($\tilde{\alpha}_n \in \mathbb{R}^6$, ξ_1 = temperature, ξ_2 = wind speed, both EOP's regression orders = 5). Threshold calculated to represent 98% of values in the training data according to a Chi-squared distribution.

As with the previous example, the trend that is present in the undamaged observations Fig. 3.13a has been removed in Fig. 3.15. However, the most significant and important difference between Fig. 3.13c and Fig. 3.15 is the change in the classification of the extreme weather condition. It is important to highlight again that the extreme weather observations belong to the undamaged observations group. Therefore, this example shows the problems that can arise from overfitted models. To illustrate why the extreme weather observations appear as damage, Fig. 3.16 shows the measured values for the training observations, the measured values for the extreme weather observations and the predicted values for both, with the 6-th natural frequency being used as an example. Fig. 3.16a and Fig. 3.16b show the differences from the manually selected model orders ($\tilde{\alpha}_n \in \mathbb{R}^6$, ξ_1 = temperature, ξ_2 = wind speed, order $\xi_1 = 2$ and order $\xi_2 = 3$) and the model where the orders are arbitrarily set to 5 ($\tilde{\alpha}_n \in \mathbb{R}^6$, ξ_1 = temperature, ξ_2 = wind speed, both EOP's regression orders = 5) respectively. Wind speed is used in this example because the effect of the overfitting is much clearer compared to plotting against temperature.

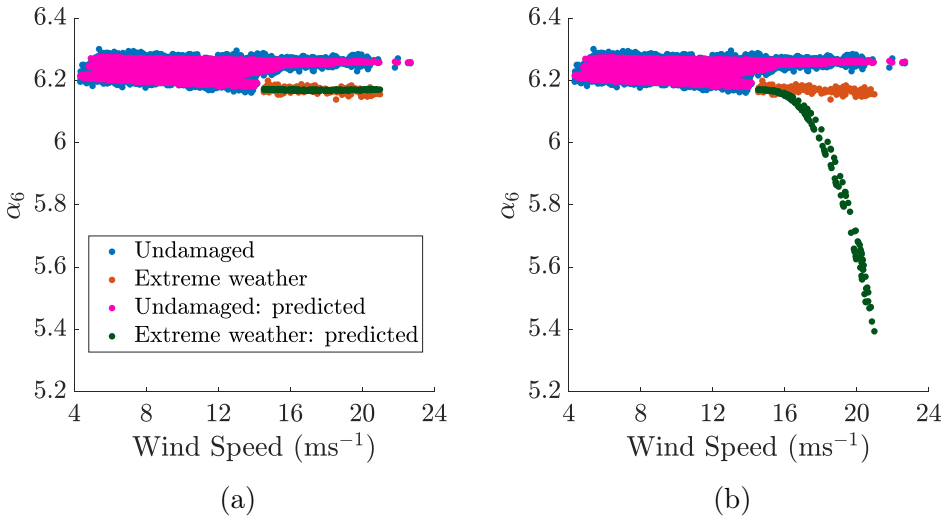

Figure 3.16: Measured and predicted values for the training and extreme weather observations for the (a) manually selected orders ($\tilde{\alpha}_n \in \mathbb{R}^6$, ξ_1 = temperature, ξ_2 = wind speed, order $\xi_1 = 2$ and order $\xi_2 = 3$) and (b) order to set to 5 for both wind speed and temperature ($\tilde{\alpha}_n \in \mathbb{R}^6$, ξ_1 = temperature, ξ_2 = wind speed).

There is very little difference between the predicted values for the undamaged data in Fig. 3.16a and Fig. 3.16b. This result is expected since the same information is available for training both regression models, consequently producing accurate models for these observations. What this also demonstrates is that the higher order models seem to make very little difference in the training of this model. The biggest difference between Fig. 3.16a and Fig. 3.16b is the way in which the extreme weather predictions begin to separate massively from the measured values in Fig. 3.16b. This separation increases the magnitude of the corrected DSFs and, thus, the value calculated in the outlier analysis. The regression models fitted to the undamaged data no longer predict the future observations accurately. The reliability of the prediction of future observations is extremely important for a robust VSHM system. This problem is further discussed in Chapter 4, where the main novelty of this work highlights the importance of designing a proper optimisation method for robust model order selection.

3.4.2.4 Adding more environmental and operational parameters to the regression approach

Further problems can occur when fitting parameters to the model that have no influence. To demonstrate the negative influence of an unrelated parameter, a new normally-distributed EOP, EOP3, is introduced to the regression model. EOP3 represents a parameter that might be available to a VSHM system, but should not be used to create models because it is non-influential. Determining which parameters are influential is non-trivial, so it can be tempting to introduce all available parameters. The following analysis highlights the detrimental effects that can occur when non-influential parameters, such as EOP3, are used in the regression modeling.

The variation of EOP3 across all damage scenarios can be found in Fig. 3.17a. Fig. 3.17b demonstrates that there is no relationship between any of the natural frequencies and EOP3 in the training data. Subsequently, the corresponding effect of EOP3 on the MSD is shown in Fig. 3.17c.

The control chart in Fig. 3.17c shows even more negative characteristics than the one in Fig. 3.15, which is already a worse version of Fig. 3.13c. Firstly, the disparity between the extreme weather observations and the rest of the undamaged observations has become worse. The most important difference, however, is the increase in the number of false positives in the validation observation set. The regression model has trained to the relationship between EOP3 and the training observations. Since EOP3 is independent of the DSFs, the relationship does not follow for observations beyond the training. Hence, creating the knock-on effect of more outliers in the validation training set. If the validation observations behave differently to the training, the system cannot be considered representative of the undamaged state of the structure, and, thus, not robust.

Interestingly, the MSD of the damaged observations changes insignificantly between Fig. 3.13c, Fig. 3.15 and Fig. 3.17c. There are a couple of factors that likely contribute to this reflection. The most significant of these is that the

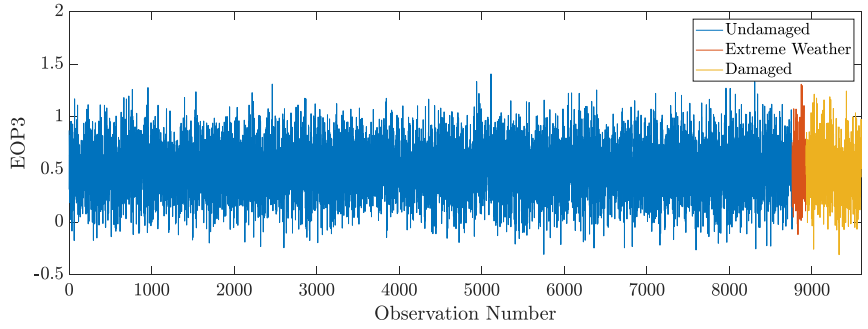

(a)

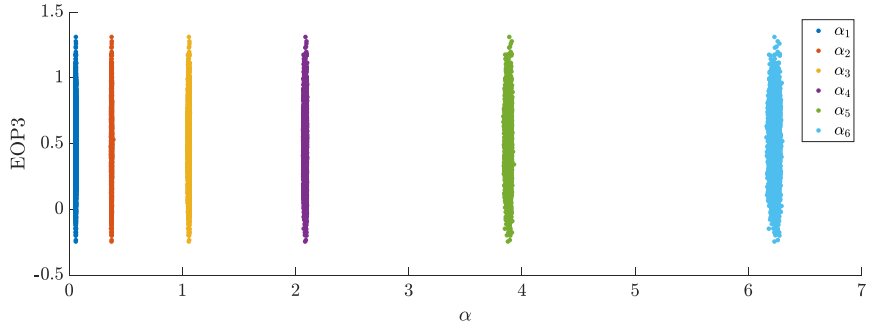

(b)

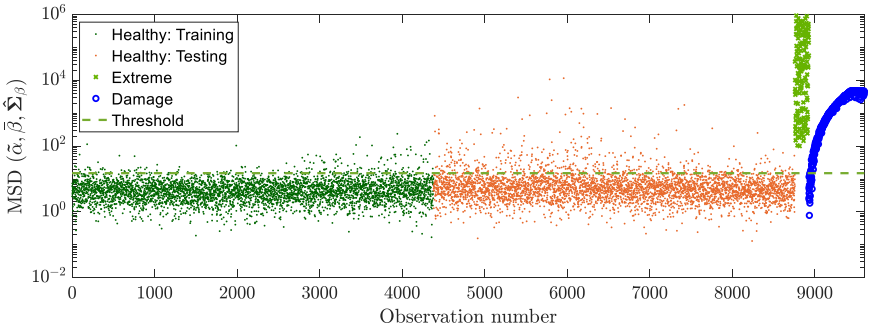

(c)

Figure 3.17: (a) Variation of introduced EOP3 over simulated wind turbine blade monitoring campaign, (b) the six natural frequencies plotted against EOP3 and (c) the control chart showing MSD against observation number of simulated data for regression corrected natural frequency DSFs with additional EOP ($\tilde{\alpha}_n \in \mathbb{R}^6$, ξ_1 = temperature, ξ_2 = wind speed, order $\xi_1 = 2$, order $\xi_2 = 3$ and order $\xi_3 = 3$).Threshold calculated to represent 98% of values in the training data according to a Chi-squared distribution

MSD is already much higher for the damaged observations since the DSFs are observably different from the undamaged and the smaller changes in the predictions do not affect the much larger spatial difference. Secondly, the conditions of the damage exist well within those of the training observations, see Fig. 3.8. Outliers often appear on the fringes of the training conditions and this problem is bypassed with the conditions of the damaged observations being well within the limits of the training conditions.

3.5 Chapter summary

This chapter introduced the fundamentals of vibration-based structural health monitoring. The basis of any VSHM system was described in detail, outlining the essential components of the system, as well as its purpose. An interpretable DSF in the form of the natural frequencies was introduced to demonstrate a number of problems that can occur in VSHM. Following this, the two core methodologies that are included within this thesis were introduced. An implicit procedure in the form of PCA was described in detail, as well as multivariate nonlinear regression as the explicit methodology.

In the latter part of the chapter, an illustrative example was introduced in order to highlight some of the advantages and disadvantages of each of the methods. The case study that was used was a simulated wind turbine blade that was subjected to varying temperatures and wind speeds. It was found that the explicit method outperformed the implicit method at removing the influence of the varying conditions. Additionally, the repercussions of overfitting the regression models was demonstrated. This section of the chapter aimed to highlight the need to avoid over-designing regression models within the context of VSHM. The following chapter aims to address this problem in more detail.

4 | Improving Regression Robustness and Reliability for VSHM applications

In this chapter, practical considerations for the robust and reliable design of a multivariate nonlinear regression methodology are discussed. These factors are all too often overlooked and have yet to be seen in the context of VSHM. This chapter forms the main contribution to knowledge of this thesis. When using regression models, there are many ways in which biases and other uncertainties can be introduced into the system. In this chapter, the following regression problems are addressed: subset selection, overfitting model orders, removing correlated variables, choosing which DSFs to regress and the correction of the novelty index. In addition to addressing these problems, a suitable optimisation framework is constructed, along with introducing an alternative optimisation method for comparison. The chapter concludes by defining measures to determine the optimal solution. The reason these problems are often left unreconciled is because they are time consuming to implement and can reduce the impact of the overall outcome. The majority of this chapter is based on my previously published works [87, 103], as well as the journal paper currently under review.

4.1 Environmental and operational parameter selection

In this section, the selection of EOPs to use will be discussed. The selection of EOPs is far from trivial and can have serious consequences in the predictability of a model if caution is not taken. Inputting all the available EOPs into a model will only lead to increased uncertainty in the system as some will have physical meaning but no effect on the data. This phenomenon has been clearly demonstrated in [103], as well as in the illustrative example in Chapter 3. Fig. 3.17c highlighted the consequences of adding an additional parameter which had no influence on the system. Once added, the extreme weather observations, which belonged to the undamaged category, appeared as more severe damage than the damage itself. Therefore, the selection and identification of the influential EOPs is of utmost importance.

However, choosing which EOPs to use is not easy as it can be difficult to identify which ones are actually influential [71]. Additionally, selecting the EOPs used in each model is also a task in itself. Some EOPs will be influential in some DSFs but not in others. Therefore, it is extremely important to choose the correct EOPs for each DSF. Fig. 3.17c showed the consequences of fitting non-influential EOPs into the regression models. If non-influential EOPs are selected, overfitting will occur.

4.1.1 Choosing from supervisory control and data acquisition data

A large amount of information about the varying environmental and operational conditions will usually be obtained from a *Supervisory Control and Data Acquisition* (SCADA) system. This will contain information on EOPs such as: temperature, wind speed, rotational speed, wind direction and many more.

The problem with SCADA systems is that they are expensive to install and not always available on every structure. This means that some of the quantities for a structure are taken from an adjacent structure, or even further away, which might not correspond well to the one being investigated. A growing area of interest in the VSHM community is determining which parameters can be estimated from structure to structure [205, 206]. If the EOPs being used to model DSFs are not representative of the structure being modelled, then this can further increase the uncertainty in a system.

With regards to which EOPs should be selected, it is wise to consider which DSFs are being used. For example, it is well established that temperature affects stiffness and that will have an effect on the natural frequencies of the system [200, 201]. However, in an ideal case, it would be good to consider all the available information and have a smart system that is capable of selecting the most influential parameters. This would add more complexity to the system but could lead to increased robustness and interpretability of the system.

4.1.2 Deriving environmental and operational parameters

In some cases, there is additional information that can be derived from other measured quantities. This additional information can often be good predictors of the DSFs. A good example of this is when natural excitation is not sufficient to excite frequencies where damage detection can be done. In these cases, a form of forced vibration is used and information on the excitation is useful to understand which frequencies have been excited.

In previous works, Roberts et al. [87] used information from an accelerometer to summarise the hit of an actuator. The measures that were used were the maximum amplitude of the vibration, as well as the standard deviation of the signal over the free decay. It was found that a number of DSFs were highly sensitive to this information.

The danger in deriving EOPs from SCADA data is that if there are already uncertainties, such as measurement errors and noisy signals, in the data, the uncertainties in the derived EOP can be even greater. This is especially true if combining information from more than one data source. As such, caution is required when using derived quantities for modelling within an VSHM system.

4.1.3 Reduction based on sensitivity analysis

A sensitivity analysis can be a powerful tool for understanding which EOPs have the largest influence on a system. In the application of the sensitivity study, the likelihoods of different models with varying numbers of EOPs are compared. When referring to the likelihood, it is a measure of the probability of receiving the value of the DSF given the EOPs for that observation. The predictive capability of each regression model can be quantified using the likelihood of the models for three different cases. The first is where all of the EOPs are considered apart from one (denoted by $\tilde{\boldsymbol{\xi}}$), the second is where only a single EOP(denoted by ξ) is considered and lastly where all are EOPs are considered (denoted by $\boldsymbol{\xi}$). The likelihoods associated with each model were calculated using the log-likelihood in Eq. 4.1a.

$$\ln \mathcal{L}(\boldsymbol{\alpha}_r|\boldsymbol{\xi}) = -\frac{N_T}{2}\ln \sigma_{\epsilon_r}^2 - \sum_{n=1}^{N_T}\frac{\left(\alpha_{n,r} - \mathbf{w}_r^{\mathrm{T}}\cdot\mathbf{f}(\boldsymbol{\xi}_n)\right)^2}{2\sigma_{\epsilon_r}^2} \tag{4.1a}$$

$$\sigma_{\epsilon_r}^2 = \frac{1}{N_T - 1}\sum_{n=1}^{N}\tilde{\alpha}_{n,r}^2 \tag{4.1b}$$

where $\ln \mathcal{L}(\boldsymbol{\alpha}_r|\boldsymbol{\xi})$ is the log-likelihood for the r-DSF considering all EOPs, σ_{ϵ_r} are the innovations (as calculated in Eq. 4.1b), $\mathbf{w}_r$ is the coefficient matrix of the r-DSF and $\alpha_{n,r}$ and $\tilde{\alpha}_{n,r}$ are the measured and corrected (from Eq. 3.15) r-DSF from the n-observation respectively.

The exclusive sensitivity $S(\boldsymbol{\alpha}_r|\tilde{\xi}_l)$ and inclusive sensitivity $S(\boldsymbol{\alpha}_r|\xi_l)$ are found by the difference between the model defined with fewer EOPs and the model

created with all the EOPs. The exclusive and inclusive sensitivities are found in Eq. 4.2a and Eq. 4.2b respectively.

$$S(\boldsymbol{\alpha}_r|\tilde{\xi}_l) = \ln \mathcal{L}(\boldsymbol{\alpha}_r|\tilde{\xi}_l) - \ln \mathcal{L}(\boldsymbol{\alpha}_r|\boldsymbol{\xi}) \tag{4.2a}$$

$$S(\boldsymbol{\alpha}_r|\xi_l) = \ln \mathcal{L}(\boldsymbol{\alpha}_r|\xi_l) - \ln \mathcal{L}(\boldsymbol{\alpha}_r|\boldsymbol{\xi}) \tag{4.2b}$$

Using the information from the exclusive and inclusive sensitivities, a decision can be made on which EOPs should be included in the regression models. If an EOP has a high sensitivity in the exclusive study, it suggests that the regression models are unable to predict well without its presence. Similarly, if an EOP has a low sensitivity in the inclusive study, the EOP is able to predict the DSF accurately on its own. If an EOP is both high in the exclusive and low in the inclusive then it is likely highly influential on the DSF.

The opposite of this is also true. If an EOP is low in the exclusive and high in the inclusive, it is likely not a good predictor for the DSF. However, this does not mean that the EOP should be discarded. If a DSF is not sensitive to one particular EOP, it does not mean that other DSFs are not. Therefore, it is important to do the sensitivity study on a DSF by DSF basis. A summary of the combinations of inclusive and exclusive studies are summarised in Table 4.1.

Table 4.1: Summary of how influential an EOP is likely to be based on the exclusive and inclusive sensitivity studies.

		Inclusive	
		Low	High
Exclusive	Low	Undetermined	Non-Influential
	High	Influential	Undetermined

It is important to note that the sensitivities being considered are only relative to the EOPs being used. A limitation to this approach, therefore, is identifying all the possible EOP that might be influential to the DSFs. Given this limitation,

it is possible that there exists EOPs that are more influential to the DSFs that have not been included as part of the analysis. However, given the known physical relationships between EOPs and vibrational behaviour, it is likely that the most influential EOPs have been included.

4.2 Optimisation of model order

The aim of this section is to discuss in detail how the order of the models within the regression method are defined, as well as the implications of how the order is selected. The order selection process can be broken down into three main categories: manual selection, trial and error (such as testing every possible model for a given range of orders) and automatic selection. Each process has its benefits and drawbacks which will be discussed further.

Choosing the correct model order is hugely important for the predictive power of regression models for observations that they have not been trained on. The DSFs themselves contain uncertainties and if a model is overfitted, these biases will become an even larger issue, which can be detrimental if not relieved [104]. Furthermore, if a model is overfitted, any future observations will be affected causing a large error even in cases where the observation belongs to the same group as the training data. This effect was previously seen in Fig. 3.15 in Chapter 3 as part of the illustrative example, where the extreme weather observations separated entirely from the rest of the undamaged observations.

4.2.1 Manual selection of order

Manual selection of model orders is the most basic form of order selection. In this method, the undamaged DSFs are studied with regard to each of the independent variables. For each independent variable, a model order is selected based on what the user believes to be the correct order of the DSF. This method is simple to implement and rarely leads to the overfitting of model orders but also has many disadvantages.

The first drawback of this method is that bias can be introduced by the user based on their opinion of the relationship. Considering the synthetic training data in Fig. 4.1a, it could be easy to misinterpret this data and assume it is based on a quadratic function. However, from Fig. 4.1b, a cubic function (displayed on figure) is actually used to model the relationship. The observations that occurred in the region beyond the training region, that belong to the same damage category but are unseen to the training model, would be poorly estimated if the quadratic function was used. The assumption of a quadratic function would have disastrous consequences for inferring the condition of the structure where the undamaged condition would be misidentified as damage.

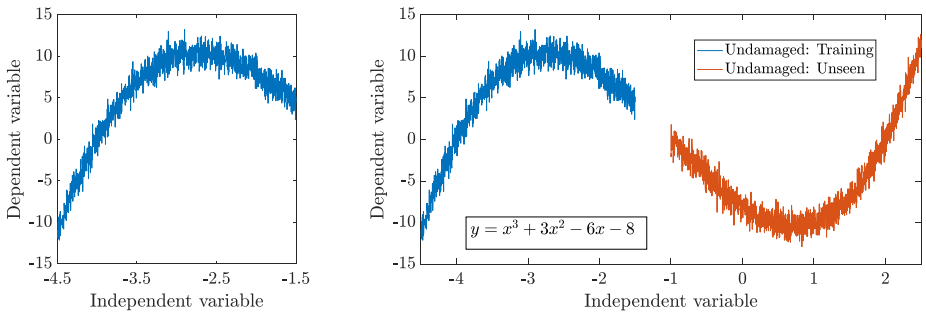

(a) (b)

Figure 4.1: (a) Example of synthetic data available for training and (b) Example of synthetic data available for training and data from the same category but unavailable for training.

Less commonly, the same problem can also work in reverse where the user selects a model which is more complex than the actual underlying relationship. Furthermore, the manual selection process can be extremely laborious in cases where there are a large number of DSFs and/or a large number of independent variables.

4.2.2 Testing all possibilities

In this trial and error method, every single possibility is tested for each independent variable and each model order, up to a limit. This method allows for

an optimum model to be chosen through testing every possible model. This method mitigates the possibility of human bias and can be completed in an automatic manner. As such, a testing all possibilities approach overcomes two of the main limitations of the manual selection method.

As an example, if a VSHM system had L independent variables and a maximum model order of Z, the number of possibilities that would have to be tested for each DSF would be L^Z. Consequently, even a basic system with $L = 5$ and $Z = 5$, a total of 3125 possibilities would have to be tested. The first disadvantage of this method is, therefore, that it takes a long time to evaluate, especially if there are a large number of DSFs.

However, the designs of the model are likely to be more accurate since a cross validation error, as described in Section 4.2.3, is considered. Having more accurate models is worthy compensation for the extra computational time. Furthermore, this method for optimisation is also able to pick up on minor relationships between independent variables within a multivariate nonlinear regression method. Once all the possibilities have been tested, the chosen model for each DSF is the one with the lowest cross validation error.

A further drawback of this method is the design of the optimisation process itself. If a large maximum order is defined at the start of the process, then it is easy for the model orders to become overfitted to the training data. Similarly, if EOPs are chosen that have no influence on the data, more uncertainty will be introduced into the system. However, this can be mitigated through considerations given in Section 4.1.

4.2.3 Evaluating models using the cross validation error

To test the accuracy of the regression models in each step, a cross validation measure can be implemented within the training regime. In a cross validation procedure, a number of observations from the same group as the training, but not within the training, are tested for their predictive accuracy. The mean

squared error is often used to quantify this. As a model becomes more and more overfitted, the mean squared error will increase showing a decrease in the predictive accuracy of the regression model.

In this thesis, the *Leave-One-Out Cross Validation* (LOOCV) is used [207]. In this method, one observation is excluded from the training data for training the model and instead its error is computed. For example, if a training set had 1000 observations, the regression model would be trained with 999 of these observations and the last used to calculate an error. This process is then repeated so that each observation has been excluded once, totalling 1000 repetitions. The LOOCV error is calculated as shown in Eq. 4.3.

$$MSE_{LOO} = \frac{1}{N_T} \cdot \sum_{n=1}^{N_T} (\hat{\boldsymbol{\alpha}}_n - \bar{\boldsymbol{\alpha}}_n)^2 \cdot \left(\sum_{n=1}^{N_T} (\boldsymbol{\alpha}_n)^2 \right)^{-1} \tag{4.3}$$

where MSE_{LOO} is the LOOCV error, $\hat{\boldsymbol{\alpha}}_n$ is the predicted value of the n-observation and $\bar{\boldsymbol{\alpha}}_n$ is the mean of the measured DSFs $\boldsymbol{\alpha}_n$.

4.3 Nonlinear forward stepwise regression

This section will outline a nonlinear forward stepwise regression method that was implemented to overcome a number of limitations previously mentioned in this chapter. Crucially, the proposed method is capable of automatically selecting the most influential EOPs, as well as determining their most appropriate model order. This type of process has never been applied in the context of VSHM, so it has been adapted for this specific purpose. Included within this method are a number of stages aimed at increasing the robustness and reducing the uncertainty in a system. With these adaptions, a reliable and logical method has been created for multivariate nonlinear regression for VSHM. The flow diagram in Fig. 4.2 outlines the overall proposed nonlinear forward stepwise regression method.

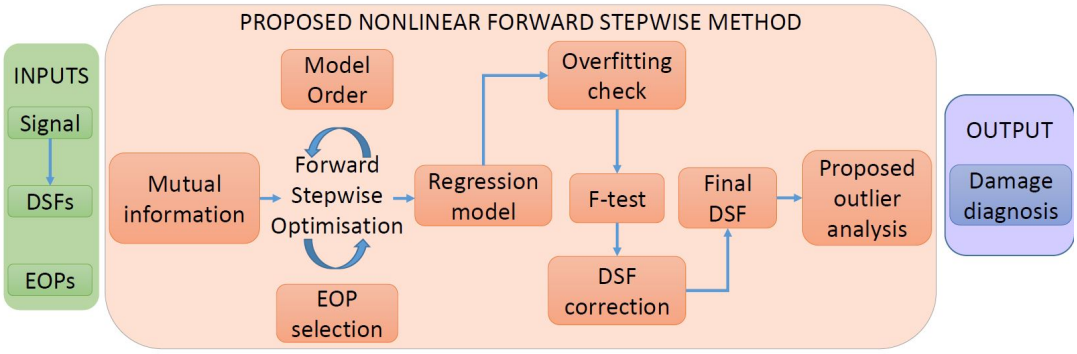

Figure 4.2: A flow diagram representing the proposed nonlinear forward stepwise regression method.

4.3.1 Removing correlated variables

Dependency between inputs can lead to severe problems with instability in parameter estimates, large sampling variances and an inability to decouple the effects of different predictors, which can hurt the interpretability of the regression model [143]. One approach to assessing the correlation between input variables is the *Pearson Correlation Coefficient* (PCC) [208]. The squared PCC gives a good measure of the linear correlation between two vectors. The closer the value is to 1, the stronger the correlation, with 0 indicating that the two vectors are independent of each other [209]. The squared PCC is calculated between two EOPs at a time, $\boldsymbol{\xi}_a$ and $\boldsymbol{\xi}_b$, as shown in Eq. 4.4.

$$\rho^2(\boldsymbol{\xi}_a, \boldsymbol{\xi}_b) = \frac{E^2(\boldsymbol{\xi}_a \boldsymbol{\xi}_b)}{\sigma^2_{\boldsymbol{\xi}_a} \sigma^2_{\boldsymbol{\xi}_b}} \tag{4.4}$$

where ρ^2 is the squared PCC, $E(\boldsymbol{\xi}_a \boldsymbol{\xi}_b)$ is the cross correlation of $\boldsymbol{\xi}_a$ and $\boldsymbol{\xi}_b$, and $\sigma_{\boldsymbol{\xi}_a}$ and $\sigma_{\boldsymbol{\xi}_b}$ are the variances of vectors $\boldsymbol{\xi}_a$ and $\boldsymbol{\xi}_b$ respectively.

However, when the models are nonlinear, the squared PCC is no longer able to detect correlated variables and so mutual information is used to assess the correlation between inputs instead. The particular approach used in this work, average mutual information in Eq. 4.5, is based on the work of Moon et al.

[210], and an existing code is used [211]. If any correlated inputs are identified, one is excluded from the construction of the regression models.

$$\overline{I}_{\boldsymbol{\xi}_a,\boldsymbol{\xi}_b} = \sum_{i,j} P_{\boldsymbol{\xi}_a,\boldsymbol{\xi}_b}(\xi_{a,i},\xi_{b,j}) \log_2 \left(\frac{P_{\boldsymbol{\xi}_a,\boldsymbol{\xi}_b}(\xi_{a,i},\xi_{b,j})}{P_{\boldsymbol{\xi}_a}(\xi_{a,i}) P_{\boldsymbol{\xi}_b}(\xi_{b,j})} \right) \tag{4.5}$$

where $\overline{I}_{\boldsymbol{\xi}_a,\boldsymbol{\xi}_b}$ is the average mutual information, $P_{\boldsymbol{\xi}_a,\boldsymbol{\xi}_b}(\xi_{a,i},\xi_{b,j})$ is the joint probability density and $P_{\boldsymbol{\xi}_a}(\xi_{a,i})$ and $P_{\boldsymbol{\xi}_b}(\xi_{b,j})$ are the marginal probability densities of predictor a and b respectively.

The joint probability density function, Eq. 4.6a, describes the probability of two or more continuous variables existing within predetermined ranges for any given time [212]. For example, $P_{\xi_a,\xi_b}(\xi_{a,i},\xi_{b,j})$ describes the probability of ξ_a happening knowing ξ_b, then multiplied by the probability of ξ_b occurring. On the other hand, the marginal probability density function, Eq. 4.6b, is the joint probability density function integrated across all variables except the one in question. For example, $P_{\xi_a}(\xi_{a,i})$ is the marginal probability density for all variables except ξ_a [213].

$$P_{\xi_a,\xi_b}(\xi_{a,i},\xi_{b,j}) = \int_{x_1}^{y_1} \int_{x_2}^{y_2} f_\xi(\xi_a,\xi_b)\, d\xi_a d\xi_b \tag{4.6a}$$

$$P_{\xi_a}(\xi_{a,i}) = \int_{-\infty}^{\infty} \cdots \int_{-\infty}^{\infty} f_\xi(\xi_b \ldots \xi_L) d\xi_L \ldots d\xi_b \tag{4.6b}$$

where $\xi_a \in [x_1, y_1]$ and $\xi_b \in [x_2, y_2]$.

Once the average mutual information has been calculated, a decision can be made on whether any of the input variables need removing. The higher the average mutual information between two variables, the more correlated they are. If two variables are identified to be correlated, one will be removed. Although it is acknowledged that if one is highly sensitive then the other will be too. Choosing a threshold value for the average mutual information can depend on the application and for this study, the threshold was chosen to be 0.8.

To demonstrate the importance of using mutual information when complex nonlinear relationships exist, a synthetic example of two correlated EOPs are

shown in Fig. 4.3. From an initial inspection, it is clear to see that the two variables are strongly nonlinearly correlated. However, if the squared PCC was to be used in this situation, it would not remove one of the variables since $\rho^2 = 0.58$. Whereas, using normalised mutual information gives $\overline{I}_{\boldsymbol{\xi}_a,\boldsymbol{\xi}_b} = 0.94$, clearly identifying the correlated variables. Mutual information is, therefore, the most sensible choice since it is capable of identifying both linear and nonlinear correlations between input variables.

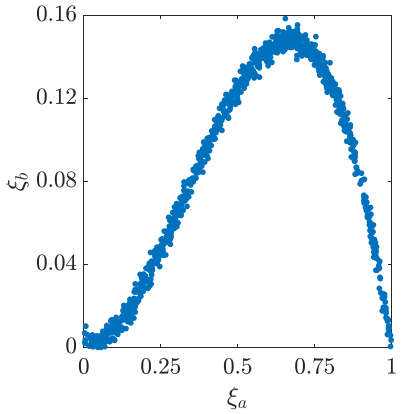

Figure 4.3: Synthetic example showing two nonlinearly correlated input variables, $\rho^2 = 0.58$ and $\overline{I}_{\boldsymbol{\xi}_a,\boldsymbol{\xi}_b} = 0.94$.

4.3.2 Nonlinear forward stepwise method for vibration-based structural health monitoring applications

In forward stepwise regression, a single predictor is added at a time to model a DSF. In most cases, forward stepwise regression has only been applied in a linear application. Only recently has linear forward stepwise regression been seen in the context of VSHM [149]. However, a nonlinear version of the forward stepwise regression has not been seen in VSHM before. In cases, not related to VSHM, where a nonlinear approach has been attempted, a linear transformation has been used to linearise the formation of the model in order to apply the regular forward stepwise procedure [152]. In this work, a more involved method has

been used which retains the nonlinear aspect of the models, if and when it is required.

The purpose of the forward stepwise method is to prevent additional predictors being added that have no influence. Since this work uses nonlinear models, each predictor has to be tested with a number of model orders, up to a predetermined limit. For the first iteration, a univariate approach is required, as shown in Eq. 4.7a. The process then follows the steps of the multivariate nonlinear regression as set out in Section 3.3.1. Once each predictor has been tested with the full range of model orders, the combination with the lowest LOOCV is kept constant through the remainder of the process, predictor and model order. The second iteration then uses the result of the first iteration and steps forwards by trying different combinations of the remaining predictors, as shown in Eq. 4.7b. Similarly, the third iteration follows the same process, as shown in Eq. 4.7c. The general procedure follows until the model can no longer be improved by adding additional predictors.

$$\mathbf{f}(\boldsymbol{\xi}_n) = \mathbf{f}_l(\xi_{n,l}) \tag{4.7a}$$

$$\mathbf{f}(\boldsymbol{\xi}_n) = \mathbf{f}_a(\xi_{n,a}) \otimes \mathbf{f}_l(\xi_{n,l_{-a}}) \tag{4.7b}$$

$$\mathbf{f}(\boldsymbol{\xi}_n) = \mathbf{f}_a(\xi_{n,a}) \otimes \mathbf{f}_b(\xi_{n,b}) \otimes \mathbf{f}_l(\xi_{n,l_{-a,b}}) \tag{4.7c}$$

where $\mathbf{f}_a(\xi_{n,a})$ is the *Univariate Functional Representation* (UFR) of the first predictor added, $\mathbf{f}_b(\xi_{n,b})$ is the UFR of the second predictor added, $\mathbf{f}_l(\xi_{n,l_{-a}})$ is the UFR of any predictor excluding the first added and $\mathbf{f}_l(\xi_{n,l_{-a,b}})$ is the UFR of any predictor excluding the first two added. An important aspect to note is that each DSF is modelled separately. The benefit of modelling each DSF separately is that they are all unique and are affected differently by EOPs. Individual models are, therefore, able capture the specific response of each DSF to the different EOPs and create the most appropriate model. The forward stepwise regression process, for a maximum order of 10, is summarised in Fig.4.4.

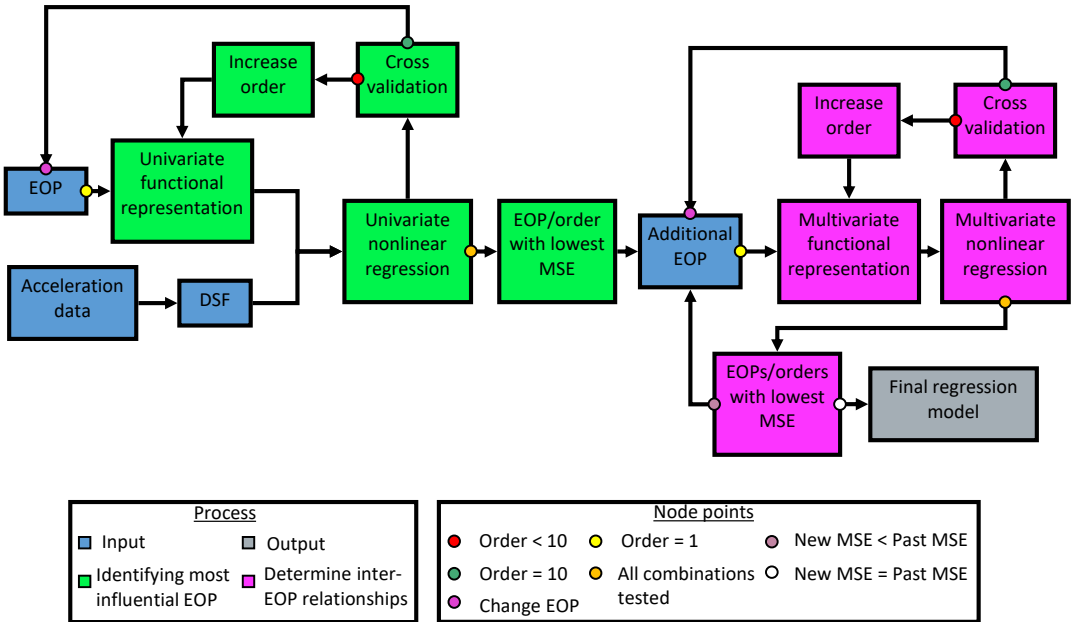

Figure 4.4: Diagrammatic representation of the forward stepwise procedure

4.3.3 Preventing overfitting

If the regression models are allowed to train to a high order, there is a reasonably high possibility that the models will be highly overfitted to the training data. However, it is also possible that there is a deeper underlying relationship which is of high order. It makes sense then to design a system that can automatically decide which models have been overfitted and which require the higher order terms.

To detect which models have been overfitted, a simple method is applied which automatically reduces the order of overfitted models. To understand the influence of each order in the model, the magnitude of the values in the model's corresponding coefficients matrix are analysed. If a model is overfitted, the coefficients for the higher order terms will be significantly less than those for the lower orders. The small coefficients have very little influence on the model and are a product of overfitting. An example of a coefficient matrix created from a synthetic dataset is included in Table 4.2.

Table 4.2: Example matrix of coefficients between two EOPs. Red cells indicate coefficients that would be removed following the application of 0.1% threshold and blue cells the remaining coefficients.

		ξ_a	ξ_a^2	ξ_a^3	ξ_a^4	ξ_a^5	ξ_a^6	ξ_a^7
	ξ_b	1256	2541	865	472	48	1.25	2.68
	ξ_b^2	954	1001	547	358	40	1.21	1.95
ξ_b	ξ_b^3	551	231	124	98	18	0.85	1.05
	ξ_b^4	54	68	23	15	4	0.71	0.45
	ξ_b^5	2.79	2.14	2.23	1.52	0.95	0.56	0.13

To remove the overfitted coefficients, a simple threshold is applied. Any coefficient that is smaller than a given percentage of the largest coefficient is deemed to be overfitted. In its essence, this approach is a basic form of pruning. From the example in Table 4.2 and using a threshold of 0.1%, the last two columns and bottom row, highlighted in red, are full of coefficients that are below the threshold. In this case, the model order would be reduced from 7 to 5 for ξ_1 and from 5 to 4 for ξ_2. The coefficients that would remain are highlighted in blue. This method is simple but effective at achieving its goal of reducing overfitted models.

4.3.4 Choosing which damage sensitive features to regress

It is possible to fit a regression model to any data set. However, this approach is inadvisable since many DSFs will not exhibit any relationship between themselves and the EOPs. For this reason, blindly applying regression models to everything can lead to uncertainties and biases in the overall VSHM system. Such uncertainties and biases can lead to a diagnosis of damage when there is none. Therefore, it is important to identify which DSFs should and should not be regressed. To determine whether the regressed DSF is to be used, a statistical F-test is applied.

An F-test is used to decide if the null hypothesis should be accepted or rejected [214]. The F-test is often used to decide whether there are any benefits

of using a higher order model. However, in this work, the F-test is used to determine if the optimised regression model provides superior prediction over the mean of the DSF. Therefore, the null hypothesis is that the mean of the DSF predicts better than the regression model. An F-test is, therefore, a quantitative measure for demonstrating which regression models provide statistically significant results. As such, it can be incorporated within the nonlinear stepwise framework as a method for determining which DSFs should be regressed.

Since the first model being considered is based only on the mean of the DSF, the model order is always 1. For the regressed DSF, the model order is determined during the nonlinear forward stepwise procedure. To calculate the F-statistic for each DSF, the following equation is used:

$$F_{0,r} = \frac{RSS_1 - RSS_2}{RSS_2} \times \frac{N_T}{p_{2,r} - 1} \tag{4.8}$$

where $F_{0,r}$ is the F-statistic of the r-DSF, $p_{2,r}$ is the model order of the the r-regressed DSF, N_T is the number of training observations and RSS_1 and RSS_2 are the *Residual Sum of Squares* (RSS) of the mean model and the regressed model respectively. The RSS for each model can be calculated using Eq. 4.9.

$$RSS = \sum_{n=1}^{N_T} (\alpha_{r,n} - \hat{\alpha}_{r,n})^2 \tag{4.9}$$

where $\alpha_{r,n}$ and $\hat{\alpha}_{r,n}$ are the measured and estimated values for the r-DSF respectively.

To make a decision on which regressed DSFs are used, a threshold must first be defined. The threshold in this case is not constant since the order of the models are different for each DSF. The threshold for decision is based on the critical value. The critical value of the F-statistic, γ, is determined by the F-distribution and the order of the two models being considered. The decision on whether the DSF is to be regressed is then based on the following hypotheses:

$$\mathrm{H}_0 : F_{0,r} \leq \gamma_r \rightarrow \text{Not regressed} \tag{4.10a}$$

$$\mathrm{H}_1 : F_{0,r} > \gamma_r \rightarrow \text{Regressed} \tag{4.10b}$$

4.3.5 Combining damage sensitive features

Once the decision has been made on which DSFs are to be regressed, according to Eq. 4.10a and Eq. 4.10b, a new DSF can be created as a combination of regressed and measured DSFs, as shown in the example in Eq. 4.11. Any DSF that has been deemed not to be regressed is simply replaced by its corresponding measured DSF so that the overall DSF length is unchanged. The new combined DSF will be both purged of its influence from varying environmental and operational conditions and free from introduced uncertainty from regressed DSFs that provide no predictive advantage over the mean of the DSF. As such, this new DSF should be more robust in the context of damage detection.

$$\breve{\boldsymbol{\alpha}} = \begin{bmatrix} \tilde{\alpha}_1 & \tilde{\alpha}_2 & \alpha_3 & \tilde{\alpha}_4 & \dots & \alpha_r & \dots & \alpha_R \end{bmatrix} \tag{4.11}$$

where $\breve{\boldsymbol{\alpha}}$ is the new combined DSF, α is the measured DSF and $\tilde{\alpha}$ is the regression corrected DSF.

4.4 Lasso regression: a comparison to nonlinear forward stepwise regression

Like the aforementioned forward stepwise method, the Lasso regression is also a method for optimising the design of regression models. Furthermore, it is another method that is typically used for linear regression but can be extrapolated for nonlinear regression. However, unlike the forward stepwise method, the Lasso is a shrinkage method. In a shrinkage method, all the possible regressors are used to begin with and it works to determine the necessary size of each.

Therefore, the Lasso is a good comparison to the forward stepwise method since it works in the opposite direction.

4.4.1 Lasso regression method

The Lasso method is based on the least squares estimate but introduces a penalty function in order to optimise the size of the regression coefficients. It was first introduced by Tibshirani [150] and serves as a method that has the same stability as ridge regression [215] whilst also having the ability to perform subset selection. The form of the Lasso is given in Eq. 4.12a [216]. To understand better the Lasso method, it is easier to view it in its Lagrangian form, as in Eq. 4.12b

$$\hat{\mathbf{W}}_r = \underset{W}{\operatorname{argmin}} \sum_{n=1}^{N} \left(\alpha_{r,n} - W_0 - \sum_{l=1}^{L} \xi_{l,n} W_l \right)^2 \tag{4.12a}$$

$$\hat{\mathbf{W}}_r = \underset{W}{\operatorname{argmin}} \left\{ \frac{1}{2} \sum_{n=1}^{N} \left(\alpha_{r,n} - W_0 - \sum_{l=1}^{L} \xi_{l,n} W_l \right)^2 + \Lambda \sum_{l=1}^{L} |W_l| \right\} \tag{4.12b}$$

where $\hat{\mathbf{W}}_r$ is the estimated coefficient matrix for the r-DSF, $\xi_{l,n}$ is the l-EOP of the n-observation, W_0 is a regression constant and W_l is the coefficient of the l-EOP. Λ is the regularisation parameter which controls the rate at which the coefficient shrinks.

Like with the forward stepwise regression discussed in Section 4.3.2, the Lasso method is capable of performing subset selection. This is possible through the design of the regularisation parameter. If Λ is sufficiently small, some of the regression coefficients will become zero because of the geometry of the l_1 normalisation penalty [151]. If the coefficients reach zero, this implies that they have no influence on the DSF being modelled. In this respect, this is how the subset selection is performed.

4.4.2 Transformation to nonlinear

The assumption that is made in both Eq. 4.12a and Eq. 4.12b is that the model used to model $\boldsymbol{\alpha}_r$ is linear. However, as discussed previously, the relationship between the EOPs and the DSFs is often nonlinear. Therefore, a nonlinear equivalent of the input variables, $\boldsymbol{\xi} = [\boldsymbol{\xi}_1, \boldsymbol{\xi}_2, \ldots, \boldsymbol{\xi}_l, \ldots, \boldsymbol{\xi}_L]^{\mathrm{T}}$, is necessary. The first option is to expand each of the input variables to the order at which they are to be tested, as shown in Eq. 4.13.

$$\begin{aligned}\mathbf{g}(\boldsymbol{\xi}) =&[\boldsymbol{\xi}_1, \boldsymbol{\xi}_1^2, \ldots, \boldsymbol{\xi}_1^z, \ldots, \boldsymbol{\xi}_1^Z, \boldsymbol{\xi}_2, \boldsymbol{\xi}_2^2, \ldots, \boldsymbol{\xi}_2^z, \ldots, \boldsymbol{\xi}_2^Z, \ldots, \\ &\boldsymbol{\xi}_l, \boldsymbol{\xi}_l^2, \ldots, \boldsymbol{\xi}_l^z, \ldots, \boldsymbol{\xi}_l^Z, \ldots, \boldsymbol{\xi}_L, \boldsymbol{\xi}_L^2, \ldots, \boldsymbol{\xi}_L^z, \ldots, \boldsymbol{\xi}_L^Z]^{\mathrm{T}}\end{aligned} \tag{4.13}$$

where Z is the maximum order to which each input variable is being tested.

The advantage of this option is that the dimension stays relatively small, given $\mathbf{g}(\boldsymbol{\xi}) \in \mathbb{R}^{(L\times Z)\times 1}$. For example, if there are 10 input variables with a maximum order of 10, then the corresponding vector has dimension 100. The disadvantage, however, is that none of the relationships between input variables are modelled. This can lead to less accurate modelling of the DSFs compared to the proposed stepwise method.

The second option is to use the Kronecker product, as given in Eq. 3.12, to expand the input variables. Unlike the first, this option does consider the relationships between the input variables. However, there can be significant issues with the dimension of the input vector when using this approach. Take for example the number of inputs and maximum order from before, the Kronecker product would give a vector with dimension 10^{10}, since $\mathbf{f}(\boldsymbol{\xi}) \in \mathbb{R}^{L^Z\times 1}$. This vector is far too large to work with and even halving each of those values, the dimension would still be 3125. Dimensions of this magnitude will lead to rank deficiencies, where the number of inputs exceeds the number of training observations [216], in the regression models since the Lasso method starts its shrinking with all possible inputs. As such, the number of input variables and

their maximum testing order are critical in the application of the Lasso in a nonlinear setting, especially in cases where little training data is available.

4.5 Correction of Mahalanobis squared distance

Whilst the MSD is a common choice for the distance metric within VSHM frameworks, it also has its limitations. The covariance matrix that represents the training data is an estimation of the overall relationships between different DSFs. However, in certain circumstances, a more appropriate covariance matrix can be used to better represent the training data based on the derivation of the DSFs. In this section, three examples of MSD correction are outlined: (I) DSFs derived from a PCA transformation, (II) DSFs that have been corrected using a regression approach and, (III) a combination of the previous two.

4.5.1 Mahalanobis squared distance with principal component analysis

When PCA is applied in the derivation of the DSFs, information on the variance of each component is available in the eigenvalues. Instead of using the covariance of the training data, the covariance can be redefined using the derivation of the PCA procedure. The process begins with the covariance of the new DSFs, as shown in Eq. 4.14. The new DSFs can now be replaced according to their projection in Eq. 3.3, see Eq. 4.15. In Eq. 4.16, the standardised extracted information matrix is expanded according to the singular value decomposition from Eq. 3.6. Finally, a number of terms can be cancelled down, since the transpose of an orthonormal matrix is equal to its inverse, to give the result in Eq. 4.17.

$$\mathbf{C}_{\mathbf{T}_j} = \frac{1}{N-1}\mathbf{T}_j\mathbf{T}_j^{\mathrm{T}} \tag{4.14}$$

$$\mathbf{C}_{\mathbf{T}_j} = \frac{1}{N-1}\mathbf{U}_j^T\mathbf{X}_j\mathbf{X}_j^{\mathrm{T}}\mathbf{U}_j \tag{4.15}$$

$$\mathbf{C}_{\mathbf{T}_j} = \frac{1}{N-1}\mathbf{U}_j^{\mathrm{T}}\mathbf{U}_j\mathbf{S}_j\mathbf{V}_j^{\mathrm{T}}\mathbf{V}_j\mathbf{S}_j^{\mathrm{T}}\mathbf{U}_j^{\mathrm{T}}\mathbf{U}_j \tag{4.16}$$

$$\mathbf{C}_{\mathbf{T}_j} = \frac{1}{N-1}\mathbf{S}_j^2 \tag{4.17}$$

where $\mathbf{U}_j$ are the eigenvectors, $\mathbf{S}_j$ are the singular values, $\mathbf{V}_j$ is the unitary matrix and $\mathbf{T}_j$ is the DSF matrix for the j-accelerometer. $\mathbf{S}_j^2$ is a diagonal matrix containing the squared singular values. All this information can be collected across all sensors to give the diagonal covariance matrix $\mathbf{\Sigma}_{\boldsymbol{\lambda}} = \frac{1}{N-1}\mathbf{S}^2$. The form of the MSD that is used for DSFs prior to correction is, therefore, given in Eq. 4.18.

$$\mathbf{MSD}(\tilde{\boldsymbol{\alpha}}_n, \mathbf{\Sigma}_{\boldsymbol{\lambda}}) = \tilde{\boldsymbol{\alpha}}_n{}^{\mathrm{T}}\mathbf{\Sigma}_{\boldsymbol{\lambda}}^{-1}\tilde{\boldsymbol{\alpha}}_n \tag{4.18}$$

The reason the square of the singular values can be used in a diagonal matrix is due to the property of the eigenvectors being orthogonal and, therefore, independent of each other. However, a limitation of the approach is then incurred when combining the eigenvectors from different sensors. Whilst the eigenvectors are orthogonal in the context of each transformation, this may not hold true across multiple sensors.

A possible solution to this problem could be to perform a second PCA transformation following the combining of the sensors in the DSF space. This process would ensure that each DSF is orthogonal to the next, thus removing the possibility of overlap between sensors. However, since one PCA transformation is already used, the DSFs have already lost some of their interpretability and performing PCA a second time would further worsen the interpretability. For this reason, the decision was made that the overlap of PCs from different sensors was assumed to be noise and could, therefore, be removed. It is possible that some of these overlaps may contain information about damage, but there would also be a large number which are specific to the training observations and are not suitable for comparison to future observations.

4.5.2 Mahalanobis squared distance with regression

Following the correction of the DSFs from the regression models, the variations for each DSF can be represented by the error in the predictions. This is also true for PCA-based DSFs corrected by regression, where the square of the singular values no longer represents the covariance between the DSFs. Instead, a better measure of the covariance are the innovations. The innovations can be calculated as a function of the sum of the regression residuals as in Eq. 4.1b. The covariance matrix can be created as a diagonal matrix of the innovations as shown in Eq. 4.19a with the corresponding modified MSD in Eq. 4.19b.

$$\boldsymbol{\Sigma}_{\epsilon} = diag(\sigma_{\epsilon_1}, \sigma_{\epsilon_2}, \cdots, \sigma_{\epsilon_r}, \cdots, \sigma_{\epsilon_R}) \tag{4.19a}$$

$$\mathbf{MSD}(\tilde{\boldsymbol{\alpha}}_n, \boldsymbol{\Sigma}_{\epsilon}) = \tilde{\boldsymbol{\alpha}}_n{}^{\mathrm{T}} \boldsymbol{\Sigma}_{\epsilon}^{-1} \tilde{\boldsymbol{\alpha}}_n \tag{4.19b}$$

where $\boldsymbol{\Sigma}_{\epsilon}$ is the diagonal matrix containing all the innovations. In this scenario, the diagonalisation of the innovations comes without the previous limitation since the regression model for each DSF is independent of any other DSF and, thus, has zero covariance.

4.5.3 Mahalanobis squared distance with the combination of regressed and measured DSFs

In the case where there are regressed DSFs mixed with measured DSFs, the covariance can be defined as in Eq. 4.20a, with the new MSD given in Eq. 4.20b.

$$\boldsymbol{\Sigma}_{tot} = \begin{bmatrix} \boldsymbol{\Sigma}_{\boldsymbol{\beta}} & 0 \\ 0 & \boldsymbol{\Sigma}_{\epsilon} \end{bmatrix} \tag{4.20a}$$

$$\mathbf{MSD}(\tilde{\boldsymbol{\alpha}}_n, \boldsymbol{\Sigma}_{tot}) = \tilde{\boldsymbol{\alpha}}_n{}^{\mathrm{T}} \boldsymbol{\Sigma}_{tot}^{-1} \tilde{\boldsymbol{\alpha}}_n \tag{4.20b}$$

4.6 System robustness metrics

A further, but no less important, consideration in the design of regression models is their robustness. In this case, when referring to robustness, the changes in the regression model due to changes in the input variables is what is of interest. In order to test this, a k-fold repetition was undertaken by creating k different training data sets and analysing the effect this had on the outlier analysis. Additionally, the stability of the coefficient matrix is analysed.

There are a number of different aspects that make one model more robust that others, the first of which is its ability to be generalised. Generalisation effectively measures the repeatability of the regression model, hence the use of the k-fold analysis. Tied into this is the performance of the regression model, and how well it can mitigate the varying conditions. In cases where mitigation has been performed effectively, it would be expected that the range of values across each damage case would be lower. Furthermore, it would be expected that there would be fewer outliers to the distribution, signifying less overfitting of model parameters. Finally, the stability of the coefficient matrix indicates how much the coefficient matrix changes with small changes to its inputs. A robust system will be less affected by these small changes.

4.6.1 Distribution of groups

One measure of the robustness of a system is how much the distribution of each damage group varies. For instance, if the distribution of one particular group changes significantly when a different training data set is used, the method cannot be said to be very robust. To compare the distributions from the different methods, the *Normalised Interquartile Range* (NIQR) of the MSD values is used, as shown in Eq. 4.21.

$$\mathrm{NIQR}_{k,d} = \frac{\mathrm{IQR}(\mathbf{MSD})_{k,d}}{\mathrm{median}(\mathbf{MSD})_{k,d}} \tag{4.21}$$

where IQR($\mathbf{MSD}$)$_{k,d}$ and median($\mathbf{MSD}$)$_{k,d}$ are the interquartile range and median of the MSD of the k-fold, d-damage group, respectively.

For a robust system, the variation in the NIQR should be as low as possible. This result would suggest that the variation in the distribution also remains similar, meaning that changes to the training set has minimal impact on the distribution of the data. In addition to this, it is more desirable to have lower NIQRs. Lower NIQRs convey tighter distributions which suggests less variability in the data. The lower variability in the data comes as a result of more appropriate regression models performing superior mitigation of the varying conditions.

4.6.2 Outlier rate

Another statistical aspect that can be analysed from a k-fold analysis is the method's outlier rate. In the analysis contained in this thesis, outliers are classified as observations that are more than 1.5 IQRs above or below either the 75th or 25th percentiles respectively. The outlier rate is then, the number of outliers divided by the total number of observations within the group, as shown in Eq.4.22. This method of defining outliers is more appropriate in data that is not normally distributed. Since the number of outliers is being examined in the MSD, this is the most appropriate measure since the MSD fits a chi-squared distribution. Consequently, the majority of outliers that are identified will be positive outliers, those above the upper bound.

$$\text{Outlier rate}_{k,d} = \frac{\text{NOut}_{k,d}}{N_{k,d}} \tag{4.22}$$

where NOut$_{k,d}$ and $N_{k,d}$ are the number of outliers in the MSD and the number of observations of the k-fold, d-damage group, respectively.

Naturally, the number of outliers to a distribution wants to be kept as small as possible. As with the NIQR, it is desirable to have observations from the same damage group to appear as similar as possible. Outliers to the group can

lead to confusion where misclassification can then occur. A large variation in the outlier rate can also indicate a lack of robustness. However, a generally lower outlier rate has a larger advantage. In terms of optimal robustness, there should be a low outlier rate with low variation.

There also exists an interaction between the outlier rate and the NIQR. As the NIQR decreases, and the distribution narrows, any observation that behaves slightly differently to others will appear as an outlier compared to a scenario where there is a higher NIQR, then it is more likely to be captured by the main distribution. Consequently, damage groups that have lower NIQRs are more likely to have outliers. An additional aspect to note here is that the outlier rate does not account for the magnitude of the outliers. Instead, it is just an indication of their presence. As such, a group might have a smaller number of outliers but they are much further distanced from the main distribution.

4.6.3 Coefficient matrix stability

To understand the stability of the coefficient matrix, it is important to consider the variance of the covariance matrix. The covariance matrix in this case is calculated using the coefficient matrix obtained from the least squares estimate from Eq. 3.14a. An estimate for the stability, variance-covariance, is given in Eq. 4.23. The expected outcome is that, the lower the variance-covariance, the more stable the coefficient matrix is. As such, the variability within the coefficient matrix is less.

$$\text{Var}(\hat{\mathbf{W}})_r = (\mathbf{F}(\mathbf{X})^{\text{T}}\mathbf{F}(\mathbf{X}))^{-1}\sigma_r^2 \tag{4.23}$$

where σ_r^2 is an estimation of the variance of the r-DSF. This variance is calculated in Eq. 4.24.

$$\tilde{\sigma}_r^2 = \frac{1}{N - p_{2,r} - 1}\sum_{n=1}^{N}\tilde{\alpha}_{n,r}^2 \tag{4.24}$$

The $N - p_{2,r} - 1$ in the above equation allows for an unbiased estimate of σ^2, such that $E(\hat{\sigma}^2) = \sigma^2$ [216].

4.7 Chapter summary

The purpose of this chapter was to address a number of problems, or drawbacks, relating to the implementation of a multivariate nonlinear regression methodology. Two different types of overfitting , overfitting of model order and overfitting of model parameters, were identified in the previous chapter, and methods to overcome these were presented in this chapter. Firstly, the problem of choosing which parameters to use in the regression model was addressed through a number of approaches. Similarly, the problem associated with model order was also discussed. A nonlinear forward stepwise regression was then proposed to tackle the two previously discussed problems, as well as addressing the issue with correlated input variables.

The second half of the chapter sought to define measures to evaluate the performance of the proposed method. Firstly, it was compared to a different optimisation procedure. The Lasso regression is a good comparison to the nonlinear forward stepwise regression since it too is a stepwise procedure, except it operates in the opposite direction. Following this, a new version of the outlier analysis is proposed based on the variances in the training data, as opposed to its covariance. Finally, statistical measures are used to conclude on the improvement of the proposed methods.

5 | Industrial Case Study: Vestas V27 Wind Turbine Blade

In this chapter, the methodology described in Chapter 3 will be applied to data taken from a real structure. To gain a true understanding of how the methods perform, they must be tested on real data where the data is more stochastic and subject to more uncertainty. For the real data, the methods will be combined with the practical aspects that were laid out in Section 4.3. A detailed description of the Vestas V27 experiment will be given first, followed by the results and a discussion of the applied methodology. Further benchmark methods are used to validate and quantify the impact of the proposed methodology. The results presented in this chapter are taken from my previously published work [103], as well as the manuscript that is under review.

5.1 Experimental set-up

The primary data set for this thesis is provided from an experiment carried out on an operational Vestas V27 wind turbine, see Fig. 5.1a, in Denmark, north-west of Copenhagen. The work was undertaken as a collaboration between the Technical University of Denmark and the measurement company Brüel & Kjær. This particular data set has become a baseline for researchers working on VSHM in relation to wind turbine blades with many previous works being completed on it [28, 32, 176, 189, 217]. A number of these works contain a description of the experiment but it will also be included in this work for completeness.

(a) (b)

Figure 5.1: (a) Image of instrumented V27 wind turbine blade used during experiment and (b) damage introduced to trailing edge of blade.

For the experiment, one of the turbine's three blades was instrumented with 12 accelerometers. Four were situated along the leading edge, four along the trailing edge and three along the spar of the blade, as shown in Fig. 5.2. In addition, another accelerometer was placed adjacent to an electro-mechanical

actuator which was fixed close to the root of the blade. The purpose of the actuator was to excite the blade to higher frequencies, ones that were unable to be excited by natural excitation. For this work, data from only 9 accelerometers was used. Data from the accelerometers found on the leading (accelerometers 1,4,7 and 10) and trailing (accelerometers 2,5,8 and 11) edges was used to create the DSFs and the accelerometer (12) closest to the actuator was used to gain information about the actuator hit itself since the signal of the impact was not available.

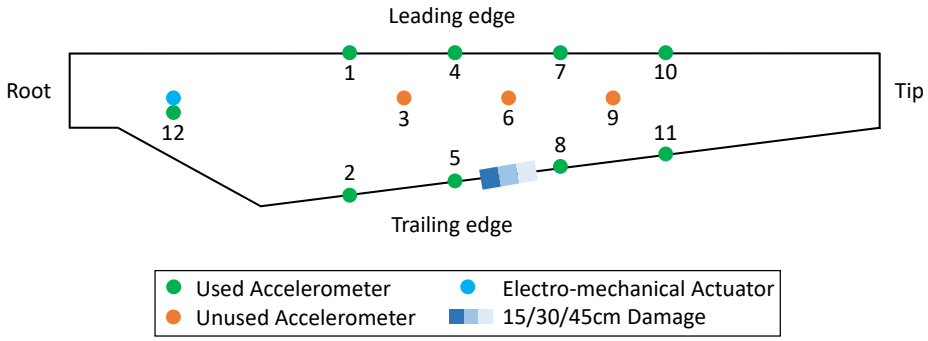

Figure 5.2: Diagram of instrumentation implemented on Vestas V27 wind turbine blade (adapted from [103]).

During the experiment, damage was introduced to the trailing edge of the blade in the form of a crack. The crack was created by debonding the upper and lower surfaces of the blade, see Fig. 5.1b, in order to emulate delamination, a common damage mechanism in wind turbine blades. This delamination represents Type 2 damage, see Section 2.4.1.2. In total, five different damage states were tested. These were: the original undamaged state, a crack of 15cm, a crack of 30cm, a crack of 45cm and a state in which the crack had subsequently been repaired. It is expected that the repaired state of the blade would perform similar, but not identical, to the original undamaged state. The increase in the crack length is a realistic evolution of the damage since it would naturally propagate through the structure. However, the propagation would not happen in steps similar to that in the experiment but, instead, would be more gradual.

The turbine that is tested is an old model of turbine. Consequently, it only operates under three different conditions, two of which are for producing energy. The operational modes are: idling, 32RPM and 43RPM. For the analysis that follows, only the acceleration data from the 43RPM operating condition is used. In future works, a method should be developed which encompasses all three of the operating modes.

5.2 Monitoring campaign

The monitoring campaign of the blade lasted from November 28-th 2014 until March 12-th 2015. As mentioned in Section 5.1, there were five different damage scenarios tested over the campaign. The three damages (15cm,30cm,45cm) were introduced on December 9-th 2014, December 15-th 2014 and January 6-th 2014 respectively. The blade was then repaired on January 19-th 2015 and the blade remained in this condition for the remainder of the campaign. The total number of observations that were available for each damage scenario are shown in Table 5.1.

Table 5.1: Total number of available observations for each damage scenario for the real wind turbine blade monitoring campaign.

Undamaged	15cm damage	30cm damage	45cm damage	Repaired
828	258	194	254	4320

During this period, the blade also experienced a range of different environmental and operational conditions. Table 5.2 shows the environmental and operational conditions that were directly measured by the SCADA system in the nacelle of the wind turbine. Additionally, Table 5.3 shows the conditions that were calculated from the measured acceleration responses. A number of different EOPs are shown in Fig. 5.3 for the duration of the campaign, for the 43RPM operating condition only. The large jumps in the values between observations

is a result of the fact that the turbine is constantly switching between operating modes and, as such, there is no continuous measurement in the 43RPM operating mode. Since some of the temperatures, among other EOPs, that are experienced by damaged states are not experienced in the initial undamaged data, it was chosen to use the repaired data in its place. Additionally, there is a lack of variation within the undamaged data.

Table 5.2: Environmental and operational conditions measured directly by the SCADA system on board the wind turbine.

Environmental	Operational
Wind speed	RPM
Temperature	Generator on/off
Wind direction	Power
Precipitation	Pitch
	Yaw

Table 5.3: Environmental and operational conditions calculated from measured acceleration responses.

Environmental	Operational
	Maximum value of actuator hit
	Standard deviation of actuator hit
	Variance of actuator hit

In an ideal case, the structure being examined would have a large number observations for training as well as being tested over a full seasonal cycle. Therefore, the repaired data was used for training and testing the models since there are significantly more observations as well as greater variability in the measured EOPs. In this work, the true undamaged observations are unused.

For each observation, recorded once every 5 minutes, the acceleration response for the actuator hit was recorded by the data acquisition system. The recording of each signal started 10 seconds before the hit and lasted for a total of 30 seconds. Since the sampling frequency of the accelerometers is 16384Hz, the 30 second recording corresponds to almost 500,000 data points. Fig. 5.4a

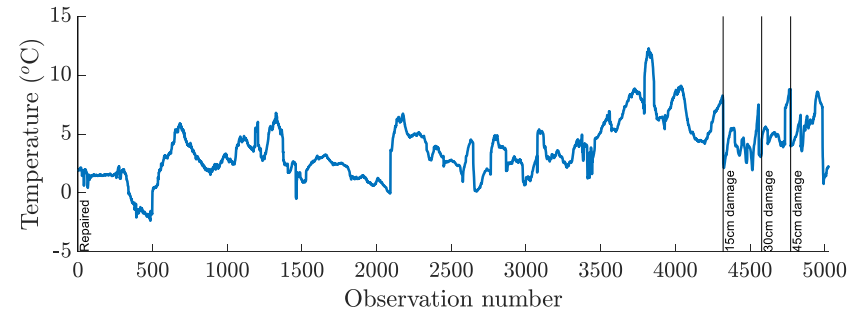

(a)

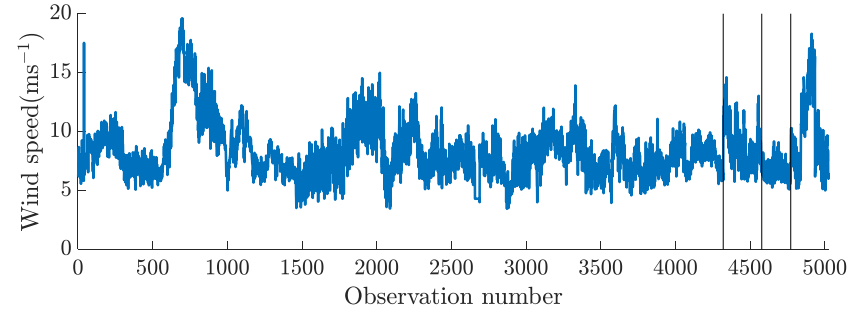

(b)

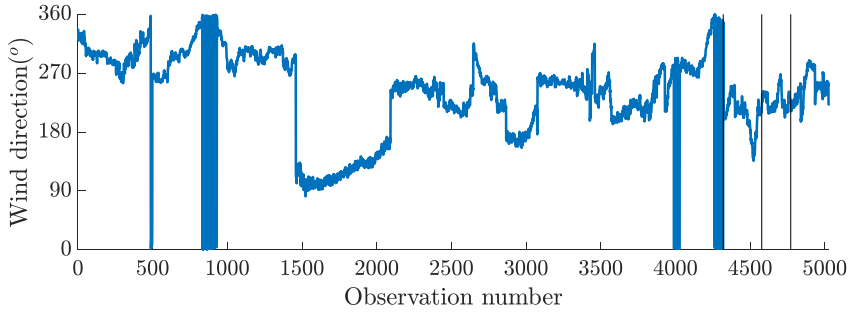

(c)

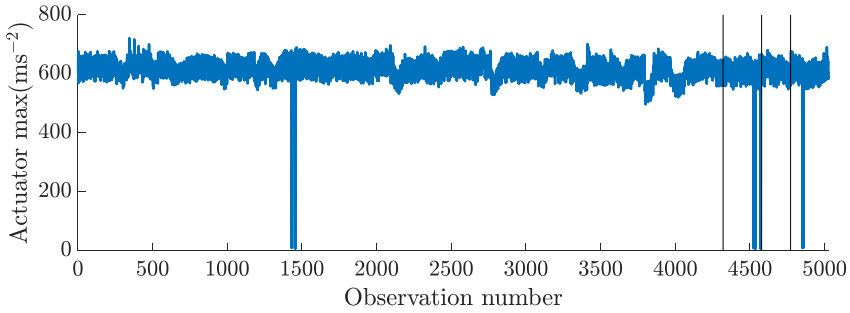

(d)

Figure 5.3: Variation of EOPs over the monitoring campaign: (a) Temperature, (b) wind speed, (c) wind direction and (d) actuator max. N.B. the observations are not in chronological order, the undamaged observations have been replaced by the repaired.

shows an example accelerometer response, with Fig. 5.4b giving a more detailed view of the moment the actuator strikes and the corresponding decay of the signal. For each acceleration signal, the responses were aligned based on the maximum amplitude experienced following the impact of the actuator.

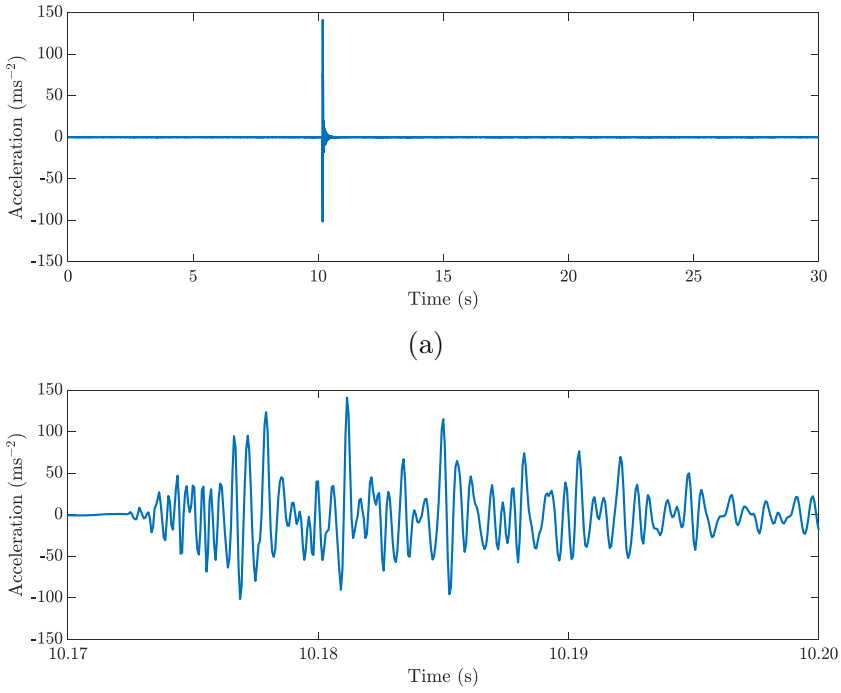

Figure 5.4: An example acceleration response from the Vestas V27 wind turbine over (a) 30 seconds and (b) 0.03 seconds. Each 30 second interval is classed as one observation.

5.3 Methodology performance

The aim of this section is to demonstrate the importance of including the considerations laid out in Chapter 4. A new VSHM system will be created by following the sections of Chapter 4, starting from the beginning. Figures will be used throughout to illustrate the effect that each stage has on the overall performance of the VSHM system. Before doing so, however, the DSFs that will be used for this case study must be defined.

5.3.1 Frequency transformation based features

The DSF used in this case study is the *Frequency Transformation Based Feature* (FTBF). Whilst the natural frequencies combine information from all sensors in question, the FTBF considers the responses of each sensor separately. The benefit of using a DSF of this type is that it utilises information on a local level which can lead to more sensitive damage detection. Additionally, the natural frequencies are hard to define in a system subjected to such varying conditions. Consequently, the FTBF has less immediate physical meaning than the natural frequencies. However, the frequency transformation still contains a large amount of information that is used in the derivation of the natural frequencies and actually contains additional information about less significant peaks.

To start the derivation of this DSF, the primary information obtained from the structure must be examined. The vibration response for a single observation, with J sensors, can be found in Eq. 5.1.

$$\mathbf{Y}_n = \begin{bmatrix} \mathbf{y}_{n,1} & \mathbf{y}_{n,2} & \cdots & \mathbf{y}_{n,j} & \cdots & \mathbf{y}_{n,J} \end{bmatrix} \tag{5.1}$$

where $\mathbf{Y}_n$ is the overall representation of the time series for the n-observation and $\mathbf{y}_{n,j}$ is the time series from the j-sensor of the n-time series.

Since the FTBF considers the contribution of each sensor individually, it makes practical sense to rearrange the information to be grouped by sensor rather than observation. The matrix in Eq. 5.2 reflects this change.

$$\mathbf{Y}_j = \begin{bmatrix} \mathbf{y}_{1,j} & \mathbf{y}_{2,j} & \cdots & \mathbf{y}_{n,j} & \cdots & \mathbf{y}_{N,j} \end{bmatrix} \tag{5.2}$$

where $\mathbf{Y}_j$ is the overall representation of the time series for the j-sensor and N is the number of observations.

Once the time series are in the form of Eq. 5.2, a Fourier transform is performed on the matrix. The Fourier transform brings the information in the time

series from the time domain into the frequency domain. In doing so, a complex vector is created. The new complex vector has the same length as the time series but it is mirrored so the second half can be immediately discarded. The real component and the real part of the complex component can be concatenated to create a vector of equal length to the time series. This process is summarised in Eqs. 5.3.

$$\mathbf{y}'_{n,j} = \mathrm{FT}(\mathbf{y}_{n,j}) \tag{5.3a}$$

$$\mathbf{y}'_{n,j} = (\Re\mathbf{y}'_{n,j} + i\Im\mathbf{y}'_{n,j}) \tag{5.3b}$$

$$\mathbf{y}''_{n,j} = (\Re\mathbf{y}'_{n,j}\Im\mathbf{y}'_{n,j})^{\mathrm{T}} \tag{5.3c}$$

where FT is the Fourier transform, $\mathbf{y}'_{n,j}$ is the first transformation of $\mathbf{y}_{n,j}$, $\Re\mathbf{y}'_{n,j}$ and $\Im\mathbf{y}'_{n,j}$ are the real and imaginary parts of $\mathbf{y}'_{n,j}$ respectively, i is equal to $\sqrt{-1}$ and $\mathbf{y}''_{n,j}$ is the concatenation of $\mathbf{y}'_{n,j}$.

The transformed data vectors can once again be grouped according to sensor, as in Eq. 5.4.

$$\mathbf{Y}''_j = \begin{bmatrix}\mathbf{y}''_{1,j} & \mathbf{y}''_{2,j} & \dots & \mathbf{y}''_{n,j} & \dots & \mathbf{y}''_{N,j}\end{bmatrix} \tag{5.4}$$

PCA is then used to reduce the dimension of matrix $\mathbf{Y}''_j$ by calculating the transformation matrix. A full explanation of PCA can be found in Section 3.2.1. Once a transformation matrix has been determined for each sensor, any observation can be projected. The overall DSF vector for each observation is then created by concatenating the individual contributions from each sensor, as shown in Eq. 5.5.

$$\boldsymbol{\alpha}_n = \begin{bmatrix}\boldsymbol{\alpha}_{n,1} & \boldsymbol{\alpha}_{n,2} & \dots & \boldsymbol{\alpha}_{n,j} & \dots & \boldsymbol{\alpha}_{n,J}\end{bmatrix}^{\mathrm{T}} \tag{5.5}$$

where $\boldsymbol{\alpha}_{n,j}$ is the projection from the j-sensor of the n-observation.

A summary of this process is given diagrammatically in Fig. 5.5.

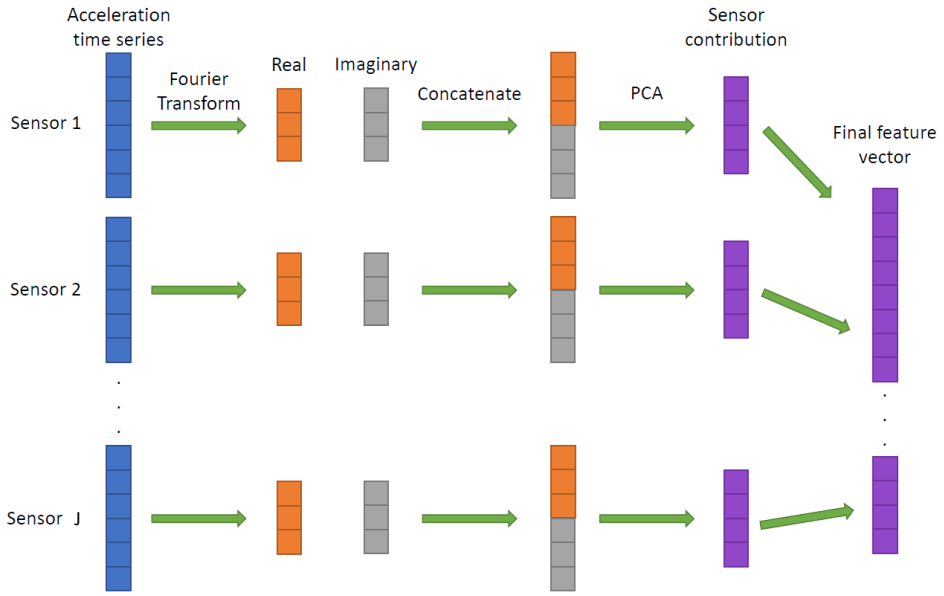

Figure 5.5: Schematic representation of the derivation of the frequency transformation based feature for each observation [103]. NB: the PCA transformation is based on all the observations available in the training condition.

As with the illustrative example from Section 3.4, it is important to check whether there exists any relationships between the DSFs and the EOPs. Fig. 5.6 gives examples of different DSFs and their relationships with an EOP. While only one relationship is shown, it does not mean that there are no other EOPs that affect the particular DSF. Temperature is used most often here since it is expected that it will have the largest influence.

5.3.2 Creating a baseline

In order to demonstrate the importance of each of the aspects discussed in Chapter 4, it is first necessary to produce a baseline from which to compare the new results. To do so, a simple and easily applied regression model will be used. In total, 5 EOPs will be used to model the DSFs: temperature, wind speed, azimuth angle, maximum value of the actuator hit and the standard deviation (STD) of the actuator hit. The order of each of the EOPs is arbitrarily set to

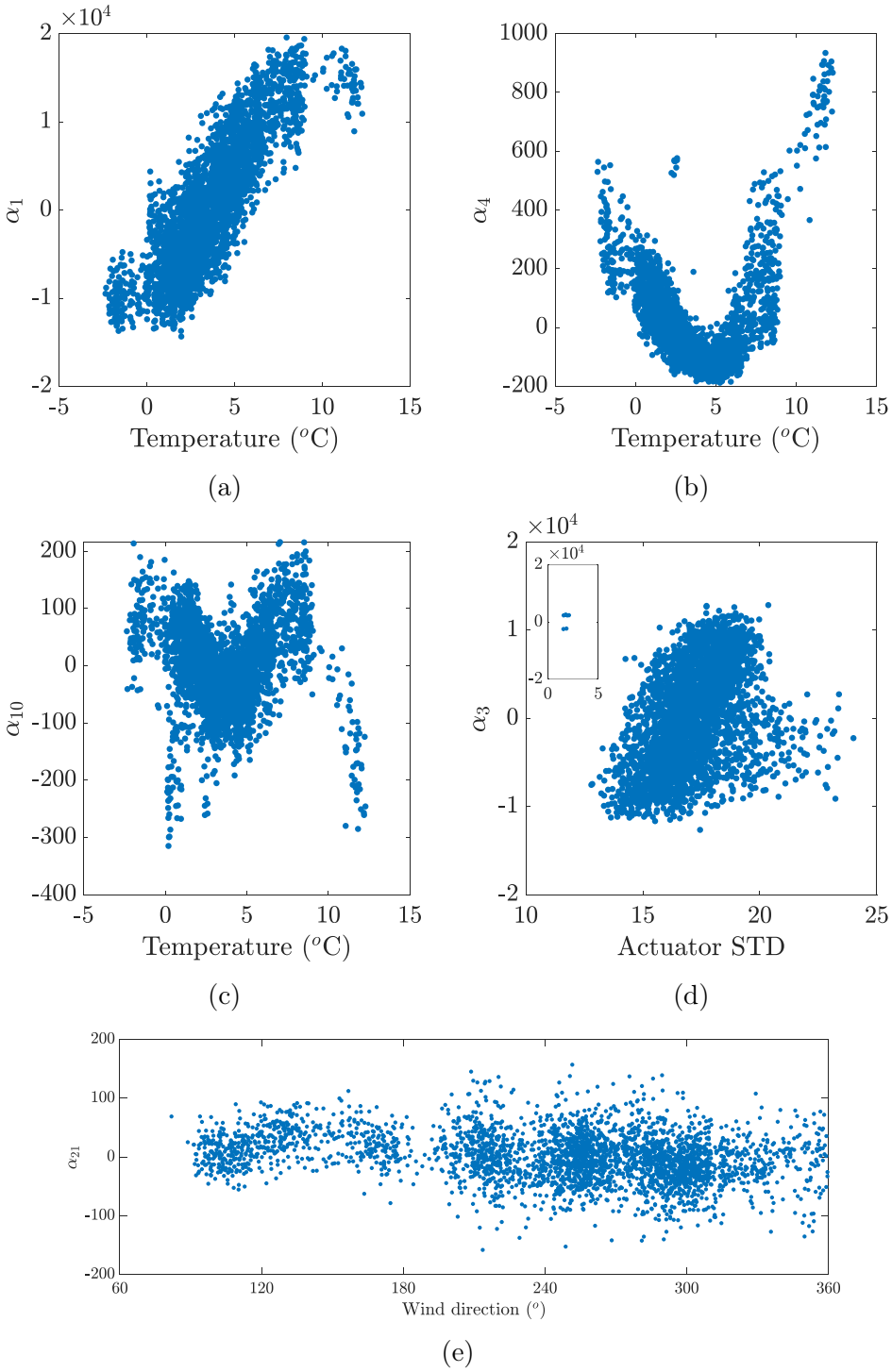

Figure 5.6: Figures displaying relationships between DSFs (from the undamaged condition) and EOPs. (a) α_1 and temperature, (b) α_4 and temperature, (c) α_{10} and temperature, (d) α_3 and actuator standard deviation and (e) α_{21} and wind direction.

3. The total number of DSFs to be modelled is 800, the first 100 projections from each of the 8 sensors.

In addition to the regression baseline model, the result of the implicit model should also be studied. If the regression models cannot outperform the implicit model, then there is no benefit to applying the more complex system. Fig. 5.7a shows the resulting control chart when only PCA is applied and Fig. 5.7b when those DSFs are regressed.

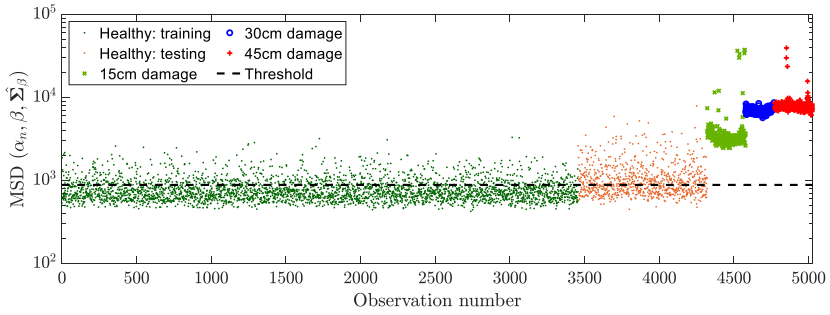

(a)

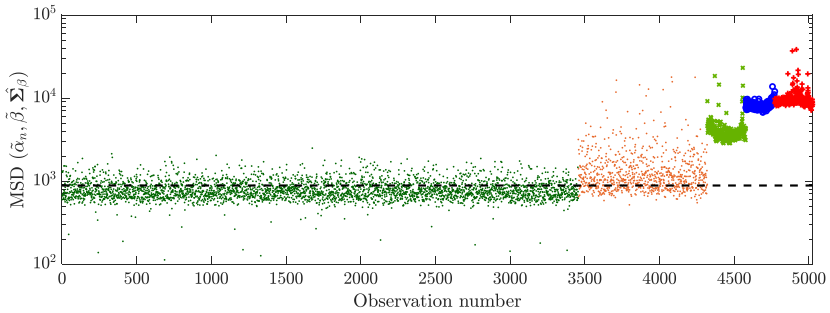

(b)

Figure 5.7: Control charts showing (a) just the implicit method applied ($\boldsymbol{\alpha}_n \in \mathbb{R}^{800}$) and (b) regression corrected DSFs based on 5 EOPs with order 3 ($\tilde{\boldsymbol{\alpha}}_n \in \mathbb{R}^{800}$, ξ_1 = temperature, ξ_2 = wind speed, ξ_3 = azimuth, ξ_4 = actuator max, ξ_5 = actuator STD, all orders = 3). Threshold calculated to represent 98% of values in the training data according to a Chi-squared distribution

There are many important differences between Fig. 5.7a and Fig. 5.7b. Starting with the training observations, the first aspect to notice is that the false positives in the training set do not tend as far from the threshold in the explicit DSFs compared to the implicit DSFs. However, there are far more false positives

in the validation set for the explicit DSFs. The reason for both of these effects is most likely due to the overfitting of the training data in the explicit model. By using 5 EOPs, the regression model is forced to create coefficients that end up fitting to the micro-trends that exist in the training data. To illustrate this more clearly, the predicted values are plotted on to a measured DSF,α_{10}, in Fig. 5.8.

Fig. 5.8a shows how well the predicted values match the measured values for α_{10}. The predicted values encapsulate the trend of the measured data, as the regression model should do. However, there are many points that deviate from the general trend, as highlighted by the boxes in Fig. 5.8b. This figure shows that the predicted try to follow these irregularities from the trend. It is difficult to know whether these irregularities arise from derivation of the DSF or as a result of another EOP. While these trends are captured by the model, the consequence on future predictions can be observed in Fig. 5.8c and Fig. 5.8d, where α_{10} is plotted for the testing data. In the regions highlight from Fig. 5.8b, the observations are no longer well predicted. Fig. 5.8d shows the more severe consequences of this overfitting, with observations appearing very far from the trend. While this does not seem like a significant problem, this is just a demonstration from a single DSF, 1 of 800. This problem will, therefore, multiply causing more substantial problems further on. The robustness of future predictions is incredibly important for a system to be trusted to make reliable estimates.

Returning to Fig. 5.7, there are also subtle differences that exist in the observations from the damaged conditions. The first effect can be seen by looking into the shape of the individual damage scenarios. Where there was little to no trend visible for the implicit features, there now is one present in the explicit DSFs. Specifically, there is now an upward trend at the end of the 30cm damage observations and a kind of arcing in the 45cm damage observations. This effect is, again, likely attributed to the overfitting of the training data. In

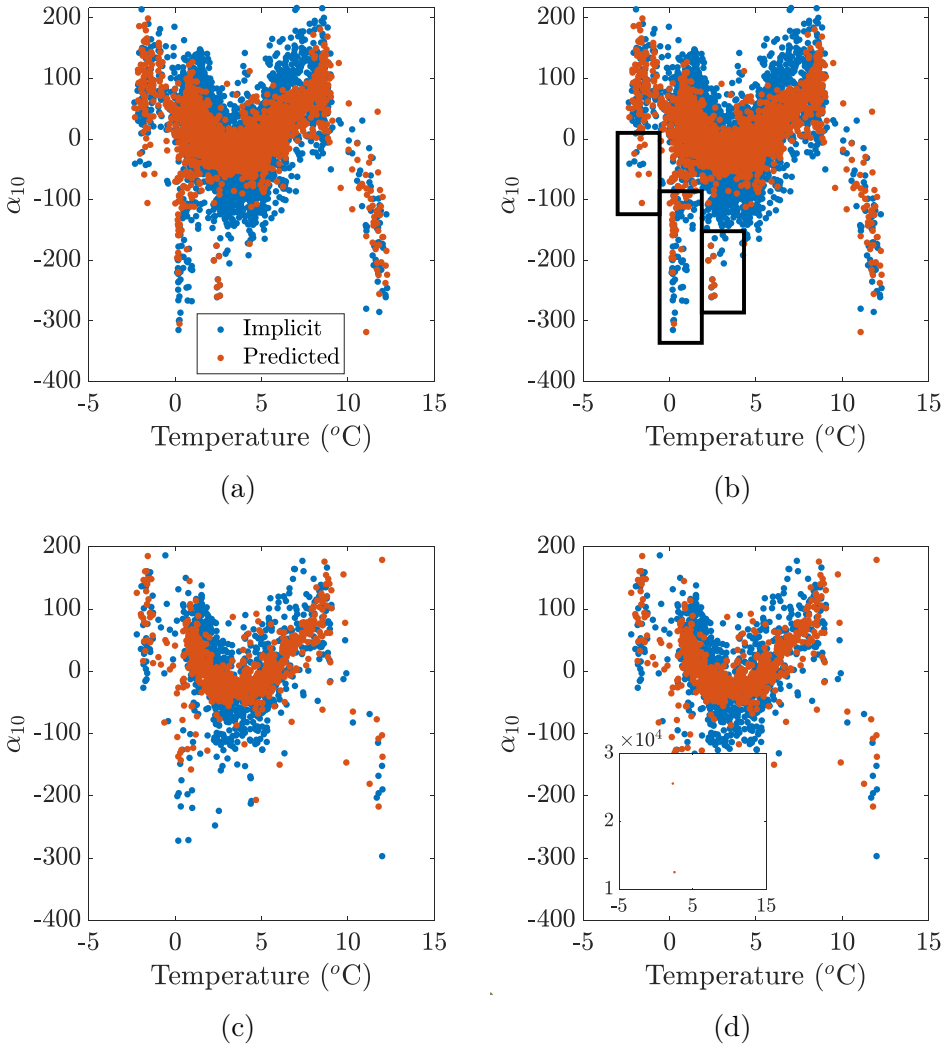

Figure 5.8: Figure demonstrating the consequences of overfitting regression model for α_{10}. (a) α_{10} from training data with superimposed predicted values, (b) α_{10} from training data with superimposed predicted values with boxes highlighting deviations from main trend, (c) α_{10} from testing data with superimposed predicted values and (d) α_{10} from testing data with superimposed predicted values with full range.

addition to this effect, there is also a slight upward shift of all the damaged observations. Whilst this could be a positive effect of increased sensitivity to damage, it is more likely the result of an introduced bias. The reason that this conclusion is more likely is due to the fact that the validation set also shifts upward for the explicit DSFs. As a whole then, the implicit features perform better than the explicit. However, with more intelligent design of the regression models using considerations from Chapter 4, the performance of the explicit DSFs should improve.

5.3.3 Environmental and operational parameter selection

From Fig. 5.7, it is clear that forcing the model to use 5 EOPs is not a good decision, at least for the given order. Therefore, it is sensible to apply a method that can be used to identify which of the EOPs are the most influential. The first option that was presented in Section 4.1 was to look at the SCADA data and see which DSFs are sensitive to which EOPs. However, given that there are 800 DSFs and 5 EOPs in the baseline case, that would mean analysing 4000 individual relationships. Thus, this is not a practical solution in this case.

A more appropriate method from Section 4.1 to test, then, is looking into the sensitivity analysis approach. Fig. 5.9 shows the results for both the exclusive and inclusive sensitivity analyses. To reiterate the interpretation of the sensitivity analysis from Table 4.1, when the sensitivity is high in the exclusive study, the suggestion is that the regression model cannot predict well without the presence of the corresponding EOP. On the contrary, if the sensitivity is high for the inclusive study, it suggests that the inclusion of the EOP only adds to the uncertainty in the regression model.

From Fig. 5.9a, temperature appears to have the largest influence on the DSFs, given the higher values for the sensitivity. Simultaneously, the sensitivity values for the temperature are lowest in the inclusive study from Fig. 5.9b. The combination of these results implies that temperature is a key EOP, and that it

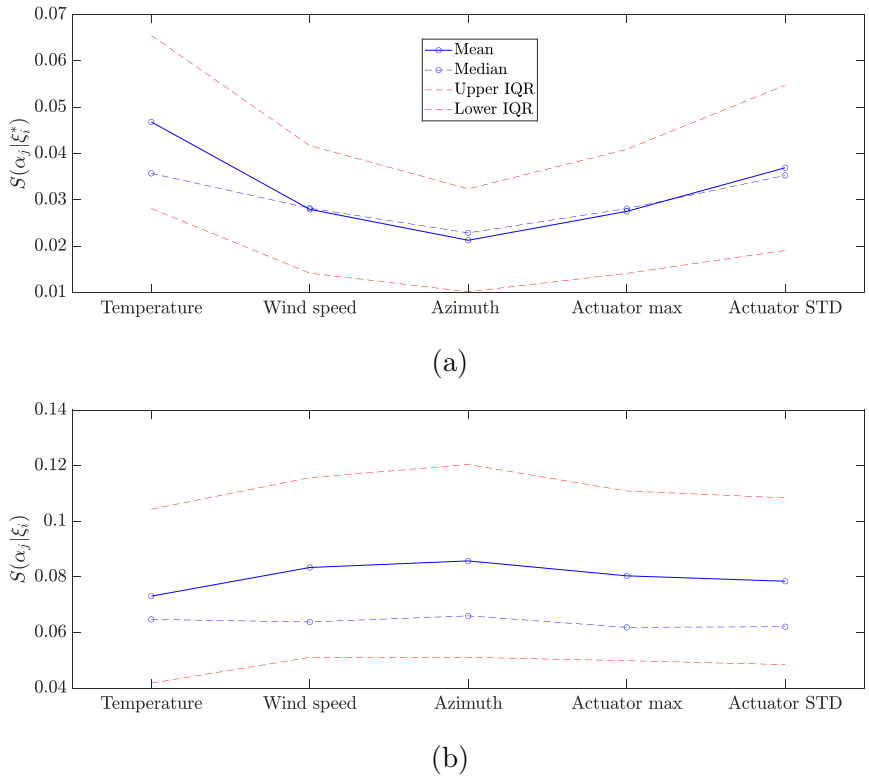

Figure 5.9: Sensitivity analysis for baseline study fitted with 5 EOPs with order 3. (a) Exclusive study and (b) inclusive study.

should be included in the regression models. This result is somewhat expected given its known physical relationship with the stiffness, which can substantially change the vibrational characteristics of the structure. An interesting point to note here is that there is a visible change in the overall trend in the DSFs below 0°C and above 10°C in Fig. 5.6a, Fig. 5.6b and Fig. 5.6c. The differing trend could be a result of the stiffness changing to the point that new distinctive vibrational frequencies are being excited.

Another notable point from Fig. 5.9 is that the maximum value of the actuator hit seems to be less influential than the STD of the hit. The STD value has both, a larger exclusive sensitivity and a lower inclusive sensitivity. Whilst the two values are likely related, there is a notable difference in their sensitivities. Studying Fig. 5.9 also shows that wind speed has a similar level influence as the actuator maximum. The azimuth angle has the least influence of the selected

EOPs. While it has the lowest exclusive and highest inclusive sensitivities, it does not mean that it has no influence at all. It simply means it has the lowest influence relative the other selected EOPs.

At this point, it is useful to compare back to the baseline case to see how removing EOPs affects the results. In the control chart in Fig. 5.10, 2 EOPs are used to model all of the DSFs, namely temperature and actuator max.

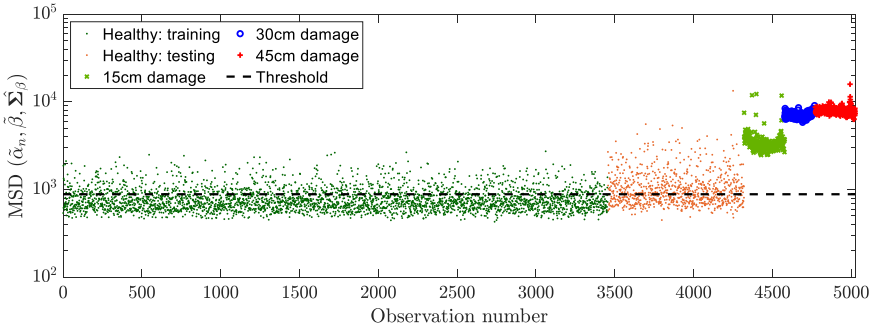

Figure 5.10: Control chart showing the explicit procedure with regression corrected DSFs based on 2 EOPs with order 3 ($\tilde{\boldsymbol{\alpha}}_n \in \mathbb{R}^{800}$, ξ_1 = temperature, ξ_2 = actuator max, both EOP's regression orders = 3). Threshold calculated to represent 98% of values in the training data according to a Chi-squared distribution

Comparing now between Fig. 5.7b and Fig. 5.10, the beginnings of some improvement is already visible. Firstly, there is less distribution among the training observations. Specifically, there are no negative outliers in the distribution of training observations in Fig. 5.10. The most significant difference, however, can be seen in the testing observations. In Fig. 5.10, there is a much greater agreement in the MSD between the training and testing. The ROC curve in Fig. 5.11 confirms this noticeable improvement. Additionally, the trends that seemed to be exaggerated in Fig. 5.7b, are no longer present in Fig. 5.10.

Given that the training and testing should be as similar as possible, the desired similarity curve should follow the diagonal between 0 and 1. Fig. 5.11 shows that there is actually very little similarity between the training and testing when 5 EOPs were used in the regression. This result is significant and should be reflected in a change in the design of the system. Whilst the ROC curve

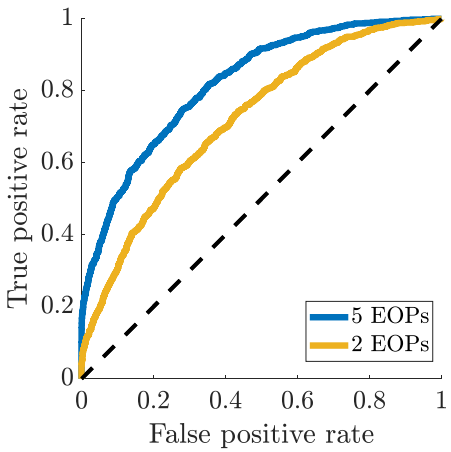

Figure 5.11: Similarity curves for crossover between training and testing for the regressed features corrected with 5 EOPs ($\tilde{\boldsymbol{\alpha}}_n \in \mathbb{R}^{800}$, ξ_1 = temperature, ξ_2 = wind speed, ξ_3 = azimuth, ξ_4 = actuator max, ξ_5 = actuator STD, all orders = 3) and 2 EOPs ($\tilde{\boldsymbol{\alpha}}_n \in \mathbb{R}^{800}$, ξ_1 = temperature, ξ_2 = actuator max, both EOP's regression orders = 3).

for the 2 EOP case is not perfect, it is still much closer to the ideal scenario. Although this simple improvement is substantial, there is still more improvement necessary to have a robust system.

With the application of a sensitivity analysis, it is possible to identify which EOPs have the largest influence. However, the study can be somewhat limited. Firstly, the EOPs perceived to have the highest influence is a generalised statement across all of the DSFs. Whereas, each DSF may be affected differently by different EOPs. By removing the low sensitivity EOPs from the regression models, a type of bias will be introduced that will poorly predict the DSFs that are not influenced by the remaining EOPs. Nonetheless, the improvements gained by not overfitting EOPs into the models shows that there is value to carefully selecting which EOPs should be used for modelling. For the sensitivity analysis to be used for this purpose, it would need to be automated in a sensible manner given the large number of DSFs.

5.3.4 Optimisation of model order

In addition to the overfitting of EOPs into the system, it is also possible to overfit the order of the variables within the model. Selecting the correct order is critical to creating representative models. In the particular case study being analysed, manually selecting the orders of each DSF would be too time consuming and, therefore, not possible. Similarly, selecting orders arbitrarily, instead of looking into each DSF, can also cause problems with overfitting. As an example, the orders of the temperature and actuator STD, from the 2 EOP example, are increased from 3 to 20. The control chart for this is shown in Fig. 5.12.

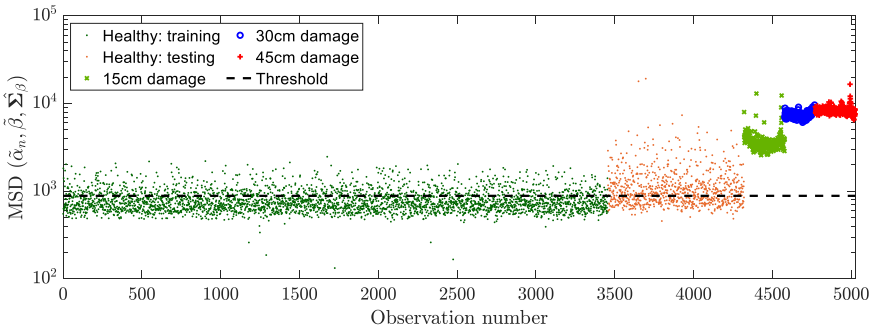

Figure 5.12: Control chart showing the explicit procedure with regression corrected DSFs based on 2 EOPs with order 20 ($\tilde{\boldsymbol{\alpha}}_n \in \mathbb{R}^{800}$, ξ_1 = temperature, ξ_2 = actuator max, both EOP's regression orders = 20). Threshold calculated to represent 98% of values in the training data according to a Chi-squared distribution

When comparing Fig. 5.10 and Fig. 5.12, there are not that many differences between them. However, there are some subtle but significant aspects that must be addressed. The first of which is that the positive outliers in the training data have compressed relative to the main distribution while simultaneously creating negative outliers that were not previously present. The combination of these factors could be a sign of overfitting. There is little change in the damage, except for the increase in a few of the observations. Again, likely a consequence of overfitting. There is also a slight shift upward in the testing data, along with more extreme outliers becoming present. The similarity curves in Fig. 5.13 show

how the overlap between training and testing has changed between model orders 3 and 20.

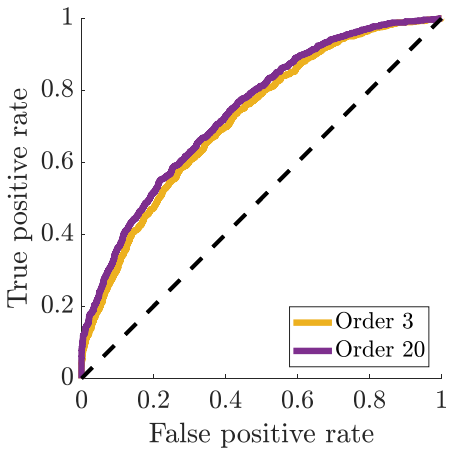

Figure 5.13: Similarity curves for crossover between training and testing for the regressed features corrected with model order 3 ($\tilde{\boldsymbol{\alpha}}_n \in \mathbb{R}^{800}$, ξ_1 = temperature, ξ_2 = actuator max, both EOP's regression orders = 3) and 20 ($\tilde{\boldsymbol{\alpha}}_n \in \mathbb{R}^{800}$, ξ_1 = temperature, ξ_2 = actuator max, both EOP's regression orders = 20), both with 2 EOPs.

From Fig. 5.13, it can be seen that when the model order is equal to 3, there is more overlap between training and testing. Therefore, by increasing the model order to 20, the effectiveness of the system has been reduced. Whilst the reduction is not significant, it is still consequential and should be avoided where possible.

Once again, by studying α_{10}, it is possible to see evidence of overfitting. Fig. 5.14a shows the measured and predicted values for α_{10} for the model made of 2 EOPs at order 20. As with before, the presence of overfitting variables has caused the system to model points that are most likely irrelevant to the trend. In the case, it is the higher order terms that have caused this as opposed to the additional non-influential EOPs. Fig. 5.14b illustrates the drop off in the magnitude of the coefficients from the regression model.

Studying the mean magnitude of the coefficients in Fig. 5.14b, it can be seen that the values drop off significantly. This happens to the point where the

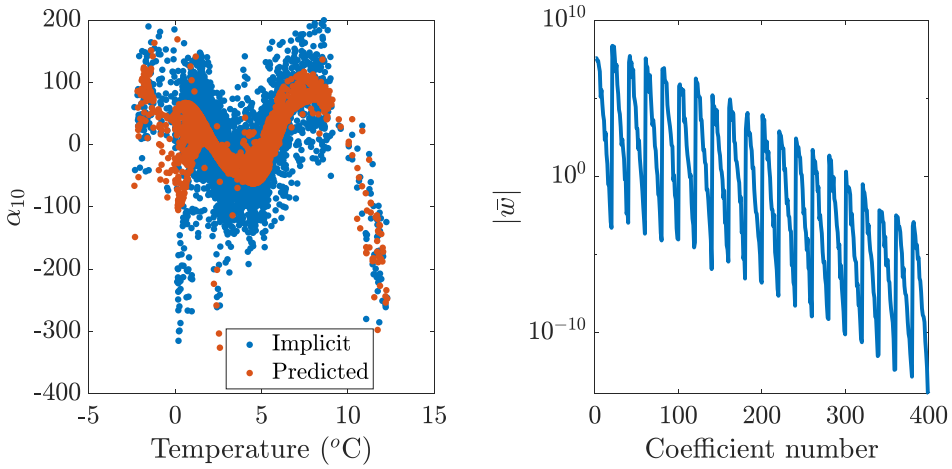

(a) (b)

Figure 5.14: (a) α_{10} from training data with superimposed predicted values from regression model with 2 EOPs at order 20 (ξ_1 = temperature, ξ_2 = actuator max, both EOP's regression orders = 20). (b) The mean of the magnitude of the coefficients of the regression model associated with α_{10}

.

higher order coefficients are a factor of 10^{10} smaller. The consequence of this is likely that the higher order coefficients are trying to model the irregularities from the trend. The result of this can be seen in Fig. 5.14a, where the model has tried to match exactly to the observations rather than modelling the more significant trend. The results for this case reflect the same phenomenon that was found in Section 3.4. Additionally, using more coefficients increases the overall computational complexity, a further downside.

Instead of using manual order selection, or choosing arbitrary values, it is possible to optimise the model order through testing all possible model orders over a given range for each EOP, as discussed in Section 4.2.2. As mentioned here, this method does not prevent overfitting outright, but instead finds the best combination of model orders for the regression. Since this method works on an automatic basis, it is also possible to create models with differing orders for each DSF. Consequently, it makes sense to reintroduce the EOPs so that their orders can be tailored accordingly.

For the example of testing all possibilities, a total of 5 EOPs (the same ones as the baseline) up to order 5 will be used. The resulting control chart from this method is shown in Fig. 5.15.

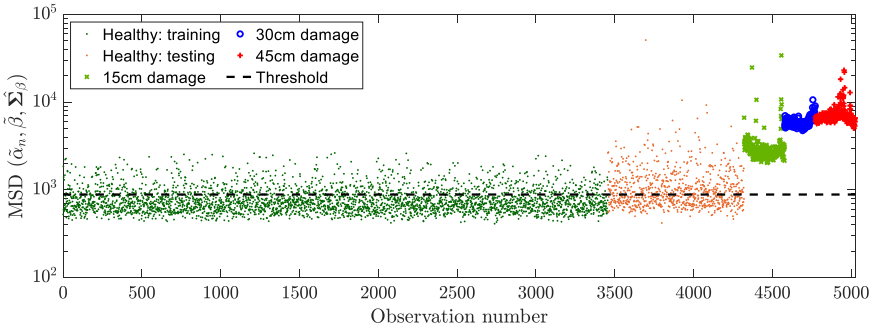

Figure 5.15: Control chart showing the explicit procedure with regression corrected DSFs based on 5 EOPs with model orders optimised with a testing all possibilities approach ($\tilde{\boldsymbol{\alpha}}_n \in \mathbb{R}^{800}$, ξ_1 = temperature, ξ_2 = wind speed, ξ_3 = azimuth, ξ_4 = actuator max, ξ_5 = actuator STD, orders vary based on optimisation). Threshold calculated to represent 98% of values in the training data according to a Chi-squared distribution

In order to have a fair comparison, Fig. 5.15 will be compared to Fig. 5.7b. Since this section is to show the effect of model order, it makes sense to compare to a model which has 5 EOPs fitted. There are many similarities between the two figures, the separation between undamaged and damaged observations is good and the distribution of the damaged observations are alike. However, the most important difference is the general shift downward of all points. This especially important in the testing observations, as these diverged significantly before. The control chart in Fig. 5.15 is actually much more similar to the one in Fig. 5.10. The ROC curves in Fig. 5.16 show the overlap of training and testing for 2 EOPs order 3 and testing all possibilities.

Firstly, from Fig. 5.16a, the testing all possibilities approach has a substantially better overlap of the training and testing observations than the 5 EOP with order 3 approach. This result indicates that the choice of model order is extremely important in fitting the data. The other possibility is that the model order for the non-influential parameters has stayed low, effectively reducing the

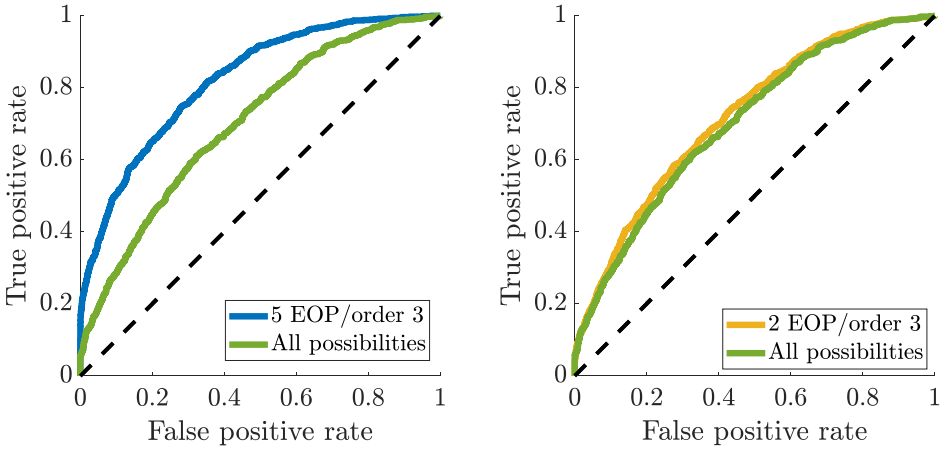

(a) (b)

Figure 5.16: Similarity curves for training and testing for: (a) 5 EOPs model order 3 ($\tilde{\boldsymbol{\alpha}}_n \in \mathbb{R}^{800}$, ξ_1 = temperature, ξ_2 = wind speed, ξ_3 = azimuth, ξ_4 = actuator max, ξ_5 = actuator STD, all orders = 3) and testing all possibilities and (b) 2 EOPs model order 3 ($\tilde{\boldsymbol{\alpha}}_n \in \mathbb{R}^{800}$, ξ_1 = temperature, ξ_2 = actuator max, both EOP's regression orders = 3) and testing all possibilities ($\tilde{\boldsymbol{\alpha}}_n \in \mathbb{R}^{800}$, ξ_1 = temperature, ξ_2 = wind speed, ξ_3 = azimuth, ξ_4 = actuator max, ξ_5 = actuator STD, all orders vary based on optimisation).

influence of them being included in the model, but not completely. However, the most significant result comes from Fig. 5.16b. This figure shows that the testing all possibilities approach is still marginally better than the 2 EOPs with order 3 approach. Again, this could suggest the importance of the model order for fitting influential EOPs. Opposingly, it could be a result of the influential EOPs being allowed to be modelled for each DSF.

In this section, it has been shown that the choice of model orders is critical in the design of the regression models. Using a method that tests every combination of model order allowed for better damage detection performance, despite some non-influential EOPs still being modelled. What is needed, then, is a method that is automatically capable of determining which EOPs are influential and what order they should be modelled at. This method is particularly important in cases where the DSFs are high dimensional and there are a large number of EOPs available. In these cases, testing all the possibilities becomes

impossible as the dimension of the matrices becomes too large. Therefore, the method also needs to work in an efficient manner so that it does not require expensive computing resources to operate.

5.3.5 Nonlinear forward stepwise regression

The concept of the nonlinear forward stepwise regression was designed to fill the need that was identified in the previous section. One of the advantages of the nonlinear forward stepwise regression procedure is its efficiency. This makes it possible to test more EOPs than before and to a higher order. It makes sense to include as many EOPs as available since the method is capable of choosing only the ones that are influential. It bypasses the need to check each one to determine its influence. For the nonlinear forward stepwise regression, a total of 10 EOPs are used: temperature, wind speed, pitch, wind direction, precipitation, azimuth angle, operating RPM, the maximum value of the actuator hit, the STD of the actuator hit and the variance of the actuator hit.

5.3.5.1 Removing correlated variables

The first new aspect that the methodology brings is the search for correlated input variables. Fig. 5.17a shows a heat-map of the normalised mutual information between each of the 10 EOPs. It can be seen that there is an exact correlation (=1) between the standard deviation of the actuator hit and the variance of the actuator hit, see Fig. 5.17c. Due to their co-nonlinearity, the actuator variance was removed from the nonlinear forward stepwise procedure. The primary reason for the removal of the variance over the STD is because it has slightly higher correlations with other EOPs. There are a few other correlated variables which would be expected to be seen. For example, the wind speed and blade pitch (see Fig. 5.17d) or the wind direction and the temperature.

The PCC has been included in Fig. 5.17b for comparison. Since the PCC is a measure of the linear relationship of two variables, it is only able to identify

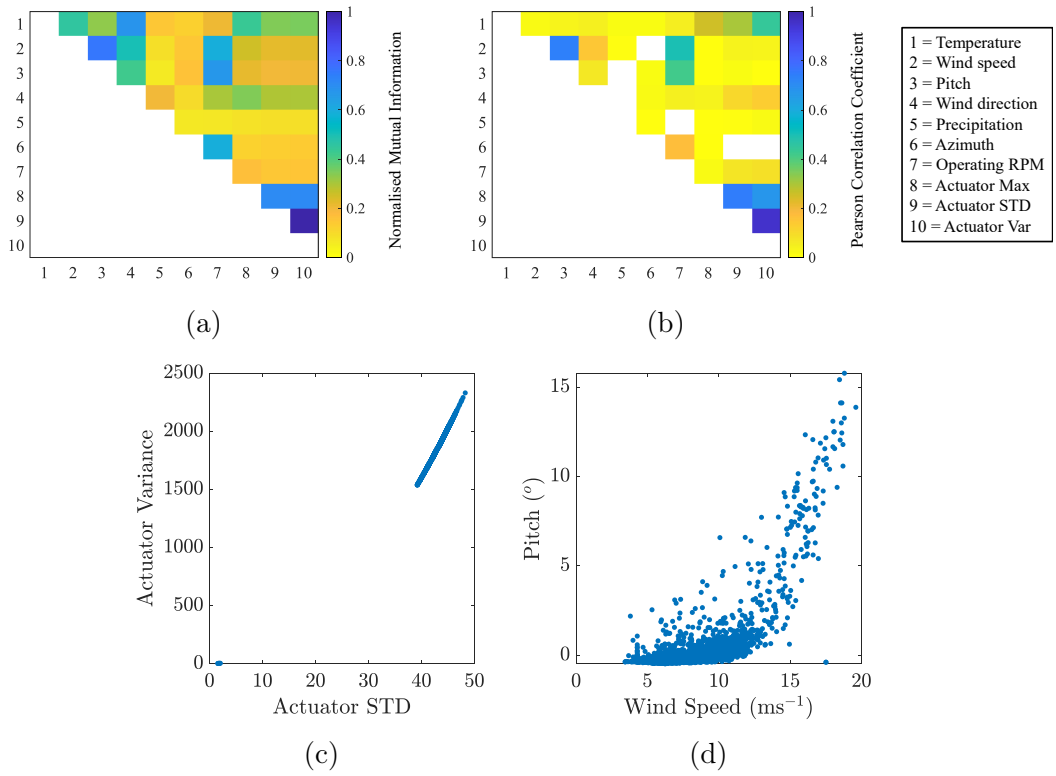

Figure 5.17: (a)Heat-map of the average mutual information between each of the 10 input variables, (b) Heat-map of the Pearson Correlation Coefficient between each of the 10 input variables, (c) Actuator variance plotted against actuator standard deviation and (d) Pitch of blade plotted against wind speed.

strongly linearly correlated inputs. However, the relationship between inputs is often nonlinear. As such, the PCC would still remove the actuator variance but does not establish more complex relationships such as that between the temperature and wind direction, one that is identified using mutual information. In this work, both the mutual information and PCC would have removed the same variable but in other cases, more complex relationships might be missed that affects the quality of the regression. For use with nonlinear models, mutual information should be used since it is capable of identifying nonlinearly correlated variables.

5.3.5.2 Initial performance

Once the correlated variables have been removed, it is possible to test the performance of the optimisation method. In this instance, the order of the variables has been allowed to go to a maximum of 10. The control chart for the nonlinear forward stepwise method is shown in Fig. 5.18. Whilst the control chart does not always give the best measure of the performance, it allows an survey of the changes.

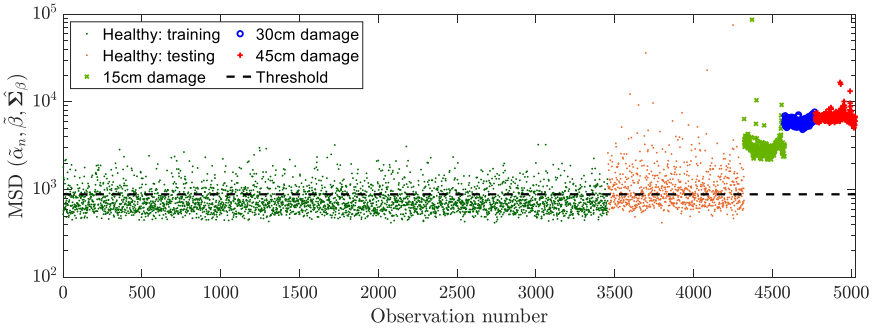

Figure 5.18: Control chart showing the explicit procedure with regression corrected DSFs ($\tilde{\boldsymbol{\alpha}}_n \in \mathbb{R}^{800}$, $\boldsymbol{\xi}_r$ and model orders vary DSF to DSF) based on a maximum of 10 EOPs with model orders optimised with a nonlinear forward stepwise procedure, maximum 10. Threshold calculated to represent 98% of values in the training data according to a Chi-squared distribution

Visually, there are not many differences between the testing all possibilities approach in Fig. 5.15 and the nonlinear forward stepwise method in Fig. 5.18. The differences in the undamaged observations is barely noticeable but there are some distinct differences in the damaged observations. Where there are quite distinct trends in Fig. 5.15, they are no longer as pronounced. To get a better quantitative measure of the differences, the ROC curves are shown in Fig. 5.19 for all the damage cases, as well as the training observations.

From Fig. 5.19, it can be seen that the performance, on a purely damage detection basis, of the nonlinear forward stepwise method is very similar to the testing all possibilities approach. The benefits of the nonlinear forward stepwise method are more subtle. The first of these being that the nonlinear

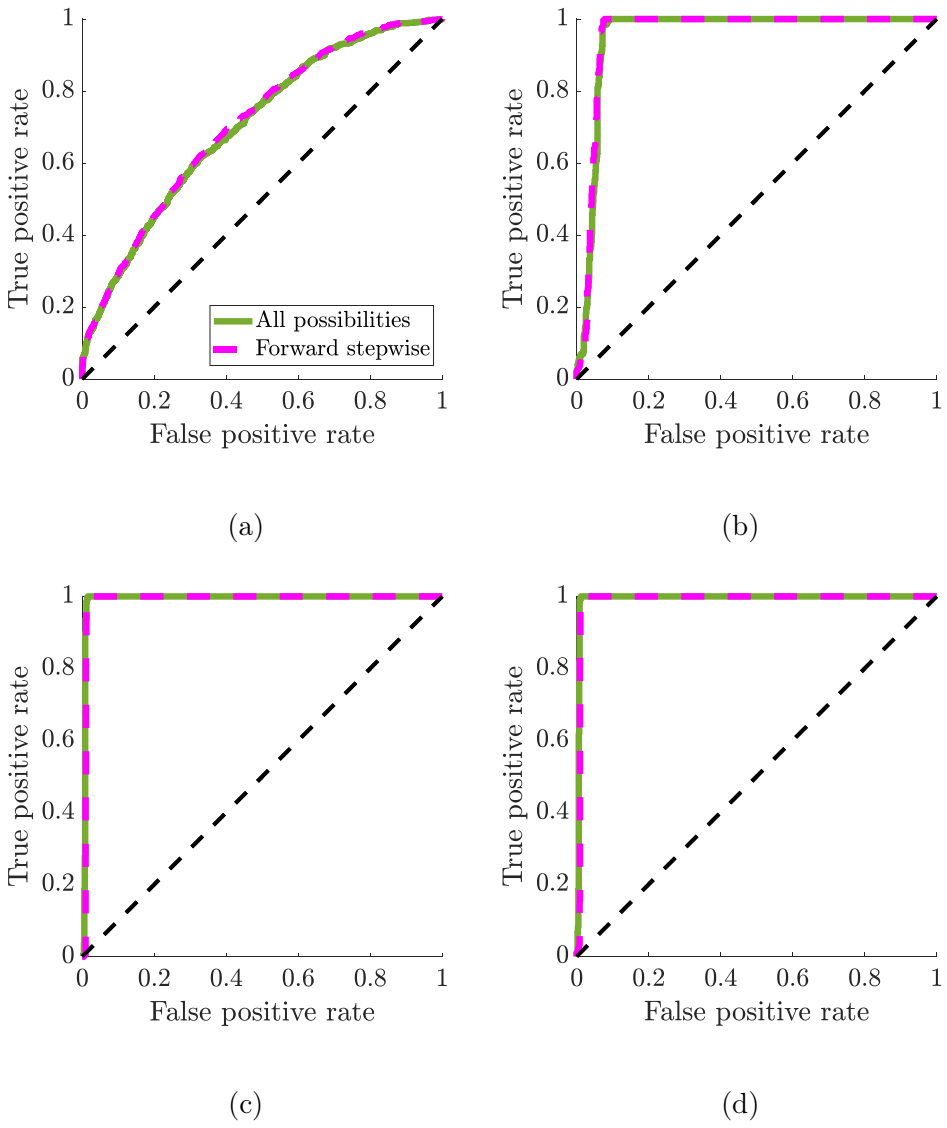

Figure 5.19: ROC curves comparing the damage detection performance for the testing all possibilities approach ($\tilde{\boldsymbol{\alpha}}_n \in \mathbb{R}^{800}$, ξ_1 = temperature, ξ_2 = wind speed, ξ_3 = azimuth, ξ_4 = actuator max, ξ_5 = actuator STD, all order varies based on optimisation) with the nonlinear forward stepwise method ($\tilde{\boldsymbol{\alpha}}_n \in \mathbb{R}^{800}$, $\boldsymbol{\xi}_r$ and model orders vary DSF to DSF). (a) testing/training (similarity curve), (b) 15cm damage/testing, (c) 30cm damage/testing and (d) 45cm damage/testing.

forward stepwise method is more efficient, taking far less time to compute. The reason being that it has fewer iterations to test, whilst achieving similar results. Furthermore, it is able to consider a wider range of EOPs. While this did not affect this particular system, it is still an important aspect for structures with more complex dynamics.

In addition to the improved efficiency, the nonlinear forward stepwise method selects only two EOPs on most occasions. The benefit of this is not immediately obvious. However, it has already been shown in Fig. 3.15 and Fig. 5.11 that selecting fewer EOPs can reduce the uncertainty and improve the similarity between the training and testing observations. Furthermore, the maximum order of 10 may be working against the nonlinear forward stepwise. The problem of overfitting model orders has already been demonstrated in Fig. 3.17c and Fig. 5.13.

5.3.5.3 Reducing model orders

To combat the problem associated with high order regression models, the method targeted at preventing overfitting, from Section 4.3.3, is applied following the nonlinear forward stepwise regression. The histograms in Fig. 5.20a and Fig. 5.20b show the distributions of regression model orders prior to and post application of the overfitting prevention scheme respectively.

The histogram in Fig. 5.20a shows that there is a tendency toward higher order models when using the nonlinear forward stepwise regression method. Whereas, Fig. 5.20b shows how the model orders have changed following the model order reduction procedure. It can be seen that the overall model orders have significantly reduced. This suggests that there were a large number of models that contained relatively small coefficients, often an indication of overfitting. The reduction in model orders should give better predictions of future data by neglecting benign trends in the training DSFs.

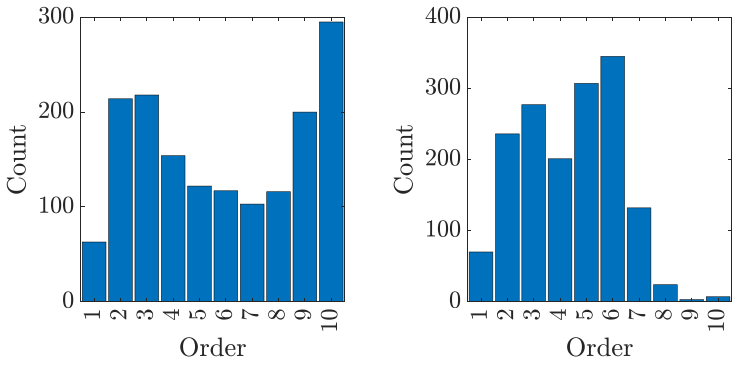

(a) (b)

Figure 5.20: (a) Histogram showing the frequency of model orders selected using nonlinear forward stepwise regression and (b) a histogram showing the frequency of the input EOP orders following an order reduction method.

Fig. 5.21 shows the resulting control chart following the application of the overfitting prevention method.

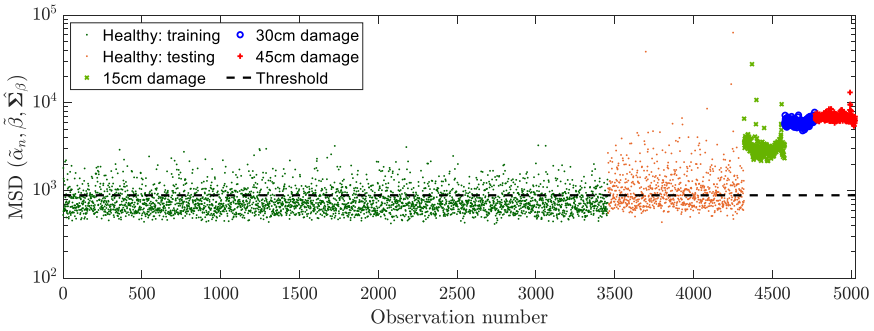

Figure 5.21: Control chart showing the explicit procedure with regression corrected DSFs based on a maximum of 10 EOPs with model orders optimised with a nonlinear forward stepwise procedure, followed by an order overfitting reduction scheme ($\tilde{\boldsymbol{\alpha}}_n \in \mathbb{R}^{800}$, $\boldsymbol{\xi}_r$ and model orders vary DSF to DSF). Threshold calculated to represent 98% of values in the training data according to a Chi-squared distribution

There is little visible difference between the result of the nonlinear forward stepwise regression, Fig. 5.18, and the reduced order version, Fig. 5.21. In this case, this result is the expected outcome given the changes to the regression models are very small. However, this can be seen as one of the great benefits of the proposed method. The regression models are more optimised but behave

as well as a higher order model. Once again, the benefits of the addition to the overall method lie in the subtle differences. The main differences in this case are reflected in the amplitude of the outliers in the damage scenarios and the reduction of trends within each damage group. The overall separation of damage and undamaged observations has changed minimally. This result is confirmed in the ROC curves in Fig. 5.22, with a slight improvement toward the reduced order method.

5.3.5.4 Choosing which features to regress

Up to this point, it has been assumed that each and every DSF has been dependent on a combination of EOPs. However, it is unlikely that all sources of variations in the system have been captured within these parameters. Therefore, it would be detrimental to try and model DSFs that lack dependency on any of the EOPs. Furthermore, the higher order PCs in the derivation make up so little variation within the data that they are likely unrelated noise.

To determine which DSFs are to be regressed, the method outlined in Section 4.3.4 is used. Fig. 5.23a and Fig. 5.23b show the F-statistic values for the DSFs obtained from one accelerometer along with their corresponding critical value, for a critical value of 1% and 0.1% respectively.

Looking, firstly, at the DSF F-statistic in Fig. 5.23. It can be seen that the F-statistic begins large and decays rapidly. This suggests that the PCs that account for the larger amounts of variance are most heavily influenced by the EOPs since the correction that is offered from the regression model gives it far more predictive power over the mean. It also implies that the higher components are most likely noise, unrelated to the EOPs, because the regression models do not provide much predictive power. In cases where the F-statistic is less than zero, the regression models actually provide worse predictions than the mean of the observations.

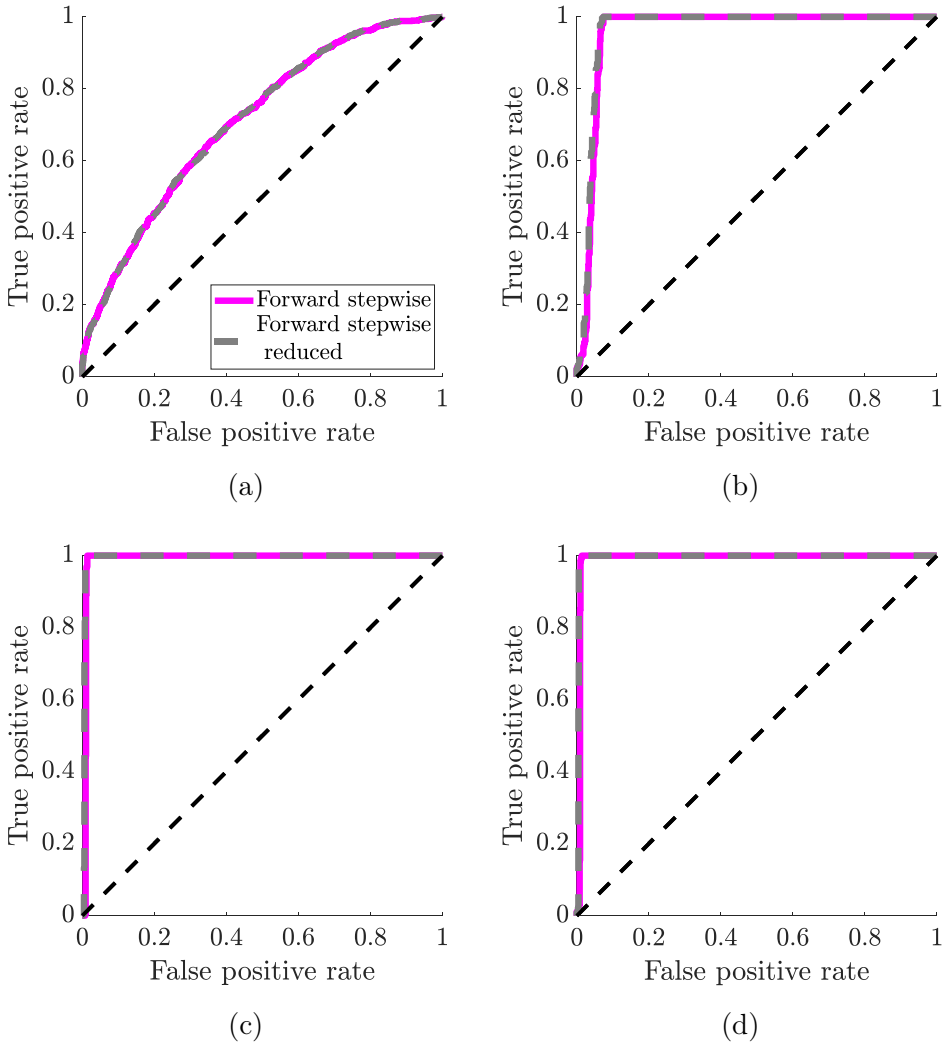

Figure 5.22: ROC curves comparing the damage detection performance for the nonlinear forward stepwise method and its associated order reduction version ($\tilde{\boldsymbol{\alpha}}_n \in \mathbb{R}^{800}$, $\boldsymbol{\xi}_r$ and model orders vary DSF to DSF). (a) testing/training (similarity curve), (b) 15cm damage/testing, (c) 30cm damage/testing and (d) 45cm damage/testing.

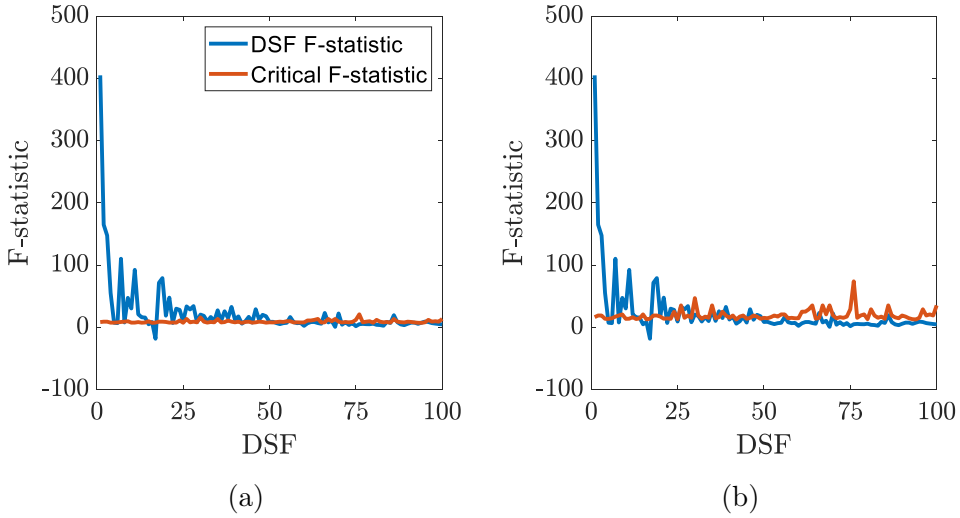

Figure 5.23: F-statistic and critical F-statistic for the regression model of each PC for accelerometer number 8, see Fig. 5.2. Critical value: (a) 1% and (b) 0.1%.

The choice for the critical value is a difficult task in itself. In this work, it was chosen that a more discriminative critical value would be used to ensure only high quality regression models are used. From Fig. 5.23b, it can be seen that far fewer regression corrected DSFs will be used in comparison to Fig. 5.23a, according to the hypotheses in Eq. 4.10a and Eq. 4.10b. Once the DSFs have been sorted according to Eq. 4.10a and Eq. 4.10b, the novelty index can be reapplied. The corresponding control chart with mixed measured and corrected DSFs is shown in Fig. 5.24.

There are very few differences between reduced order nonlinear forward stepwise, Fig. 5.21 and the combination of regressed and measured DSFs, Fig. 5.24. This result is not too surprising given there is also not too many differences between the implicit procedure, measured DSFs in Fig. 5.7a, and any of the nonlinear forward stepwise iterations. The benefit of the nonlinear forward stepwise method is that it targets sources of variations and removes them as well as is possible. Whilst this seems like a small improvement, it adds to the robustness of the VSHM system as a whole. The observations that are then

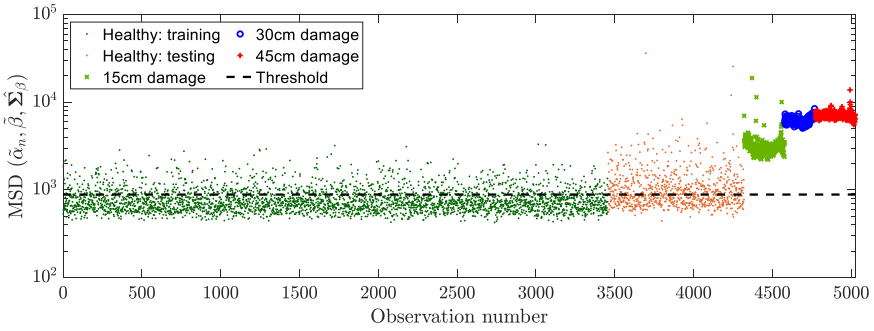

Figure 5.24: Control chart showing the result of combining regression corrected DSFs and implicit DSFs according to a critical F-statistic of 0.1% ($\breve{\boldsymbol{\alpha}}_n \in \mathbb{R}^{800}$, for regression corrected DSFs: $\boldsymbol{\xi}$ and model orders vary DSF to DSF). Threshold calculated to represent 98% of values in the training data according to a Chi-squared distribution

seen in the control charts can be better relied upon.

5.3.5.5 Varying the damage sensitive feature dimension

Until now, the changes that have been seen between the steps of the nonlinear forward stepwise method have been very small. When looking at the changes, the control charts have been exclusively for 100 PCs from each sensor. However, it is possible to use a different number of PCs. Part of having a robust system is knowing that the results will be reliable irrespective of the amount of information that is input into the system. In this section, two different scenarios will be considered. First, a case where 100 PCs from only one accelerometer will be presented; followed by a case where varying numbers of PCs are taken from all 8 accelerometers.

Using one accelerometer

For this example, the DSF that will be used is comprised of the first 100 PCs from the accelerometer located right-centre, number 8, on the trailing edge of the blade, see Fig. 5.2. Since the DSF vector is of dimension 100, as opposed to 800 from before, it is expected that the damage will not be as well detected since less information about the damage will be contained within the DSF vector.

The control charts for the implicit, explicit and combined models are shown in Fig. 5.25.

As predicted, the damaged observations are not as well separated from the undamaged compared to the cases where the DSF is of dimension 800. However, what can be seen is an upward shift of the damaged observation in the regression corrected DSFs, Fig. 5.25b, relative to the measured DSFs, Fig. 5.25a. In all cases, the initial damage is not very well detected. Since the combined DSF vector is a mix of the implicit and explicit methods, the observations in the resulting control chart, Fig. 5.25c, are a middle ground between the two other methods. One of the advantages that can be seen by observing a single accelerometer is that there is no longer a large discrepancy between the testing and training observations. This is hugely beneficial for the robustness of the system. The ROC curves in Fig. 5.26 highlight the improvement in the detection rate between the implicit and explicit methods.

The upward shift between Fig. 5.25a and Fig. 5.25b has translated to an increased damage detection rate for all the damage cases, see Fig. 5.26b, Fig. 5.26c and Fig. 5.26d. The most notable change is in the detection of the early damage, Fig. 5.26b. However, the detection rate for this damage case is still very low, only marginally above the testing observations. As noted in the control charts, the overlap between the training and testing observation in Fig. 5.26a is much closer to the desired black dashed line compared to when 8 accelerometers were being considered in Fig. 5.22a. Notably, there is more of an overlap between the testing and early damage in Fig. 5.26b than there is between the training and testing in Fig. 5.22a. This result is undesirable in both cases. What is evident is that the information from all of the accelerometers is required to make an informed decision on damage diagnosis.

Whilst the results for the regression corrected DSFs are superior to the measured DSFs, it is important to remember that there are still sources of uncertainty present by regressing DSFs that are not influenced by the input

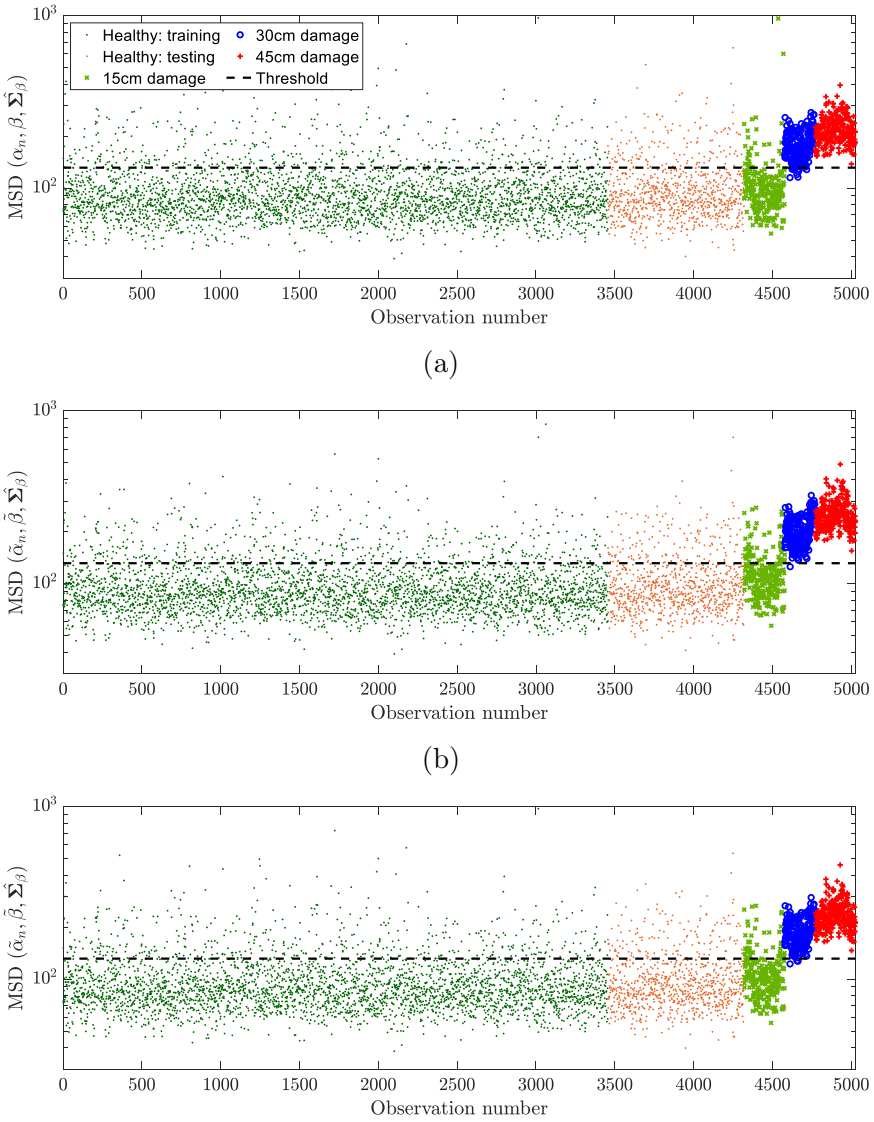

(a)

(b)

(c)

Figure 5.25: Control chart showing (a) the implicit method for 100 PCs taken from one accelerometer (accelerometer number 8, see Fig. 5.2)($\boldsymbol{\alpha}_n \in \mathbb{R}^{100}$), (b) regression corrected DSFs optimised with the reduced order forward stepwise method using the same feature set ($\tilde{\boldsymbol{\alpha}}_n \in \mathbb{R}^{100}$, $\boldsymbol{\xi}$ and model orders vary DSF to DSF) and (c) the combined DSF vector based on a critical F-statistic of 0.1% ($\breve{\boldsymbol{\alpha}}_n \in \mathbb{R}^{100}$, for regression corrected DSFs: $\boldsymbol{\xi}$ and model orders vary DSF to DSF). Threshold calculated to represent 98% of values in the training data according to a Chi-squared distribution

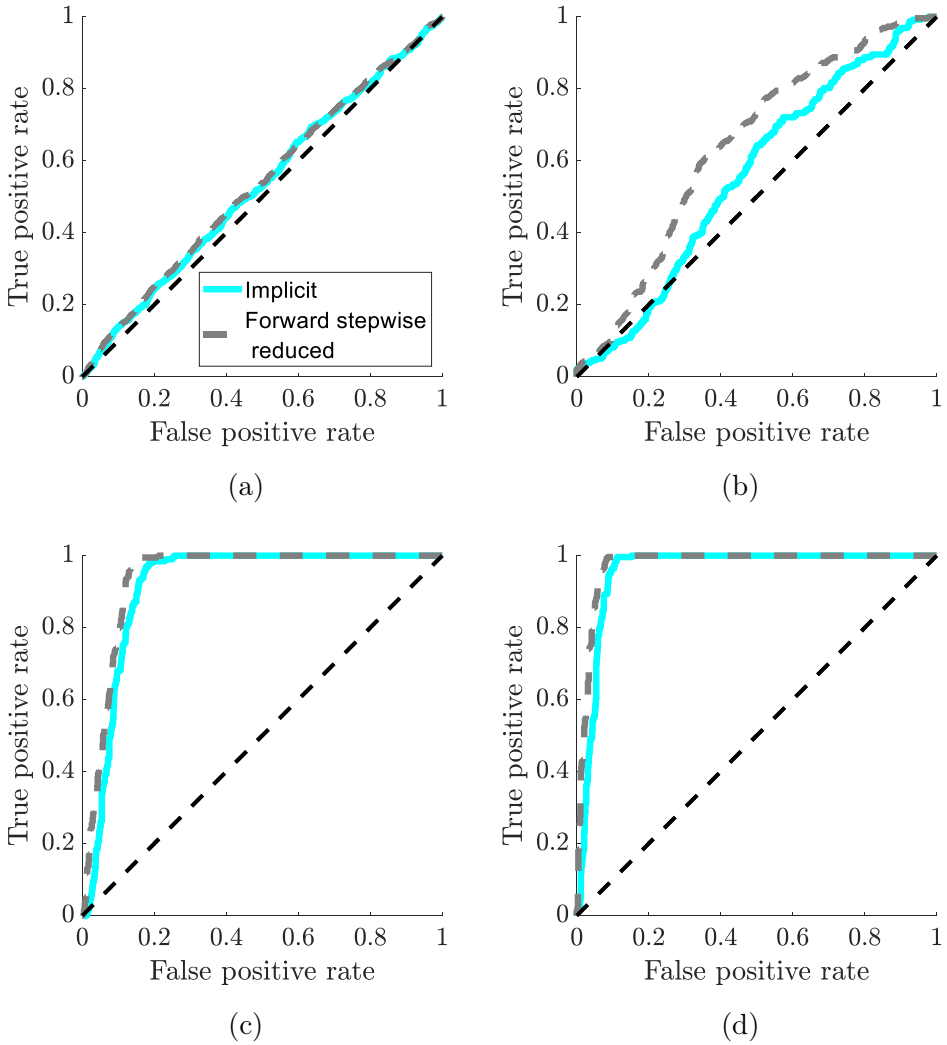

Figure 5.26: ROC curves comparing the damage detection performance for the implicit method ($\boldsymbol{\alpha}_n \in \mathbb{R}^{100}$) and reduced order forward stepwise method ($\tilde{\boldsymbol{\alpha}}_n \in \mathbb{R}^{100}$, $\boldsymbol{\xi}$ and model orders vary DSF to DSF) when using only one accelerometer. (a) testing/training (similarity curve), (b) 15cm damage/testing, (c) 30cm damage/testing and (d) 45cm damage/testing.

parameters. The uncertainties introduced have consequently inflated the values of the MSD, making the observations appear more different than they truly are. As such, the combined DSFs should be used. The results may not be as good as the regression corrected DSFs, but they are more reliable.

Varying the number of principal components

The second way in which the number of DSFs can be varied is by changing the number of PCs that are taken from each of the accelerometers. As with the previous example, when fewer PCs are used, it is expected that the damage will not be detected as well since less information about the damage is likely to be present. However, it is possible that the higher order PCs that are added contain little to no information about the damage since they are more likely to be related to benign noise contained within the system. This example will use information from the 8 accelerometers that were used in previous examples. The PCs that are introduced to the system will be cumulative. For example, the first case will use only the first PC from each accelerometer, the second case will used the first two PCs from each accelerometer and so on and so forth.

The measure of damage detection that will be used will be the AUC. In the case of damage detection, it is desirable to have the AUC as close to 1 as possible, giving perfect separation between damaged and undamaged observations. For the overlap between training and testing, an ideal value would be 0.5, giving an even and overlapping distribution between the two sets of observations. The variation of the AUC is given in Fig. 5.27 for all damage cases, plotted against the cumulative number of PCs added to the system from each accelerometer.

Beginning with the commonalities between the damage cases in Fig. 5.27b, Fig. 5.27c and Fig. 5.27d, the measured DSFs outperform both the nonlinear forward stepwise reduced DSFs and the combined DSFs. However, at the lower order PCs, the ones that are most affected by the EOPs, the result is the opposite. This result suggests that correcting for the EOPs in the lower order PCs can help to highlight the presence of damage. Beyond this, when the measured DSFs overtake the regressed, the resulting improvement could be due to variations that are not related to the condition of the structure. In this case, the method for creating the combined DSFs would become redundant. But since

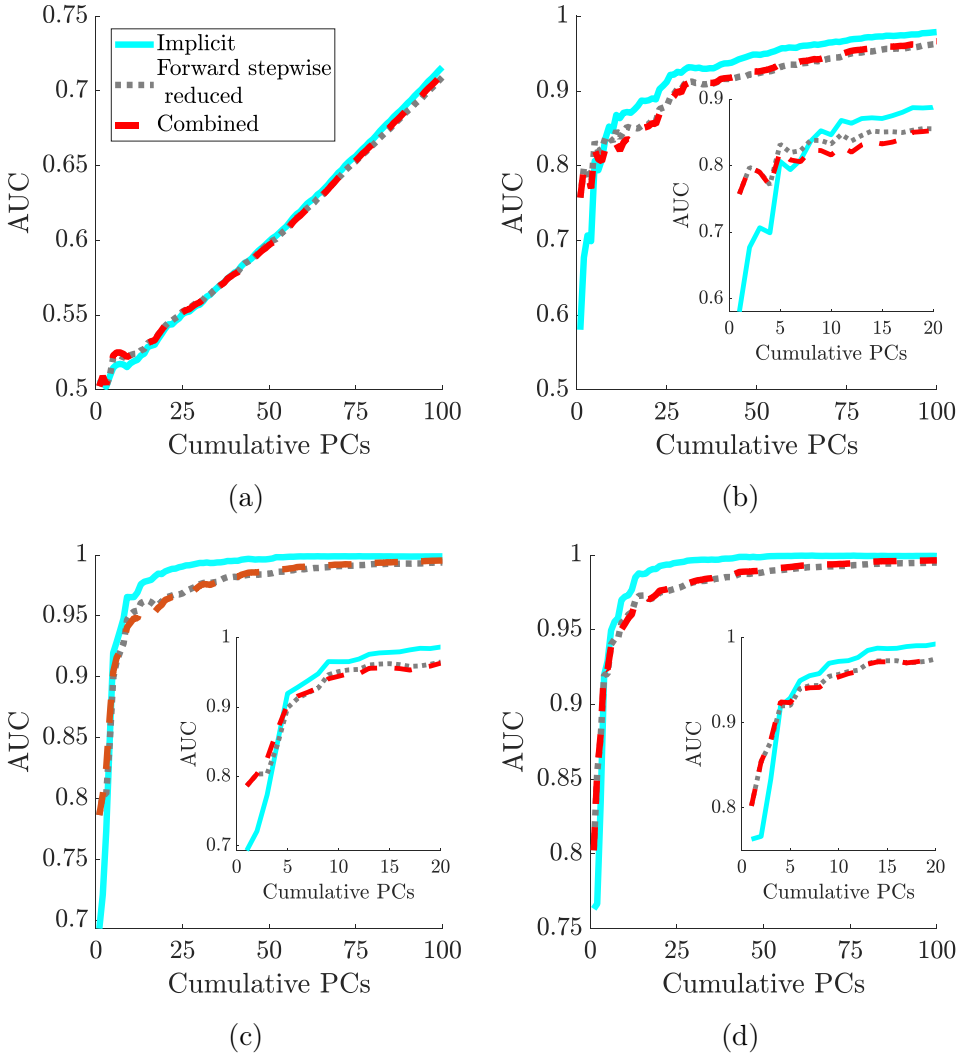

Figure 5.27: Comparing the AUC for the implicit method ($\alpha_n \in \mathbb{R}^{8\to800}$), the reduced order forward stepwise method ($\tilde{\boldsymbol{\alpha}}_n \in \mathbb{R}^{8\to800}$, $\boldsymbol{\xi}$ and model orders vary DSF to DSF) and the combined DSF method ($\breve{\boldsymbol{\alpha}}_n \in \mathbb{R}^{8\to800}$, for regression corrected DSFs: $\boldsymbol{\xi}$ and model orders vary DSF to DSF). (a) testing/training, (b) 15cm damage/testing, (c) 30cm damage/testing and (d) 45cm damage/testing.

the purpose is to try and retain as much information as possible, it would be desirable to also keep the higher order PCs. As expected, the combined DSFs exist in the region between the measured and regression corrected DSFs.

Another key commonality between the damage cases is that the AUC continues to increase as more PCs are added. This would suggest that each DSF contains information about the damage. However, this could also be a result of the previously mentioned point of adding variabilities not related to the condition of the structure. A notable point is also that the AUC rapidly increases at the beginning and tails off towards the end. This confirms the assumption that the lower order PCs contain more information about the damage and, thus, discarding them is not conducive to effective damage detection.

From Fig. 5.27a, it can be seen that the separation between training and testing increases as more PCs are added. This is a very undesirable effect and can lead to problems with reliability for the user. An interesting aspect to notice is that it does not begin to rapidly increase until the point where the measured DSFs begin to outperform the regressed and combined DSFs in Fig. 5.27b, Fig. 5.27c and Fig. 5.27d. This finding could also supplement the evidence of the higher order PCs containing variabilities that are not related to the condition of the structure. Despite the fact the combined DSFs do not perform the best, it would be recommended to still use them since the most effort has been made to reduce the uncertainties and variations within the system. However, the results found in this iteration are still undesirable given the increase in the separation between the training and testing, a large issue in creating a robust system.

5.3.6 Lasso regression

The Lasso regression is introduced as an alternative to the nonlinear forward stepwise regression. The particular model used in this study was created using 5 EOPs for orders up to 5. The input vector of EOPs was expanded to allow

orders of up to 5 by using Eq. 4.13. The resultant control chart for the Lasso regression is shown in Fig. 5.28.

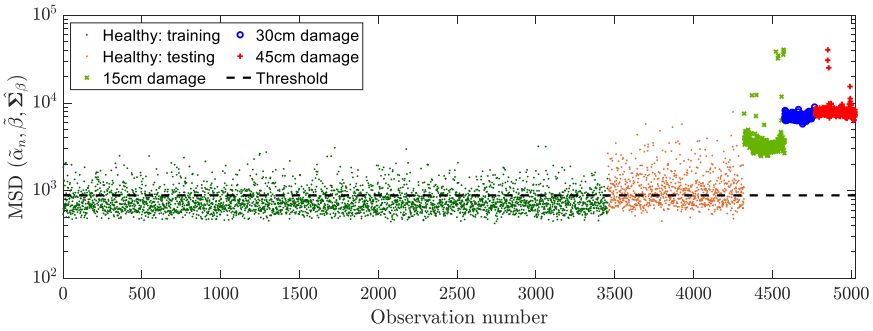

Figure 5.28: Control chart showing the outcome of the Lasso regression method constructed with 5 EOPs up to a maximum order of 5 ($\tilde{\boldsymbol{\alpha}}_n \in \mathbb{R}^{800}$, ξ_1 = temperature, ξ_2 = wind speed, ξ_3 = azimuth, ξ_4 = actuator max, ξ_5 = actuator STD, all orders maximum = 5). Threshold calculated to represent 98% of values in the training data according to a Chi-squared distribution

Once again, the control chart in Fig. 5.21 for the reduced order nonlinear forward stepwise method and the control chart for the Lasso regression, Fig. 5.28, are very similar. The distribution of the groups of observations is similar and so too is the value of the threshold, suggesting the training sets are very similar. However, the biggest difference between the two is a slight upward shift in the damaged observations for the Lasso. This shift might suggest that the Lasso outperforms the nonlinear forward stepwise method. However, studying the ROC curves in Fig. 5.29 shows that it is not as simple as that.

The first thing that can be said is that both methods perform on a very similar level. There is a slight improvement in the separation of damaged and undamaged observations, as seen in Fig. 5.29b, Fig. 5.29c and Fig. 5.29d. However, this comes at the cost of a reduced overlap between the testing and the training, see Fig. 5.29a. While it is important for the system to differentiate between damaged and undamaged observations, it is more important that it can identify when the observations are still undamaged beyond the training. It

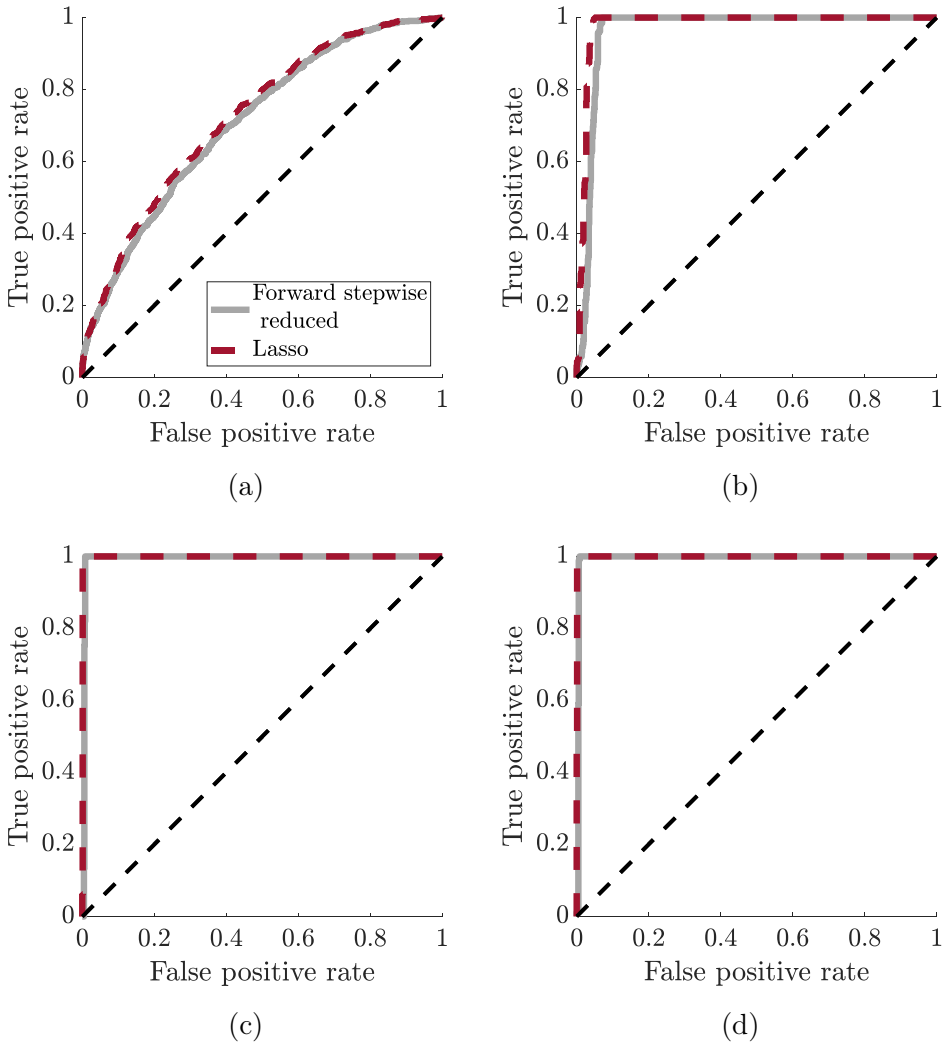

Figure 5.29: ROC curves comparing the damage detection performance for the reduced order forward stepwise method ($\tilde{\boldsymbol{\alpha}}_n \in \mathbb{R}^{800}$, $\boldsymbol{\xi}$ and model orders vary DSF to DSF) and the Lasso regression method ($\tilde{\boldsymbol{\alpha}}_n \in \mathbb{R}^{800}$, ξ_1 = temperature, ξ_2 = wind speed, ξ_3 = azimuth, ξ_4 = actuator max, ξ_5 = actuator STD, all orders maximum = 5). (a) testing/training (similarity curve), (b) 15cm damage/testing, (c) 30cm damage/testing and (d) 45cm damage/testing.

can be difficult, then, to justify which of these methods is superior, instead it is important to recognise that each method has its benefits and drawbacks.

In the reduced order nonlinear forward stepwise method, there are many stages that take place. It is impossible to check at each stage what is happening and there is a possibility of uncertainties creeping in. However, the benefit of the method is that it automatically removes highly correlated EOPs but is still able to model less significant relationships between the EOPs. In instances of extreme weather, the relationship that is estimated may be key in correctly identifying the condition of the structure without further intervention. Furthermore, the nonlinear forward stepwise method has fewer iterations to attempt since it will stop when it cannot find more influential EOPs.

On the other hand, the Lasso regression consists of only one stage, reducing the likelihood of errors being introduced. However, it is not able to model the relationships between EOPs. While this has little effect on this particular example, future monitoring campaigns might be hindered by their absence. In addition, the 5 EOPs that were chosen for the Lasso were already suspected to be influential. In systems with complex DSFs, it might not be possible to guess which EOPs will be influential. Increasing the number of EOPs increases the dimension of the matrix that needs to be optimised in Lasso regression. Therefore, without a lot of computing power, the Lasso regression cannot consider as many EOPs as the nonlinear forward stepwise method.

Considering again the reliability of the methods with varying amounts of information, the AUC is plotted against cumulative components for the nonlinear forward stepwise and Lasso methods in Fig. 5.30.

It can be seen that for the damage cases in Fig. 5.30b, Fig. 5.30c and Fig. 5.30d, there is a general improvement from the Lasso regression method across all cumulative PCs. This suggests that the Lasso method is superior to the nonlinear forward stepwise method. The potential implication here is that the nonlinear forward stepwise method is over-complicated and unnecessary.

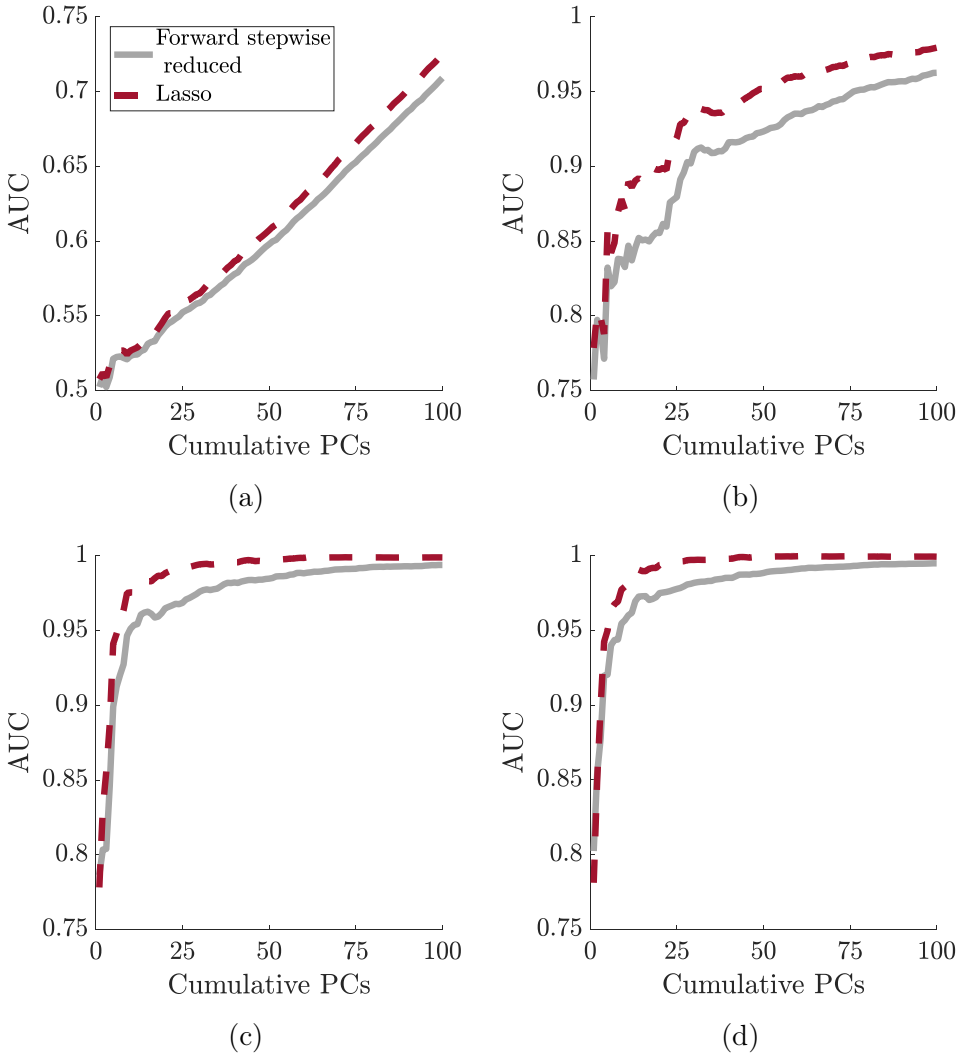

Figure 5.30: Comparing the AUC for the reduced order forward stepwise method ($\tilde{\boldsymbol{\alpha}}_n \in \mathbb{R}^{8\to 800}$, $\boldsymbol{\xi}$ and model orders vary DSF to DSF) and the Lasso regression method ($\tilde{\boldsymbol{\alpha}}_n \in \mathbb{R}^{8\to 800}$, ξ_1 = temperature, ξ_2 = wind speed, ξ_3 = azimuth, ξ_4 = actuator max, ξ_5 = actuator STD, all orders maximum = 5). (a) testing/training, (b) 15cm damage/testing, (c) 30cm damage/testing and (d) 45cm damage/testing.

However, the reliability of the Lasso is affected by the larger separation of the testing and training observations, see Fig. 5.27a.

The results in Fig. 5.30 reflect and expand upon those found in Fig. 5.29. The use of the Lasso regression over the nonlinear forward stepwise regression is application specific. In cases where there are few available EOPs, that also show little correlation, the Lasso method can be implemented quickly and with success. However, in cases where there are many EOPs available, or complex DSFs, the nonlinear forward stepwise regression would be more appropriate as it is able to search more variations to determine the best possible model.

5.3.7 Correction of Mahalanobis squared distance

While the design of regression models can be a source of uncertainty within a VSHM system, the measure for the outlier analysis must also be chosen carefully. Substantial measures have been taken already in this chapter to reduce the variabilities in the system, but the separation between testing and training remains a significant problem. Instead, corrections to the covariance within the MSD, described in Section 4.5, can be implemented.

5.3.7.1 Correction to implicit damage sensitive features

In this case, the covariance of the baseline is instead replaced with the eigenvalues from the applied PCA method. Since the eigenvectors are orthogonal, the PCs are independent of each other and, thus, there should be no correlation between PCs from the same accelerometer. The control chart with the corrected MSD for the implicit DSFs is shown in Fig. 5.31.

The biggest difference due to the change in the MSD can be seen clearly when comparing Fig. 5.31 with the baseline implicit method in Fig. 5.7a. There is a very noticeable downward shift of all the future observations beyond the

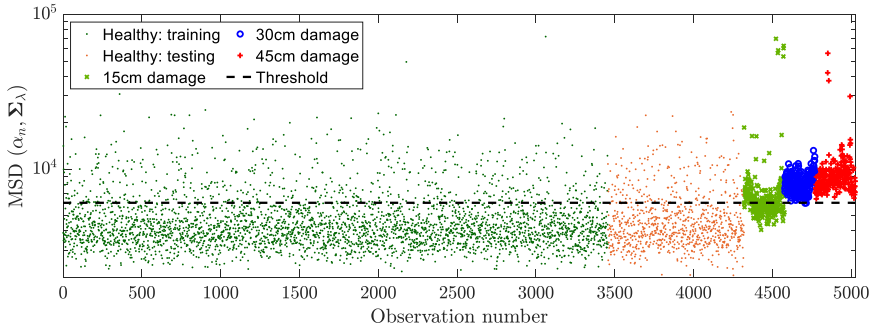

Figure 5.31: Control chart showing the recalculated MSD for the DSFs obtained in the implicit method ($\boldsymbol{\alpha}_n \in \mathbb{R}^{800}$). Threshold calculated to represent 98% of values in the training data according to a Chi-squared distribution

training. Whilst this results in a lower rate of damage detection, the more important aspect of the overlap between training and testing is resolved. Resolving this issue goes a long distance towards creating a more robust system.

To explore the reason for the correction of the MSD, the auto-covariance for the baseline training data and testing data are shown in Fig. 5.32a and Fig. 5.32b respectively. Only the first 20 PCs from each sensor are shown.

In an ideal scenario, the auto-covariance of the testing data should match as closely as possible to the auto-covariance of the baseline data. Studying Fig. 5.32, it is difficult to see any differences between Fig. 5.32a and Fig. 5.32b. One thing that can be seen in both figures is that there is no correlation between the orthogonal vectors from the same sensor, a result that is expected given the derivation of the DSFs. To get a better idea of the differences between the auto-covariances of the training and testing, Fig. 5.33 shows the ratio between the two auto-covariances.

An initial inspection of Fig. 5.33 reveals a large number of DSFs that correlate well between the baseline training and testing. In particular, the main diagonal shows excellent correlation between the two sets. This correlation shows that the eigenvalues of the PCs remain very similar in the two sets. The correlated DSFs do not appear to follow any pattern and are, therefore, most

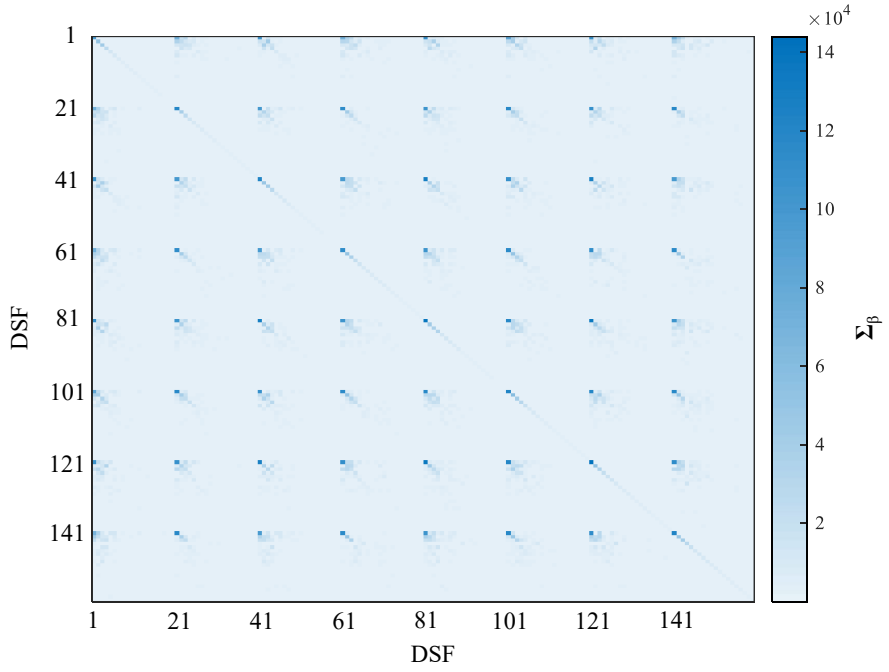

(a)

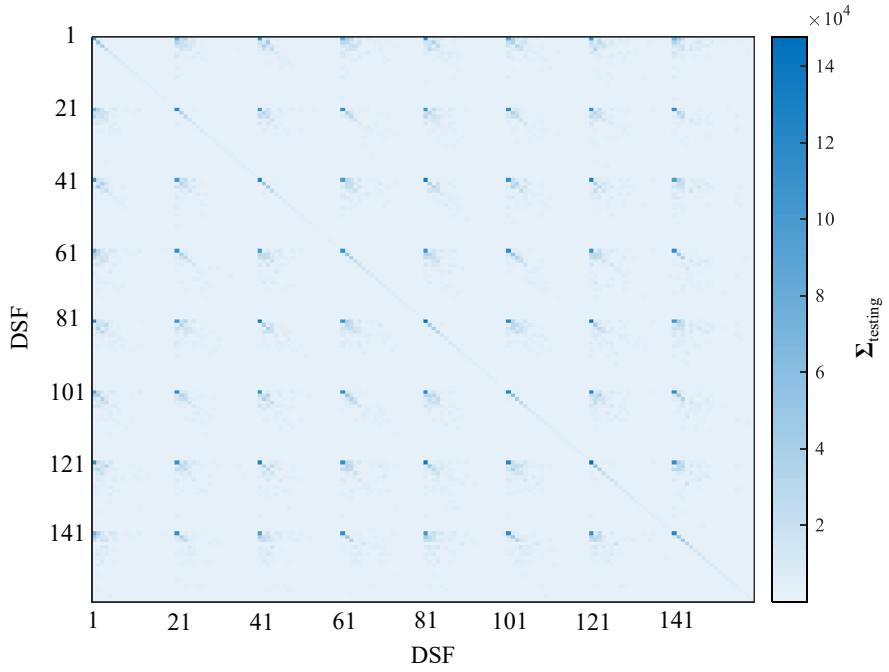

(b)

Figure 5.32: Auto-covariance of (a) baseline training data and (b) testing data, an important component of the MSD.

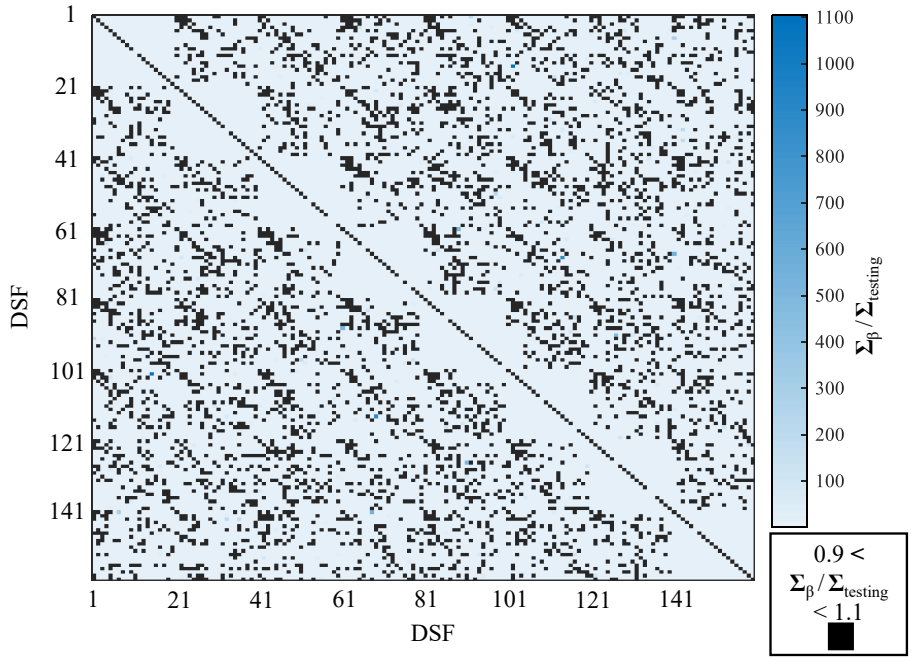

Figure 5.33: Ratio of auto-covariance between the baseline training data and testing data of the implicit DSFs. Highlighted in black are the DSFs where the auto-covariances are within 10% of perfect correlation.

likely specific between the training and testing. As a result, these are considered to be noise and are not considered as part of the eigenvalue derivation. Furthermore, there are a number of points where there is no correlation at all, with some as much as 1000 times out. These anomalies could explain the reason for the dissimilarity in the MSD for the training and testing prior to correction.

Ultimately, the results in Fig. 5.33 show that the covariance of the training data is not a good representation of the undamaged condition given the lack of correlation with the testing data. Ignoring this finding can create relationships between DSFs that do not exist, causing more uncertainty in the VSHM system. The subsequent ramification being that the increase in the MSD between the undamaged and damaged observations is a work of fiction, a result of an improperly defined distance metric. Perhaps, it is not possible to detect the early onset of damage as well as first thought.

5.3.7.2 Correction to regressed damage sensitive features

Since the regression is performed on the DSFs from the implicit method, the fact that the eigenvectors within PCA are orthogonal means that the DSFs remain unrelated. However, instead of using the square of the eigenvalues to explain the variance in each feature, the innovations variance is used. The resulting control chart for the reduced order nonlinear forward stepwise regression method is shown in Fig. 5.34.

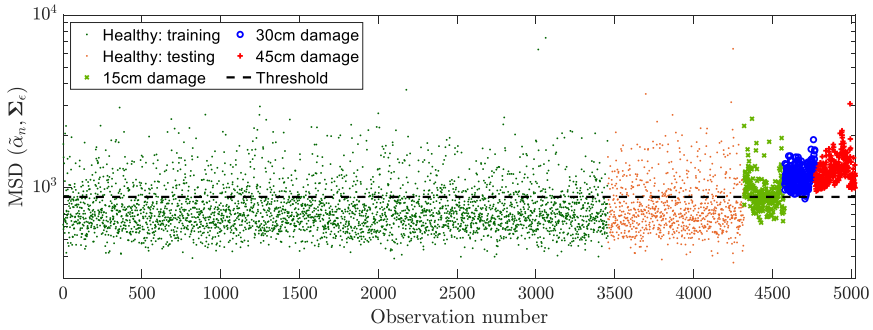

Figure 5.34: Control chart showing the recalculated MSD for the DSFs obtained through the reduced order nonlinear forward stepwise method ($\tilde{\boldsymbol{\alpha}}_n \in \mathbb{R}^{800}$, $\boldsymbol{\xi}$ and model orders vary DSF to DSF). Threshold calculated to represent 98% of values in the training data according to a Chi-squared distribution

Like with Fig. 5.31, Fig. 5.34 also shows the downward shift of the observations beyond the training. As such, the same conclusion regarding the increased robustness at a cost of lower damage detection can be made, given that there is much better overlap between training and testing in Fig. 5.34 compared to pre-MSD-correction in Fig. 5.21. The main visible difference between Fig. 5.34 and Fig. 5.31 is that the magnitude of the outliers within the damage groups has reduced. However, there may be further, more subtle, differences between the two control charts, ones which are difficult to see on a control chart.

Fig. 5.35 shows the ratio of the auto-covariance of the baseline training data, the one used in a normal MSD calculation, and testing data.

Similar to Fig. 5.33, Fig. 5.35 has good correlation between the baseline training and testing along the main diagonal. Furthermore, there is also no

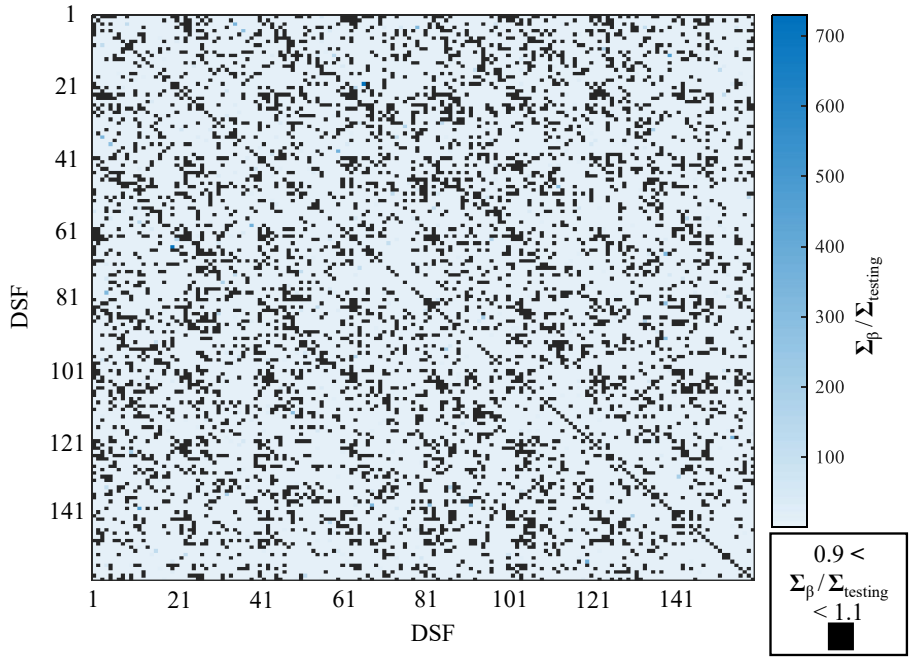

Figure 5.35: Ratio of auto-covariance between the baseline training data and testing data of the regression corrected DSFs. Highlighted in black are the DSFs where the auto-covariances are within 10% of perfect correlation.

discernible pattern in the DSFs outside of the diagonal. Once again, this can be considered to be noise that should be removed to lower the uncertainty in the VSHM system. The correction to the MSD for the regression corrected DSFs uses the innovations in place of the eigenvalues. Fig.5.36 demonstrates that there is good correlation between the innovations of the training and testing, making it an appropriate representation of the undamaged data.

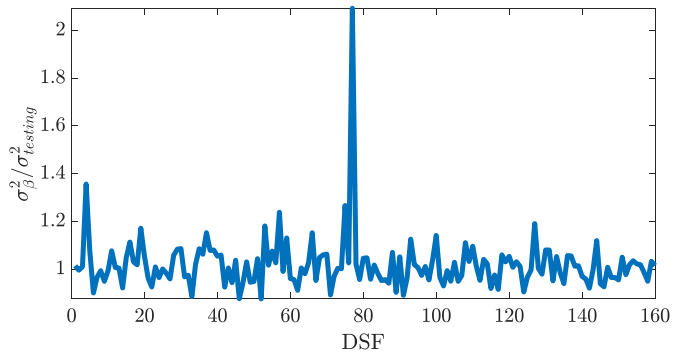

Figure 5.36: Ratio of innovations of the baseline training data and testing data of the regression corrected DSFs.

Similar to the eigenvalues with the PCA corrected DSFs, the well correlated off-diagonal values are likely to be specific to the training and testing. Discarding a large number of highly correlated DSFs does reduce the system's sensitivity to damage. It is likely that these correlations hold information on the damage, but without knowing which, it is impossible to keep them all without introducing uncertainty into the VSHM system.

5.3.7.3 Correction to combined damage sensitive features

The combination of the two types of DSF, implicit and explicit, means that both the correction methods for the MSD must be used. Once the corresponding correction has been made to the covariance term in the MSD for each DSF, a new control chart can be created, as shown in Fig. 5.37.

Alongside Fig. 5.31 and Fig. 5.34, Fig. 5.37 also shows the shift downward of all observations beyond training. Once more, the earliest damage is not very well detected but the 30cm and 45cm more so. Once again, the magnitude of the outliers within the damage groups has reduced. However, to get a better idea of the differences between the methods, the ROC curves in Fig. 5.38 and the AUC charts in Fig. 5.39 should be studied.

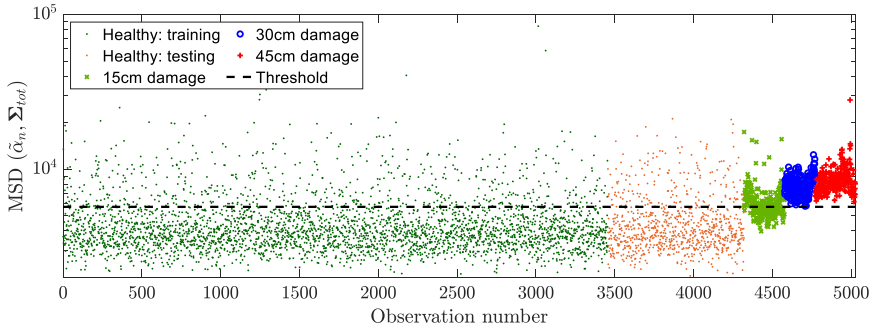

Figure 5.37: Control chart showing the recalculated MSD for the combined DSF vector created using an F-statistic of 0.1% ($\breve{\boldsymbol{\alpha}}_n \in \mathbb{R}^{800}$, for regression corrected DSFs: $\boldsymbol{\xi}$ and model orders vary DSF to DSF). Threshold calculated to represent 98% of values in the training data according to a Chi-squared distribution

5.3.7.4 Varying the damage sensitive feature dimension

As with Section 5.3.5.5, it is important to consider how the ability of the system to detect damage changes with respect to the amount of input information.

Using one accelerometer

As with the previous example, only the first 100 PCs of the accelerometer located right-centre on the trailing edge of the blade will be used. The ROC curves in Fig. 5.38 illustrate the changes in the separation between damaged and undamaged observations for the measured (implicit), reduced order forward stepwise and combined DSFs.

For all cases, it can be seen that the overlap between training and testing, Fig. 5.38a, is similar and close to the ideal diagonal. Accordingly, it is not possible to draw a conclusion on which approach is best in this respect. However, it can be seen that the damage detection is slightly improved for the smallest damage, Fig. 5.38b, when using the nonlinear forward stepwise method. Once again, the improvement from the regression model could be artificial, a result of fitting models where no trends are present. Therefore, the method using combined DSFs is the one that should be considered. This DSF set still outperforms the measured DSFs but in a more robust manner than regressing all DSFs no

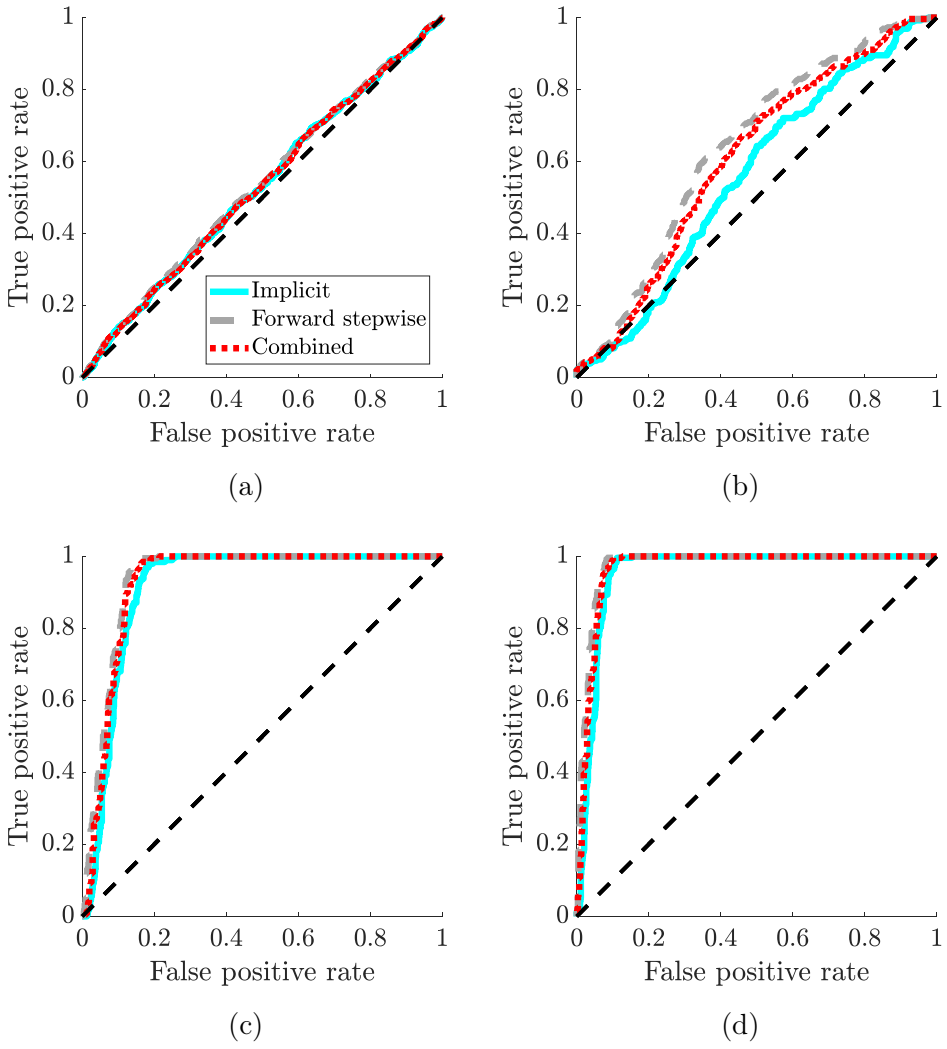

Figure 5.38: Comparing the ROC curves for the measured ($\boldsymbol{\alpha}_n \in \mathbb{R}^{100}$), reduced order forward stepwise ($\tilde{\boldsymbol{\alpha}}_n \in \mathbb{R}^{100}$, $\boldsymbol{\xi}$ and model orders vary DSF to DSF) and combined DSFs ($\breve{\boldsymbol{\alpha}}_n \in \mathbb{R}^{100}$, for regression corrected DSFs: $\boldsymbol{\xi}$ and model orders vary DSF to DSF) when only considering 1 accelerometer (accelerometer number 8, see Fig. 5.2). (a) testing/training (similarity curve), (b) 15cm damage/testing, (c) 30cm damage/testing and (d) 45cm damage/testing.

matter what. As a whole, the detection of the smallest damage when using once accelerometer is not very good, likely owing to a lack of information. The two larger damages in Fig. 5.38c and Fig. 5.38d are better detected. The same trend of the DSF sets that was witnessed in Fig. 5.38b is present in the larger damages. Whilst the larger damages are detected well, the poor detection of the initial damage justifies the need to include more information, predominantly in the form of information from a wider array of sensors.

Varying the number of principal components

Once more, the number of cumulative PCs from all 8 accelerometers are varied to study the effect on the AUC, as with Section 5.3.5.5. Fig. 5.39 highlights the variations in the AUC for all damage cases for the measured (implicit), reduced order forward stepwise and combined DSFs.

The most noticeable difference between Fig. 5.27a and Fig. 5.39a is that with the correction of the MSD, the overlap between training and testing has significantly improved. Previously, Fig. 5.27a, the two groups separated as more PCs were considered. With the correction of MSD, the overlap between the training and testing is far more stable across varying amounts of information, whilst remaining close to the desirable value of 0.5. Therefore, the additional consideration given to the true nature of the covariance of the training data can provide additional robustness. Confidence in the overlap between observations belonging to the same damage state, particularly undamaged, subsequently increases the confidence in observations that indicate damage, a key aspect in the application of VSHM for real structures.

Observing Fig. 5.39b-5.39d, it can be seen that the combined DSFs are largely made up using regression corrected DSFs for the earlier PCs. This aligns with the assumption that the high variance PCs are the ones which are most effected by EOVs. In agreement with Fig. 5.27, the measured DSFs in Fig. 5.39 outperform the regression corrected DSFs when larger number of PCs are considered. However, in Fig. 5.39a, the combined DSFs now have the superior damage detection, unlike Fig. 5.27. Whilst the overall damage detection is lower, the decision making is more reliable by accounting for sources of uncertainty. Overall then, the correction of the MSD is a necessary measure to ensure more reliable and robust decision making.

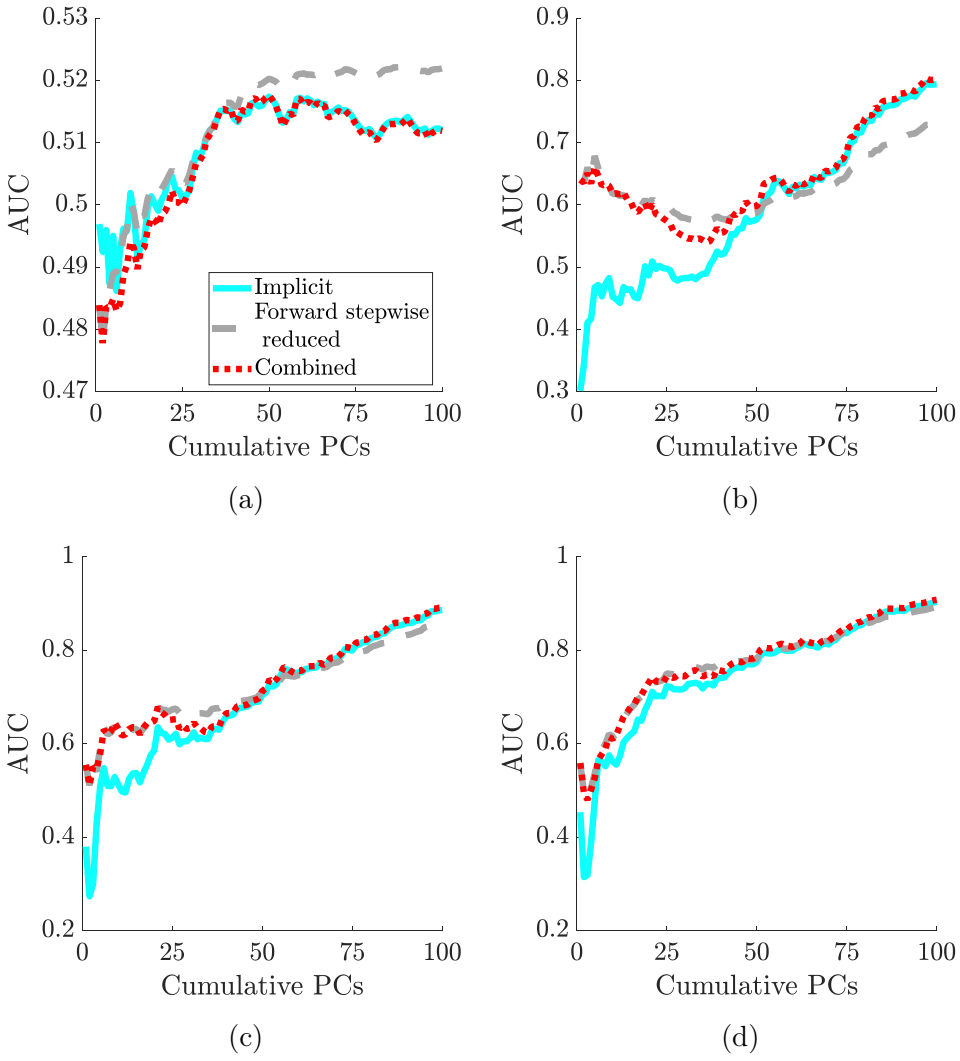

Figure 5.39: Comparing the AUC for the measured ($\alpha_n \in \mathbb{R}^{8\to800}$), reduced order forward stepwise ($\tilde{\boldsymbol{\alpha}}_n \in \mathbb{R}^{8\to800}$, $\boldsymbol{\xi}$ and model orders vary DSF to DSF) and combined DSFs ($\breve{\boldsymbol{\alpha}}_n \in \mathbb{R}^{8\to800}$, for regression corrected DSFs : $\boldsymbol{\xi}$ and model orders vary DSF to DSF). (a) testing/training, (b) 15cm damage/testing, (c) 30cm damage/testing and (d) 45cm damage/testing.

5.3.7.5 Conservative design practices

Prior to the correction of the MSD, there is evidence that conservative design can aid in the confidence in the value of the outlier analysis for each observation. When only DSFs from one sensor was considered in Fig. 5.25c, the separation in the training and testing that was seen in Fig. 5.24, where all sensors were combined, is no longer present. The implication of this is that the covariance values between sensors in the MSD adds bias towards the training model. However, without the presence of all sensors, it is difficult to detect damage, as there is less information available. This finding further highlights the need to better design the covariance within the MSD so that it represents the training observations without the same bias.

What is evident in all cases where the correction of the MSD is implemented, is that the system's sensitivity to damage is severely affected. The trade-off for this is that the training and testing observations have a much better overlap. The design of the VSHM system is, therefore, dependent on the requirements of the user. They user can decide whether to have a conservative system that is less sensitive to damage but more interpretable, robust and reliable or to have one that is more sensitive to damage but at the cost of less confidence in the decision making process.

5.3.8 System robustness

To get a better understanding of how well the models perform, the observations beyond the training must be explored. As discussed previously, the testing data should perform as similarly as possible to the training data. For this analysis, the DSFs are evaluated following the application of the novelty index.

5.3.8.1 Distribution of groups

To assess the changes in the distributions amongst the different damage cases, the NIQR in Fig. 5.40 is plotted. A number of the previously analysed regression

models and all of the damage cases are considered. A k-fold analysis was used to gain a better understanding of the variations in these factors [218]. A total of 25 different training sets were used for building the regression models, a different subset of 3456 of the total 4320 repaired observations each fold, see Table 5.1. In Fig. 5.40, the Lasso regression is excluded due to its computational time since 100 PCs from each sensor are considered for the DSF.

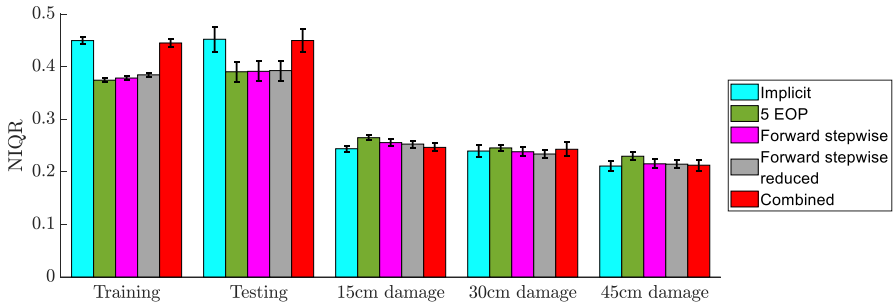

Figure 5.40: The normalised interquartile range plotted against each damage case for each regression method, excluding Lasso. Regression procedure repeated 25 times with different training data sets. ($\boldsymbol{\alpha}_n \in \mathbb{R}^{800}$, $\tilde{\boldsymbol{\alpha}}_n \in \mathbb{R}^{800}$, $\breve{\boldsymbol{\alpha}}_n \in \mathbb{R}^{800}$).

In a perfect regression case, it would be possible to remove all the variation within data. However, previous works [87, 103] showed that there were expansive distributions of data, an indicator of poor regression models, that must be addressed when multivariate nonlinear regression was applied. From Fig. 5.40, there is a pattern in the training distributions that can be attributed to the overfitting of models. Starting with 5 EOP trial and error approach, the distribution of the data is smaller than that of the proposed reduced order nonlinear forward stepwise method. However, there is the least change between training and testing for the proposed method, a desirable aspect in the context of VSHM. As the optimisation scheme becomes more strict on its inputs, the training models become less accurate but more generalised. The benefits of this are immediately apparent in the smaller distributions among the damage cases.

Between the forward stepwise and the reduced order forward stepwise, there is a reduction in the distribution, as well as the variability in the size of the distributions, as observed in Fig. 5.40 for all the damage cases. A really important outcome is that the NIQR for both the training and testing are very similar, thanks to the MSD implemented in Section 4.5. This adds confidence to the decisions that are made beyond the training. The DSFs created using measured and regression corrected DSFs tend to have lower NIQRs for the damage cases. Unsurprisingly, the NIQR for the combined DSFs is higher for the training and testing since the DSF sets contain mostly measured DSFs. Ultimately, the combined DSFs can be considered the most robust as they contain the least variation in the unseen observations.

By reducing the number of PCs taken from each sensor, it is possible to rerun the analysis to include the Lasso regression. In Fig. 5.41, 20 PCs are taken from each sensor.

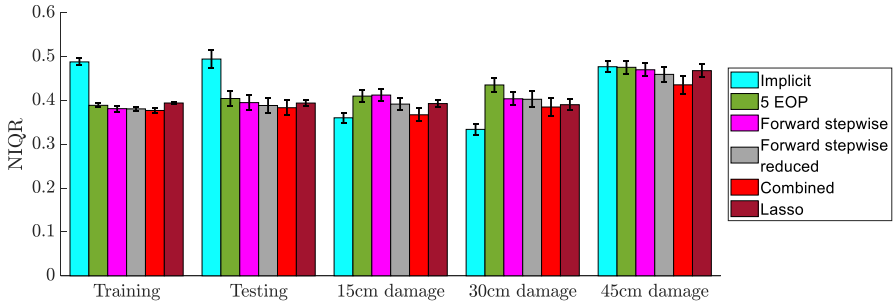

Figure 5.41: The normalised interquartile range plotted against each damage case for each regression method. Regression procedure repeated 25 times with different training data sets. ($\boldsymbol{\alpha}_n \in \mathbb{R}^{160}$, $\tilde{\boldsymbol{\alpha}}_n \in \mathbb{R}^{160}$, $\breve{\boldsymbol{\alpha}}_n \in \mathbb{R}^{160}$).

There are many interesting aspects that can be seen in Fig. 5.41. Firstly, the reduced order nonlinear forward stepwise regression performs the best across all of the damage cases, including the training and testing unlike in Fig. 5.40. In this instance, the majority of the DSFs should be regressed according to the F-statistic. This suggests that the more complex models only benefit to model

the lower order components more accurately. A factor that becomes irrelevant once the F-statistic has been applied. The result of this is that the combined DSFs are now the superior choice across almost all of the damage cases since fewer measured DSFs will be used. Given the combined is now lower than both the reduced order nonlinear forward stepwise and the measured DSFs, it shows that the inclusion of measured DSFs over regression corrected DSFs can actually reduce the distribution of the within group observations. Similarly, regressing DSFs that should not be regressed can be conclusively shown to add uncertainty to the system.

Looking specifically into the Lasso regression in Fig. 5.41, it can be seen that the Lasso increases the distribution of within group observations compared to the proposed reduced order nonlinear forward stepwise regression method. Whilst it performs worse, the difference is not that significant. However, the computational costs associated with running the Lasso are far greater than the proposed method, further making it a less desirable choice. The NIQR does not give a measure of the damage detection, but it is an important aspect in creating robust and reliable systems. Purely based on the results from the NIQR study, the optimal solution is the combination of the reduced order nonlinear forward stepwise regression corrected DSFs with the measured DSFs according to their corresponding F-statistic.

5.3.8.2 Outlier rate

The outlier rate in Fig. 5.42 is given by the number of outliers in the selected distribution divided by the total number of observations in the damage group. As with the NIQR in Fig. 5.40, 25 different training data sets were used, with a total of 100 PCs from each sensor.

Observing firstly the training observations in Fig. 5.42, it can be seen that nonlinear forward stepwise regression has a lower outlier rate than reduced order nonlinear forward stepwise regression, the measured DSFs and marginally less

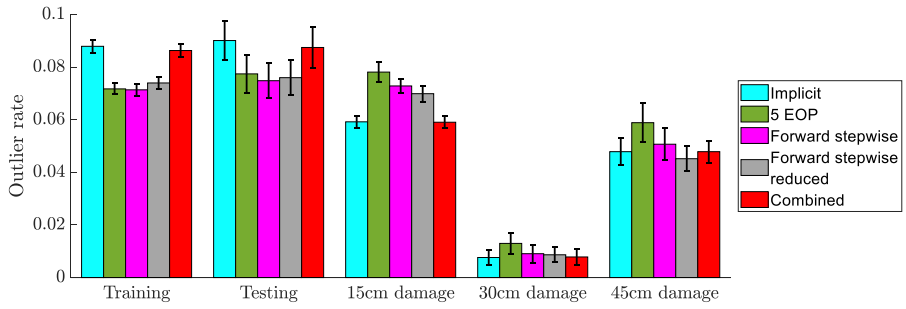

Figure 5.42: The outlier rate plotted against each damage case for each regression method, excluding Lasso. Regression procedure repeated 25 times with different training data sets. ($\boldsymbol{\alpha}_n \in \mathbb{R}^{800}$, $\tilde{\boldsymbol{\alpha}}_n \in \mathbb{R}^{800}$, $\breve{\boldsymbol{\alpha}}_n \in \mathbb{R}^{800}$).

than the 5 EOP trial and error approach. This result could be due to overfitting to the training data in the regular nonlinear forward stepwise regression but less accurate fitting due to the order reduction in the reduced order version. As with the NIQR in Fig.5.40, the number of outliers is consistent between training and testing.

Beyond the undamaged data in Fig. 5.42, there is a general pattern that emerges. Each step that is taken to improve the quality of the regression models improves the outlier rate, starting from the 5 EOP model right through to the combined DSFs. Additionally, the variation in the outlier rate for the combined DSFs is consistently the lowest across most damage scenarios. Whilst the outlier rate is higher in the undamaged cases, the benefits of the stability in the damage cases demonstrates an improvement over the other regression based methods. The lower outlier rate is made more impressive by the smaller NIQRs observed in Fig. 5.40, where it would be expected to have more outliers given a small distribution of points within the interquartile range.

Once again, the Lasso regression can be added to the analysis by reducing the number of PCs from each sensor from 100 to 20. Fig. 5.43 shows the analysis with the addition of the Lasso regression.

An important difference between Fig. 5.42 and Fig. 5.43 is that the magnitude of the outlier rate is lower for the regression models in Fig. 5.43. The

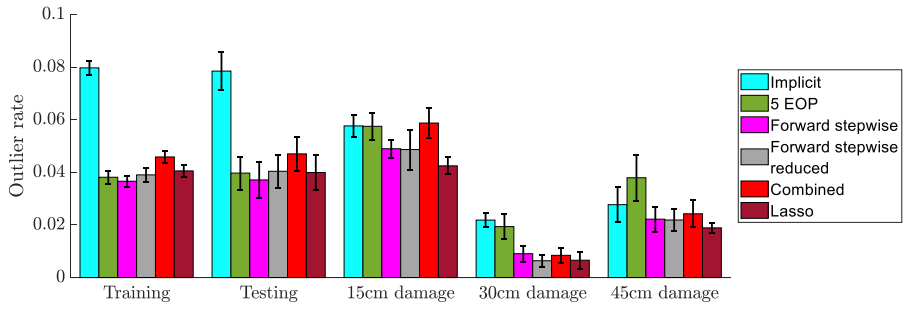

Figure 5.43: The outlier rate plotted against each damage case for each regression method. Regression procedure repeated 25 times with different training data sets. ($\boldsymbol{\alpha}_n \in \mathbb{R}^{160}$, $\tilde{\boldsymbol{\alpha}}_n \in \mathbb{R}^{160}$, $\breve{\boldsymbol{\alpha}}_n \in \mathbb{R}^{160}$).

reason for this is likely down to the fact that most of the lower order PCs contain information that is affected by EOVs and, thus, have relationships with the EOPs. The models can, therefore, be more accurately created and contain fewer outliers once the DSFs have been examined with the outlier analysis. In this case, the outlier rate for the combined DSFs is heavily influenced by the outlier rate of the measured DSFs within it.

Unlike the NIQR in Fig. 5.41, the Lasso regression appears to have a positive effect on the outlier rate. In almost all cases, the Lasso regression produces the lowest outlier rate compared to the other regression methods. In this work, the Lasso was not designed to establish the relationships between input variables and perhaps this aspect in the other regression methods cause a level of overfitting. As before, it is difficult to tell how the Lasso would perform over a larger range of DSFs given its large computational cost.

5.3.8.3 Coefficient matrix stability

A secondary aspect of each model that was tested was the coefficient matrix stability. The values for the coefficient matrix stability from Eq. 4.23 are shown in Fig. 5.44.

Fig. 5.44 shows that the trial and error (5EOP) approach has the most stable coefficient matrices. That is followed by the reduced order forward stepwise

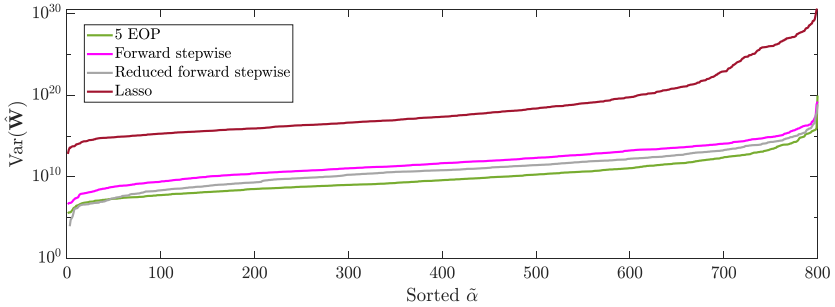

Figure 5.44: Coefficient matrix stability values against assorted DSFs using trial and error optimisation (5 EOP), forward stepwise optimisation, reduced order forward stepwise optimisation and Lasso optimisation.

method, the forward stepwise method and, finally, the Lasso. While the trial and error approach has the highest stability, previous works [87, 103] have shown that this approach suffers in the prediction of future observations, as well as being more computationally expensive compared to the nonlinear forward stepwise regression. On the other hand, the reduced order forward stepwise was able to predict future observations better through the methods within it that aimed to reduce overfitting. The result in Fig. 5.44 also shows that the reduction of model orders help with the matrix stability. Given previous results and those in Fig. 5.44, the best choice for robust and reliable mitigation would be the reduced order nonlinear forward stepwise method.

5.4 Chapter summary

In this chapter, a dataset from an operational wind turbine blade was introduced for the purpose of testing the proposed method in Chapter 4. The data was recorded from the structure over a period of around 3 months, where damage was introduced to the trailing edge in the form of a crack. The damage was extended twice before being repaired and the structure retested. During the monitoring campaign, the blade naturally experienced a range of different EOVs. To test the methodology, DSFs were extracted from the acceleration responses based on their frequency transformation.

A number of critical aspects related to the design of regression models, explored in Chapter 3, were addressed on the operational data. This proposed methodology was demonstrated to:

- Identify, using mutual information, and discard nonlinearly correlated input variables.
- Reduce the order that EOPs were modelled at in order to improve the estimation of future observations by lessening the effect of overfitted models.
- Identify the most influential EOPs to model the DSFs, reducing subset selection and improving the estimation of future observations.
- Determine which DSFs should or should not be regressed according to an F-test for the purpose of reducing the amount of uncertainty within the VSHM system.
- Remain effective when presented with varying amounts of information from the accelerometers.
- Remove biases created in the MSD by addressing the nature of the covariance of the training data.
- Simultaneously design regression models that were capable of improved damage detection compared to established methods, as well as reducing the distribution of observations of the same group whilst maintaining stable coefficient matrices.

A number of the aspects implemented from Chapter 4 appear to negatively affect the damage detection capabilities of the VSHM system as a whole, particularly the correction of the MSD. Whilst this is true, it is more important to address the effects of overfitting and bias in order to create a truly robust and

reliable monitoring system. Ignored uncertainties will artificially increase the MSD of observations beyond the training stage, making them appear as damaged when they are not. Without addressing these problems then, it is difficult to say with confidence which observations were outliers or damage. By establishing a framework that overcomes the problems, confidence in the decision making process can be restored.

The aim of this chapter was to demonstrate the importance of implementing methods to reduce uncertainty in VSHM systems. Whilst this was achieved in relation to the presented case study, it is important to consider the nature and requirements of each system that this type of methodology is applied on. Each system will experience different conditions and function for different purposes. The following section presents more general guidelines and advice on applying VSHM systems for wider applications.

6 | Comprehensive Guidelines for the Robust Mitigation of Environmental and Operational Variabilities

This chapter gives a guide towards the implementation of the different aspects of structural health monitoring, and explores the advantages and disadvantages of both implicit and explicit methods. The aim is to outline considerations when applying the types of method used in this thesis. Some of the content of this chapter is published in the works I authored [103] and co-authored [71] in which the advantages and disadvantages, as well as limitations, were discussed.

6.1 Vibration-based structural health monitoring system design

Vibration-Based Structural health monitoring can be a useful tool in the maintenance and operation of large civil structures. However, precautions must be taken to ensure that the system that is implemented is fit for the purpose for which it has been designed. In an ideal world, there would be a one-size fits-all method but sadly this is not the case at the moment. Therefore, it is necessary to examine what information is available from the structure, as well as assessing what will be the most appropriate DSF to use. It is highly likely that the optimal DSF for monitoring a wind turbine blade will not be the same as the DSF used for monitoring the supports of a long-span bridge. However, there are a few factors that can be considered transferable using similar frameworks. Even taking this account, the design of VSHM systems is an intricate and often difficult task, but an important one nonetheless.

An important first consideration is to assess the amount of data that is available for training the VSHM system. With most VSHM methods, a substantial amount of data is required to understand the intricate relationships that exist within the DSFs. If there is insufficient data, ideally more observations will should be collected. Should that not be possible, then it must be acknowledged that a large amount of uncertainty likely exists within the system. There are methods which require less training data, but methods such as deep learning call for extensive training data to ensure the patterns are learned effectively. Whilst the explicit method used in Section 5 does not require as large a training set, the number of undamaged observations, highlighted in Table 5.1, would not have been sufficient to create reliable models. This is why the repaired observations are used for training instead. A lack of sufficient training information can cause severe consequences in the prediction of future observations, making it challenging to differentiate between damaged and undamaged cases.

In most instances, once an appropriate DSF has been identified, the design of the VSHM can proceed to the next stage. However, in some cases, the dimension of the DSF is very large and impractical to work with. The computing cost will only increase as the dimension of the DSF increases. Since this is undesirable, a dimensional reduction scheme may be applied to assuage the issue. However, the difficulty then lies in how much information should be kept and how much discarded. Without any knowledge of the damage, it can be easy to inadvertently remove information from the DSF that might be sensitive to the occurrence of damage. Therefore, in an ideal scenario, it would be advantageous to preserve as much of the original information as possible. The results from Fig. 5.39 confirm, where as more PCs are added to the training model, the greater the AUC becomes. This suggests that even low variance components can contain information about the damage.

The range of conditions experienced by the structure during the training period is also an important aspect to consider. While this may seem like an obvious statement in relation to explicit models, it is also important for implicit models. Whilst the varying conditions are not being monitored, they will still affect the DSFs, unless in a very unlikely scenario that the entire DSF set is insensitive to any kind of varying conditions. If a full range of conditions is not included as part of the training, then it is likely that there will be an increase in outliers due to the structure experiencing unfamiliar conditions. This is best demonstrated in Fig. 3.13a where the introduction of extreme weather conditions causes unusual behaviour which could be mistaken for a change in the condition of the structure. The mitigation provided by the explicit model in Fig. 3.13c avoids this issues by directly modelling the effect of the changing conditions. However, there are still a number of outliers unaccounted for. Therefore, ensuring the training data has seen as wide a range of conditions as possible will add to the reliability and robustness of any VSHM system.

An additional factor to consider is the structure of the chosen model. The types of aspects to consider vary depending on the method that is being applied, but are typically made up of: model type, functional family, structural complexity and model order. Choosing an unsuitable model structure can adversely affect the predictions of future observations, as well as needlessly increasing the computational time. For example, by selecting a 10-th order polynomial to model a linear system, the model will try and fit unnecessary terms to account for the variability in the data, a phenomenon that is clear in Fig. 3.16b. Future observations that exist outside the training range can then be massively over or underestimated, indicating damage where none is present, such as the extreme weather in Fig. 3.15. Therefore, the incorrect model structure will create bias in the damage indices. Whilst it is not possible to assess each model structure, careful choices can mitigate against an inability to perform exhaustive modelling.

When designing a robust and reliable VSHM system, it is important to realise that not every step taken to remove uncertainty is going to result in superior results, at least not from a damage detection perspective. Not all uncertainty contained within a system will impede the differentiation between undamaged and damaged observations. Instead, the uncertainty can act as a pseudo-damage, making observations appear damaged when they are not. Ultimately, the measures taken to reduce uncertainty should still be carried out despite their potential effect on the outcome. It is possible that damage that was previously thought as detected merely could be a consequence of unaddressed uncertainty. An example of this was demonstrated when applying the novelty index correction in Section 4.5 to better represent the training data. The resulting AUC performs worse than prior to correction for all damage cases. However, this does not mean that it should not be implemented. The major improvement in the overlap between the training and testing observations is testament to the ability of the system to remove uncertainty.

6.2 Implicit models

One of the advantages of implicit methods is that they do not require any additional information beyond what is used to create the DSFs. Therefore, implicit methods bypass the need for additional computing power to synchronise and merge data streams. Consequently, implicit methods are either less accurate or need additional computing power to run more sophisticated and complex models. However, there are many pre-built algorithms that can easily be applied for a VSHM system. This can make implicit systems more user friendly and more accessible to those who do not have formal training. Unfortunately however, it creates a recurring problem where methods are implemented in instances where they are not appropriate. Without a full understanding of the individual methods, presumed assumptions about the data might not be met or overly complex methods might be implemented where simpler models fit the data better.

Without prior knowledge or context, implicit methods attempt to decipher patterns and relationships within the DSFs. However, the manifolds obtained in healthy and damaged states often overlap, particularly at the onset of damage. Given the overlap, there is the possibility that the system will be less sensitive to damage because of the similarities between the two states. Compounding the problem is the previously discussed dilemma, see Section 6.1, surrounding the decision on the amount of information to retain. To resolve this, more complex algorithms can be implemented, but again at the cost of increased computing power. Moreover, the addition of EOPs could once again assist in resolving the overlapped sections. However, where implicit methods are being applied, it is possible that there is no information available on the EOPs. As a result, implicit procedures often come with a limited sensitivity to damage but require less synchronisation.

One of the factors that often hinders implicit methods is their interpretability. Without the measurements of the EOPs, it can be difficult to directly

understand the occurrence of outliers. Whilst the features can be created using known physical relationships, they are often still affected by changes in the varying conditions. Therefore, it is not always possible to decouple the effects of the varying conditions from the influence of the damage. Once again, this has a negative effect on the damage sensitivity of the system. Complex models are capable of capturing the effect implicitly, but this is often on DSFs that have less direct physical meaning. To retain the interpretability, implicit models must find a balance between extremely complex and computationally expensive models and features that contain more physical meaning.

Principal component analysis is one of the most commonly applied implicit methods in the field of VSHM. It is one of many purely dimensional reduction methods that have been implemented in the definition of the DSFs. As mentioned previously, the largest difficulty in these methods is deciding which information to keep and which to discard, see Section 2.3.1.1. In most cases, it is assumed that certain components are more likely to be influenced by EOPs and should, therefore, be discarded. However, a second assumption here is that, again, the effects of damage and EOPs are decoupled. Without information on the EOPs, it is almost impossible to be certain of what is and is not affected by the varying conditions. Similarly, in implicit methods that do not involve dimensional reduction, any trends that are captured and mitigated cannot be directly attributed to any particular source. Once again, this decreases the level of interpretability of the system.

When it comes to implementation, implicit methods require as much training data as possible in order to understand the relationships between the DSFs. While it is not always possible to acquire the optimum amount of data, extremely powerful algorithms can often make up for this, but again at the cost of their interpretability. With the constantly advancing field of informatics, the accuracy and modelling capabilities of computer systems will continue to

improve. However, it is likely that for implicit systems to preserve any interpretability, they will have to be combined with measurements of the EOPs to create a holistic model.

6.3 Explicit models

One of the downsides to explicit methods is that they require more measurements. Additional equipment is often necessary to capture information from the structure's environment, as well as sensors for measuring its operating condition. The measurements taken from the structure itself can also be used for mitigating variations in the measured data. As a result, additional processing power is required to handle all of the information coming from the different sources. Caution must also be exercised in the synchronisation of the data so that the information from all of the sensors can be aligned perfectly, ensuring the measurements correspond globally across the structure. However, many structures already have the desirable information with systems that automatically synchronise the data. Nonetheless, it is an aspect that must be considered when working with data from multiple streams.

In addition to the increased computing power required to synchronise and gather information from the sensors, power is also required to run the algorithms that are used in the analysis stage. This is especially true in cases where there are a large number of input measurements and/or very complex models. Given that regression models are typically single output only, a new model must be created for each DSF. Consequently, when there are a large number of DSFs, a significant amount of power is required to model each feature. One solution to this is to use dimensional reduction, such as PCA in Section 5.3.1, to reduce the total number of DSFs. However, if the DSFs are based on physical relationships, interpretability of the data can be lost. Consequently, a balance must be struck between the amount of information being measured, the dimension of the feature vectors and the available computing power.

A fundamental problem, that is often overlooked, can also occur in high dimensional data. The problem is centred on the application of regression models to DSFs that appear insensitive to the available EOPs. By attempting to regress DSFs where no trend is present is an easy way to introduce more uncertainty into the system, as discussed in Section 4.3.4. Techniques like the F-statistic can be employed to determine whether a regression model is able to predict observations more accurately than the mean of the data. As such, the system becomes more flexible and robust by regressing only the components which evidence significant dependence on varying conditions. Given that the any system should be purged of as much uncertainty as possible, this problem is one that must be addressed, even if it seemingly decreases the rate of damage detection. Ultimately, by combining measured and regression corrected DSFs, it is possible to create a more robust system which has comparatively better damage detection, as shown in Fig. 5.39.

As the number of DSFs and input variables increase, the optimisation procedure becomes substantially more complex. There are many aspects to the regression models that must be addressed to ensure a robust model is created. That is to say, the observations beyond the training will be suitably predicted. The most significant problem that occurs is the overfitting of models. To alleviate this problem, coefficients with magnitude significantly smaller than those within the same matrix are identified and used to redefine the model orders, as detailed in Section 4.3.3. Given a large magnitude of input variables and DSFs, it is certainly not possible to examine each model individually to assess its quality. Therefore, an automatic procedure, such as the one presented in Section 4.3, is required to carry out the task. Unfortunately, this adds computational expense.

Having many environmental and operational sensors can also be detrimental in other ways. Firstly, when there are a large number of available measurements,

it can be difficult to identify which particular measurements are actually influential on the system. As discussed previously, Section 4.1, adding parameters that have no influence can have severe consequences on the regression model's predictive capability, especially in observations beyond the training. This effect is clearly shown in Fig. 5.11, where the overlap between training and testing is significantly improved when fewer EOPs are used for modelling. However, through the implementation of controlled optimisation procedures, this problem can be reduced. Another aspect is that with a large number of measurements, there is likely to be a large amount of correlation. The correlation of input variables can lead to problems in uniquely defining regression coefficients. This was addressed in Section 4.3.1 by removing highly correlated variables through assessing their mutual information. Although PCC identified the same correlated variables to remove in Fig. 5.17, it is recommended to use mutual information in any system where complex inter-EOP relationships are present. An alternative method could be to use dimensional reduction methods such as principal component analysis, factor analysis or singular spectrum analysis. However, dimensionally reduced input variables can lose a significant amount of physical interpretability. Whilst physical interpretability is not always essential, it is often a reason for using an explicit method rather an implicit one.

However, one of the great benefits of explicit procedures comes from the presence of the EOPs in the training model. If the aforementioned problems have been addressed in an appropriate manner then a more controlled system can be created. Consequently, the results obtained as part of the structural health monitoring system are more robust and reliable, as well as being more interpretable. Part of this increased interpretability comes from the modelling of the cause-effect relationship between the EOPs and the DSFs. When large variances occur in the DSFs, these can then be directly traced back to changes in the EOPs. Whilst the magnitude of complexity increases with the addition of the EOPs, explicit models are still considered the preferable option. This

is because, on top of the aforementioned points, they are influenced less by the presence of outliers, are less prone to overfitting and in cases of stochastic models, uncertainty bounds can be computed. However, this does not mean that these aspects should not be investigated. If disregarded, the quality of the model can be severely impacted, as demonstrated in this work.

In many structures, there are a large number of sensors for measuring environmental conditions, but this is not always the case. Especially in the case of large structures, such as dams and bridges, it is not practical to have a fine grid of sensors throughout the structure. In this case, environmental measurements taken may experience fractionally, but not insignificantly, different conditions to the sensors measurements used in the definition of the DSFs, which will then cause inaccuracies in the explicit model. For instance, Murgia et al. [219] found that whilst a wind turbine gearbox bearing temperature was a good predictor of gearbox failure, the gear oil temperature was not. This highlights the importance of taking the EOP measurements at each individual point of interest in examples where there is likely to be a variation of temperature across the structure. Had the bearing temperature been assumed to be the same as the oil, the forthcoming failure would not be detected. This can also be a problem in smaller structures where there may only be one available measurement for the entire structure. In some cases, such as wind farms, there is only one measurement of each parameter that is measured at one structure and used for all neighbouring structures. This aspect should be considered during monitoring as outliers may occur when the measurements do not correspond well.

Another advantage of explicit procedures can be observed when considering structures that experience large variations in their dynamic behaviour when switching operating regimes. A prime example of this can be found in the operation of wind turbines. The dynamic characteristics of the structure change vastly when it transfers from an idling regime to an energy production regime. In addition to changes in operational conditions, changes to external boundary

conditions of a structure, such as the water level behind a dam due to drought or during wet seasons, can significantly affect the structural dynamics. Similarly, the height of waves that offshore wind turbines experience varies the overall stiffness of the system. The solution, then, is to construct independent models for each discrete, or range of, operational conditions. Ultimately, this is a large benefit of explicit procedures where the changing conditions are continuously monitored.

For an explicit procedure to see implementation, there are many factors that must be addressed for it to produce meaningful results. In addition to the substantial computational power required for data synchronisation, regression modelling and optimisation, an initial monitoring period of ample length is required to capture a sufficient range of conditions to ensure high quality regression models. Failure to address the many potential pitfalls of explicit methods will result in unreliable and possibly dangerous results.

7 | Conclusions and Future Work

The purpose of this chapter is to bring together the results and discussions from throughout this thesis. Conclusions are drawn on each of the applied methods, reflecting on their efficacy. Subsequently, areas of future research interest are proposed in order to continue the improvement of VSHM for wind turbine blades.

7.1 Conclusions

Due to their exposure to harsh weather conditions, wind turbines are susceptible to damage due to hail, rain, and lightning strikes. In addition to these factors, damage can also occur as a result of manufacturing errors, particle impacts and many more events. Manual inspection of the wind turbine blades can be very time consuming and difficult to conduct when the turbines are located in remote areas. VSHM has been proposed as an alternative method for maintenance as it can be operated in real-time and online, bypassing the need to visit the turbines each inspection. However, the varying environmental and operational conditions can make it difficult to differentiate between damaged and undamaged observations.

The challenge of mitigating the effects of varying conditions has been the subject of a great deal of research. Methods such as principal component analysis, cointegration and neural networks have been applied and have shown some success. However, the methods have lacked sufficient robustness to see implementation on real structures. This work aimed to overcome this challenge through considered design of multivariate nonlinear regression models. The proposed solution uses an adapted forward stepwise optimisation procedure to address common problems associated with the overfitting of model orders and the subset selection problem. The holistic method also recognises the effect of correlated input variables, the value of regression and the definition of the of outlier metric. For the purpose of comparison, the proposed method was compared to a PCA-based approach, as well as against Lasso regression, a backward stepwise regression method.

7.1.1 Implicit method

The implemented implicit method was based on a dimensionally reduced frequency response using PCA. The implicit method was capable of detecting

damage when presented with a large amount of information. However, when using lower numbers of PCs, the implicit method was unable to differentiate any degree of damage from the undamaged observations. The implication of this is that the lower order PCs are the ones which are most affected by EOVs. Since only direct comparisons were tested, the scenario where the lower order PCs are removed was not tested. Furthermore, since the information about damage and EOVs is difficult to decouple, it is desirable to keep as much of the original information as possible since most PCs will contain some information about damage. In addition, a number of assumptions have to be made about which PCs to remove. The implicit method fundamentally lacks the interpretability of an explicit method, meaning that the consequence of each action to the VSHM system cannot be fully understood.

7.1.2 Explicit method

To demonstrate the importance of regression architecture and model design, multivariate nonlinear regression was implemented. Subsequently, a nonlinear forward stepwise regression was applied to improve the robustness towards EOVs of a damage detection algorithm. The aim of this work was to address important challenges that occur in multivariate regression, such as the overfitting of model orders, redundant input variables and collinearity between input variables. The proposed method was able to identify and remove correlated input variables by either mutual information or Pearson's correlation coefficient. However, since Pearson's correlation coefficient is suited towards linear correlation, it is recommended to continue to use mutual information for future applications. The optimisation method used in the forward stepwise regression was capable of creating models that were comparably as accurate as a laborious trial and error approach. Furthermore, the optimisation was able to recognise and and remove overfitted variables.

The proposed methodology was able to outperform a trial and error approach to optimisation and a Lasso regression, as well as the original measured DSFs. Furthermore, it was demonstrated that reducing the model orders aids in preventing overfitting, a crucial aspect to the accurate estimation of future observations. However, the most important finding in this work was that the proposed methodology allows the creation of a tailored nonlinear regression model that obtains a DSF vector that combines DSFs which are normalised against different numbers of EOPs depending on their influence.

In addition to creating more accurate and representative models, the proposed methodology also automatically analysed each DSF to determine whether the regression model provided value to the prediction. The value of each regression model was tested using the F-statistic for the regression model against the mean of the DSF. In cases where the regression model did not add significant value, the regressed DSF was replaced with the measured DSF. The combination of these factors contribute to a more robust DSF, where no biases or uncertainties are unintentionally introduced. Ultimately, a more reliable VSHM system is created, one that can accurately mitigate the effects of EOVs.

7.2 Limitations and future work

In order for the proposed method to develop further, a number of future directions have been identified. Whilst the proposed method was demonstrated to construct more robust and reliable regression models, work is still required before VSHM will be commercially viable. The first suggestion aims to target a number of the limitations that arose from the utilised dataset while the second proposes a methodology that could be implemented to improve the quality of the training model.

7.2.1 Utilising a more expansive dataset

One of the main limitations of the dataset was first identified in Section 5.2. The lack of available observations for the undamaged observations meant that the repaired observations had to be used in their place. Whilst it is possible to train regression models with fewer observations, the presence of each outlier creates a larger bias in the training phase of the model. As such, the more observations that are available for training, the more reliable the predictions are likely to be. Hence, this is why the repaired observations were used for training. In future work, it would be interesting to test the outcome of a case study where significantly more undamaged observations are available. This would allow the analysis of the effect of bias as a result of outliers, as well as whether model order overfitting remains an issue.

In addition to the lack of observations in the undamaged data, the range of the environmental and operational parameters is not sufficient to create robust regression models. Even while using the repaired observations for training, it would be desirable to have a wider range of conditions. Without seeing a full range of parameters, the regression models are more likely to overfit to the range of values that are available. Since the monitoring campaign of the case study was over winter, the regression models are unlikely to understand hotter summer conditions. Therefore, in addition to an increased number of observations, the proposed method should be tested on a dataset that has experienced a full seasonal cycle. In an ideal world, data available from multiple full seasonal cycles would enhance the understanding of any VSHM method. Testing the proposed method on a case study with such available observations will give a better understanding of the potential benefits, as well as any disadvantages of the method. Such a test could put VSHM in a better position in terms of implementation on operational structures.

7.2.2 Updating the training model

In the monitoring of operational structures, it will be unlikely that information about damage is available. As such, it is important that as many steps are taken to ensure that the baseline represents the undamaged state of the structure as best as possible. While having information on a full seasonal cycle is important, this is also not always practical. A possible solution to this problem is to have a constantly evolving training set. If the VSHM system can confidently assume a new observation is undamaged, it can then retrain the models with the additional point.

The major difficulty with this method is determining whether a new observation is undamaged. Typically the MSD is used for this purpose. However, this is insufficient in itself since it will constantly change and the presence of outliers will cause bias. Therefore, the essence of the problem lies in understanding the nature of the outliers; whether they can be explained or not. For this reason, explicit methods are particularly well suited to this application because the relationship between EOP and DSF is estimated. Fig. 7.1 demonstrates a possible visible representation for determining whether a new observation is undamaged. In this case, ψ represents a function of the EOPs.

From Fig. 7.1, it can be seen that there are four main regions under which any new observation can fall. The first group is the undamaged (known) group and it is made up of observations where there is high likelihood that they are undamaged. This group is the most important as it contains the observations that will be used for retraining of the baseline model. As the value of ψ increases, there is less confidence in the state of the observation since the training conditions are outside what is understood by the regression models. This group could also be used for retraining in order to expand the range of conditions that the system is trained with. Above a threshold in the MSD, the observations can belong to one of two groups. With lower values of ψ, the system can be

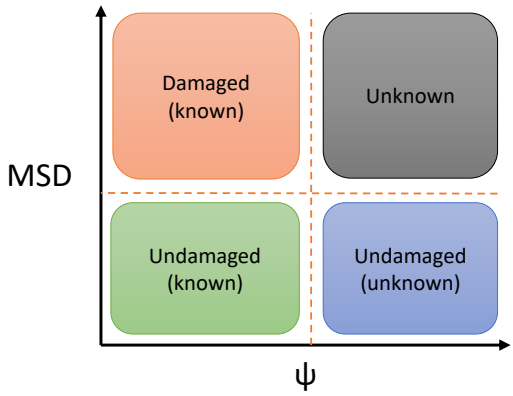

Figure 7.1: MSD plotted against function of EOPs, used for determining if new observation should be used for retraining regression model.

more confident that something unusual is happening and can stop using the observations for training. Finally, the unknown group in the top right consists of observations that have high values for the MSD paired with high values of ψ. This group lacks the information to understand fully what is happening with the structure.

The idea behind Fig. 7.1 can be integrated into the explicit method, Fig. 2.3, as a type of closed loop optimisation. Fig. 7.2 demonstrates where the loop should be placed so that the DSFs associated with the undamaged (known) group can be fed back into the training model.

The addition of the loop allows for a more accurate training dataset to be created. However, there is a risk that small changes in damage will be included into training which will accumulate over time. This scenario would then hinder the ability of the VSHM system to differentiate between undamaged and damaged observations. The addition of Bayesian probability could further help to initially differentiate between undamaged and damaged observations. However, more research is needed to explore the exact nature of the loop. Successful implementation could greatly increase the number of observations used

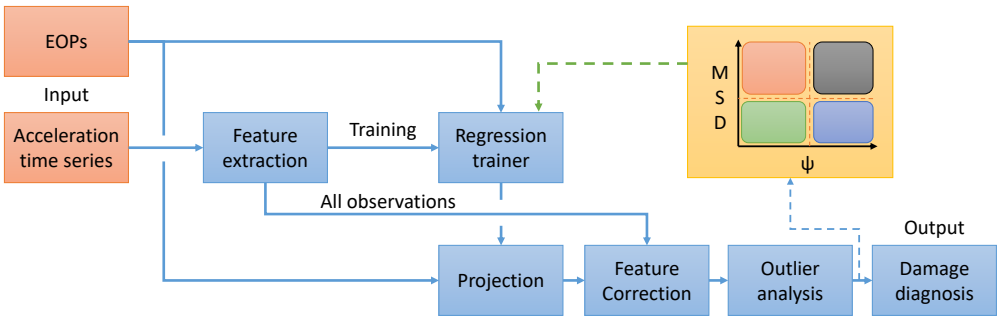

Figure 7.2: Schematic representation of the overall explicit method for VSHM with closed loop for introducing new observations into the training observation set.

for training, thus creating a more robust VSHM system.

7.2.3 Summary

The lack of implementation of VSHM on operational structures is often attributed to lack of evidence of robustness. To overcome this obstacle, the proposed methodology should be tested on a variety of large datasets, ones which have experienced a full seasonal cycle. A large number of observations are required to create robust and reliable VSHM systems. If a large amount of data is not available, then methods that make the most of available data should be implemented. Once the methodology has been shown to be robust, it is far more likely to installed on operational structures.

Bibliography

[1] J. Houghton, *Global warming: the complete briefing*. Cambridge university press, 2009.

[2] J. Houghton, "Global warming," *Reports on progress in physics*, vol. 68, no. 6, p. 1343, 2005.

[3] P. Agreement, "Paris agreement," in *Report of the Conference of the Parties to the United Nations Framework Convention on Climate Change (21st Session, 2015: Paris). Retrived December*, vol. 4, p. 2017, HeinOnline, 2015.

[4] M. McGrath, "Climate change: Us formally withdraws from paris agreement," Nov. 2020.

[5] C. Schumer, S. Boehm, T. Fransen, K. Hausker, and C. Dellesky, "6 takeaways from the 2022 ipcc climate change mitigation report," Apr. 2022.

[6] P. Shukla, J. Skea, R. Slade, A. Al Khourdajie, R. van Diemen, D. McCollum, M. Pathak, S. Some, R. Vyas, R. Fradera, M. Belkacemi, A. Hasija, G. Lisboa, S. Luz, and J. Malley, "Climate change 2022: Mitigation of climate change. contribution of working group iii to the sixth assessment report of the intergovernmental panel on climate change.," 2022.

[7] J. K. Kaldellis and D. Zafirakis, "The wind energy (r) evolution: A short review of a long history," *Renewable energy*, vol. 36, no. 7, pp. 1887–1901, 2011.

[8] S. Renewables, "Energy consumption by sector."

[9] BBC, "Renewables met 97% of scotland's electricity demand in 2020," Mar. 2021.

[10] W. Europe, "North sea offshore wind to help repower the eu," May 2022.

[11] M. A. Djeziri, S. Benmoussa, and R. Sanchez, "Hybrid method for remaining useful life prediction in wind turbine systems," *Renewable Energy*, vol. 116, pp. 173–187, 2018.

[12] J. S. Nielsen and J. D. Sørensen, "Bayesian estimation of remaining useful life for wind turbine blades," *Energies*, vol. 10, no. 5, p. 664, 2017.

[13] C. Loraux and E. Brühwiler, "The use of long term monitoring data for the extension of the service duration of existing wind turbine support structures," in *Journal of Physics: Conference Series*, vol. 753, p. 072023, IOP Publishing, 2016.

[14] J. Cotrell, T. Stehly, J. Johnson, J. Roberts, Z. Parker, G. Scott, and D. Heimiller, "Analysis of transportation and logistics challenges affecting the deployment of larger wind turbines: summary of results," tech. rep., National Renewable Energy Lab.(NREL), Golden, CO (United States), 2014.

[15] J. Zhang, G. Cosma, and J. Watkins, "Image enhanced mask r-cnn: A deep learning pipeline with new evaluation measures for wind turbine blade defect detection and classification," *Journal of Imaging*, vol. 7, no. 3, p. 46, 2021.

[16] H. Zhang and J. Jackman, "A feasibility study of wind turbine blade surface crack detection using an optical inspection method," in *2013 International Conference on Renewable Energy Research and Applications (ICRERA)*, pp. 847–852, IEEE, 2013.

[17] C. C. Ciang, J.-R. Lee, and H.-J. Bang, "Structural health monitoring for a wind turbine system: a review of damage detection methods," *Measurement science and technology*, vol. 19, no. 12, p. 122001, 2008.

[18] D. García, I. Trendafilova, and D. J. Inman, "A study on the vibration-based self-monitoring capabilities of nano-enriched composite laminated beams," *Smart Materials and Structures*, vol. 25, no. 4, p. 045011, 2016.

[19] Y. Ying, J. H. Garrett Jr, I. J. Oppenheim, L. Soibelman, J. B. Harley, J. Shi, and Y. Jin, "Toward data-driven structural health monitoring: application of machine learning and signal processing to damage detection," *Journal of Computing in Civil Engineering*, vol. 27, no. 6, pp. 667–680, 2013.

[20] C. Heilmann, A. Grunwald, M. Melsheimer, R. Liebich, and R. Kamieth, "Reconstruction of a wind turbine's endured load spectrum using a short-time load measurement and operational data," *Proceeding of EWEA 2014*, 2014.

[21] S. M. Kojidi, M. Döhler, D. Bernal, and Y. Liu, "Linear projection techniques in damage detection under a changing environment," in *Topics in Modal Analysis, Volume 7*, pp. 325–332, Springer, 2014.

[22] G. Manson, "Identifying damage sensitive, environment insensitive features for damage detection," in *Proceedings of the third international conference on identification in engineering systems*, pp. 187–197, 2002.

[23] B. Peeters and G. De Roeck, "One-year monitoring of the z24-bridge: environmental effects versus damage events," *Earthquake engineering & structural dynamics*, vol. 30, no. 2, pp. 149–171, 2001.

[24] H. Sohn, M. Dzwonczyk, E. G. Straser, K. H. Law, T. H.-Y. Meng, and A. S. Kiremidjian, "Adaptive modeling of environmental effects in modal parameters for damage detection in civil structures," in *Smart structures and materials 1998: Smart systems for bridges, structures, and highways*, vol. 3325, pp. 127–138, International Society for Optics and Photonics, 1998.

[25] C. Devriendt, F. Magalhães, W. Weijtjens, G. De Sitter, Á. Cunha, and P. Guillaume, "Structural health monitoring of offshore wind turbines using automated operational modal analysis," *Structural Health Monitoring*, vol. 13, no. 6, pp. 644–659, 2014.

[26] F. Gharibnezhad, L. E. Mujica, J. Rodellar, and C. P. Fritzen, "Damage detection using principal component analysis based on wavelet ridges," in *Key Engineering Materials*, vol. 569, pp. 916–923, Trans Tech Publ, 2013.

[27] L. Mujica, J. Rodellar, A. Fernandez, and A. Güemes, "Q-statistic and t2-statistic pca-based measures for damage assessment in structures," *Structural Health Monitoring*, vol. 10, no. 5, pp. 539–553, 2011.

[28] C. Roberts, D. Garcia, and D. Tcherniak, "A comparative study on data manipulation in pca-based structural health monitoring systems for removing environmental and operational variations," in *Proceedings of the 13th International Conference on Damage Assessment of Structures*, pp. 182–198, Springer, 2020.

[29] E. J. Cross and K. Worden, "Cointegration and why it works for shm," in *Journal of Physics: Conference Series*, vol. 382, p. 012046, IOP Publishing, 2012.

[30] B. A. Qadri, M. D. Ulriksen, L. Damkilde, and D. Tcherniak, "Cointegration for detecting structural blade damage in an operating wind turbine: An experimental study," in *Dynamics of Civil Structures, Volume 2*, pp. 173–180, Springer, 2020.

[31] H. Shi, K. Worden, and E. Cross, "A nonlinear cointegration approach with applications to structural health monitoring," in *Journal of Physics: Conference Series*, vol. 744, p. 012025, IOP Publishing, 2016.

[32] A. Movsessian, D. G. Cava, and D. Tcherniak, "An artificial neural network methodology for damage detection: Demonstration on an operating wind turbine blade," *Mechanical Systems and Signal Processing*, vol. 159, p. 107766, 2021.

[33] L. Yang and Z. Zhang, "A conditional convolutional autoencoder-based method for monitoring wind turbine blade breakages," *IEEE Transactions on Industrial Informatics*, vol. 17, no. 9, pp. 6390–6398, 2020.

[34] Y. Yu, H. Cao, X. Yan, T. Wang, and S. S. Ge, "Defect identification of wind turbine blades based on defect semantic features with transfer feature extractor," *Neurocomputing*, vol. 376, pp. 1–9, 2020.

[35] J. M. Brownjohn, "Structural health monitoring of civil infrastructure," *Philosophical Transactions of the Royal Society A: Mathematical, Physical and Engineering Sciences*, vol. 365, no. 1851, pp. 589–622, 2007.

[36] G. James III, "Development of structural health monitoring techniques using dynamics testing," tech. rep., Sandia National Lab.(SNL-NM), Albuquerque, NM (United States), 1996.

[37] F.-K. Chang, "A summary report of the 2nd workshop on structural health monitoring, held at stanford university on september 8-10, 1999," tech.

rep., STANFORD UNIV CA DEPT OF AERONAUTICS AND ASTRONAUTICS, 2000.

[38] A. Rytter, *Vibrational based inspection of civil engineering structures*. PhD thesis, Dept. of Building Technology and Structural Engineering, 1993.

[39] C. R. Farrar, K. Worden, and J. Dulieu-Barton, "Principles of structural degradation monitoring," *Encyclopedia of structural health monitoring*, 2009.

[40] A. Mita, "Emerging needs in japan for health monitoring technologies in civil and building structures," in *Proc. Second International Workshop on Structural Health Monitoring*, pp. 56–67, Citeseer, 1999.

[41] R. Moss and S. Matthews, "In-service structural monitoring. a state of the art review," *Structural Engineer*, vol. 73, no. 2, 1995.

[42] D. Ziaja and P. Nazarko, "Shm system for anomaly detection of bolted joints in engineering structures," in *Structures*, vol. 33, pp. 3877–3884, Elsevier, 2021.

[43] D. Montalvao, N. M. M. Maia, and A. M. R. Ribeiro, "A review of vibration-based structural health monitoring with special emphasis on composite materials," *Shock and vibration digest*, vol. 38, no. 4, pp. 295–324, 2006.

[44] C. Rainieri, I. Rosati, L. Cieri, and G. Fabbrocino, "Development of the digital twin of a historical structure for shm purposes," in *European Workshop on Structural Health Monitoring*, pp. 639–646, Springer, 2023.

[45] C. Ye, L. Butler, B. Calka, M. Iangurazov, Q. Lu, A. Gregory, M. Girolami, and C. Middleton, "A digital twin of bridges for structural health monitoring," *Structural Health Monitoring 2019*, 2019.

[46] F. Concli, L. Pierri, and C. Sbarufatti, "A model-based shm strategy for gears—development of a hybrid fem-analytical approach to investigate the effects of surface fatigue on the vibrational spectra of a back-to-back test rig," *Applied Sciences*, vol. 11, no. 5, p. 2026, 2021.

[47] P. Antunes, A. Żmij // i jewska Rocha, N. Ferreira, J. Viana, and G. Dias, "Finite element model-based structural health monitoring (shm) systems of critical structural components under vibrations," *researchgate*, 2009.

[48] E. Z. Moore, J. M. Nichols, and K. D. Murphy, "Model-based shm: Demonstration of identification of a crack in a thin plate using free vibration data," *Mechanical systems and signal processing*, vol. 29, pp. 284–295, 2012.

[49] J. E. Warner, G. F. Bomarito, J. D. Hochhalter, W. P. Leser, P. E. Leser, and J. A. Newman, "A computationally-efficient probabilistic approach to model-based damage diagnosis," *International journal of prognostics and health management*, vol. 8, no. 2, 2017.

[50] M. Mróz, A. Świercz, P. Kołakowski, and J. Holnicki-Szulc, "Model-based identification of structural parameters using strain measurements–simulation and experiment," *IPPT PAN*, 2009.

[51] T. Nagayama, B. Spencer, G. Agha, and K. Mechitov, "Model-based data aggregation for structural monitoring employing smart sensors," in *Proc. of INSS*, pp. 1–8, 2006.

[52] D. A. Tibaduiza Burgos, R. C. Gomez Vargas, C. Pedraza, D. Agis, and F. Pozo, "Damage identification in structural health monitoring: A brief review from its implementation to the use of data-driven applications," *Sensors*, vol. 20, no. 3, p. 733, 2020.

[53] M. Azimi, A. D. Eslamlou, and G. Pekcan, "Data-driven structural health monitoring and damage detection through deep learning: State-of-the-art review," *Sensors*, vol. 20, no. 10, p. 2778, 2020.

[54] A. Entezami, H. Sarmadi, M. Salar, C. De Michele, and A. N. Arslan, "A novel data-driven method for structural health monitoring under ambient vibration and high-dimensional features by robust multidimensional scaling," *Structural Health Monitoring*, p. 1475921720973953, 2021.

[55] D. García and D. Tcherniak, "An experimental study on the data-driven structural health monitoring of large wind turbine blades using a single accelerometer and actuator," *Mechanical Systems and Signal Processing*, vol. 127, pp. 102–119, 2019.

[56] B. C. Love, "Comparing supervised and unsupervised category learning," *Psychonomic bulletin & review*, vol. 9, no. 4, pp. 829–835, 2002.

[57] S. Li, S. Li, S. Laima, and H. Li, "Data-driven modeling of bridge buffeting in the time domain using long short-term memory network based on structural health monitoring," *Structural Control and Health Monitoring*, vol. 28, no. 8, p. e2772, 2021.

[58] E. J. Cross, S. Gibson, M. Jones, D. Pitchforth, S. Zhang, and T. Rogers, "Physics-informed machine learning for structural health monitoring," in *Structural Health Monitoring Based on Data Science Techniques*, pp. 347–367, Springer, 2022.

[59] B. Peeters, J. Maeck, and G. De Roeck, "Vibration-based damage detection in civil engineering: excitation sources and temperature effects," *Smart materials and Structures*, vol. 10, no. 3, p. 518, 2001.

[60] S. Alampalli, "Effects of testing, analysis, damage, and environment on modal parameters," *Mechanical Systems and Signal Processing*, vol. 14, no. 1, pp. 63–74, 2000.

[61] H. Sohn, M. Dzwonczyk, E. G. Straser, A. S. Kiremidjian, K. H. Law, and T. Meng, "An experimental study of temperature effect on modal parameters of the alamosa canyon bridge," *Earthquake engineering & structural dynamics*, vol. 28, no. 8, pp. 879–897, 1999.

[62] V. Askegaard and P. Mossing, "Long term observation of rc-bridge using changes in natural frequency. nordic concrete research. publication no 7," *Publication of: NORDIC CONCRETE FEDERATION*, 1988.

[63] W. Hu, K. Choi, and H. Cho, "Reliability-based design optimization of wind turbine blades for fatigue life under dynamic wind load uncertainty," *Structural and multidisciplinary optimization*, vol. 54, no. 4, pp. 953–970, 2016.

[64] W. Hu, K. Choi, O. Zhupanska, and J. H. Buchholz, "Integrating variable wind load, aerodynamic, and structural analyses towards accurate fatigue life prediction in composite wind turbine blades," *Structural and multidisciplinary optimization*, vol. 53, no. 3, pp. 375–394, 2016.

[65] M. Liu, D. M. Frangopol, and S. Kim, "Bridge safety evaluation based on monitored live load effects," *Journal of Bridge Engineering*, vol. 14, no. 4, pp. 257–269, 2009.

[66] Y. Xia and Y. Ni, "Extrapolation of extreme traffic load effects on bridges based on long-term shm data," *Smart structures and systems*, vol. 17, no. 6, pp. 995–1015, 2016.

[67] M. Khazaee, P. Derian, and A. Mouraud, "A comprehensive study on structural health monitoring (shm) of wind turbine blades by instrumenting tower using machine learning methods," *Renewable Energy*, 2022.

[68] W.-H. Hu, S. Thöns, R. G. Rohrmann, S. Said, and W. Rücker, "Vibration-based structural health monitoring of a wind turbine system part ii: Environmental/operational effects on dynamic properties," *Engineering Structures*, vol. 89, pp. 273–290, 2015.

[69] T. Bull, M. D. Ulriksen, and D. Tcherniak, "The effect of environmental and operational variabilities on damage detection in wind turbine blades," in *9th European Workshop on Structural Health Monitoring*, p. 84, NDT net, 2018.

[70] A. Staino and B. Basu, "Dynamics and control of vibrations in wind turbines with variable rotor speed," *Engineering Structures*, vol. 56, pp. 58–67, 2013.

[71] D. García Cava, L. D. Avendaño-Valencia, A. Movsessian, C. Roberts, and D. Tcherniak, "On explicit and implicit procedures to mitigate environmental and operational variabilities in data-driven structural health monitoring," in *Structural Health Monitoring Based on Data Science Techniques*, pp. 309–330, Springer, 2022.

[72] A. Deraemaeker and K. Worden, "A comparison of linear approaches to filter out environmental effects in structural health monitoring," *Mechanical systems and signal processing*, vol. 105, pp. 1–15, 2018.

[73] G. F. Gomes, Y. A. D. Mendez, P. da Silva Lopes Alexandrino, S. S. da Cunha, and A. C. Ancelotti, "A review of vibration based inverse methods for damage detection and identification in mechanical structures using optimization algorithms and ann," *Archives of computational methods in engineering*, vol. 26, no. 4, pp. 883–897, 2019.

[74] G. Capellari, E. Chatzi, and S. Mariani, "Cost–benefit optimization of structural health monitoring sensor networks," *Sensors*, vol. 18, no. 7, p. 2174, 2018.

[75] G. Capellari, E. Chatzi, and S. Mariani, "Structural health monitoring sensor network optimization through bayesian experimental design," *ASCE-ASME Journal of Risk and Uncertainty in Engineering Systems, Part A: Civil Engineering*, vol. 4, no. 2, p. 04018016, 2018.

[76] E. Migoya, A. Crespo, J. Garcia, F. Moreno, F. Manuel, A. Jimenez, and A. Costa, "Comparative study of the behavior of wind-turbines in a wind farm," *Energy*, vol. 32, no. 10, pp. 1871–1885, 2007.

[77] N. Dervilis, K. Worden, and E. Cross, "On robust regression analysis as a means of exploring environmental and operational conditions for shm data," *Journal of Sound and Vibration*, vol. 347, pp. 279–296, 2015.

[78] A. Movsessian, D. G. Cava, and D. Tcherniak, "Interpretable machine learning in damage detection using shapley additive explanations," *ASCE-ASME Journal of Risk and Uncertainty in Engineering Systems, Part B: Mechanical Engineering*, vol. 8, no. 2, p. 021101, 2022.

[79] K. I. Kim, K. Jung, and H. J. Kim, "Face recognition using kernel principal component analysis," *IEEE signal processing letters*, vol. 9, no. 2, pp. 40–42, 2002.

[80] G. Byrne, P. Crapper, and K. Mayo, "Monitoring land-cover change by principal component analysis of multitemporal landsat data," *Remote sensing of Environment*, vol. 10, no. 3, pp. 175–184, 1980.

[81] J. Tang, "Frequency response based damage detection using principal component analysis," in *2005 IEEE International Conference on Information Acquisition*, pp. 6–pp, IEEE, 2005.

[82] F. Song, Z. Guo, and D. Mei, "Feature selection using principal component analysis," in *2010 international conference on system science, engineering design and manufacturing informatization*, vol. 1, pp. 27–30, IEEE, 2010.

[83] P. E. Hart, D. G. Stork, and R. O. Duda, *Pattern classification*. Wiley Hoboken, 2000.

[84] D. Tibaduiza, L. Mujica, and J. Rodellar, "Comparison of several methods for damage localization using indices and contributions based on pca," in *Journal of Physics: Conference Series*, vol. 305, p. 012013, IOP Publishing, 2011.

[85] G. Lederman, Z. Wang, J. Bielak, H. Noh, J. H. Garrett, S. Chen, J. Kovacevic, F. Cerda, and P. Rizzo, "Damage quantification and localization algorithms for indirect shm of bridges," in *Proc. Int. Conf. Bridge Maint., Safety Manag., Shanghai, China*, pp. 640–647, 2014.

[86] L. D. Avendaño-Valencia, E. N. Chatzi, and D. Tcherniak, "Gaussian process models for mitigation of operational variability in the structural health monitoring of wind turbines," *Mechanical Systems and Signal Processing*, vol. 142, p. 106686, 2020.

[87] C. Roberts, D. G. Cava, and L. D. Avendaño-Valencia, "Understanding the influence of environmental and operational variability on wind turbine blade monitoring," in *European Workshop on Structural Health Monitoring*, pp. 109–118, Springer, 2020.

[88] A.-M. Yan, G. Kerschen, P. De Boe, and J.-C. Golinval, "Structural damage diagnosis under varying environmental conditions—part i: a linear analysis," *Mechanical Systems and Signal Processing*, vol. 19, no. 4, pp. 847–864, 2005.

[89] B. A. Qadri, L. Avendaño-Valencia, J.-O. Hooghoudt, D. Tcherniak, and M. D. Ulriksen, "Removal of environmental and operational effects in damage detection: A comparative study with an operating wind turbine," *Structural health monitoring (submitted)*, 2020.

[90] K. Kumar, P. K. Biswas, and N. Dhang, "Time series-based shm using pca with application to asce benchmark structure," *Journal of Civil Structural Health Monitoring*, vol. 10, no. 5, pp. 899–911, 2020.

[91] K. Worden, T. Baldacchino, J. Rowson, and E. J. Cross, "Some recent developments in shm based on nonstationary time series analysis," *Proceedings of the IEEE*, vol. 104, no. 8, pp. 1589–1603, 2016.

[92] C. Zang and M. Imregun, "Structural damage detection using artificial neural networks and measured frf data reduced via principal component projection," *Journal of sound and vibration*, vol. 242, no. 5, pp. 813–827, 2001.

[93] L. E. Mujica, J. Vehí, M. Ruiz, M. Verleysen, W. Staszewski, and K. Worden, "Multivariate statistics process control for dimensionality reduction in structural assessment," *Mechanical Systems and Signal Processing*, vol. 22, no. 1, pp. 155–171, 2008.

[94] S. Park, J.-J. Lee, C.-B. Yun, and D. J. Inman, "Electro-mechanical impedance-based wireless structural health monitoring using pca-data compression and k-means clustering algorithms," *Journal of intelligent material systems and structures*, vol. 19, no. 4, pp. 509–520, 2008.

[95] J.-C. Golinval, P. De Boe, A. Yan, and G. Kerschen, "Structural damage detection based on pca of vibration measurements," in *58th Meeting of the Soc. for Mach. Failure Prevention Tech, Virginia Beach, 2004*, 2004.

[96] I. Trendafilova, M. P. Cartmell, and W. Ostachowicz, "Vibration-based damage detection in an aircraft wing scaled model using principal component analysis and pattern recognition," *Journal of Sound and Vibration*, vol. 313, no. 3-5, pp. 560–566, 2008.

[97] E. J. Cross, K. Worden, and Q. Chen, "Cointegration: a novel approach for the removal of environmental trends in structural health monitoring data," *Proceedings of the Royal Society A: Mathematical, Physical and Engineering Sciences*, vol. 467, no. 2133, pp. 2712–2732, 2011.

[98] H. Shi, K. Worden, and E. J. Cross, "A regime-switching cointegration approach for removing environmental and operational variations in structural health monitoring," *Mechanical Systems and Signal Processing*, vol. 103, pp. 381–397, 2018.

[99] H. Shi, K. Worden, and E. J. Cross, "A cointegration approach for heteroscedastic data based on a time series decomposition: an application to structural health monitoring," *Mechanical Systems and Signal Processing*, vol. 120, pp. 16–31, 2019.

[100] S. Johansen, *Likelihood-based inference in cointegrated vector autoregressive models*. OUP Oxford, 1995.

[101] B. Peeters and G. De Roeck, "Reference-based stochastic subspace identification for output-only modal analysis," *Mechanical systems and signal processing*, vol. 13, no. 6, pp. 855–878, 1999.

[102] L. D. Avendaño-Valencia, E. N. Chatzi, K. Y. Koo, and J. M. Brownjohn, "Gaussian process time-series models for structures under operational variability," *Frontiers in Built Environment*, vol. 3, p. 69, 2017.

[103] C. Roberts, D. G. Cava, and L. D. Avendaño-Valencia, "Addressing practicalities in multivariate nonlinear regression for mitigating environmental and operational variations," *Structural Health Monitoring*, 2022.

[104] Y.-W. Wen, Y.-W. Tsai, D. B.-C. Wu, and P.-F. Chen, "The impact of outliers on net-benefit regression model in cost-effectiveness analysis," *PLoS one*, vol. 8, no. 6, p. e65930, 2013.

[105] M. A. Babyak, "What you see may not be what you get: a brief, nontechnical introduction to overfitting in regression-type models," *Psychosomatic medicine*, vol. 66, no. 3, pp. 411–421, 2004.

[106] N. Dervilis, I. Antoniadou, R. J. Barthorpe, E. J. Cross, and K. Worden, "Robust methods for outlier detection and regression for shm applications.," *International Journal of Sustainable Materials and Structural Systems*, vol. 2, no. 1/2, 2016.

[107] M. Schlechtingen and I. F. Santos, "Comparative analysis of neural network and regression based condition monitoring approaches for wind turbine fault detection," *Mechanical systems and signal processing*, vol. 25, no. 5, pp. 1849–1875, 2011.

[108] W. S. L. Wah, Y.-T. Chen, and J. S. Owen, "A regression-based damage detection method for structures subjected to changing environmental and operational conditions," *Engineering Structures*, vol. 228, p. 111462, 2021.

[109] C. Xu, J. G. Chase, and G. W. Rodgers, "Nonlinear regression based health monitoring of hysteretic structures under seismic excitation," *Shock and Vibration*, vol. 2015, 2015.

[110] H. Sohn, "Effects of environmental and operational variability on structural health monitoring," *Philosophical Transactions of the Royal Society*

A: Mathematical, Physical and Engineering Sciences, vol. 365, no. 1851, pp. 539–560, 2007.

[111] E. Schulz, M. Speekenbrink, and A. Krause, "A tutorial on gaussian process regression: Modelling, exploring, and exploiting functions," *Journal of Mathematical Psychology*, vol. 85, pp. 1–16, 2018.

[112] A. G. Wilson, D. A. Knowles, and Z. Ghahramani, "Gaussian process regression networks," *arXiv preprint arXiv:1110.4411*, 2011.

[113] D. Duvenaud, J. Lloyd, R. Grosse, J. Tenenbaum, and G. Zoubin, "Structure discovery in nonparametric regression through compositional kernel search," in *International Conference on Machine Learning*, pp. 1166–1174, PMLR, 2013.

[114] Q.-A. Wang and Y.-Q. Ni, "Measurement and forecasting of high-speed rail track slab deformation under uncertain shm data using variational heteroscedastic gaussian process," *Sensors*, vol. 19, no. 15, p. 3311, 2019.

[115] A. M. Alani, F. Tosti, L. B. Ciampoli, V. Gagliardi, and A. Benedetto, "An integrated investigative approach in health monitoring of masonry arch bridges using gpr and insar technologies," *NDT & E International*, vol. 115, p. 102288, 2020.

[116] Q.-A. Wang, C. Zhang, Z.-G. Ma, and Y.-Q. Ni, "Modelling and forecasting of shm strain measurement for a large-scale suspension bridge during typhoon events using variational heteroscedastic gaussian process," *Engineering Structures*, vol. 251, p. 113554, 2022.

[117] L. D. Avendaño-Valencia, I. Abdallah, and E. Chatzi, "Virtual fatigue diagnostics of wake-affected wind turbine via gaussian process regression," *Renewable Energy*, vol. 170, pp. 539–561, 2021.

[118] C. T. Wickramarachchi, D. S. Brennan, W. Lin, E. Maguire, D. Y. Harvey, E. J. Cross, and K. Worden, "Towards population-based structural health monitoring, part v: Networks and databases," in *Data Science in Engineering, Volume 9*, pp. 1–8, Springer, 2022.

[119] N. Dervilis, H. Shi, K. Worden, and E. Cross, "Exploring environmental and operational variations in shm data using heteroscedastic gaussian processes," in *Dynamics of Civil Structures, Volume 2*, pp. 145–153, Springer, 2016.

[120] T. J. Rogers, G. Manson, K. Worden, and E. J. Cross, "On the choice of optimisation scheme for gaussian process hyperparameters in shm problems," *Structural Health Monitoring 2017*, vol. 1, 2017.

[121] S. Zhang, T. J. Rogers, and E. J. Cross, "Gaussian process based grey-box modelling for shm of structures under fluctuating environmental conditions," in *European Workshop on Structural Health Monitoring*, pp. 55–66, Springer, 2020.

[122] K. Qu, D. G. Cava, S. Killbourn, and A. Logan, "Operational modal analysis for scour detection in mono-pile offshore wind turbines," in *European Workshop on Structural Health Monitoring*, pp. 668–678, Springer, 2023.

[123] L. D. Avendaño-Valencia and E. N. Chatzi, "Sensitivity driven robust vibration-based damage diagnosis under uncertainty through hierarchical bayes time-series representations," *Procedia engineering*, vol. 199, pp. 1852–1857, 2017.

[124] E. Figueiredo, I. Moldovan, A. Santos, P. Campos, and J. C. Costa, "Finite element–based machine-learning approach to detect damage in bridges under operational and environmental variations," *Journal of Bridge Engineering*, vol. 24, no. 7, p. 04019061, 2019.

[125] J. Peng, S. Zhang, D. Peng, and K. Liang, "Application of machine learning method in bridge health monitoring," in *2017 Second International Conference on Reliability Systems Engineering (ICRSE)*, pp. 1–7, IEEE, 2017.

[126] H. Sarmadi, "Investigation of machine learning methods for structural safety assessment under variability in data: comparative studies and new approaches," *Journal of Performance of Constructed Facilities*, vol. 35, no. 6, p. 04021090, 2021.

[127] M. Mishra, "Machine learning techniques for structural health monitoring of heritage buildings: A state-of-the-art review and case studies," *Journal of Cultural Heritage*, vol. 47, pp. 227–245, 2021.

[128] M. H. Rafiei and H. Adeli, "A novel machine learning-based algorithm to detect damage in high-rise building structures," *The Structural Design of Tall and Special Buildings*, vol. 26, no. 18, p. e1400, 2017.

[129] P. Singh, U. F. Ahmad, and S. Yadav, "Structural health monitoring and damage detection through machine learning approaches," in *E3S Web of Conferences*, vol. 220, p. 01096, EDP Sciences, 2020.

[130] P. Assumpção, C. Oliveira, W. Melo, and L. Carmo, "Sensors fingerprints using machine learning: a case study on dam monitoring systems," in *2022 IEEE International Instrumentation and Measurement Technology Conference (I2MTC)*, pp. 1–6, IEEE, 2022.

[131] Y. Li, T. Bao, Z. Gao, X. Shu, K. Zhang, L. Xie, and Z. Zhang, "A new dam structural response estimation paradigm powered by deep learning and transfer learning techniques," *Structural Health Monitoring*, vol. 21, no. 3, pp. 770–787, 2022.

[132] K. Chandrasekhar, N. Stevanovic, E. J. Cross, N. Dervilis, and K. Worden, "Damage detection in operational wind turbine blades using a new approach based on machine learning," *Renewable Energy*, vol. 168, pp. 1249–1264, 2021.

[133] N. Dervilis, *A machine learning approach to structural health monitoring with a view towards wind turbines*. PhD thesis, University of Sheffield, 2013.

[134] T. Regan, C. Beale, and M. Inalpolat, "Wind turbine blade damage detection using supervised machine learning algorithms," *Journal of Vibration and Acoustics*, vol. 139, no. 6, 2017.

[135] M. Flah, I. Nunez, W. Ben Chaabene, and M. L. Nehdi, "Machine learning algorithms in civil structural health monitoring: a systematic review," *Archives of computational methods in engineering*, vol. 28, no. 4, pp. 2621–2643, 2021.

[136] A. Arcos Jiménez, C. Q. Gómez Muñoz, and F. P. García Márquez, "Machine learning for wind turbine blades maintenance management," *Energies*, vol. 11, no. 1, p. 13, 2017.

[137] A. Reddy, V. Indragandhi, L. Ravi, and V. Subramaniyaswamy, "Detection of cracks and damage in wind turbine blades using artificial intelligence-based image analytics," *Measurement*, vol. 147, p. 106823, 2019.

[138] A. A. Jiménez, F. P. G. Márquez, V. B. Moraleda, and C. Q. G. Muñoz, "Linear and nonlinear features and machine learning for wind turbine blade ice detection and diagnosis," *Renewable energy*, vol. 132, pp. 1034–1048, 2019.

[139] A. A. Jiménez, L. Zhang, C. Q. G. Muñoz, and F. P. G. Márquez, "Maintenance management based on machine learning and nonlinear features in wind turbines," *Renewable Energy*, vol. 146, pp. 316–328, 2020.

[140] A. A. Jiménez, C. Q. G. Muñoz, and F. P. G. Márquez, "Dirt and mud detection and diagnosis on a wind turbine blade employing guided waves and supervised learning classifiers," *Reliability Engineering & System Safety*, vol. 184, pp. 2–12, 2019.

[141] J. X. Leon-Medina, N. Parés, M. Anaya, D. Tibaduiza, and F. Pozo, "Imbalanced multi-class classification of structural damage in a wind turbine foundation," in *European Workshop on Structural Health Monitoring*, pp. 492–500, Springer, 2023.

[142] L. Wang, Z. Zhang, J. Xu, and R. Liu, "Wind turbine blade breakage monitoring with deep autoencoders," *IEEE Transactions on Smart Grid*, vol. 9, no. 4, pp. 2824–2833, 2016.

[143] C. F. Dormann, J. Elith, S. Bacher, C. Buchmann, G. Carl, G. Carré, J. R. G. Marquéz, B. Gruber, B. Lafourcade, P. J. Leitão, *et al.*, "Collinearity: a review of methods to deal with it and a simulation study evaluating their performance," *Ecography*, vol. 36, no. 1, pp. 27–46, 2013.

[144] X. Ying, "An overview of overfitting and its solutions," in *Journal of physics: Conference series*, vol. 1168, p. 022022, IOP Publishing, 2019.

[145] G. N. Karystinos and D. A. Pados, "On overfitting, generalization, and randomly expanded training sets," *IEEE Transactions on Neural Networks*, vol. 11, no. 5, pp. 1050–1057, 2000.

[146] D. Blalock, J. J. Gonzalez Ortiz, J. Frankle, and J. Guttag, "What is the state of neural network pruning?," *Proceedings of machine learning and systems*, vol. 2, pp. 129–146, 2020.

[147] K. Ullrich, E. Meeds, and M. Welling, "Soft weight-sharing for neural network compression," *arXiv preprint arXiv:1702.04008*, 2017.

[148] A. R. Barron, "Complexity regularization with application to artificial neural networks," in *Nonparametric functional estimation and related topics*, pp. 561–576, Springer, 1991.

[149] F. Turrisi and S. Lucà, "On the use of multiple linear regression to compensate for the effect of environmental parameters in large structures tilt measurements," in *IV Forum Nazionale delle Misure*, pp. 1–10, 2020.

[150] R. Tibshirani, "Regression shrinkage and selection via the lasso," *Journal of the Royal Statistical Society: Series B (Methodological)*, vol. 58, no. 1, pp. 267–288, 1996.

[151] N. Gauraha, "Introduction to the lasso," *Resonance*, vol. 23, no. 4, pp. 439–464, 2018.

[152] A. Yasar, M. Bilgili, and E. Simsek, "Water demand forecasting based on stepwise multiple nonlinear regression analysis," *Arabian Journal for Science and Engineering*, vol. 37, no. 8, pp. 2333–2341, 2012.

[153] P. Bortolotti, D. S. Berry, R. Murray, E. Gaertner, D. S. Jenne, R. R. Damiani, G. E. Barter, and K. L. Dykes, "A detailed wind turbine blade cost model," tech. rep., National Renewable Energy Lab.(NREL), Golden, CO (United States), 2019.

[154] O. T. Thomsen, "Sandwich materials for wind turbine blades—present and future," *Journal of Sandwich Structures & Materials*, vol. 11, no. 1, pp. 7–26, 2009.

[155] A. Sareen, C. A. Sapre, and M. S. Selig, "Effects of leading edge erosion on wind turbine blade performance," *Wind Energy*, vol. 17, no. 10, pp. 1531–1542, 2014.

[156] K. Pugh, J. Nash, G. Reaburn, and M. Stack, "On analytical tools for assessing the raindrop erosion of wind turbine blades," *Renewable and Sustainable Energy Reviews*, vol. 137, p. 110611, 2021.

[157] Y. Liu, H. Cheng, X. Kong, Q. Wang, and H. Cui, "Intelligent wind turbine blade icing detection using supervisory control and data acquisition data and ensemble deep learning," *Energy Science & Engineering*, vol. 7, no. 6, pp. 2633–2645, 2019.

[158] C. Hochart, G. Fortin, J. Perron, and A. Ilinca, "Wind turbine performance under icing conditions," *Wind Energy: An International Journal for Progress and Applications in Wind Power Conversion Technology*, vol. 11, no. 4, pp. 319–333, 2008.

[159] P. Frohboese and A. Anders, "Effects of icing on wind turbine fatigue loads," in *Journal of Physics: Conference Series*, vol. 75, p. 012061, IOP Publishing, 2007.

[160] S. Yokoyama, "Lightning protection of wind turbine blades," *Electric power systems research*, vol. 94, pp. 3–9, 2013.

[161] A. C. Garolera, S. F. Madsen, M. Nissim, J. D. Myers, and J. Holboell, "Lightning damage to wind turbine blades from wind farms in the us," *IEEE Transactions on Power Delivery*, vol. 31, no. 3, pp. 1043–1049, 2014.

[162] I. Cotton, N. Jenkins, and K. Pandiaraj, "Lightning protection for wind turbine blades and bearings," *Wind Energy: An International Journal for Progress and Applications in Wind Power Conversion Technology*, vol. 4, no. 1, pp. 23–37, 2001.

[163] J. G. Njiri, N. Beganovic, M. H. Do, and D. Söffker, "Consideration of lifetime and fatigue load in wind turbine control," *Renewable energy*, vol. 131, pp. 818–828, 2019.

[164] S. Lee, M. Churchfield, P. Moriarty, J. Jonkman, and J. Michalakes, "Atmospheric and wake turbulence impacts on wind turbine fatigue loadings," in *50th AIAA Aerospace Sciences Meeting including the New Horizons Forum and Aerospace Exposition*, p. 540, 2012.

[165] F. Zhu and F. Li, "Reliability analysis of wind turbines," *Stability Control & Reliable Performance of Wind Turbines*, pp. 169–186, 2018.

[166] C. Debel, "Identification of damage types in wind turbine blades tested to failure," in *Dansk Metallurgisk Selskabs vintermøde 2004*, pp. 123–127, Dansk Metallurgisk Selskab, 2004.

[167] B. F. Sørensen, E. Joergensen, C. P. Debel, F. Jensen, H. Jensen, T. Jacobsen, and K. Halling, "Improved design of large wind turbine blade of fibre composites based on studies of scale effects (phase 1)-summary report," *U.S. Department of Energy*, 2004.

[168] H. Zhou, H. Dou, L. Qin, Y. Chen, Y. Ni, and J. Ko, "A review of full-scale structural testing of wind turbine blades," *Renewable and Sustainable Energy Reviews*, vol. 33, pp. 177–187, 2014.

[169] F. P. G. Márquez and A. M. P. Chacón, "A review of non-destructive testing on wind turbines blades," *Renewable Energy*, vol. 161, pp. 998–1010, 2020.

[170] G. Marsh, "Meeting the challenge of wind turbine blade repair," *Reinforced plastics*, vol. 55, no. 4, pp. 32–36, 2011.

[171] K. Kong, K. Dyer, C. Payne, I. Hamerton, and P. M. Weaver, "Progress and trends in damage detection methods, maintenance, and data-driven monitoring of wind turbine blades–a review," *Renewable Energy Focus*, 2022.

[172] D. Y. Kim, H.-B. Kim, W. S. Jung, S. Lim, J.-H. Hwang, and C.-W. Park, "Visual testing system for the damaged area detection of wind power plant blade," in *IEEE ISR 2013*, pp. 1–5, IEEE, 2013.

[173] P. Kaewniam, M. Cao, N. F. Alkayem, D. Li, and E. Manoach, "Recent advances in damage detection of wind turbine blades: A state-of-the-art review," *Renewable and Sustainable Energy Reviews*, vol. 167, p. 112723, 2022.

[174] S. Das and P. Saha, "A review of some advanced sensors used for health diagnosis of civil engineering structures," *Measurement*, vol. 129, pp. 68–90, 2018.

[175] P. Schubel, R. Crossley, E. Boateng, and J. Hutchinson, "Review of structural health and cure monitoring techniques for large wind turbine blades," *Renewable energy*, vol. 51, pp. 113–123, 2013.

[176] D. Tcherniak and L. L. Mølgaard, "Active vibration-based structural health monitoring system for wind turbine blade: Demonstration on an operating vestas v27 wind turbine," *Structural Health Monitoring*, vol. 16, no. 5, pp. 536–550, 2017.

[177] X. Wei, M. Verhaegen, and T. Van den Engelen, "Sensor fault diagnosis of wind turbines for fault tolerant," *IFAC Proceedings Volumes*, vol. 41, no. 2, pp. 3222–3227, 2008.

[178] H. Huang and Y. Hew, "Wireless vibration sensing without a battery," in *Smart Materials, Adaptive Structures and Intelligent Systems*, vol. 45097, pp. 885–890, American Society of Mechanical Engineers, 2012.

[179] A. Behnia, H. K. Chai, A. A. Mousa, and S. A. Ravanfar, "A novel damage index for online monitoring of rc slabs under monotonic loading by integration of process controlling into acoustic emission technique," *Mechanical Systems and Signal Processing*, vol. 119, pp. 547–560, 2019.

[180] H. Kamei, Y. Sato, J. Mitsugi, K. Egawa, Y. Kawakita, and H. Ichikawa, "Frequency efficient concurrent data streaming with passive backscatter wireless sensors," in *2018 6th IEEE International Conference on Wireless for Space and Extreme Environments (WiSEE)*, pp. 107–109, IEEE, 2018.

[181] A. Rytter, *Vibrational Based Inspection of Civil Engineering Structures*. PhD thesis, Building Technology and Structural Engineering, Denmark, 1993. Ph.D.-Thesis defended publicly at the University of Aalborg, April 20, 1993 PDF for print: 206 pp.

[182] C. Farrar, G. Park, and K. Worden, "Complexity: A new axiom for structural health monitoring?," tech. rep., Los Alamos National Lab Nm, 2010.

[183] K. Worden, C. R. Farrar, G. Manson, and G. Park, "The fundamental axioms of structural health monitoring," *Proceedings of the Royal Society A: Mathematical, Physical and Engineering Sciences*, vol. 463, no. 2082, pp. 1639–1664, 2007.

[184] Y. Ou, K. E. Tatsis, V. K. Dertimanis, M. D. Spiridonakos, and E. N. Chatzi, "Vibration-based monitoring of a small-scale wind turbine blade under varying climate conditions. part i: An experimental benchmark," *Structural Control and Health Monitoring*, vol. 28, no. 6, p. e2660, 2021.

[185] S. R. Vadyala, S. N. Betgeri, J. C. Matthews, and E. Matthews, "A review of physics-based machine learning in civil engineering," *Results in Engineering*, p. 100316, 2021.

[186] J. P. Santos, C. Crémona, L. Calado, P. Silveira, and A. D. Orcesi, "On-line unsupervised detection of early damage," *Structural Control and Health Monitoring*, vol. 23, no. 7, pp. 1047–1069, 2016.

[187] R. de Almeida Cardoso, A. Cury, F. Barbosa, and C. Gentile, "Unsupervised real-time shm technique based on novelty indexes," *Structural Control and Health Monitoring*, vol. 26, no. 7, p. e2364, 2019.

[188] L. Bull, K. Worden, and N. Dervilis, "Towards semi-supervised and probabilistic classification in structural health monitoring," *Mechanical Systems and Signal Processing*, vol. 140, p. 106653, 2020.

[189] M. D. Ulriksen, D. Tcherniak, and L. Damkilde, "Damage detection in an operating vestas v27 wind turbine blade by use of outlier analysis," in *2015 IEEE Workshop on Environmental, Energy, and Structural Monitoring Systems (EESMS) Proceedings*, pp. 50–55, IEEE, 2015.

[190] D. García, D. Tcherniak, and I. Trendafilova, "Damage assessment for wind turbine blades based on a multivariate statistical approach," in *Journal of Physics: Conference Series*, vol. 628, p. 012086, IOP Publishing, 2015.

[191] A. P. Bradley, "The use of the area under the roc curve in the evaluation of machine learning algorithms," *Pattern recognition*, vol. 30, no. 7, pp. 1145–1159, 1997.

[192] T. Fawcett, "An introduction to roc analysis," *Pattern recognition letters*, vol. 27, no. 8, pp. 861–874, 2006.

[193] C. Roberts, S. Isbister, C. Murphy, C. Nisbet, P. Sweeney, D. Garcia Cava, and D. Tcherniak, "Strain estimation using modal expansion approach via virtual sensing for structural asset management," in *1st International Conference on Structural Integrity for offshore energy industry*, 2018.

[194] S. Adhikari, *Damping models for structural vibration*. PhD thesis, Citeseer, 2001.

[195] W. Timmer, "An overview of naca 6-digit airfoil series characteristics with reference to airfoils for large wind turbine blades," in *47th AIAA aerospace sciences meeting including the new horizons forum and aerospace exposition*, p. 268, 2009.

[196] F. O. of Meteorology and C. MeteoSwiss, "Historic measured meteorological data," 2017.

[197] T. website for wind energy data in Switzerland, "Monthly wind speed values," 2022.

[198] J. I. Rojas and D. Crespo, "Modeling of the effect of temperature, frequency, and phase transformations on the viscoelastic properties of aa 7075-t6 and aa 2024-t3 aluminum alloys," *Metallurgical and Materials Transactions A*, vol. 43, no. 12, pp. 4633–4646, 2012.

[199] B. J. Jonkman, "Turbsim user's guide: Version 1.50," tech. rep., National Renewable Energy Lab.(NREL), Golden, CO (United States), 2009.

[200] P. Moser and B. Moaveni, "Environmental effects on the identified natural frequencies of the dowling hall footbridge," *Mechanical Systems and Signal Processing*, vol. 25, no. 7, pp. 2336–2357, 2011.

[201] F. Ubertini, G. Comanducci, N. Cavalagli, A. L. Pisello, A. L. Materazzi, and F. Cotana, "Environmental effects on natural frequencies of the san

pietro bell tower in perugia, italy, and their removal for structural performance assessment," *Mechanical Systems and Signal Processing*, vol. 82, pp. 307–322, 2017.

[202] W. Weijtjens, T. Verbelen, G. De Sitter, and C. Devriendt, "Data normalization for foundation shm of an offshore wind turbine: a real-life case study," in *EWSHM-7th European Workshop on Structural Health Monitoring*, 2014.

[203] Y.-C. Liu, C.-H. Loh, and Y.-Q. Ni, "Stochastic subspace identification for output-only modal analysis: application to super high-rise tower under abnormal loading condition," *Earthquake Engineering & Structural Dynamics*, vol. 42, no. 4, pp. 477–498, 2013.

[204] E. Cheynet, "Operational modal analysis with automated ssi-cov algorithm," 2020.

[205] X. Jin, H. Wang, Z. Kong, Z. Xu, and W. Qiao, "Condition monitoring of wind turbine generators based on scada data and feature transfer learning," *IEEE Access*, 2023.

[206] Y. Li, W. Jiang, G. Zhang, and L. Shu, "Wind turbine fault diagnosis based on transfer learning and convolutional autoencoder with small-scale data," *Renewable Energy*, vol. 171, pp. 103–115, 2021.

[207] M. Magnusson, M. R. Andersen, J. Jonasson, and A. Vehtari, "Leave-one-out cross-validation for bayesian model comparison in large data," *arXiv preprint arXiv:2001.00980*, 2020.

[208] A. G. Asuero, A. Sayago, and A. González, "The correlation coefficient: An overview," *Critical reviews in analytical chemistry*, vol. 36, no. 1, pp. 41–59, 2006.

[209] J. Benesty, J. Chen, Y. Huang, and I. Cohen, "Pearson correlation coefficient," in *Noise reduction in speech processing*, pp. 1–4, Springer, 2009.

[210] Y.-I. Moon, B. Rajagopalan, and U. Lall, "Estimation of mutual information using kernel density estimators," *Physical Review E*, vol. 52, no. 3, p. 2318, 1995.

[211] T. Lee, "Mutual information -2 variabllee," Oct 2010.

[212] X. Liu and G. S. Chen, *Friction Dynamics: Principles and Applications*. Woodhead Publishing, 2016.

[213] M. Taboga, "Marginal probability density function," 2021.

[214] A. Iwasaki, A. Todoroki, T. Sugiya, and S. Sakai, "Damage diagnosis for shm of existing civil structure with statistical diagnostic method," in *Health Monitoring and Smart Nondestructive Evaluation of Structural and Biological Systems III*, vol. 5394, pp. 411–418, International Society for Optics and Photonics, 2004.

[215] D. W. Marquardt and R. D. Snee, "Ridge regression in practice," *The American Statistician*, vol. 29, no. 1, pp. 3–20, 1975.

[216] T. Hastie, R. Tibshirani, J. H. Friedman, and J. H. Friedman, *The elements of statistical learning: data mining, inference, and prediction*, vol. 2. Springer, 2009.

[217] A. Movsessian, D. Garcia, and D. Tcherniak, "Adaptive feature selection for enhancing blade damage diagnosis on an operational wind turbine," in *Proceedings of the 13th International Conference on Damage Assessment of Structures*, pp. 594–605, Springer, 2020.

[218] D. Anguita, L. Ghelardoni, A. Ghio, L. Oneto, and S. Ridella, "The 'k'in k-fold cross validation," in *20th European Symposium on Artificial Neural Networks, Computational Intelligence and Machine Learning (ESANN)*, pp. 441–446, i6doc. com publ, 2012.

[219] A. Murgia, R. Verbeke, E. Tsiporkova, L. Terzi, and D. Astolfi, "Discussion on the suitability of scada-based condition monitoring for wind turbine fault diagnosis through temperature data analysis," *Energies*, vol. 16, no. 2, p. 620, 2023.

.